Multiple Model Based Real Time Estimation Of Wheel-Rail Contact Conditions

Imtiaz Hussain

School of Computing, Science and Engineering
College of Science and Technology
University of Salford
Salford, UK

Submitted in Partial Fulfillment of the Requirement of the Degree of Doctor of Philosophy, August 2012

Table Of Contents

Abstract

The issue of low adhesion between the wheel and the rail has been a problem for the design and operation of the railway vehicles. The level of adhesion can be influenced by many different factors, such as contamination, climate, and vegetation, and it is extremely difficult to predict with certainty. Changes in the adhesion conditions can be rapid and short-lived, and values can differ from position to position along a route, depending on the type and degree of contamination. All these factors present a significant scientific challenge to effectively design a suitable technique to tackle this problem. This thesis presents the development of a unique, vehicle based technique for the real-time estimation of the contact conditions using multiple models to represent variations in the adhesion level and different contact conditions. The proposed solution exploits the fact that the dynamic behaviour of a railway vehicle is strongly affected by the nonlinearities and the variations in creep characteristics. The purpose of the proposed scheme is to interpret these variations in the dynamic response of the wheelset, developing useful contact condition information. The proposed system involves the use of a number of carefully selected mathematical models (or estimators) of a rail vehicle to mimic train dynamic behaviours in response to different track conditions. Each of the estimators is tuned to match one particular track condition to give the best results at the specific design point. Increased estimation errors are expected if the contact condition is not at or near the chosen operating point. The level of matches/mismatches is reflected in the estimation errors (or residuals) of the models concerned when compared with the real vehicle (through the measurement output of vehicle mounted inertial sensors). The output residuals from all the models are then assessed using an artificial intelligence decision-making approach to determine which of the models provides a best match to the present operating condition and, thus, provide real-time information about track conditions.

Acknowledgements

I want first to thank my supervisor Professor T X Mei for all the encouragement he has given to me. He has enlightened me through his vast knowledge of this subject and his deep intuitions about where it should go and what is necessary to reach that point. It would not have been possible to write this doctoral thesis without his help, support, and patience. I appreciate all his contributions of time and ideas to make my Ph.D. experience productive.

I would like to give special thanks to Professor Tim Ritchings for his valuable time to help me through the last chapter. His opinion as an expert in intelligent system design helped me to complete the fuzzy logic part of this thesis.

I also thank Professor Mukhtiar Unar, Professor Ahsan Ursani, Professor Athar Asif, Mr Aslam Laghari, and Dr Shahid Abro for their support during my high school, undergraduate, and post-graduate studies. It was under their tutelage that I became interested in engineering. They provided me with direction and technical support; they became my mentors and friends in addition to being my teachers. I doubt that I will ever be able to convey my appreciation fully, but I owe them my eternal gratitude.

It was a pleasure to share doctoral studies with wonderful people like Ben, Roy, and Fred, my first office mates, and with Ahmed, May, Mo, and Indra, among others who are very close friends now. The last few months of writing—which is a rather frustrating period—were made more pleasant by the company of my country mate Dr Ziauddin Ursani. The year spent in Leeds would not have been as wonderful without my friends, including Wanod, Arif, Javed, and Asghar.

I would like to acknowledge the financial, academic, and technical support of the Mehran University of Engineering and Technology, University of Salford and University of Leeds, particularly the award of scholarship that provided me the necessary financial support for this research, library facilities, and the computer facilities.

Above all, my deepest gratitude goes to my family for their unflagging love and support throughout my life; this dissertation is simply impossible without them. For my parents, who have given me their unequivocal support throughout, as always, for which my mere

expression of thanks likewise does not suffice. I am indebted to my father, Muhammad Shaban Kalwar, for his care and love. He worked industriously to support our family and spared no effort to provide the best possible environment for me to grow up and attend school. I cannot ask for more from my mother, Hamida Kalwar, as she is simply perfect. I have no suitable words to fully describe her everlasting love for me. I remember her constant support when I encountered difficulties, and I remember, most of all, her delicious dishes. I owe my loving thanks to my wife Sajida, my daughter Sumayya and my son Sufiyan. They have sacrificed a lot due to my research abroad. Without their encouragement and understanding it would have been impossible for me to finish this work. My special gratitude is due to my brothers Dr Altaf and Dr Aftab, my sister Dr Rehana and their families for their loving support.

Last but not least, thanks be to Almighty God for my life through all tests in the past four years. You have made my life more bountiful. May your name be exalted, honoured, and glorified.

List Of Figures

List Of Tables

1. Introduction

1.1 Introduction

Since the beginning of rail travel, adhesion between the wheel and the rail has been a crucial parameter in the design and operation of the railway vehicles, particularly during the autumn leaf falls, when the leaves are crushed to form a low-adhesion contaminant film on the rail surface, which is extremely difficult to remove. Poor adhesion can either be caused by naturally occurring weather conditions or the local environmental or industrial conditions. Some of the causes, such as leaf contamination, snow, ice, oil spills, etc., may be obvious and well known, while others such as industrial pollutions are not so obvious. However, they all have a similar effect in that they reduce the level of adhesion.

Figure-1.1: Contaminants on railway tracks

The level of adhesion between wheel and rail has a major impact on a vehicle's ability to brake and to accelerate properly. If the wheels deliver a higher force to the rail than they can transmit, they start to slip in traction or slide in braking, causing surface damage to the wheels, such as flats, skid marks and shelling, and to the rails, which also

suffer from wheel burns and deterioration caused by damaged wheels. Wheelsets then need re-profiling or replacing and the rails need regrinding, thus causing additional costs to the rail industry. Furthermore, there is loss of train availability during the period of repair [1]. Wear due to wheel slip/slides and disruption to train schedules is the most important aspect from an economic perspective. However, from the safety point of view, when the friction levels are very low a train might not be able to brake within the available distance, making this aspect of even higher importance. Extremely low friction values between the wheel and the rail have been reported worldwide, leading to severe delays and sometimes even to accidents.

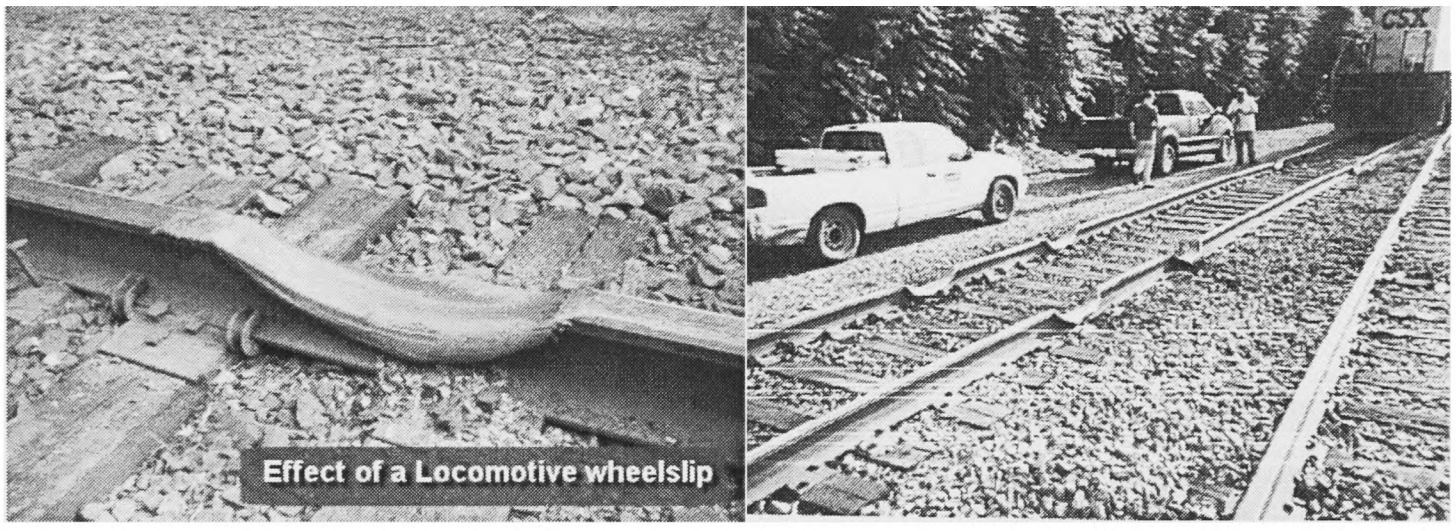

Figure-1.2: Damaged track after severe wheel slip

Another side effect is that it tends to influence the behaviour of the driver. Basic knowledge about low adhesion is limited and based largely on subjective observations offered, for the most part, by drivers. Therefore it is up to the drivers, and because they shoulder great responsibility, they tend to be overly cautious on the basis of their 'feeling' concerning the condition of the track. When one driver encounters a slippery track during braking or accelerating, he may immediately communicate to other drivers that they ought to exert caution [2]. Of course, such behaviour is 'over-safe' when the friction levels are at acceptable limits, leading undoubtedly to delays and wasted drive time.

Many railway organisations still suffer from low adhesion problems as a consequence of the extensive use of the rail infrastructure. In autumn 2005, in the UK, nearly 400 adhesion-related incidents were reported, including nine signals passed at danger and 390 stations overrun wholly or partially as a result of low adhesion conditions [3]. In the Netherlands, slippery tracks caused the almost complete failure of train services in the autumn of 2002, as an important part of the rolling stock of the

Dutch train operator NS-Reizigers suffered flat wheels due to excessive sliding, leaving thousands of travellers stranded overnight on their way home. In the following week, thorough maintenance was carried out on the rolling stock, but the lack of available train carriages made it impossible for the operator to run on schedule [2]. Low adhesion costs the railway industry significant sums of money each year, not only for various railhead treatments to minimise the occurrence of low adhesion conditions, but also for reduced operational performance and for the repair of wheels and rails where railhead treatments are not successful. According to adhesion working group (AWG) reports, the annual cost of low adhesion to the UK's rail industry as a whole exceeds £50 million [2, 4]. A large number of measures have been developed; nevertheless, the problems caused by low adhesion still persist.

Several measures have been taken by the railway operators around the world to improve the level of adhesion in severe weather conditions. The most commonly used methods include the use of sandites, water jetting and vegetation management, but the effectiveness of these methods has long been doubted. Wheel slip/slide protection (WSP) technologies for traction and braking systems are incorporated into rail vehicles to maximise the use of available adhesion, by controlling the slip ratio (relative speed between a wheel and the train) below a predefined threshold. These controllers find it difficult to obtain optimal performance and also require the accurate measurement of wheel slip. In general, WSPs are effectively reactive systems, i.e. only 'activated' to stop wheels slipping or sliding when detected by sensors. In some rail networks, a LAWS (low adhesion warning system) or an AMS (adhesion management system) is used to provide estimates of track conditions based on a large pool of trackside measurements such as site topography, track geometry, microclimates and contamination. Such systems are inevitably very complex, expensive to implement and potentially inaccurate because of the large number of sensors that need to be installed across a network and the amount of data to be collected and processed. Despite the measures taken by the railway industry, problems caused by low adhesion still occur because the adhesion varies all the time on any given date and time, so it cannot be predicted with certainty. Changes in adhesion conditions can be rapid and also short-lived, and values can differ from position to position along a route depending upon the type and degree of contamination, which presents a great scientific challenge to design a suitable technique to tackle this problem.

For at least 150 years, research has been conducted on how to improve the transmission of power. The need for faster, more efficient and safer transportation over the past decade has made it increasingly important to improve the transmission of force. As a result, NS (the largest train operator in the Netherlands) and ProRail (Dutch infrastructure management company) have initiated the low adhesion research programme AdRem (Adhesion Remedy) [5]. The railway industry in the UK is currently taking formative steps in using the real-time condition monitoring of railway vehicles [6-7], several techniques for which have been proposed, with the main emphasis on detecting areas of low adhesion as the train travels along the track [6, 8-11]. These condition monitoring techniques rely on available measurements, estimates and observations of the required parameters (such as creep forces) during normal running conditions of railway vehicle.

1.2 Motivation, aims and objectives of the study

The problem of low adhesion costs the railway industry significant amounts of money each year and raises several safety and reliability issues. Although in last few decades the railway industry has been able to manage low adhesion to some extent, currently available measures are not sufficient to eliminate safety incidents and train delays. Over one million scientific publications have been produced by researchers around the world alluding to this subject, including topics such as material technology, organic chemistry, rolling stock technology (also braking techniques, control techniques, traction installation), transportation processes, driver behaviour, safety, infrastructure, signalling systems, timetables, tribology, the dynamic behaviour of trains, weather and measuring techniques [5, 12]. Nevertheless, this volume of work has not resulted in an acceptable reduction in the problem, mainly because adhesion varies continually.

The lack of knowledge on low adhesion is the result of the absence of a measurement tool that can establish the problem as it occurs. Therefore, in this research a novel technique is proposed to solve this issue. The main purpose of this research is to develop a technique for the real-time estimation of wheel-rail contact conditions as the train travels along the track. The real-time information obtained from such a system would not only be helpful to drivers for determining the maximum acceleration or braking forces they can apply, but also would help network operators to optimise train schedules and make timetabling adaptive to track conditions.

The wheel slip/slide phenomenon and associated damages and repair costs will be a thing of the past. The technique will also save time because the train will be driven more efficiently at speeds associated with the maximum use of available adhesion rather than using the current guidelines. It will also have a great impact on the quality of service in terms of passenger ride comfort and noise levels.

1.3 Railway vehicle dynamics

Wheel-rail contact conditions and the level of adhesion also play a significant part in the dynamic properties and behaviour of railway vehicles, especially those pertaining to wheelsets. The focus of this thesis therefore centres on the dynamics of the most fundamental element of railway transport vehicles, namely the wheelset. Railway wheels are different from the wheels on road vehicles in that both wheels are mounted rigidly on a common axle, the whole arrangement being known as a wheelset. There are exceptions, such as the Spanish high-speed train, the Talgo Express, which has independent wheels (as do many rail vehicles used in coal mines), but most conventional rail vehicles use the solid axle wheelset [13-15].

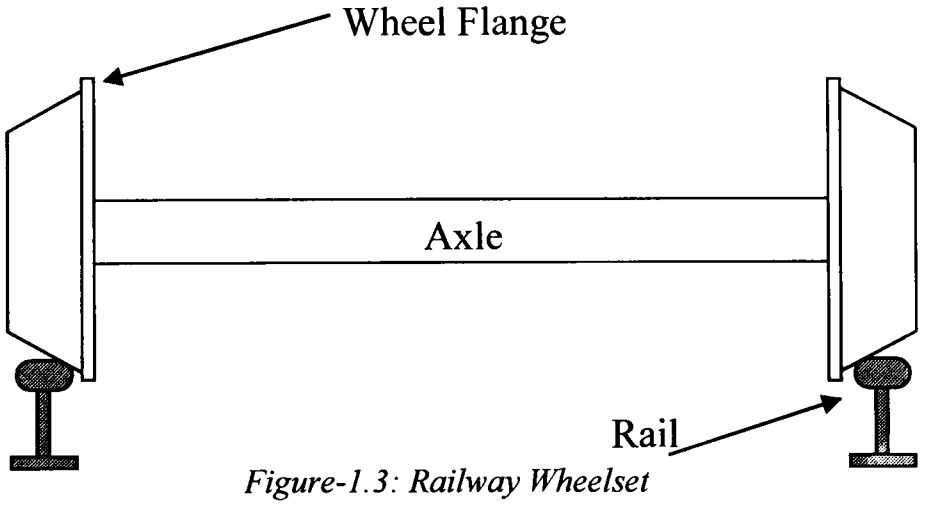

Figure-1.3: Railway Wheelset

The conventional railway wheelset has a long history and seems to have evolved through a process of trial and error. The conventional wheelset of today (Figure-1.3) consists of two wheels mounted rigidly on a common axle, so that both wheels rotate at common angular velocity and a constant distance between the two wheels is maintained. Flanges are provided on the inside edge of the treads and the flangeway clearance allows, typically, ±7-10 mm of lateral displacement to occur before flange contact [16]. The actual wheelset has a profiled tread, but in this thesis it is considered linear – as shown in Figure-1.3. The coned/profiled tread helps to steer the wheelset on curves by providing natural feedback, but this kind of wheelset exhibits kinematic oscillations at any non-

zero speeds. This type of motion, when the wheelset moves in oscillatory form, is known as 'hunting', a problem which has been known to railway engineers since the very early days, although with very little scientific understanding at that time [13]. It is only in about last fourty years that an adequate theory for hunting has been available for vehicle suspension designers to use. One of the solutions to avoid hunting is by means of yaw stiffness, but choosing a suitable yaw stiffness value is another problem, as low stiffness limits the maximum speed of the vehicle and high stiffness degrades the curving performance of the wheelset. Another important factor that affects wheelset dynamics is the adhesion level during wheel-rail contact.

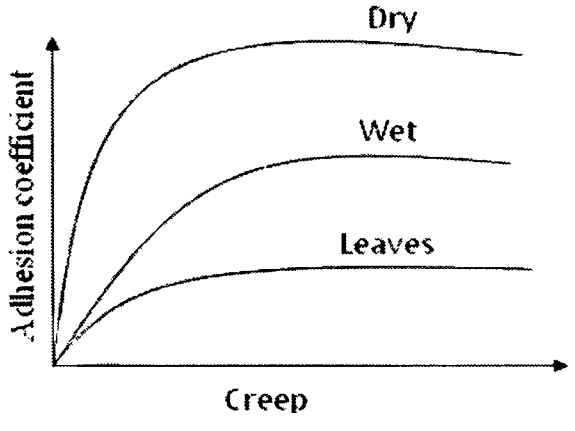

Figure-1.4: Adhesion coefficient vs. creep, representing different contact conditions

The contact between wheel and track is fundamental to railway operation. All the forces supporting and guiding the railway vehicle are transmitted through the contact patch, which is very small (about $1cm^2$) compared to its overall dimensions and shape. One of the most important factors in the transmission of these forces is adhesion level at the wheel-rail contact patch. However, the relationship between these forces and adhesion is very complex and depends upon the concept of creep, a phenomenon that occurs due to the elastic behaviour of the material at the wheel-rail contact patch.

The relationship between adhesion and the creep is nonlinear and can vary substantially and quickly from one section of the track to another, influenced by a wide range of factors and parameters. Figure-1.4 shows the typical variation of the adhesion coefficient with creep. The figure also demonstrates how the creep curve is affected dramatically by the presence of a third body layer, e.g. crushed leaves, water or ice, during wheel-rail contact. This could be formed by a substance used to increase/decrease friction or by naturally occurring material acting to decrease friction. In order to have

proper traction and braking performance, a minimum level of adhesion (typically 0.25 for traction and up to 0.1 for braking) is required. In poor contact conditions, the maximum adhesion available can be far below what is needed for the normal provision of traction or braking.

1.4 Thesis structure

This thesis consists of seven chapters. In this chapter the problem of low adhesion in railway vehicles is described briefly. The basic operation of the solid axle railway wheelset and the effect of contact conditions on the dynamics of the wheelset are also described briefly.

In Chapter 2, the literature review gives a comprehensive introduction to the importance of adhesion in line with the traction and braking performance of the vehicle. The causes of low adhesion and its consequences on the performance of the vehicle are presented in detail. Later, the measures taken by railway operators around the world to improve adhesion are discussed in detail. Conventional wheel slip/slide protection techniques are also covered. Finally, the use of model-based estimation for railway condition monitoring is discussed. Based on the literature review, a brief conclusion is drawn to support the importance and approach of this research.

In Chapter 3, wheelset dynamics are discussed and a comprehensive mathematical model of a single solid axle wheelset is developed. In order to provide a better insight of complex wheel-rail mechanics the dynamics of the wheelset are analysed using various methods (Eigen value analysis, root locus, etc.) at different speeds and in different contact conditions.

In Chapter 4, simplifications in the wheelset model are introduced in order to simplify the design of the estimators. The design detail of the Kalman filter is presented and preliminary estimation results are presented to show the working of Kalman filters in different contact conditions.

In Chapter 5, multiple model-based contact condition estimation scheme is presented. Two designs with the same basic principle are proposed. The design detail of each scheme and the simulation results with detailed discussions are presented.

In Chapter 6, basic idea of the fuzzy logic reasoning is presented. Then a brief introduction to the fuzzy inference systems is presented. Design of the fuzzy logic-based decision making systems for Design-I and Design-II are discussed in detail (including choice of type fuzzy system, type of membership functions and choice of defuzzification method). In the end, simulation results are presented for Design-I and Design-II to show the potential of this research.

In Chapter 7, primary aim of this thesis and progress made towards this goal is summarised. In the end some suggestions for the future research directions are presented.

2. Literature Review

The railway wheelset is a very complex mechanical system, its dynamics are influenced by many factors and uncertain variations in the contact condition make it even more complex. This chapter provides a literature review of the modelling and dynamics studies that have been carried out previously by other researchers. More relevantly, adhesion, factors affecting adhesion, solutions and proposed solutions for improvements based on previous research findings are detailed.

2.1 Railway wheelset modelling and dynamics

Railway wheelset dynamics are governed by the forces generated at the wheel-rail contact patch. These forces are nonlinear in nature and can be calculated in a number of ways, depending upon the mode of the wheelset operation. A common approach for the wheel-rail contact model is to use a linearised model based on Kalker coefficients [9] because during normal running conditions creep is small and the creep forces vary linearly with creep. Therefore, in many studies of railway vehicle modelling and control, the linear model of the wheelset is considered [6, 8-9, 11, 17-23]. For example, the linear dynamic model is used to study the dynamic stability of the wheelset on straight and curved tracks, in order to apply active control [18]. In condition monitoring applications a linear wheelset model is used also to estimate the creep forces generated at on the wheel-rail contact patch [6]. However, when creep is large and the traction and braking modes of railway vehicles are considered, the linear model is deemed an inappropriate choice and nonlinear equations are used to describe the relation between creep force and creepage. The nonlinear relation of creep forces with creepage is due to the presence of nonlinearities such as the nonlinear wheel-rail profile and the nonlinear friction-creep characteristics of the wheel-rail contact geometry [24]. Various factors such as vehicle speed, adhesion level, track geometry and suspension parameters influence creep forces and in turn wheelset dynamics, but adhesion level is a very significant factor here because adhesion is highly unpredictable and can vary to a great extent from site to site. When adhesion is low and the vehicle is accelerated with a tractive effort, wheel micro-slip occurs. Eventually, maximum adhesion is reached, in which case the vehicle fails to exert further increases in tangential force. Since the tractive effort in the wheel shaft is

still increased, wheel macro-slip takes place and increases [25]. Wheel macro-slip can be avoided by means of an appropriate braking and traction control system.

2.2 Adhesion and adhesion management

A train is driven as a result of traction on the contact patches between steel wheels and steel rails. The advantage of using steel wheels on steel rails is low rolling resistance. This advantage, however, also poses a disadvantage: the wheel can only transmit relatively limited braking and traction forces to the rail. Therefore, the maximum values of traction are limited by the adhesion coefficient, known as the ratio of tangential force to the normal load [26]. Adhesion is one of the most significant factors influencing the dynamic response of the wheelset. The dynamic behaviour of a wheelset running on the railway track is governed by contact forces in lateral and longitudinal directions, which in turn are related closely to different contact conditions. In the last few decades, the railway network has been increasingly exploited, resulting in greater demand for faster services; consequently, the traction and braking capabilities of rail vehicles have been increased. However, the friction conditions between wheel and rail have not been improved, so the low adhesion problem remains a key issue in many railway networks around the world [25].

A lack of knowledge about the issue is an important reason why slippery tracks are still a problem, which makes it difficult to take effective and efficient measures [27]. Poor adhesion can be caused by a large number of different factors, and there is often enormous variation in local adhesion conditions along a particular section of a route. The main causes of decreasing wheel-rail adhesion are forms of contamination such as water, rust, oil and leaves [25-26, 28-35]. Although low adhesion can occur virtually anywhere on the network, there are some locations that are more vulnerable than others. Common example of these sites can be 'leaf fall sites', coastal lines where sea spray settles on railway lines and industrial areas where industrial pollution such as coal dust from nearby factories can contaminate the rails. Previous studies have shown that particles of solid debris are always present on the railhead, even where the rail looks clean. These particles adhere quite strongly to the rail, and evidence shows that as they become trapped beneath the wheels, they transmit a proportion of traction or braking forces. The most significant property of the particles appears to be the size of the surface area over which oil can spread [36]. Evidence suggests that water reduces adhesion through two

causes. On debris-free rails it acts as an additional boundary lubricant, while with debris present it forms a low shear strength mixture which, in minimally wet conditions, remains on the wear band where wheels contact the rail. In steady rain the debris mixture is squeezed aside and adhesion is possibly improved [30]. In dry weather, debris particles have apparently little influence on the overall adhesion coefficient. Oils on rails are present in minute quantities and are found to be complex mixtures containing an unusually high proportion of chemically active compounds. Laboratory experiments have studied how such oils and related compounds affect friction when present in surface concentrations similar to those found on the track [31]. Ever since the early days of railways, autumn leaves have been a source of disruption to train services in those areas where trees grow close to the trackside [37]. In the UK, train operations can be affected significantly during autumn leaf fall due to the resulting reduced adhesion, as the leaves are crushed to form a hard, slippery layer on the rail, which is extremely difficult to remove [8, 34, 38-39]. A typical variation of the adhesion coefficient with the relative wheel slip for dry and wet contacts is given in Figure-1.4.

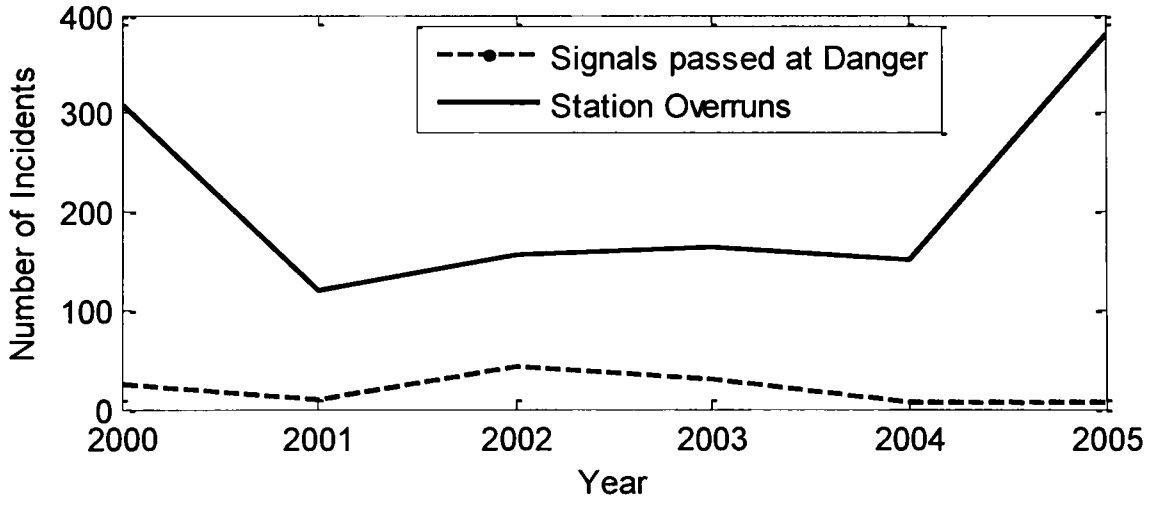

Figure-2.1: RAIB Statistics on adhesion-related incidents

Low adhesion has an entirely negative impact on the safety and performance of railway networks. Poor adhesion in braking is a particular safety issue, as it leads to extended and unpredictable stopping distances, whereas poor adhesion in traction is primarily an operational issue because it leads to reduced performance [29, 33]. Insufficient adhesion can result in severe wheel slipping or sliding, the former causing a rapid increase in the speed of the wheels, which leads to heavy wear to the wheel and rail profile and reduces the lives of mechanical parts, thus increasing overall maintenance costs. Furthermore, torsional vibrations in the axle are produced, which in turn are

transmitted to the passenger part of the vehicle create discomfort in the ride. Extremely low friction values between the wheel and the rail also lead to severe delays and sometimes even to accidents. When viewed from a historical perspective, the risk from adhesion-related incidents can be characterised as high in frequency but low in consequence. There have been very few accidents arising from low adhesion, but the most significant occurred in November 1985, when two trains collided at Copyhold Junction in Sussex, resulting in 40 people being injured, 11 of them seriously [3]. In 1994, in the UK, nearly 600 adhesion-related incidents were reported including 91 signals passed at danger, seven buffer stop collisions, one collision with another vehicle and 503 stations overrun wholly or partially as the result of low adhesion conditions. Figure-2.1 shows the adhesion-related incidents from autumn 2000 to autumn 2005 reported by the Rail Accident Investigation Branch (RAIB). Railway industries around the world have suffered a great deal due to the problems caused by low adhesion.

The need for increased wheel-rail adhesion has been recognised for a long time, as it results in better operating performance and system cost savings. Investigations have been conducted going over the past 150 years, but despite their efforts rail engineers still have not found any definitive solution to overcome the problems caused by low adhesion because the adhesion coefficient is very sensitive to environmental conditions and vehicle parameters such as speed, axle-loads, wheel and rail profiles, contamination of contact surfaces and weather [26] and can vary randomly from one site to another in a short period of time. In order to fight low adhesion, in affected countries some practical measures have been applied such as vegetation management, rail cleaning and friction modification [40-42]. However, the usefulness of these methods for friction control has long been doubted. Friction modifiers use various techniques to enhance the adhesion level of the rail surface such as by cleaning the track of contaminants such as tree leaves and snow with a specially designed vehicle [43-44] or by spraying adhesion-enhancing material such as sand on the rail surface [45-51]. The most common solution still used today is to spread sand at the front of the wheel-rail contact to enhance adhesion along the railroad [2]. Of course, the lasting effect of the sand is minimal, as due to air flow underneath the train, only part of the sand actually makes contact [52]. Sand also increases the risk of rail insulation, resulting in a dangerous situation whereby a train cannot be detected by the signalling equipment [1, 4]. Although this problem is minimised by using a mixture of sand and metal particles, often called 'sandite' [2], there

are several other issues involved such as limited quantities of sandite available on board and the slower speed at which it has to be applied [3]. High pressure water jets were used in 1972 to remove leaf films from the rail surface [53-54], but the conclusion was that water alone was not effective at practical train speeds, although the monitoring of wheel flats on treated tracks suggested that some improvement in adhesion was attained [55-56]. During 1974, a number of liquid systems were tested for their ability to increase wheel-rail adhesion when applied to the railhead by trackside applicators [57-58]. Network Rail, in the UK, applied sandite and water jets to eliminate low adhesion during the leaf fall season in 2005 [3]. There is an important distinction between the effect of water jetting and sandite, as the purpose of water jetting is to clean the railhead, whereas the purpose of applying sandite is to enhance adhesion at the wheel-rail interface. As such, in severe low adhesion conditions, sandite would be required in addition to water jetting [3]. Network Rail and its predecessor, performing the role of infrastructure manager for the national network, experimented with novel methods including surface scrubbing and laser cleaning. However, these methods proved to be impractical (lasers only work at very low speed and brushes wear out very quickly). Another problem in using a modifier is that it does not have exact information about the actual adhesion coefficient that sometimes results in excessive sanding and causes accelerated wheel wear and material waste damage to the track structure because of ballast fouling, drains and switch points, disruption to train detection systems and the premature rotting of ties. Certain commercial adhesion enhancers currently promoted involve rubbing a solid stick on the wheel, which leaves a layer of material on the wheel that comes in contact with the rail, therefore acts as a third layer and modifies friction between the two surfaces [44]. Although this approach improves friction in certain conditions, the extra layer of material left on the rails can have some negative effects on the non-tractive wheels.

Railhead treatment has helped rail operators to improve train performance to some extent, but it is not considered a sufficient step to cope with problems posed by low adhesion because the choice of an effective measure for certain conditions is difficult. In recent advancements, automatic devices that control wheel slip during traction and braking are used. They are generally known as wheel slip/slide protection systems (WSP), the objective of which, in general, is to reduce stopping distance under low adhesion conditions and to reduce the risk of wheel damage [1]. An ideal WSP system would find the maximum adhesion for the given contact conditions and try to keep the

braking and traction efforts as close to that maximum as possible [25]. WSP systems usually consist of two elements, one for detecting wheel slip/slide and another that has to be able to adjust traction and braking force [59]. The most common WSPs are developed by measuring the difference between the train speed and the wheel rotational speed [60-61], and they rely on relative speeds measured by sensors that gauge the angular speed of the wheel and the absolute speed of the vehicle.

There are several practical issues involved in detecting these parameters. According to [62], the absolute speed of a train is normally obtained from a trailer bogie (or axle), but the provision of a reliable train speed is a problem when all the axles are affected, e.g. in braking. The requirement of robust/reliable sensors for what can be harsh working environments limits the accuracy of measurements. In a different research study, estimated vehicle speeds were used instead to improve performance in noisy mechanical environments [63], but conventional re-adhesion control techniques are not particularly sensitive to condition changes and only large variations tend to be detectable. Effectively, WSPs are reactive systems, i.e. only 'activated' to stop wheel slip/slide when detected by sensors. In some rail networks, LAWS (low adhesion warning system) or AMS (adhesion management systems) are used to provide estimates of track conditions based on a large pool of trackside measurements such as site topography, track geometry, microclimates and contamination. It is widely recognised that such localised adhesion conditions can be very beneficial to train drivers and to network operators, as they can take preventative measures and plan train journeys and schedules accordingly in order to maximise network capacity and efficiency within the constraints of the track conditions. Such systems are inevitably very complex and expensive to implement, and it is potentially difficult to deliver reliable estimates because of the large number of sensors that need to be installed across a network and the amount of data that must be collected and processed.

Tribometer trains were used between 1970 and 1995 to investigate the problem of low adhesion between the wheel and rail. A Tribometer train is usually a heavily instrumented train, equipped with various sensors, which is used to carry out the measurements necessary to determine adhesion levels on rail surfaces. The European Rail Research Institute (ERRI) has been doing thorough research into adhesion behaviour. The first test was conducted in 1960 using a specially designed bogie to

investigate the influence of basic parameters on adhesion [1]. It was concluded that the value of adhesion decreases as the axle load increases and that the influence of the curve is not significant. The National Traction Power Laboratory (NTPL), in China, undertook a detailed experimental investigation of the adhesion problem using a specially designed, full-scale roller rig with actual wheel and rail profiles [64]. The roller could not only rotate to simulate different train running speeds, but it could also vibrate independently in the vertical and lateral directions to simulate track irregularities. The adhesion coefficient was measured under water-contaminated, machine oil-contaminated, dry and clean surface conditions. British Rail (BR) Tribometer trains were also used to measure the longitudinal creep coefficients [135], which measures the relative longitudinal creepage between a braked and freely rotating wheelset. The actual brake force is determined via instrumented brake and suspension elements. A series of runs at various brake force levels gives a series of points on the creep curve.

Although various different experiments in the laboratory and on real tracks have attempted to prove the reliability of the measured value, there are several issues that need to be addressed such as roller rigs and Tribometer trains differing from actual trains in terms of axle load, speed and other important parameters that can affect the adhesion coefficient.

Complete and accurate information on available adhesion would be very helpful to prevent slippage before it occurs. Several attempts have been made, but the data measurements are not considered practicable from an economic perspective. Methods using estimation techniques have also used available measurements. In an indirect method used to identify friction forces between the wheel and rail, friction forces were recognised by using values attributed to the traction motor armature current. The proposed model was validated using computer simulations as well as a scaled model, but the systems were required to become active only when wheel grip was lost, as only in this way could the maximum allowable traction forces be utilised [65]. Due to the involvement of nonlinearities in wheel-rail mechanics, the neural network-based identification of the friction coefficient is proposed [66]. Neural networks have been used to estimate parameters and the influence of varying friction coefficients. Different neural network-based algorithms have provided adequate results; however, the influence of variable running velocity and track disturbance, which have a great influence on the

creep coefficient, have not been considered. In [67], a method for the identification of friction force is proposed. The identification is realised by means of observations carried out in the mathematical model of the physical system and of the driving motor. This method uses the derivative of the adhesive effort with respect to the slip velocity to determine the saturation point, which is difficult because the derivation of the slip velocity is highly sensitive to measurement noise caused by the limited resolution of practical speed sensors. In a similar work, the derivative of friction force is estimated to eliminate the problem of sensor resolution [68]. The derivative of friction force is estimated by means of a high-pass digital filter.

Another approach to re-adhesion control is based on disturbance observation [69], which estimates disturbance torque by using rotor speed and torque current information. However, the performances of anti-slip schemes based on a disturbance observer are affected to a large extent by noises in the system, which can be very substantial in the wheel-rail contact environment.

In recent research an indirect approach was used for wheel slip detection and explored changes in wheelset dynamics and in wheel-rail contact conditions [62, 70-71]. The study showed that torsional vibrations of specific frequencies (associated with material damping) in the axle are produced when creep forces are saturated. This finding provided an opportunity to develop a novel re-adhesion control technique that could detect axle vibrations of specific frequencies – and hence wheel slip. Two detection methods proposed are running FFT to detect the spectrum variation of a particular frequency, while the other uses bandpass and low-pass filters to obtain magnitude information on the frequency of interest.

2.3 Condition monitoring

The area of fault detection and identification (FDI) is well known and well developed, especially in the discipline of control engineering [72]. FDI is a generic term that applies to all systems, and it is aimed at detecting and identifying faults as they occur. Condition monitoring can be considered an offshoot of FDI and is applicable mainly to systems that deteriorate over time [73]. Condition monitoring is the process of monitoring the real-time condition of a system, and its use allows maintenance to be scheduled, or other actions to be taken, in order to avoid the consequences of failure, before the failure

occurs. Monitoring can either be used to improve maintenance procedures for railway vehicles or to determine the current running conditions of in-service vehicles, without the use of cost-prohibitive sensors [6]. The generic railway condition monitoring system uses some level of knowledge of the system in the form of a mathematical model, expert system, learnt behaviour, etc. and measured outputs to perform its diagnosis, but unlike other condition monitoring applications the dynamic response of the system is driven by irregularities in the track, which are difficult to measure and therefore cannot be applied to a condition monitoring system [9, 74]. The use of condition monitoring techniques to identify local adhesion conditions along with other condition monitoring parameters has recently been adopted by several researchers. A number of ideas have been proposed to detect the running conditions of the wheel-rail interface [6, 9-11, 75-77]. A model-based scheme for condition monitoring at the wheel-rail interface is proposed in [9] whereby the adhesion level is identified by measuring the dynamic response of the vehicle to lateral track irregularities under normal running. This work is carried out further in [6, 78-81], with the primary aim to estimate creep forces generated at the wheel-rail contact. Estimating these forces has many applications such as local adhesion level estimation, the prediction of rolling contact fatigue, the prediction of wheel tread wear, the estimation of track damage caused by specific vehicles and potentially as a cost-effective method of assessing engineering design changes to wheel tread geometry. An inverse modelling approach for the estimation of creep coefficients, using measured car body acceleration, is proposed in [75-77]. There are also a number of other applications in railway vehicle research that used the interacting multiple model (IMM) algorithm for condition monitoring [21, 82-85]. In [83], IMM is used to detect and identify failures in suspension. In addition, multiple Kalman filters are used to describe different modes of suspension failure.

2.4 Model-based estimation

The Kalman filter is a model-based estimation technique applied in many advanced control systems in vehicle dynamics applications such as the driver assistance system, which helps drivers maintain stability, avoid roll-over and customise handling characteristics, anti-lock brake systems (ABS), used to prevent wheel lock-up, and traction control systems, which are also becoming popular because they prevent the drive wheels from losing grip when accelerating [86]. The Kalman filter, due to its robustness

and accuracy in the presence of stochastic noises, provides an opportunity to estimate key vehicle parameters such as vehicle mass, tyre cornering stiffness, under-steer gradient, roll stiffness and the roll damping coefficient. Once vehicle parameters have been estimated precisely, parameterised vehicle dynamics models with properly estimated parameters can be used for a wide variety of applications including highway automation, vehicle stability control and rollover prevention systems [87-90]. The Kalman filter has also been used in a variety of rail vehicle applications such as actively controlled railway vehicle suspension, fault detection of railway vehicle suspension, low adhesion estimation and in re-adhesion control schemes to estimate important parameters [8, 14, 83, 91].

Adhesion between the wheel and rail varies stochastically and depending upon several factors. The Kalman filter has been applied successfully in various condition monitoring applications to detect adhesion variation [8-9], and [38] presents a Kalman filter-based estimation scheme to estimate the adhesion force coefficient. A half vehicle model, consisting of two wheelsets, one bogie and a half vehicle body, is used to simulate behaviour. The dynamics of the wheelset are modelled using linearised creep forces valid only in the low creep region of the creep curve. In [9], model-based condition monitoring at the wheel-rail interface is presented. Two applications of model based condition monitoring are proposed – one for wheel-rail profile estimation and the other for low adhesion detection. A Kalman filter is used to estimate the wheel-rail profile and estimation is carried out on a linearised simulation model. In an indirect adhesion estimation method, the Kalman filter was used to detect slip [62]. Traction motor speed was used to estimate torsional oscillations, and the results showed that the Kalman filter provided a level of estimation sufficient for slip detection and it was robust in a variety of different slip conditions.

The multiple model method is an estimation method using multiple dynamic models. This method can cope with changes in the structure and parameters of a system. Using a bank of Kalman filters was pioneered by Magill [92], who employed a parallel structure of estimators in order to estimate a sampled stochastic process. In recent years, Kalman filter based localisation has become common practice in robotics literature [93-94]. The basic philosophy of the method is to use analytical redundancy in the form of several models. The Kalman filter-based framework provides disparity (typically called a

'residual') between the measured sensor values and the values predicted by the model embedded within the filter [94]. The model selection takes place based on the value of the residual signal. The multiple model-based estimation has also been used in railway vehicle research [21, 83, 85], especially in fault detection application where system parameters are changed over time. For example, in [21] a multiple model approach to detect faults in suspension using on-board measured data is proposed.

2.5 Fuzzy logic

There is a variety of vehicle dynamic applications in which the fuzzy logic is used, especially in automatic steering and intelligent control for vehicle systems in which the vehicle dynamics have various structured uncertainties and nonlinear characteristics. Not only are uncertainties unknown or poorly known, but they also may be subject to change as the vehicle goes about its navigation [95]. In such situations, the lack of information about parameters makes it difficult to design a conventional control scheme, so fuzzy logic is considered better suited for such types of application. Other applications include the use of logic-based control for the purpose of determining and assigning desired wheel slips for each corner of a vehicle [96], a fuzzy logic controller to control the lateral motion of the vehicle [97], yaw moment control based on fuzzy logic to improve vehicle handling and stability [98] and a fuzzy rule-based Kalman filtering technique for an accurate estimation of the true speed of a vehicle [99]. There are various railway vehicle applications where fuzzy logic is used either for estimation or for control [100-103], and [100-101, 103] present techniques based on fuzzy logic to control the steering and traction torque of the wheelset, while [102] presents fuzzy logic-based gain scheduling control for a nonlinear suspension system.

Gaining accurate adhesion information is not only a problem in rail vehicles but also road vehicles, which also require adhesion information for efficient traction performance. Similar types of approaches can be applied to road and rail vehicles in order to estimate adhesion forces. A re-adhesion control scheme for wheeled robots based on fuzzy logic using estimated adhesion force is presented in [104]. Adhesion information is obtained through an ordinary disturbance observer, and fuzzy logic is used to control the driving torque to prevent the slip phenomenon. Furthermore, there are various industrial applications in which fuzzy logic is used as a data/model selector [105-108]. The data selection process is required particularly in multiple model-based

applications in which various models produce different sets of data. Therefore, some sort of decision-making system is required that can compare the actual result with the output produced by various models and identify the most valid model among several. Fuzzy logic is useful in circumstances where it is practically impossible to describe all the nonlinearities and changes in parameters using a multiple model-based system; therefore, fewer models are used to design the system, and the possible behaviours of the system are described using these fewer models.

2.6 Summary

The presence of contaminations on rails such as snow, water, oil, tree leaves etc. presents a serious challenge to traction and braking control systems. There is currently a paucity of knowledge regarding low adhesion and it is based largely on subjective observations, for the most part offered by drivers. Available techniques for railhead treatment are not sufficient to cope with the problems arising from low adhesion, and the absence of an adhesion measurement tool is the major reason why slippery tracks are still a problem. In order to make the current measures more effective, it is necessary to provide real-time information about track conditions as the train travels along the track. This will help traction and braking control systems (WSPs) to maximise the use of available adhesion and thus maintain the stable operation of the railway vehicle.

The dynamic response of the railway wheelset on any creep curve depends on the location of the operating point on the creep curve. As the operating point moves up and down due to the application of traction and braking forces, the dynamic response varies accordingly. Specifically the dynamic response of the wheelset at a particular operating point on any given curve depends upon the slope of the creep curve ($\frac{d\mu}{d\gamma}$) and on the traction ratio ($\frac{\mu}{\gamma}$).

This thesis proposes a novel technique to identify adhesion conditions by using the afore stated fact that the dynamic properties of the wheelset are affected strongly by nonlinearities and changes in the contact condition. The proposed idea involves the use of a number of carefully selected mathematical models (or estimators) to mimic dynamic train behaviours in response to different track conditions. Each of the estimators is tuned to match one particular track condition in order to give the best results at the specific

design point. Increased estimation errors are expected if the contact condition is not at or near to the chosen operating point, while the level of matches/mismatches is reflected in the estimation errors (or residuals) of the models concerned, when compared with the real vehicle (through the measurement output of vehicle-mounted inertial sensors). A fuzzy reasoning procedure is developed to translate and map the estimation residuals from all the models into direct information on track conditions and adhesion levels, which in turn can be used by train drivers and network operators (or traction/braking control systems). All the simulations are carried out in the MATLAB/SIMULINK environment.

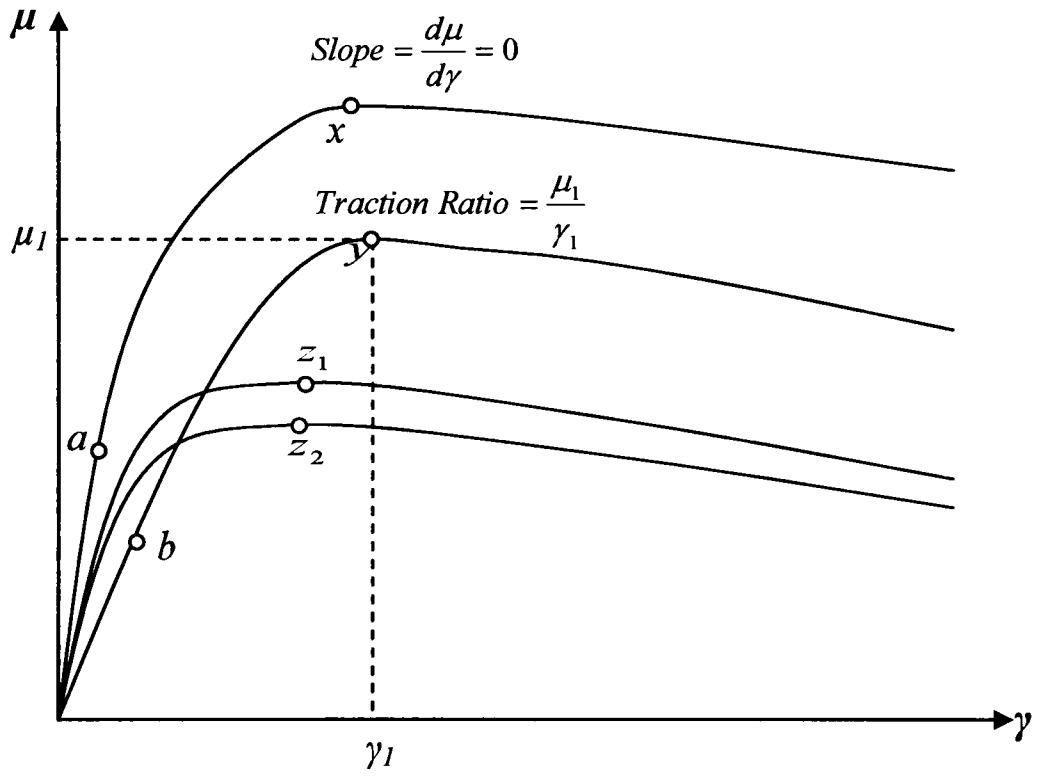

Figure-2.2. Basic concept of contact condition identification

The basic idea of the proposed model can be explained with the help of Figure 2.2. In this Figure, at operating points *a* and *b,* the slopes and the traction ratios are different, so the residual would also be different. In addition the amount of tractive effort would also be different and, by analysing the residual values and the tractive torque, it is possible to identify these two operating points. It is possible too that two operating points have the same traction ratio or same slope. For instance, in this same Figure, the slopes of the operating points *x* and *y* are the same but the traction ratios are different. Therefore the residual values would be different and therefore the contact condition is identifiable. However, in some cases, such as z_1 and z_2, where the slopes and the traction ratios are approximately the same, no significant difference is expected from the residual values. In such cases, tractive torque can provide additional information to differentiate between

two operating points. It is highly unlikely that two operating points can have the same slope, traction ratio and same amount of tractive effort. Therefore it is concluded that the contact condition may be identified by analysing the residuals and the tractive torque.

A similar kind of work is also presented in [10-11], which uses the vehicle mounted inertial sensors to estimate the creep force during normal running condition. Apart from methodology the major difference between this work and the work carried out in [10-11] is that, in this thesis normal running condition as well as traction mode are considered.

3. WHEELSET MODELLING

3.1 Railway vehicles

Railway vehicles employ steel wheels that run on steel rail tracks, which provide support and guidance functions. The interface between the two is established at contact point(s) between the wheels and the rail surface, and both the vehicle configuration and the track greatly influence how vehicles behave [109]. Figure-3.1 shows the configuration of the most modern passenger-carrying railway vehicles. Each car consists of two bogies, each of which has two sets of wheels. The purpose of the bogie is to carry the weight of a vehicle along the track at the required speed and with a high degree of safety. In so doing, and as far as practicable, it isolates the vehicle from dynamic forces and vibrations resulting from motion. The car body is connected to bogies via suspensions (secondary suspension), the purpose of which is to provide good ride quality by isolating the car body from vibrations induced by track irregularities. The wheelsets are connected to the bogie via primary suspensions, whose elements are much stiffer than in the secondary suspension system and are designed to satisfy the vehicle's stability and guidance requirements. The left and right side wheels in each wheelset are connected rigidly via a common axle (known as the solid-axle wheelset) such that the two wheels have to rotate at the same speed.

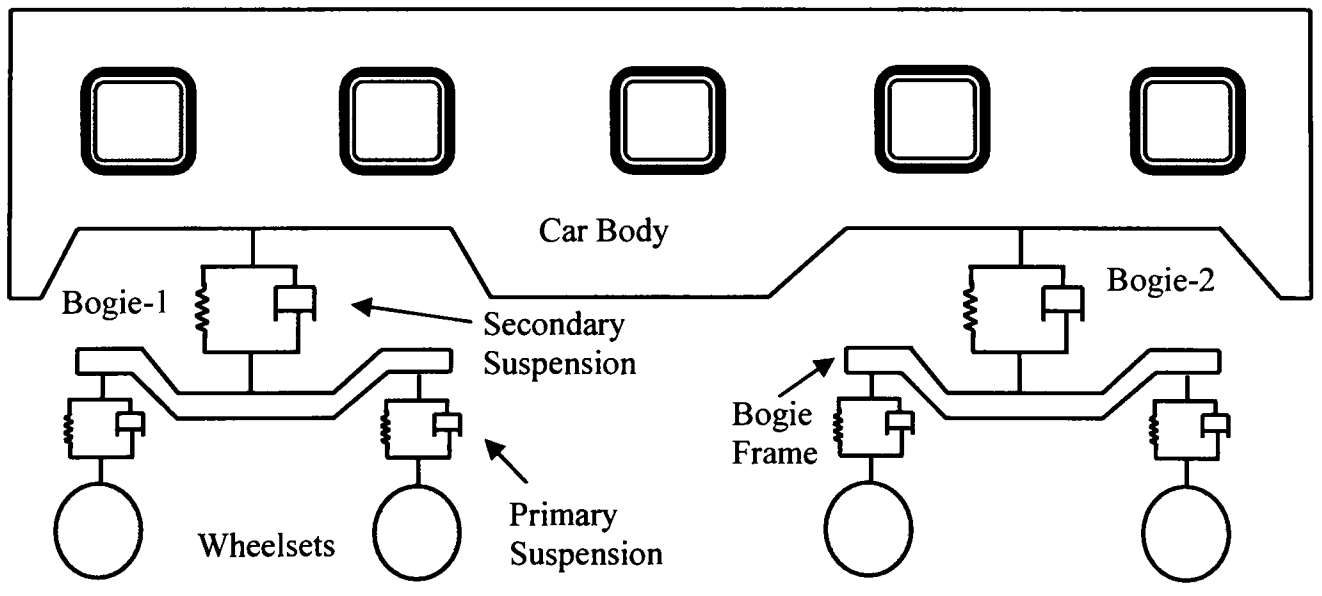

Figure-3.1: Railway vehicle configuration

A wheelset is a vital element of railway transport and is in direct contact with the track, so its dynamics are influenced directly by changing contact conditions. This study is fundamentally focussed on a single solid axle wheelset which has a direct interaction

with the track. Therefore, a single solid axle wheelset is considered in this study. The dynamics of the bogie do have some effect on the wheelset dynamics but the end result is not too different from single wheelset and also in various other stability and guidance studies the primary focus of the study has been on a single wheelset which can be easily extended to two axles and a full vehicle with some modifications [9, 14, 17-20, 23, 31, 70-71, 110-111]. The simplified plan view of the wheelsets in a bogie frame is shown in Figure-3.2. The single solid axle wheelset consists of two wheels connected rigidly to an axle (hence the name 'solid axle wheelset'). The wheels are considered as two rigid cones, although in practice they are of a profiled structure. The flanges are a necessary precaution and they should never touch the rails except on sharp curves to meet an accidental, lateral force [112].The coned tread helps the wheelset to maintain a pure rolling motion in a curve, if it moves outward and adopts a radial position [15].

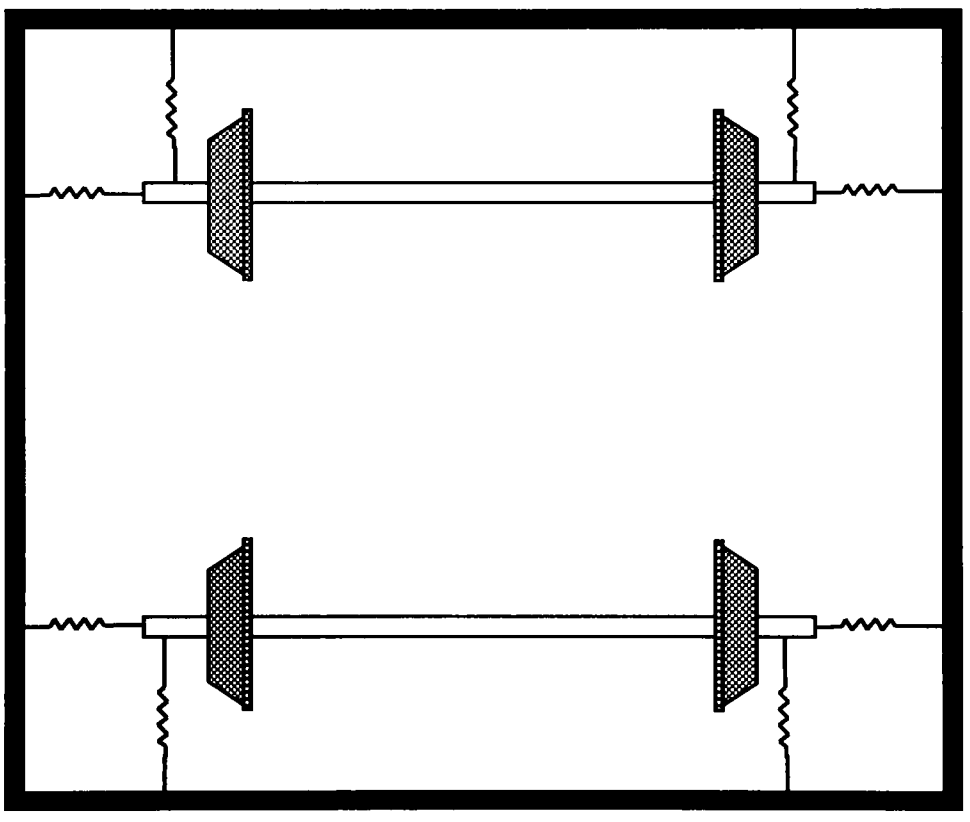

Figure-3.2: Railway wheelsets in a bogie frame

When the wheelset is moved laterally, the rolling radius of the one side increases, which means that one wheel has to cover more distance than the other wheel, but as both wheels are fixed rigidly and they have to run at the same speed, the wheelset is forced to yaw about the vertical axis (Figure-3.3), and this yaw angle causes the wheelset to align back into the centre position if pure rolling is maintained. However, an unconstrained solid axle wheelset is unstable at non-zero speeds, crosses the central line and overshoots to the other side, exhibiting sustained oscillation in the lateral plane, a phenomenon known as 'wheelset hunting' [111]. In 1883, Klingel presented the first mathematical

analysis of kinematic oscillation [113] and derived the relationship between the frequency f and the wheelset conicity λ_w, wheel radius r_o and the lateral distance between the contact points between wheels and rails $2L_g$ as [15].

$$f = \frac{v_s}{2\pi}\sqrt{\frac{\lambda_w}{L_g r_o}} \tag{3.1}$$

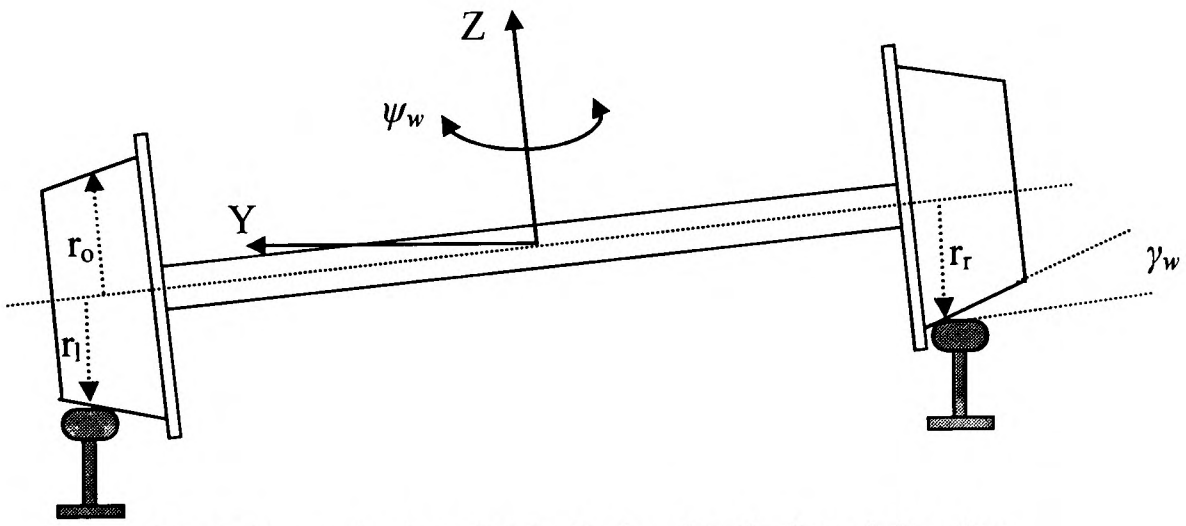

Figure-3.3: Railway wheelset slightly displaced in the lateral direction

The wheelset is connected to a vehicle body or bogie via suspension elements set in lateral and longitudinal directions. The longitudinal connections between the wheelset and the bogie are assumed to be solid, as the stiffness is normally very high and associated dynamics are not of significant relevance to this study [114]. The lateral springs are necessary to transmit the curving forces, so they are therefore not considered for further study, as in this thesis only a straight track is taken into consideration.

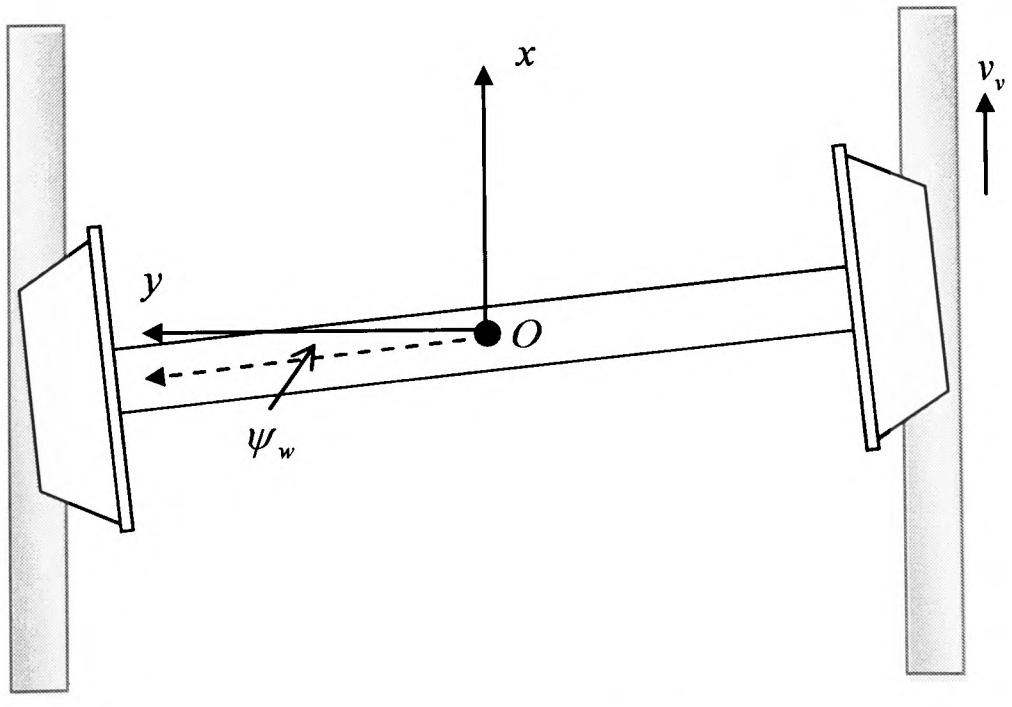

Figure-3.4: Wheelset degrees of freedom

Figure-3.4 shows a wheelset running on a straight track. The coordinate system *oxyz* moves synchronously with the wheelset at the speed of the vehicle, while origin O is constrained along the centre line of the undistorted track. The x-axis points along the rails in the rolling direction are also known as the 'longitudinal direction', and the y-axis (lateral direction) is a 90° lag to complete a right-hand coordinated system. The z-axis points vertically upwards. The yaw angle (ψ_w) is the angular displacement around the vertical axis.

3.2 Creep and creep forces

Creep is said to exist when a wheel deviates from pure rolling, that is the distance covered by the wheel in one revolution is not equal to the circumference of the wheel. Pure rolling rarely takes place, and wheels and rails are not rigid [115]. The normal load between the wheel and rail causes local elastic deformation, and an area of contact, the contact patch, is formed. In the contact patch the material is compressed at entry before a section where adhesion takes place then a section where the material slips out of compression and finally exits in tension [19]. Creep is defined as the relative speed of the wheels to the rail and is characterised as lateral and longitudinal creep in accordance with the direction of motion. If a longitudinal force is applied to the wheel, a deviation from the pure rolling motion occurs. The deviation in relative velocity, divided by the forward speed of the wheel, is referred to as longitudinal creep (γ_x) [116].

$$\gamma_x = \frac{v_w - v_v}{v_v} \tag{3.1}$$

where v_v is the vehicle's forward speed and v_w the equivalent linear speed of the wheel, which is given by

$$v_w = \omega_w . r \tag{3.2}$$

where r is the contact radius of the wheel and ω_w the wheel rotational speed. The linear speeds of the left and right wheels are not equal if the wheelset is displaced laterally from its centre position (because of the different contact radii). In that case, the wheel's linear speeds are formulated in equations (3.3) and (3.4) for the left and right wheels respectively, considering the wheelset is laterally displaced to the right.

$$v_{wL} = \omega_{wL} . [r_o + \lambda_w (y_w - y_t)] \tag{3.3}$$

$$v_{wR} = \omega_{wR}.[r_o - \lambda_w(y_w - y_t)] \tag{3.4}$$

where ω_{wL} is the left wheel's angular speed, ω_{wR} the right wheel angular speed, r_o the radius of each wheel when the wheelset is running in a centre position, λ_w the wheelset conicity and y_t the disturbance applied by the track in a lateral direction. Usually there are four inputs to the vehicle from the track: vertical profile, cross level, lateral alignment and gauge [13], but only lateral disturbance is considered here because of its direct effect on yaw and lateral dynamics. Irregularities in the gauge are very small as compare to y_t therefore, are not considered in this study. Yaw movement will also contribute to the longitudinal creepage in opposite directions for the two wheels [70]. Creepage for the left (γ_{xL}) and right (γ_{xR}) wheels can then be written as

$$\gamma_{xL} = \frac{r_o\omega_{wL} - v_v}{v_v} + [\frac{L_g\dot{\psi}_w}{v_v} + \frac{\omega_{wL}\lambda_w(y_w - y_t)}{v_v}] \tag{3.5}$$

$$\gamma_{xR} = \frac{r_o\omega_{wR} - v_v}{v_v} - [\frac{L_g\dot{\psi}_w}{v_v} + \frac{\omega_{wR}\lambda_w(y_w - y_t)}{v_v}] \tag{3.6}$$

where L_g is the track's half gauge, ψ_w the yaw angle of the wheelset and y_w the lateral motion of the wheelset. When a wheelset is displaced laterally, yaw torque steers the wheelset against the restraining effect of the suspension. If a wheelset is forced to run at an angle of attack to the rails, lateral creepage (γ_y) is produced [13], which is defined as the relative lateral velocity divided by the forward speed [115].

$$\gamma_y = \gamma_{yR} = \gamma_{yL} = \frac{\dot{y}_w}{v_v} - \psi_w \tag{3.7}$$

Spin creepage has an important value when flanging [19], but in this study flange contact is not taken into account. The total creepage for each wheel is given by

$$\gamma_L = \sqrt{\gamma_{xL}^2 + \gamma_y^2} \tag{3.8}$$

$$\gamma_R = \sqrt{\gamma_{xR}^2 + \gamma_y^2} \tag{3.9}$$

The delivery of traction and braking is achieved through longitudinal creep. Lateral creep is usually minimal compared to longitudinal creep, unless a vehicle is operating on the curves, but it still plays a significant role in the stable operations of the wheelset.

Figure-3.5 shows a typical nonlinear variation of the adhesion coefficient with creep. The creep curve can be divided into three regions to describe the stable and unstable behaviour of the wheelset. The initial part of the curve is linear and a low creep section, in which almost the entire contact area is occupied by the non-slip region; the wheelset operates in this region when the vehicle is operating in steady conditions. With the increase in tractive effort, the slip region at the wheel-rail contact patch increases and the non-slip region decreases. When the tractive force reaches its saturation value, the non-slip regions disappear and the entire contact area is in a state of pure sliding.

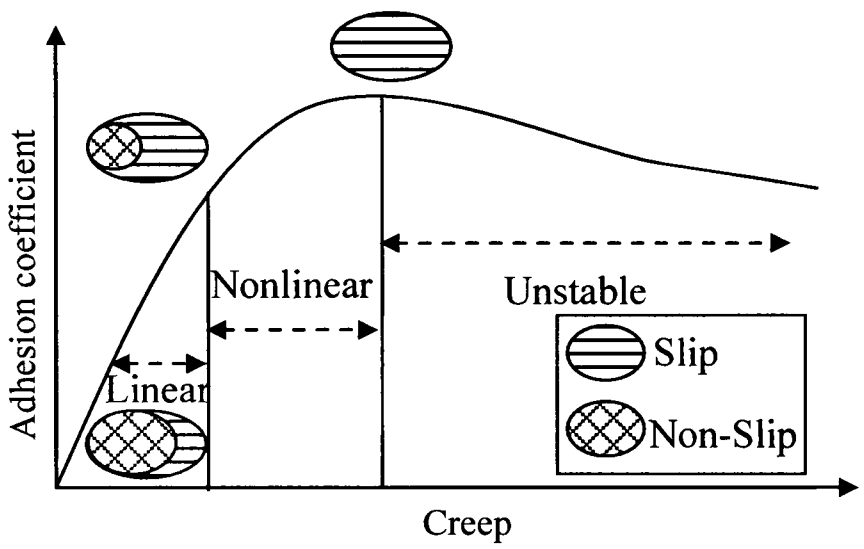

Figure-3.5: Creep vs. adhesion coefficient

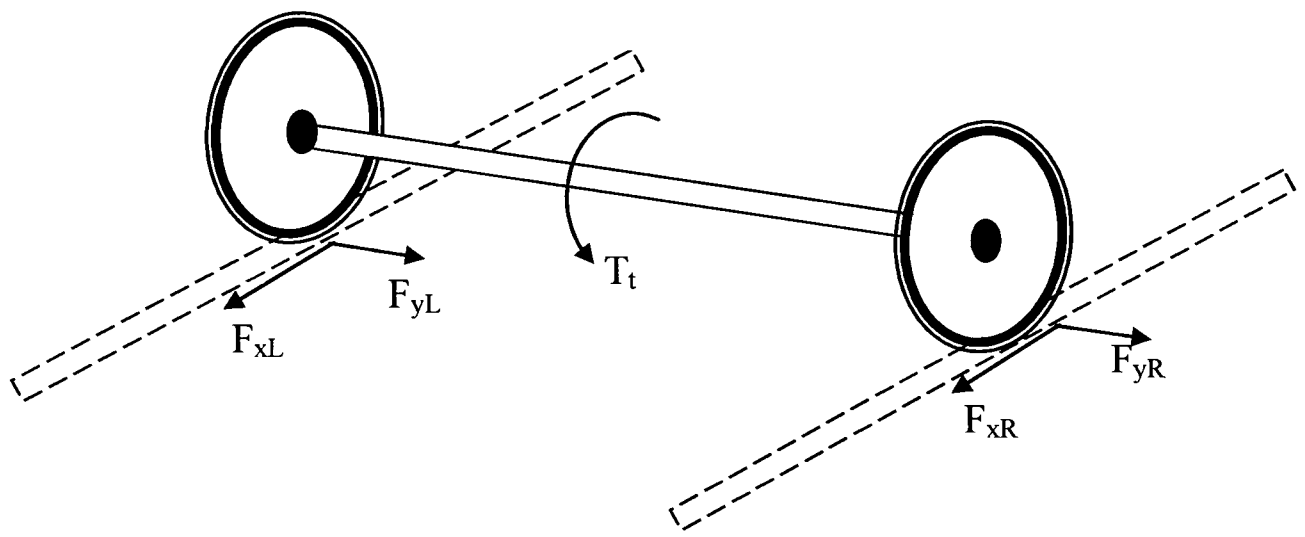

Figure-3.6: Creep forces at the contact patch

3.2.1. Creep forces

Creep force occurs as a result of the difference between the relative speeds of the wheel and of the rail [17]. When a wheel deviates from pure rolling, during acceleration, braking or curving or when subject to lateral forces through the suspensions, forces tangential to the normal force are transmitted to the rail at the contact patch. These are

called creep forces and occur due to micro-slippage or creepage in the area of contact [19]. The relationship between creep and creep forces has been studied thoroughly by Kalker [117] and his equations are widely used in simulations. The following figure illustrates creep forces generated at the contact patch.

The forces between the wheel and rail due to creepage are of fundamental importance to the dynamic behaviour of railway vehicles because they are widely recognised to present nonlinear characteristics as a function of creep, as shown in Figure-3.7. In normal running conditions where creep is small (area before μ_L in Figure-3.7), the contact forces provide a damping effort to the dynamic modes of a wheelset and are very useful in stabilising those modes, which would otherwise be almost critically damped. In this case there is adhesion over the complete contact area (according to the Hertz theory) and there is a linear relationship between creep forces and creepage [15].This is in the form

$$F_{xj} = f_{11}\gamma_{xj} \qquad j = L,\ R \tag{3.10}$$

$$F_{y} = f_{22}\gamma_{y} \tag{3.11}$$

where f_{11} and f_{22} are creep force coefficients and represent the slope of the creep curve at the operating point of the wheelset. As creep increases, contact forces can operate in the nonlinear region (between μ_L and $\mu_{\max}$), where the rate of change of the creep forces and their associated damping effect is much lower. For large creep sections of the creep curve, the representation of creep forces in longitudinal and lateral directions for the left and right wheels is given in the following equations:

$$F_{iR} = F_R.\frac{\gamma_{iR}}{\gamma_R}, \qquad i = x, y \tag{3.12}$$

$$F_{iL} = F_L.\frac{\gamma_{iL}}{\gamma_L}, \qquad i = x, y \tag{3.13}$$

where F_{xR}, F_{xL}, F_{yR} and F_{yL} are creep forces in longitudinal and lateral directions for the right and left wheels respectively, and F_R and F_L are total creep forces for the left and right wheels at the wheel-rail contact patch and are a function of the adhesion coefficient (μ) and normal force (N).

$$F_j = \mu_j N_j, \qquad j = L, R \tag{3.14}$$

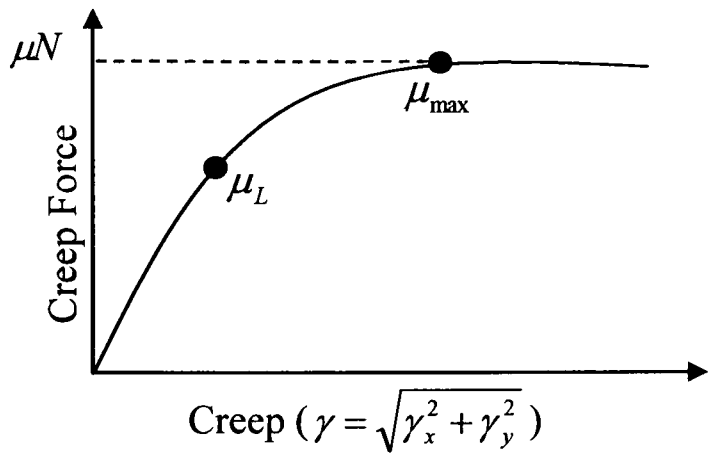

Figure-3.7: Creep vs. creep force

When creep is beyond the point of the maximum adhesion available (μ_{max} in Figure-3.7) at the wheel-rail interface and enters the slip and unstable region, contact forces will then become a destabilising element, which not only causes the well-known problem of wheel slip (in traction) and slide (in braking), but also can lead to other undesirable mechanical oscillations in the wheelset.

3.3 Wheelset dynamics

It is essential in the study of wheelset dynamics to develop and use a comprehensive model that includes all relevant motions related to the contact forces, because strong interactions between different motions of the wheelset through creep forces during wheel-rail contact act in both the longitudinal and lateral directions. In this section a comprehensive wheelset model is introduced, which considers all the relevant motions. A single solid axle-powered wheelset is considered for basic study, with a traction motor mounted on the right side of the wheelset. Therefore, traction torque (T_t) is applied directly to the right wheel. It is assumed that the normal load on either side of the wheelset is the same. Railway wheelset has several degrees of freedom. The lateral displacement and the yaw angle are two small movements relative to the track. The displacement along Ox and the rotational motion around Oy are determined by longitudinal speed v_v. The rolling radius r of the wheel, the wheelset centre of gravity height z and the roll angle around Ox are linked to rails when there is contact on both rails [109]. The longitudinal motion of the wheelset is a result of left and right wheel creep forces in the longitudinal directions.

$$M_v \ddot{x} = F_{xR} + F_{xL} \tag{3.15}$$

where M_v is the mass of the vehicle (referred to the wheelset). The wheelset yaw angle is considered positive in the anticlockwise direction and is the result of the difference in longitudinal creep force between the two wheels.

$$I_w\ddot{\psi}_w = F_{xR}L_g - F_{xL}L_g - k_w\psi_w \tag{3.16}$$

where I_w is the yaw moment of inertia and k_w is the stiffness of the yaw spring that connects the wheelset with the bogie. When the wheelset is moved in the lateral direction, one of the wheels has greater contact radius than the other, which introduces a small roll motion, the roll motion formulated as [19].

$$\phi_w = \frac{r_R - r_L}{2L_g} = \frac{\gamma_w y_w}{L_g} \tag{3.17}$$

Lateral dynamics are determined by the total creep force of the two wheels in the lateral direction.

$$m_w\ddot{y}_w = -F_{yR} - F_{yL} + F_c + F_g \tag{3.18}$$

where F_c is the centrifugal force which is taken into consideration when the wheelset runs on a curved track (given in equation (3.19)) and F_g is a gravitational stiffness force depending on the lateral displacement and roll angle of the wheelset [19] (given by equation (3.20)).

$$F_c = \frac{m_w v_v^{\,2}}{R_c} \tag{3.19}$$

$$F_g = -m_w g\phi_w = -\frac{m_w g\gamma_w y_w}{L_g} \tag{3.20}$$

R_c in equation (3. 19) is the radius of the curve. The wheelset is driven by the traction motor mounted on one side (the right side in this case) of the wheelset. The other wheel is driven by torsional torque transmitted through the axle.

$$I_R\dot{\omega}_{wR} = T_t - T_s - T_R \tag{3.21}$$

$$I_L\dot{\omega}_{wL} = T_s - T_L \tag{3.22}$$

where T_s is torsional torque and T_R and T_L are the tractive torques of the right and left wheels respectively. The torsional torque along the shaft is determined by the difference in rotation between the two wheels [70]:

$$T_s = k_s\int(\omega_{wR} - \omega_{wL})dt + C_s(\omega_{wR} - \omega_{wL}) \tag{3.23}$$

where C_s is the material damping of the axle, which is usually very small and therefore can be neglected. It is assumed that there is no bounce motion (off the rail), in which case roll motion is constrained by the track and does not have a significant effect on creepage. Consequently, it is not considered for further study. After substituting the creep force equations, the equations for the motions of the wheelset are given below.

$$M_v\ddot{x} = \frac{\mu_R N_R}{\sqrt{\gamma_{xR}^2+\gamma_{yL}^2}}\left[\frac{r_o\omega_{wR}-v_v}{v_v}-[\frac{L_g\dot{\psi}_w}{v_v}+\frac{\omega_{wR}\lambda_w(y_w-y_t)}{v_v}]\right] + \frac{\mu_L N_L}{\sqrt{\gamma_{xL}^2+\gamma_{yL}^2}}\left[\frac{r_o\omega_{wL}-v_v}{v_v}+[\frac{L_g\dot{\psi}_w}{v_v}+\frac{\omega_{wL}\lambda_w(y_w-y_t)}{v_v}]\right] \tag{3.24}$$

$$I_w\ddot{\psi}_w = \frac{\mu_R N_R}{\sqrt{\gamma_{xR}^2+\gamma_{yL}^2}}\left[\frac{r_o\omega_{wR}-v_v}{v_v}-[\frac{L_g\dot{\psi}_w}{v_v}+\frac{\omega_{wR}\lambda_w(y_w-y_t)}{v_v}]\right]L_g - \frac{\mu_L N_L}{\sqrt{\gamma_{xL}^2+\gamma_{yL}^2}}\left[\frac{r_o\omega_{wL}-v_v}{v_v}+[\frac{L_g\dot{\psi}_w}{v_v}+\frac{\omega_{wL}\lambda_w(y_w-y_t)}{v_v}]\right]L_g - k_w\psi_w \tag{3.25}$$

$$m_w\ddot{y}_w = -\frac{\mu_L N_L}{\sqrt{\gamma_{xL}^2+\gamma_{yL}^2}}\left[\frac{\dot{y}_w}{v_v}-\psi_w\right]-\frac{\mu_R N_R}{\sqrt{\gamma_{xR}^2+\gamma_{yL}^2}}\left[\frac{\dot{y}_w}{v_v}-\psi_w\right] \tag{3.26}$$

$$I_R\dot{\omega}_{wR} = T_t - K_s\theta_s - r_o\frac{\mu_R N_R}{\sqrt{\gamma_{xR}^2+\gamma_{yL}^2}}\left[\frac{r_o\omega_{wR}-v_v}{v_v}-[\frac{L_g\dot{\psi}_w}{v_v}+\frac{\omega_{wR}\lambda_w(y_w-y_t)}{v_v}]\right] \tag{3.27}$$

where $\theta_s = \int(\omega_{wR}-\omega_{wL})dt$

$$I_L\dot{\omega}_{wL} = K_s\theta_s - r_o\frac{\mu_L N_L}{\sqrt{\gamma_{xL}^2+\gamma_{yL}^2}}\left[\frac{r_o\omega_{wL}-v_v}{v_v}+[\frac{L_g\dot{\psi}_w}{v_v}+\frac{\omega_{wL}\lambda_w(y_w-y_t)}{v_v}]\right] \tag{3.28}$$

Equations (3.24) to (3.28) show the complexity of the wheelset dynamics with all the motions of the wheelset interdependent on each other. A Simulink model, shown in Figure-3.8, based on these equations is developed. A random track input y_t is generated to simulate wheelset dynamics in the presence of track irregularities. Figure-3.9 shows the creep curves used during the simulation. Curve 1 represents a good dry contact condition, providing a sufficient adhesion level for the proper operation of a railway vehicle, and Curve-2 represents a contaminated track. It is well-known in railway vehicle dynamics that an unconstrained solid axle wheelset (i.e. without yaw stiffness) is unstable and will produce kinematic oscillations at all non-zero speeds. Figure-3.10 shows the step response of unconstrained wheelset dynamics when the wheelset is running at a speed of 20m/sec. The contact condition used in this simulation is represented by creep curve-1. A small step disturbance of 5mm is applied in the lateral direction after 1 second of the simulation during normal running condition of the vehicle under zero tractive effort. The frequency of kinematic oscillations in Figure-3.10 is 2Hz, which can be calculated using Klingel's formula given in equation (3.1).

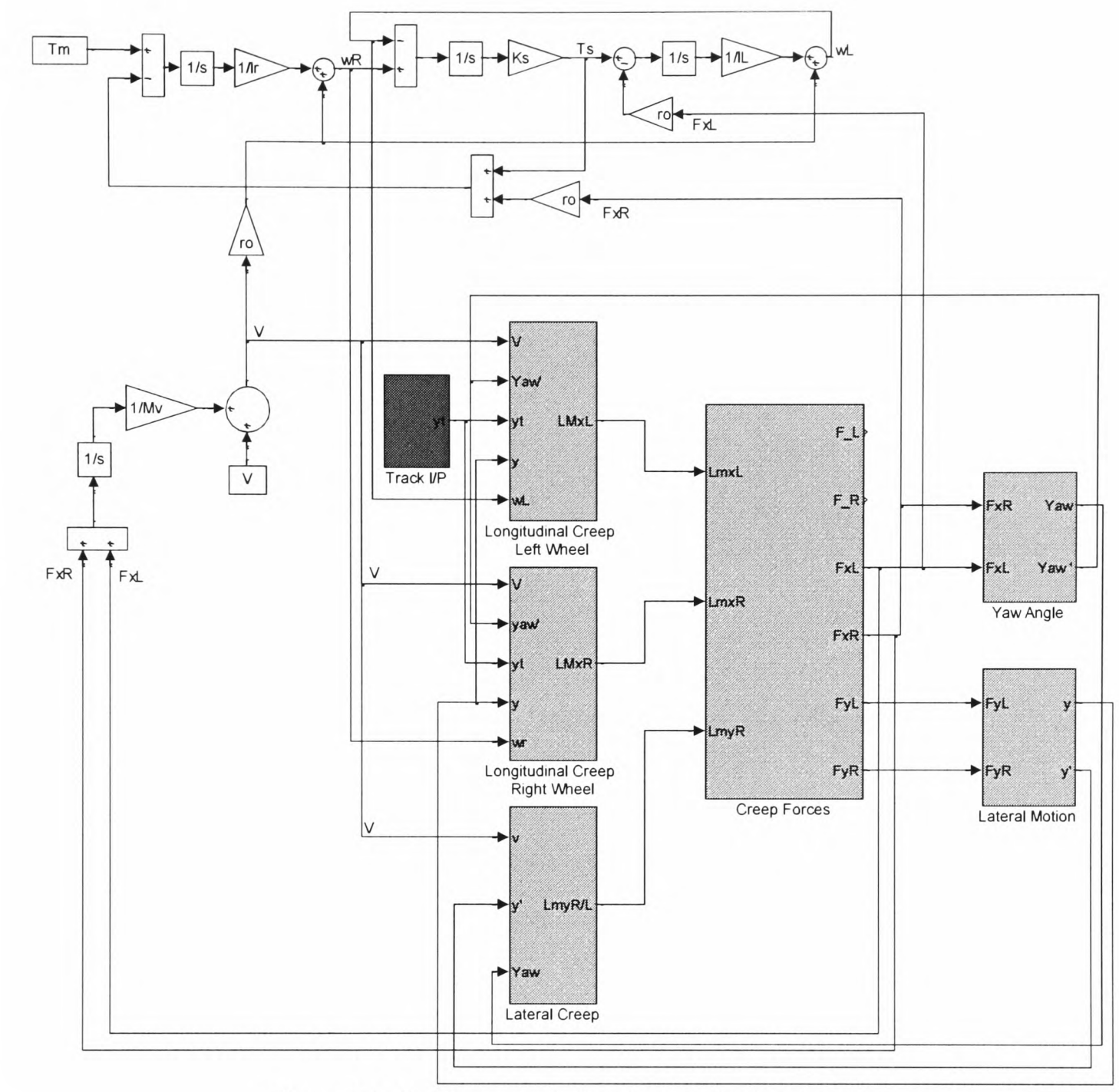

Figure-3.8: Simulink model of nonlinear wheelset dynamics

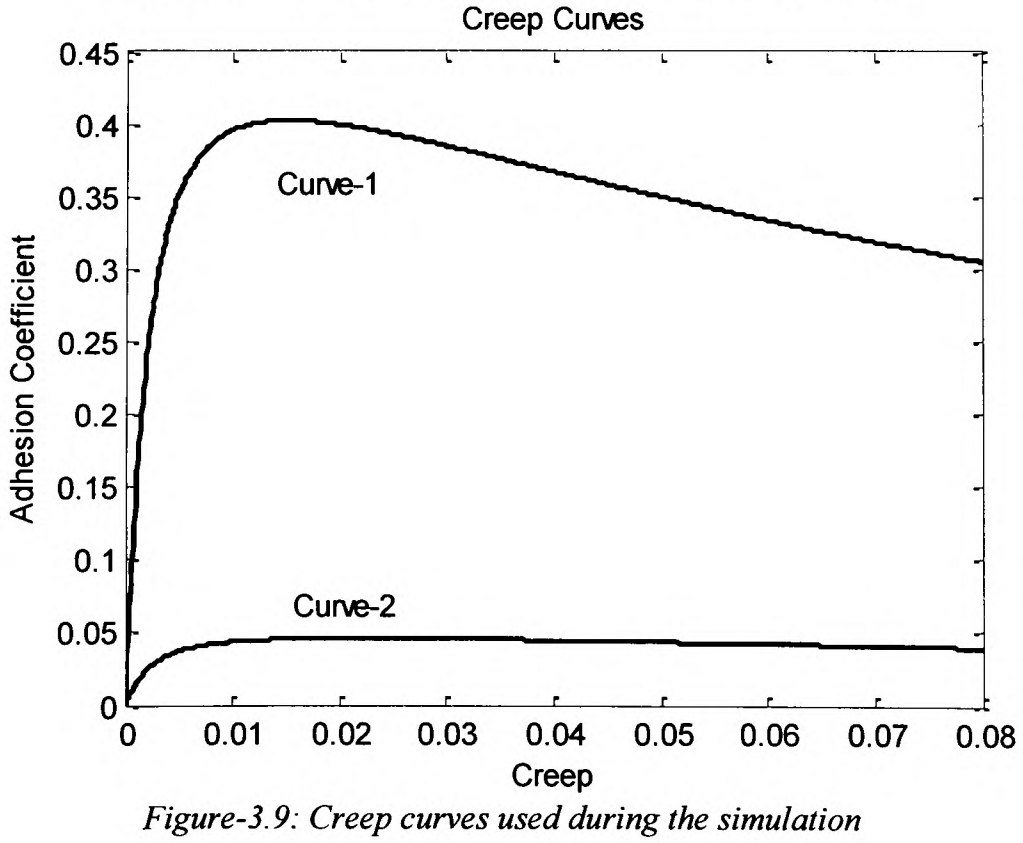

Figure-3.9: Creep curves used during the simulation

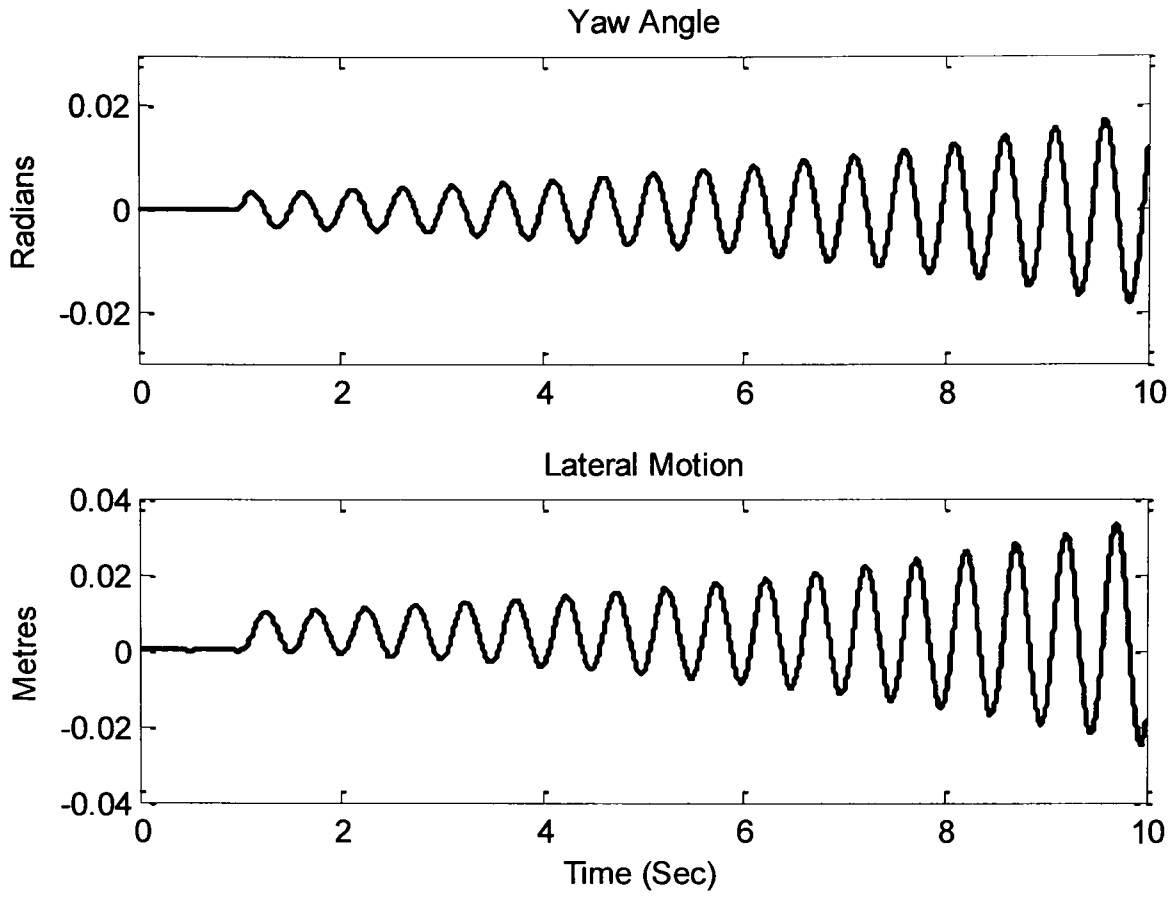

Figure-3.10: Step response of an unconstrained solid axle wheelset at 20m/s

When yaw stiffness is provided to the wheelset, the yaw and lateral dynamics are stabilised for range of speed values, depending upon the amount of stiffness provided. Figure-3.11 demonstrates this phenomenon when the wheelset is operated at 20m/sec with yaw stiffness.

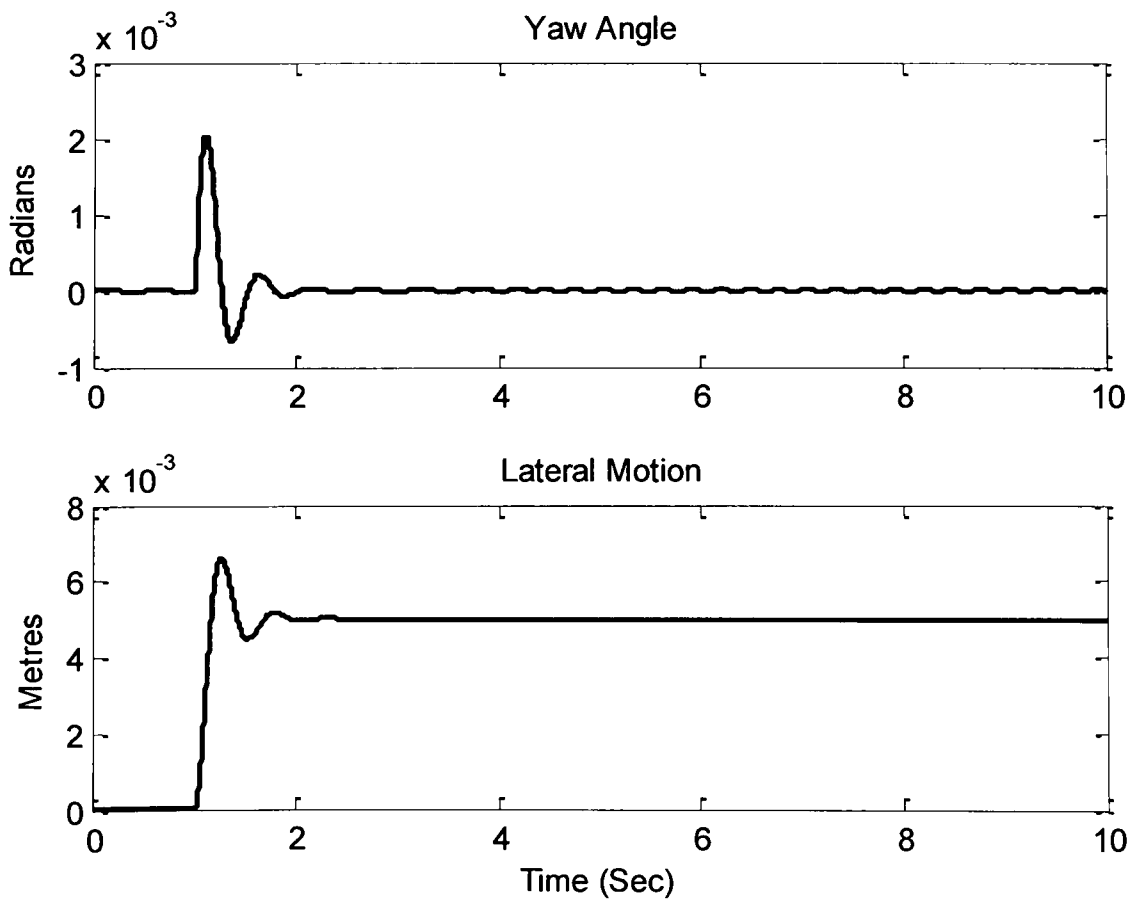

Figure-3.11: Step response of a constrained solid axle wheelset at 20m/s and K_w=5×10^{6}N/rad

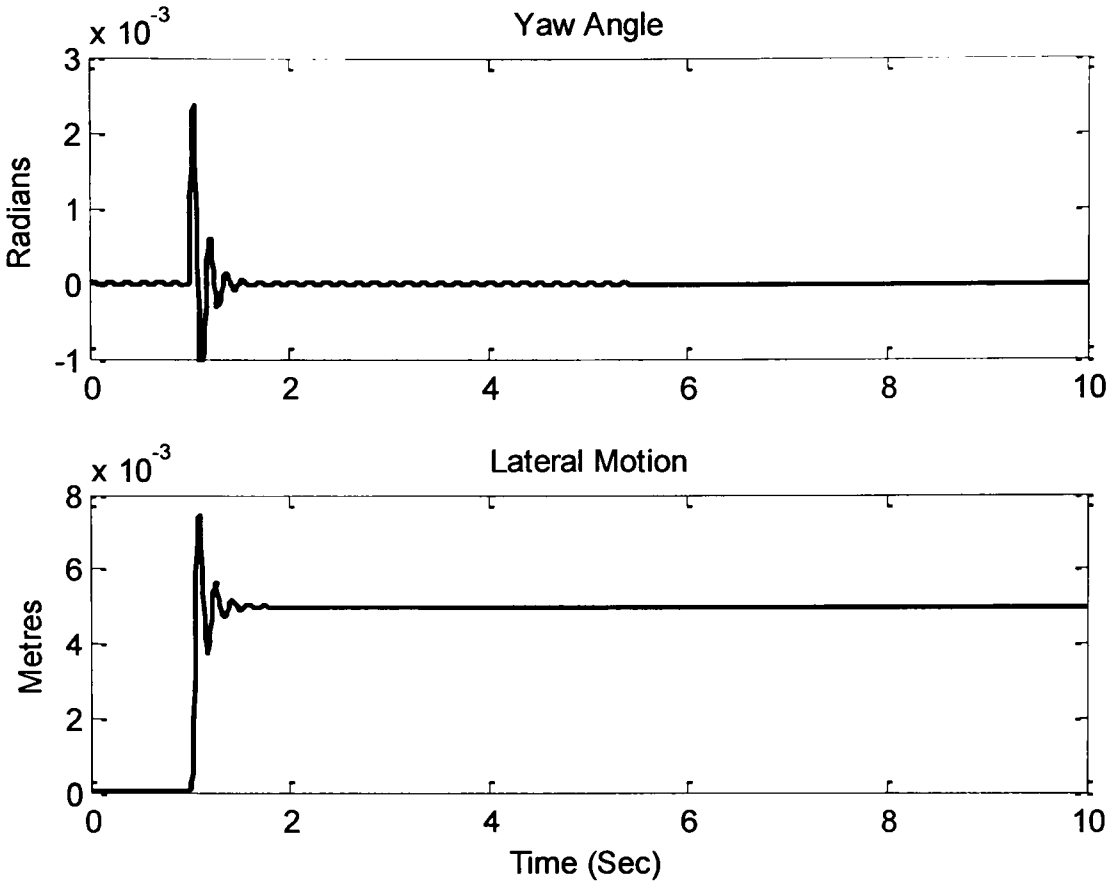

Figure-3.12: Step response of a constrained solid axle wheelset at 60m/s and K_w=5×10^{6}N/rad

Figure-3.12 and Figure-3.13 show the results of yaw and lateral dynamics when the wheelset is operated at the same speed and with different yaw stiffness. In Figure-3.12 the yaw stiffness is higher, so the wheelset dynamics are stable at a higher speed (whereas, in Figure-3.13 with a less stiff spring, the wheelset is unstable at higher speeds). Nonetheless, the problem with high stiffness is that it degrades the natural curving ability of the wheelset.

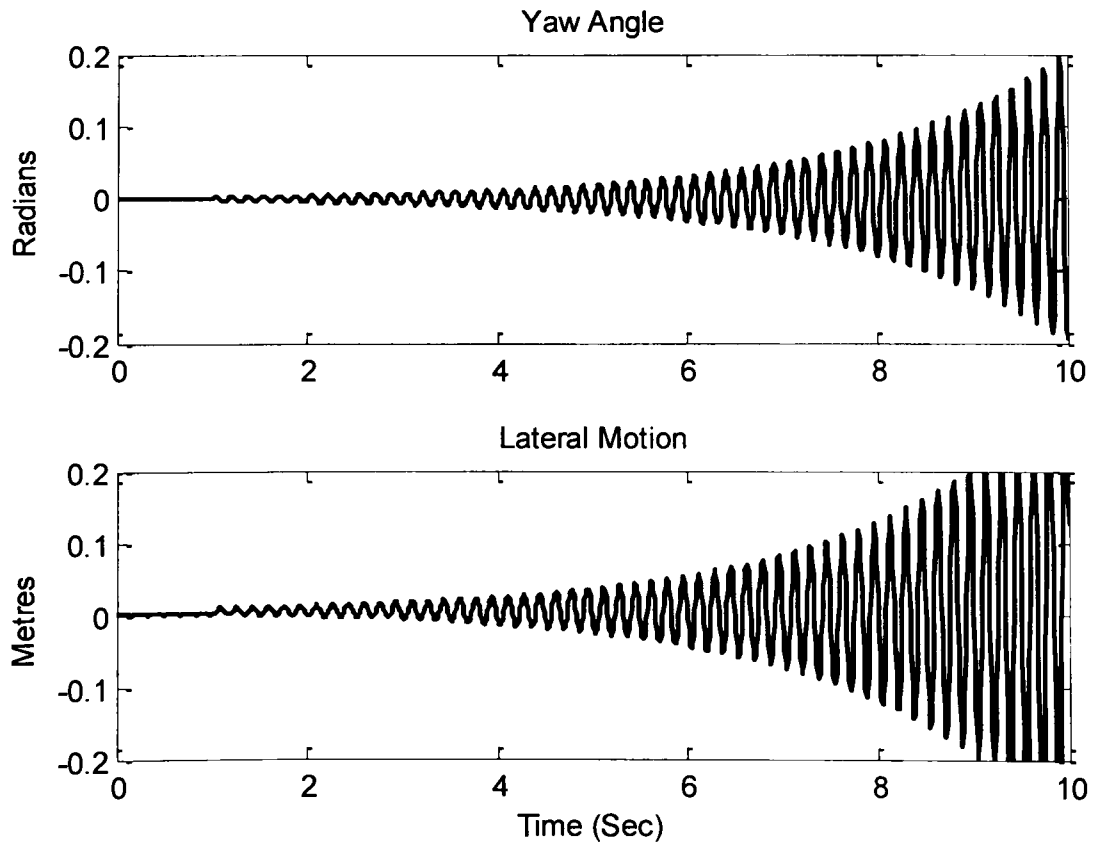

Figure-3.13: Step response of constrained solid axle wheelset at 60m/s and K_w=1.8×10^{6}N/rad

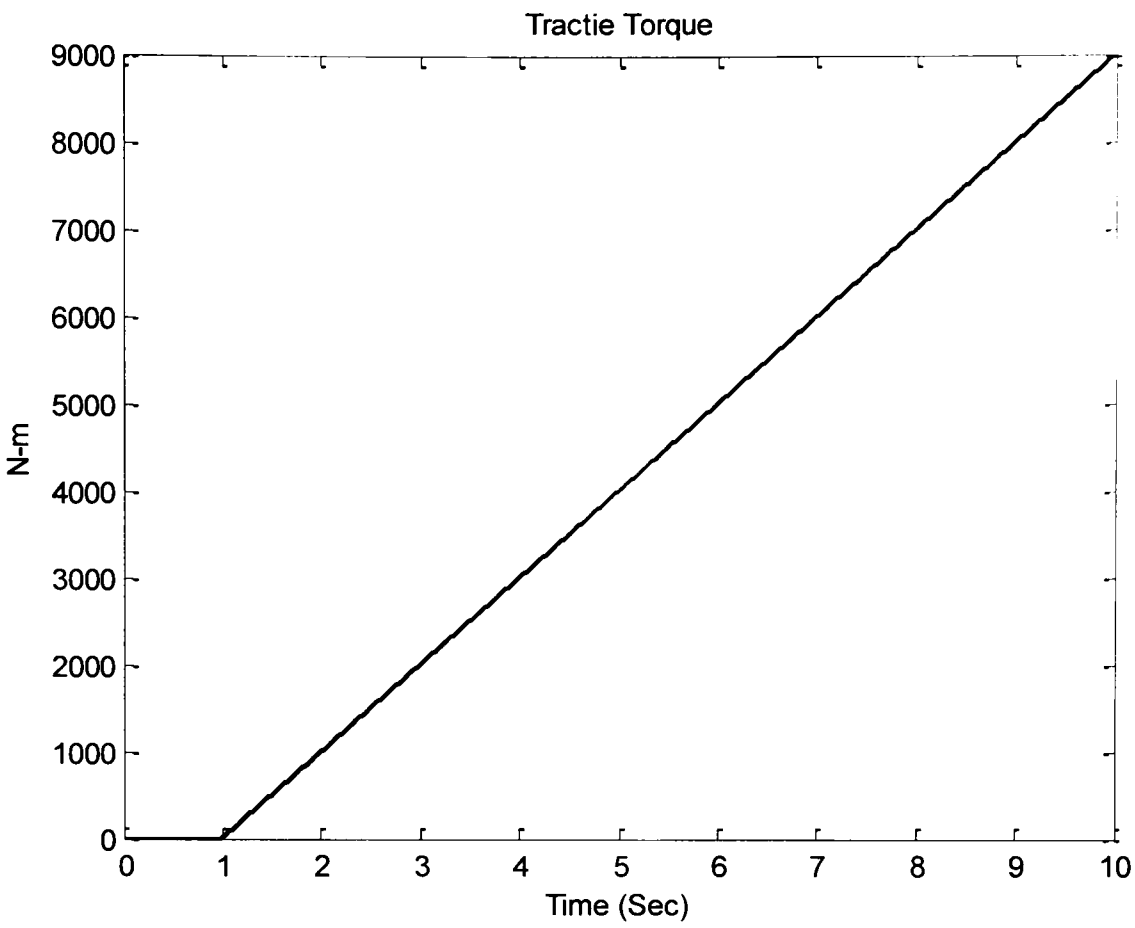

Figure-3.14: Applied tractive torque

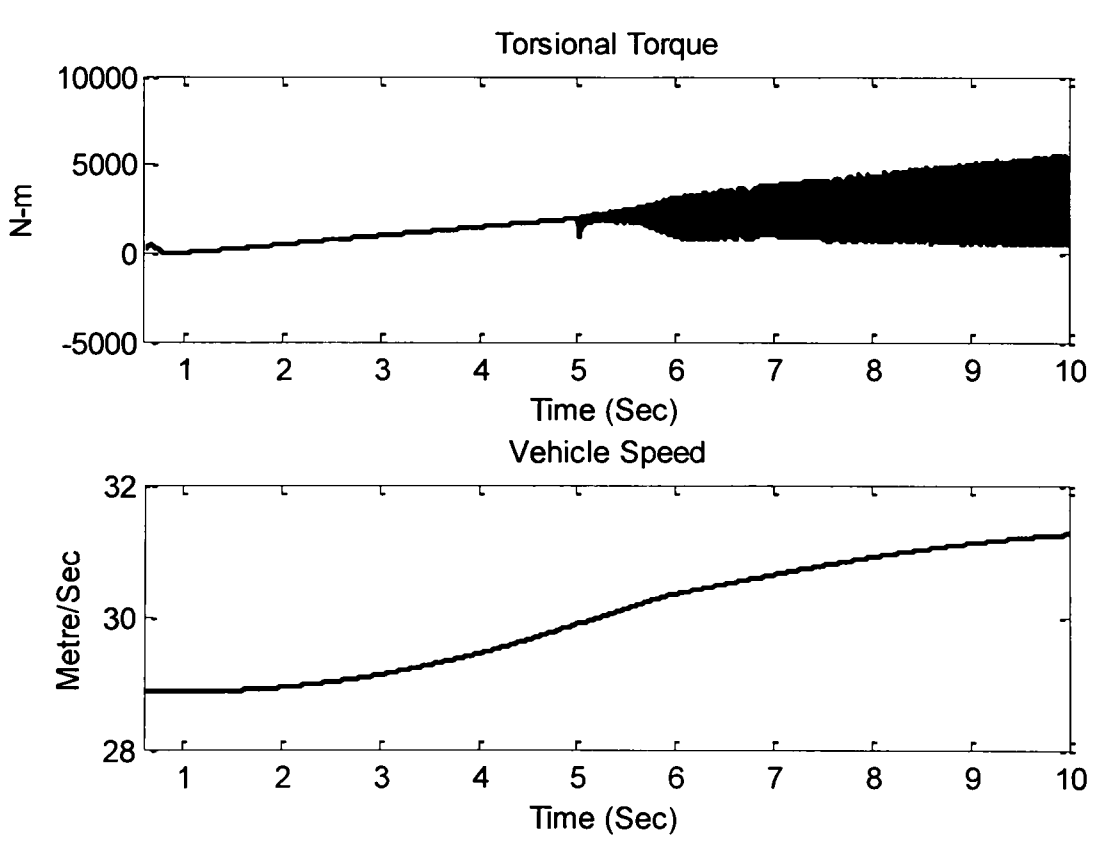

Figure-3.15: Wheelset dynamics in different contact conditions

Another unwanted phenomenon in wheelset dynamics is the wheel slip, which is result of the presence of insufficient adhesion to apply acceleration and brakes properly. Figure-3.15 demonstrates the consequences of a low adhesion condition on wheelset dynamics. Tractive effort is gradually increased during the simulation, as shown in figure-3.14, and the adhesion level is dropped during the simulation (at t=5 sec), which results in the torsional vibrations of the specific frequency, defined by the material

stiffness and material damping of the axle, as shown in Figure-3.15. Because of the slip the speed of the wheels increases abruptly (Figure-3.16), causing the mechanical parts of the rolling stock to wear down quickly and waste of power, whereas the increase in vehicle speed is much slower (Figure-3.15) because of the wheel slip.

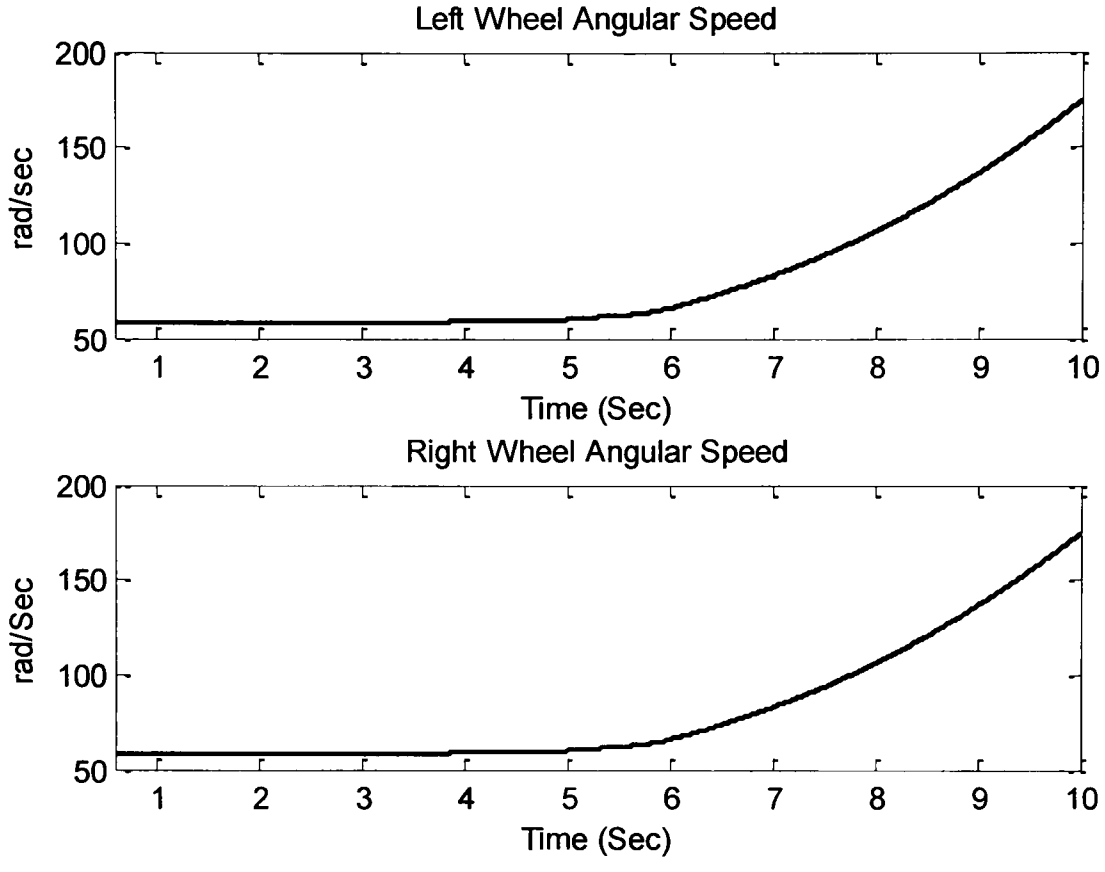

Figure-3.16: Wheelset dynamics in different contact conditions

4. ESTIMATORS DESIGN

4.1 Simplification of wheelset dynamics

The main objective of this study is to develop a new model-based technique to detect changes in wheel-rail contact conditions by using the least number of on-board sensors. One of the major steps in doing so is to estimate the wheelset dynamics in different contact conditions. For practicality purposes, it is necessary that the design of the estimators should be as simple as possible by considering those wheelset dynamics related directly to contact conditions. Previous studies have shown that lateral and yaw dynamics are sufficient to detect these changes [8-9, 14, 118-121]. Therefore, some simplifications in the wheelset model are introduced for the estimator design. The simplified equation of creepage involving only yaw and lateral dynamics is given below. The longitudinal creep of the left wheel is given in equation (4.1).

$$\gamma_{xL} = \frac{L_g \dot{\psi}_w}{v_v} + \frac{\omega_{wL} \lambda_w (y_w - y_t)}{v_v} \tag{4.1}$$

where $\frac{\omega_{wL}}{v_v} = \frac{v_v / r_o}{v_v} = \frac{1}{r_o}$. As such, equation (4.1) is rewritten as

$$\gamma_{xL} = \frac{L_g \dot{\psi}_w}{v_v} + \frac{\lambda_w (y_w - y_t)}{r_o} \tag{4.2}$$

Right wheel longitudinal creep and lateral creep are given in equations (4.3) and (4.4) respectively.

$$\gamma_{xR} = -\frac{L_g \dot{\psi}_w}{v_v} - \frac{\lambda_w (y_w - y_t)}{r_o} \tag{4.3}$$

$$\gamma_y = \gamma_{yR} = \gamma_{yL} = \frac{\dot{y}_w}{v_v} - \psi_w \tag{4.4}$$

The simplified equations of lateral and yaw dynamics can then be written as:

$$I_w \ddot{\psi}_w = F_{xR} L_g - F_{xL} L_g - k_w \psi_w \tag{4.5}$$

$$I_w \ddot{\psi}_w = \frac{\mu_R N_R}{\sqrt{\gamma_{xR}^2 + \gamma_{yL}^2}} \left[-\frac{L_g \dot{\psi}_w}{v_v} + \frac{\lambda_w (y_w - y_t)}{r_o} \right] L_g - \frac{\mu_L N_L}{\sqrt{\gamma_{xL}^2 + \gamma_{yL}^2}} \left[\frac{L_g \dot{\psi}_w}{v_v} + \frac{\lambda_w (y_w - y_t)}{r_o} \right] L_g - k_w \psi_w \tag{4.6}$$

$$m_w \ddot{y}_w = -F_{yR} - F_{yL} + F_c + F_g \tag{4.7}$$

$$m_w \ddot{y}_w = -\frac{\mu_L N_L}{\sqrt{\gamma_{xL}^2 + \gamma_{yL}^2}}\left[\frac{\dot{y}_w}{v_v} - \psi_w\right] - \frac{\mu_R N_R}{\sqrt{\gamma_{xR}^2 + \gamma_{yL}^2}}\left[\frac{\dot{y}_w}{v_v} - \psi_w\right] \tag{4.8}$$

The simplified model has several advantages in estimator design, without having a significant effect on the results [119-121]. The major advantage is the simple design of the estimator with a minimum number of states that allow the estimator to converge quickly. The yaw and lateral dynamics are excited by lateral track irregularities; hence, torque input is not required for the estimators in the simplified model.

4.2 Linearisation of creep forces

In equations (4.5 and 4.7) creep forces F_{xR}, F_{xL}, F_{yR} and F_{yL} have a nonlinear relationship with creepages γ_x and γ_y. Therefore, these creep forces are linearised at specific operating points on the creep curve in order to design the Kalman filters. The first order approximation of longitudinal creep force for the right wheel around an operating point (γ_{xRo}, γ_{yRo}) is given in the following equation:

$$F_{xR} = F_R.\frac{\gamma_{xR}}{\gamma_R} = F_{xRo} + \frac{\partial F_{xR}}{\partial \gamma_{xR}}\bigg|_{(\gamma_{xRo},\gamma_{yRo})} \times \Delta\gamma_{xR} + \frac{\partial F_{xR}}{\partial \gamma_{yR}}\bigg|_{(\gamma_{xRo},\gamma_{yRo})} \times \Delta\gamma_{yR} \tag{4.9}$$

where

$$\frac{\partial F_{xR}}{\partial \gamma_{xR}}\bigg|_{(\lambda_{xRo},\lambda_{yRo})} = \left[\frac{\partial}{\partial \gamma_{xR}}\left(F_R \frac{\gamma_x}{\sqrt{\gamma_{xR}^2 + \gamma_{yR}^2}}\right)\right]_{(\gamma_{xRo},\gamma_{yRo})} \tag{4.10}$$

Placing $F_R = \mu_R N_R$ into the above equation and considering $\frac{\partial \gamma_R}{\partial \gamma_{xR}} = \frac{\gamma_x}{\sqrt{\gamma_{xR}^2 + \gamma_{yR}^2}}$ gives

$$\frac{\partial F_{xR}}{\partial \gamma_{xR}}\bigg|_{(\gamma_{xRo},\gamma_{yRo})} = \left[N_R\left(\frac{\gamma_{xR}^2}{\gamma_R^2}\frac{\partial \mu_R}{\partial \gamma_R} + \frac{\gamma_{yR}^2 \mu_R}{\gamma_R^3}\right)\right]_{(\gamma_{xRo},\gamma_{yRo})} = g_{R11} \tag{4.11}$$

where $\frac{\partial \mu_R}{\partial \gamma_R}$ is the slope of the creep curve at point (γ_{xRo}, γ_{yRo}) and N_R is the normal force applied to the right wheel. As only singe wheelset is considered in this study therefore only quarter of the vehicle mass is considered for the calculation of normal force on single wheelset, which is further divided into half for the left and right wheels. For the vehicle running on straight track lateral creep is very small as compare to longitudinal creep. Therefore, when the vehicle runs on straight track, the value of g_{R11} at any operating point depend upon the slope of the creep curve at operating point and the

normal force. Assuming normal force is constant then g_{R11} only depends upon the slope of the creep curve. In the other half of equation (4.9),

$$\frac{\partial F_{xR}}{\partial \gamma_{yR}}\Big|_{(\gamma_{xRo},\gamma_{yRo})} = \left[\frac{\partial}{\partial \gamma_{yR}}\left(F_R \frac{\gamma_x}{\sqrt{\gamma_{xR}^2+\gamma_{yR}^2}}\right)\right]_{(\gamma_{xRo},\gamma_{yRo})}$$

$$= \left[N_R \frac{\gamma_{xR}\gamma_{yR}}{\gamma_R^2}\left(\frac{\partial \mu_R}{\partial \gamma_R} - \frac{\mu_R}{\gamma_R}\right)\right]_{(\gamma_{xRo},\gamma_{yRo})} = g_{R12} \tag{4.12}$$

The value of g_{R12} depends upon the difference between slope of creep curve and traction ratio at operating point. It is positive when the wheelset is operated in the linear region of the creep curve because of the high slope and is negative when the operating point is moved up on the creep curve where traction ratio ($\frac{\mu_R}{\gamma_R}$) is high and the slope of the creep curve is decreased. Substituting values g_{R11} and g_{R12}in equation (4.9) gives

$$F_{xR} = F_{xRo} + g_{R11}\Delta\gamma_{xR} + g_{R12}\Delta\gamma_{yR} \tag{4.13}$$

or in small signal form

$$\Delta F_{xR} = F_{xR} - F_{xRo} = g_{R11}\Delta\gamma_{xR} + g_{R12}\Delta\gamma_{yR} \tag{4.14}$$

where

$$\Delta\gamma_{xR} = \gamma_{xR} - \gamma_{xRo} = \left(-\frac{L_g\dot{\psi}_w}{v_v} - \frac{\lambda_w(y_w - y_t)}{r_o}\right) - \left(-\frac{L_g\dot{\psi}_{wo}}{v_v} - \frac{\lambda_w(y_{wo} - y_{to})}{r_o}\right) \tag{4.15}$$

$$\Delta\gamma_{xR} = -\frac{L_g(\dot{\psi}_w - \dot{\psi}_{wo})}{v_v} - \frac{\lambda_w(y_w - y_{wo})}{r_o} + \frac{\lambda_w(y_t - y_{to})}{r_o} \tag{4.16}$$

$$\Delta\gamma_{xR} = -\frac{L_g\Delta\dot{\psi}_w}{v_v} - \frac{\lambda_w\Delta y_w}{r_o} + \frac{\lambda_w\Delta y_t}{r_o} \tag{4.17}$$

and

$$\Delta\gamma_{yR} = \gamma_{yR} - \gamma_{yRo} = \left(\frac{\dot{y}_w}{v_v} - \psi_w\right) - \left(\frac{\dot{y}_{wo}}{v_v} - \psi_{wo}\right) \tag{4.18}$$

$$\Delta\gamma_{yR} = \frac{\dot{y}_w}{v_v} - \frac{\dot{y}_{wo}}{v_v} - \psi_w + \psi_{wo} = \frac{\Delta\dot{y}_w}{v_v} - \Delta\psi_w \tag{4.19}$$

Finally, the small signal form of the right wheel's longitudinal creep force is given as:

$$\Delta F_{xR} = g_{R11}\left[-\frac{L_g\Delta\dot{\psi}_w}{v_v} - \frac{\lambda_w\Delta y_w}{r_o} + \frac{\lambda_w\Delta y_t}{r_o}\right] + g_{R12}\left[\frac{\Delta\dot{y}_w}{v_v} - \Delta\psi_w\right] \tag{4.20}$$

Similarly, the first order approximation of the longitudinal creep force for the left wheel around an operating point (γ_{xLo}, γ_{yLo}) is given as

$$F_{xL} = F_L.\frac{\gamma_{xL}}{\gamma_L} = F_{xLo} + \frac{\partial F_{xL}}{\partial \gamma_{xL}}\bigg|_{(\gamma_{xLo},\gamma_{yLo})} \times \Delta\gamma_{xL} + \frac{\partial F_{xL}}{\partial \gamma_{yL}}\bigg|_{(\gamma_{xLo},\gamma_{yLo})} \times \Delta\gamma_{yL} \quad (4.21)$$

where

$$\frac{\partial F_{xL}}{\partial \gamma_{xL}}\bigg|_{(\gamma_{xLo},\gamma_{yLo})} = \left[N_L\left(\frac{\gamma_{xL}^2}{\gamma_L^2}\frac{\partial \mu_L}{\partial \gamma_L} + \frac{\gamma_{yL}^2 \mu_L}{\gamma_L^3}\right) \right]_{(\gamma_{xLo},\gamma_{yLo})} = g_{L11} \quad (4.22)$$

and

$$\frac{\partial F_{xL}}{\partial \gamma_{yL}}\bigg|_{(\gamma_{xLo},\gamma_{yLo})} = \left[N_L \frac{\gamma_{xL}\gamma_{yL}}{\gamma_L^2}\left(\frac{\partial \mu_L}{\partial \gamma_L} - \frac{\mu_L}{\gamma_L}\right) \right]_{(\gamma_{xLo},\gamma_{yLo})} = g_{L12} \quad (4.23)$$

and the small signal representation of e equation (4.21) is given as

$$\Delta F_{xL} = g_{L11}\left[\frac{L_g \Delta\dot{\psi}_w}{v_v} + \frac{\lambda_w \Delta y_w}{r_o} - \frac{\lambda_w \Delta y_t}{r_o}\right] + g_{L12}\left[\frac{\Delta\dot{y}_w}{v_v} - \Delta\psi_w\right] \quad (4.24)$$

Now, the lateral creep force of the right wheel is linearised as below:

$$F_{yR} = F_{yRo} + \frac{\partial F_{yR}}{\partial \gamma_{xR}}\bigg|_{(\gamma_{xRo},\gamma_{yRo})} \times \Delta\gamma_{xR} + \frac{\partial F_{yR}}{\partial \gamma_{yR}}\bigg|_{(\gamma_{xRo},\gamma_{yRo})} \times \Delta\gamma_{yR} \quad (4.25)$$

$$\Delta F_{yR} = N_R \frac{\gamma_{xR}\gamma_{yR}}{\gamma_R^2}\left[\frac{\partial \mu_R}{\partial \gamma_R} - \frac{\mu_R}{\gamma_R}\right]_{(\gamma_{xRo},\gamma_{yRo})} \times \Delta\gamma_{xR} + N_R\left[\frac{\gamma_{yR}^2}{\gamma_R^2}\frac{\partial \mu_R}{\partial \gamma_R} + \frac{\gamma_{xR}^2}{\gamma_R^2}\frac{\mu_R}{\gamma_R}\right]_{(\gamma_{xRo},\gamma_{yRo})} \times \Delta\gamma_{yR} \quad (4.26)$$

and considering

$$g_{R21} = N_L \frac{\gamma_{xL}\gamma_{yL}}{\gamma_L^2}\left[\frac{\partial \mu_L}{\partial \gamma_L} - \frac{\mu_L}{\gamma_L}\right]_{(\gamma_{xLo},\gamma_{yLo})} \quad and \quad g_{R22} = N_L\left[\frac{\gamma_{yL}^2}{\gamma_L^2}\frac{\partial \mu_L}{\partial \gamma_L} + \frac{\gamma_{xL}^2}{\gamma_L^2}\frac{\mu_L}{\gamma_L}\right]_{(\gamma_{xLo},\gamma_{yLo})}$$

For a vehicle running on a straight track, g_{R21} depends upon the slope of the creep curve and the traction ratio, while g_{R22} depends only upon the traction ratio calculated at the operating point of the wheelset.

$$\Delta F_{yR} = g_{R21}\left[-\frac{L_g \Delta\dot{\psi}_w}{v_v} - \frac{\lambda_w \Delta y_w}{r_o} + \frac{\lambda_w \Delta y_t}{r_o}\right] + g_{R22}\left[\frac{\Delta\dot{y}_w}{v_v} - \Delta\psi_w\right] \quad (4.27)$$

Similarly, the linearised lateral creep force for the left wheel is given by

$$F_{yL} = F_{yLo} + \left.\frac{\partial F_{yL}}{\partial \gamma_{xL}}\right|_{(\gamma_{xLo},\gamma_{yLo})} \times \Delta\gamma_{xL} + \left.\frac{\partial F_{yL}}{\partial \gamma_{yL}}\right|_{(\gamma_{xLo},\gamma_{yLo})} \times \Delta\gamma_{yL} \tag{4.28}$$

$$\Delta F_{yL} = N_L \frac{\gamma_{xL}\gamma_{yL}}{\gamma_L^2}\left[\frac{\partial \mu_L}{\partial \gamma_L} - \frac{\mu_L}{\gamma_L}\right]_{(\gamma_{xLo},\gamma_{yLo})} \times \Delta\gamma_{xL} + N_L\left[\frac{\gamma_{yL}^2}{\gamma_L^2}\frac{\partial \mu_L}{\partial \gamma_L} + \frac{\gamma_{xL}^2}{\gamma_L^2}\frac{\mu_L}{\gamma_L}\right]_{(\gamma_{xLo},\gamma_{yLo})} \times \Delta\gamma_{yL} \tag{4.30}$$

$$\Delta F_{yL} = g_{L21}\left[\frac{L_g \Delta\dot{\psi}_w}{v_v} + \frac{\lambda_w \Delta y_w}{r_o} - \frac{\lambda_w \Delta y_t}{r_o}\right] + g_{L22}\left[\frac{\Delta\dot{y}_w}{v_v} - \Delta\psi_w\right] \tag{4.29}$$

4.3 Small signal representation of the wheelset dynamics

The small signal model is only valid at the specific point on the creep curve where linearisation is carried out. The small signal representation of the yaw dynamics of the wheelset is given in the following equation:

$$I_w \Delta\ddot{\psi}_w = L_g(\Delta F_{xR} - \Delta F_{xL}) - k_w \Delta\psi_w \tag{4.31}$$

Substituting the creep forces equation from equations (4.20) and (4.24) gives

$$\begin{aligned}\Delta\ddot{\psi}_w = \frac{L_g}{I_w}\Big[&g_{R11}\left(-\frac{L_g\Delta\dot{\psi}_w}{v_v} - \frac{\lambda_w(\Delta y_w - \Delta y_t)}{r_o}\right) + g_{R12}\left(\frac{\Delta\dot{y}_w}{v_v} - \Delta\psi_w\right) - \\ &g_{L11}\left(\frac{L_g\Delta\dot{\psi}_w}{v_v} + \frac{\lambda_w(\Delta y_w - \Delta y_t)}{r_o}\right) - g_{L12}\left(\frac{\Delta\dot{y}_w}{v_v} - \Delta\psi_w\right)\Big] - \frac{k_w}{I_w}\Delta\psi_w\end{aligned} \tag{4.32}$$

Assuming that the normal force on both wheels is the same and the contact condition on either side of the rails is also the same (i.e. $g_{R11} = g_{L11}$ and $g_{R12} = g_{L12}$), equation (4.32) can be simplified as

$$\Delta\ddot{\psi}_w = -\frac{2L_g^2 g_{11}}{v_v I_w}\Delta\dot{\psi}_w - \frac{2L_g g_{11}\lambda_w}{r_o I_w}\Delta y_w + \frac{2L_g g_{11}\lambda_w}{r_o I_w}\Delta y_t - \frac{k_w}{I_w}\Delta\psi_w \tag{4.33}$$

Similarly, the small signal representation of the lateral dynamics is given as

$$m_w \Delta\ddot{y}_w = -\Delta F_{yR} - \Delta F_{yL} \tag{4.34}$$

$$\begin{aligned}\Delta\ddot{y}_w = -\frac{1}{m_w}\Big[&g_{R22}\left(\frac{\Delta\dot{y}_w}{v} - \Delta\psi_w\right) + g_{R21}\left(-\frac{L_g\Delta\dot{\psi}_w}{v_v} - \frac{\lambda_w(\Delta y_w - \Delta y_t)}{r_o}\right) + g_{L22}\left(\frac{\Delta\dot{y}_w}{v_v} - \Delta\psi_w\right) \\ &+ g_{L21}\left(\frac{L_g\Delta\dot{\psi}_w}{v_v} + \frac{\lambda_w(\Delta y_w - \Delta y_t)}{r_o}\right)\Big]\end{aligned} \tag{4.35}$$

If the contact condition and normal force are the same on both wheels (i.e. $g_{R22}=g_{L22}$ and $g_{L21}=g_{R21}$), equation (4.35) is further simplified as

$$\Delta\ddot{y}_w = -\frac{2g_{22}}{m_w v_v}\Delta\dot{y}_w + \frac{2g_{22}}{m_w}\Delta\psi_w \tag{4.36}$$

The final small signal model of the simplified wheelset model is given in the following equation in the state space form:

$$\frac{d}{dt}\begin{bmatrix}\Delta y_w\\ \Delta\psi_w\\ \Delta\dot{y}_w\\ \Delta\dot{\psi}_w\end{bmatrix}=\begin{bmatrix}0 & 0 & 1 & 0\\ 0 & 0 & 0 & 1\\ 0 & \frac{2g_{22}}{m_w} & -\frac{2g_{22}}{v_v m_w} & 0\\ -\frac{2L_g\lambda_w g_{11}}{r_o I_w} & -\frac{k_w}{I_w} & 0 & -\frac{2L_g^2 g_{11}}{v_v I_w}\end{bmatrix}\begin{bmatrix}\Delta y_w\\ \Delta\psi_w\\ \Delta\dot{y}_w\\ \Delta\dot{\psi}_w\end{bmatrix}+\begin{bmatrix}0\\ 0\\ 0\\ \frac{2L_g\lambda_w g_{11}}{r_o I_w}\end{bmatrix}\Delta y_t \quad (4.37)$$

From equation (4.37) it is clear that the dynamics of the wheelset are dependent upon changes in the contact condition. More significantly, the dynamics of the wheelset vary with changes in the operating point of the wheelset and depend upon the slope of the creep curve and the traction ratio at the point where the wheelset is operating. This shows that not only a change in contact condition has significant effect on wheelset dynamics but the dynamics are also varied during the application of traction and braking. Therefore, it is important to monitor tractive effort and wheelset dynamics together in order to identify the available contact conditions.

4.4 Assessment of wheelset dynamics

Eigenvalue analysis describes the small signal behaviour of the model and allows a much deeper view into a system by observing characteristics such as the frequency of oscillation and damping of different modes. The dynamic behaviour of the railway wheelset varies if the vehicle's speed, contact conditions or yaw stiffness are varied. Adequate understanding of the dynamic behaviour of a wheelset requires an in-depth analysis of wheelset dynamics in different contact conditions and at different speeds. An analysis of the wheelset dynamics based on the small signal model given in equation (4.37) is provided in this section. Variations in natural frequency, damping and the root locus plots with respect to variation in contact conditions and at different values of speed and yaw stiffness are provided. The minimum and maximum values for the creep coefficients used are $g_{11}=g_{22}=1\times10^6$ and $g_{11}=g_{22}=1\times10^7$ respectively. Figure-4.1 shows the frequency and damping variations of the kinematic mode when the vehicle is moving at a speed of 10m/sec. The stiffness of the yaw spring used in simulations is 1.5×10^6N/rad. The natural frequency of the kinematic mode changes slightly as the contact condition is varied, whereas the damping ratio is decreased significantly with an increase in creep coefficient values.

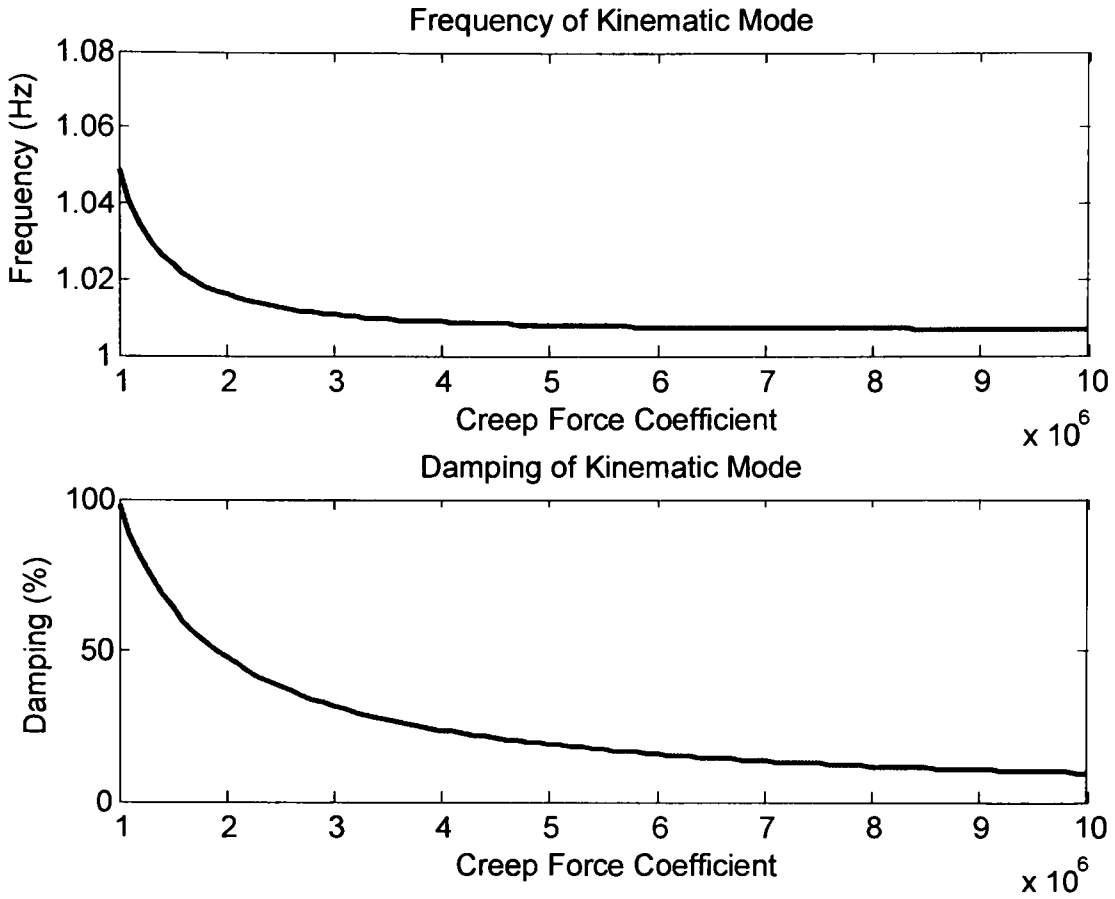

Figure 4.1: Damping and frequency variation of kinematic mode (v_v=10m/s and K_w=1.5×10^6 N/rad)

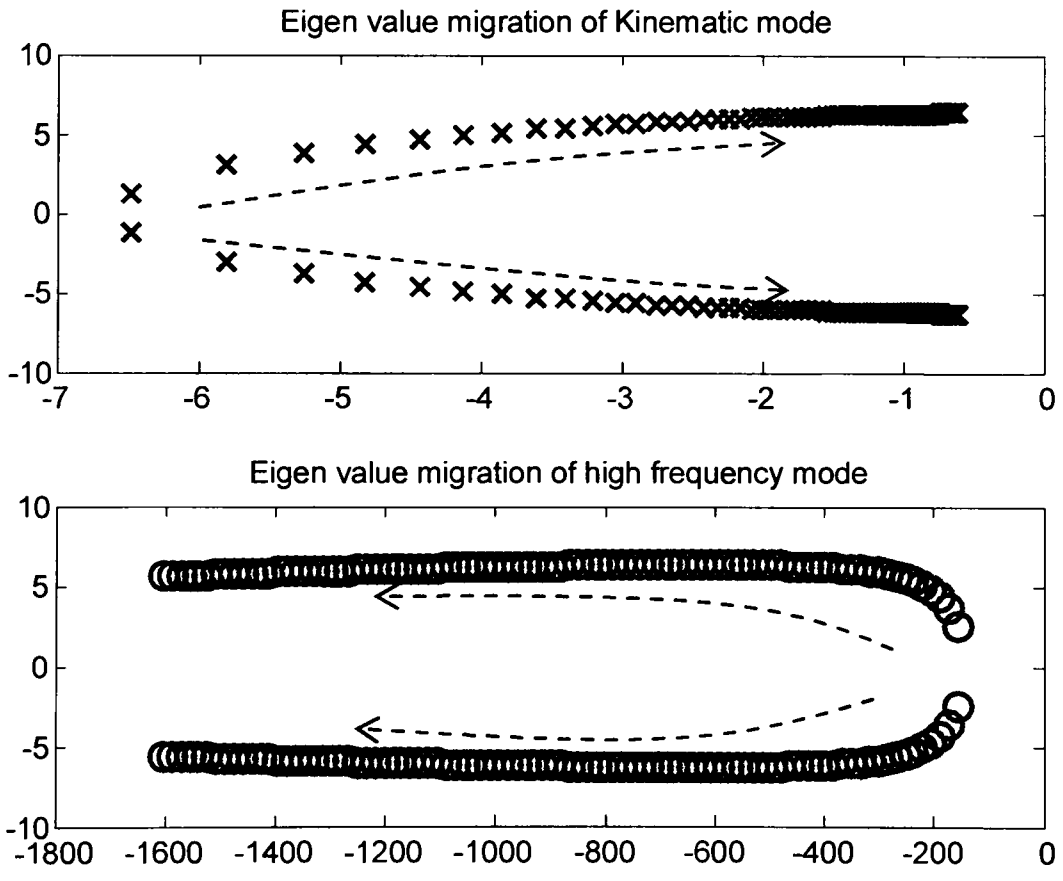

Figure-4.2: Eigen value migration of the kinematic and high frequency modes (v_v=10m/s and K_w=1.5×10^6 N/rad)

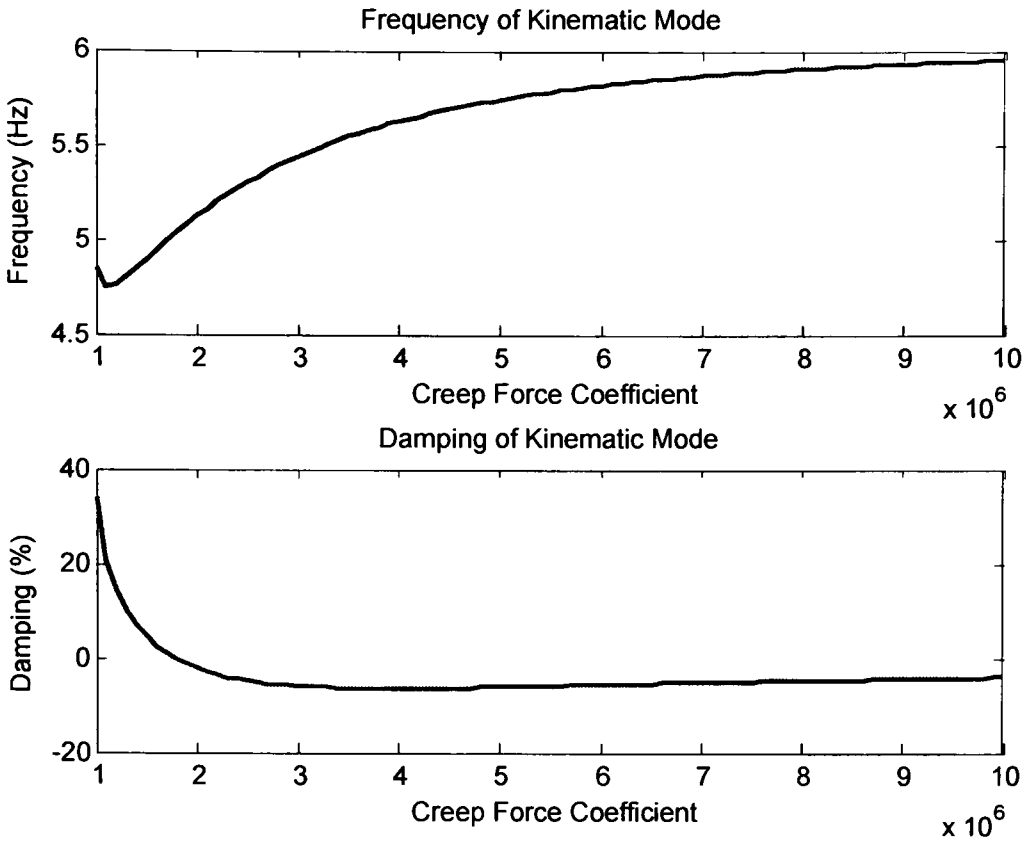

Figure-4.3: Damping and frequency variation of kinematic mode (v_v=60m/s and K_w=1.5×10^6 N/rad)

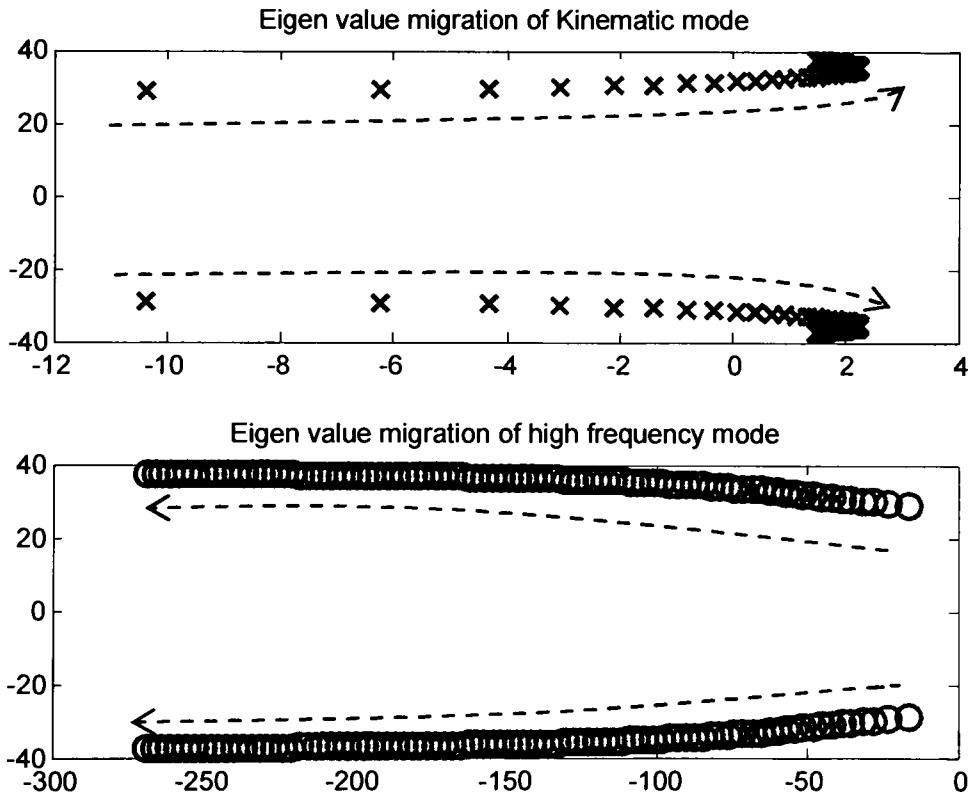

Figure-4.4: Eigen value migration of the kinematic and high frequency modes (v_v=60m/s and K_w=1.5×10^6 N/rad)

Figure-4.2 shows the eigenvalue migration of the kinematic and high frequency modes for the same speed and yaw stiffness used in the previous figure. The direction of the arrow shows the locus of the eigenvalues as the creep coefficient is increased. The values on the right-hand side of the zero on the horizontal axis represent the stable part of the plane, and the right-hand side of the plane is an unstable portion. As the creep

coefficient is increased, the kinematic mode eigenvalues move towards instability, whereas in the high frequency mode the eigenvalues are moving further away from the unstable region.

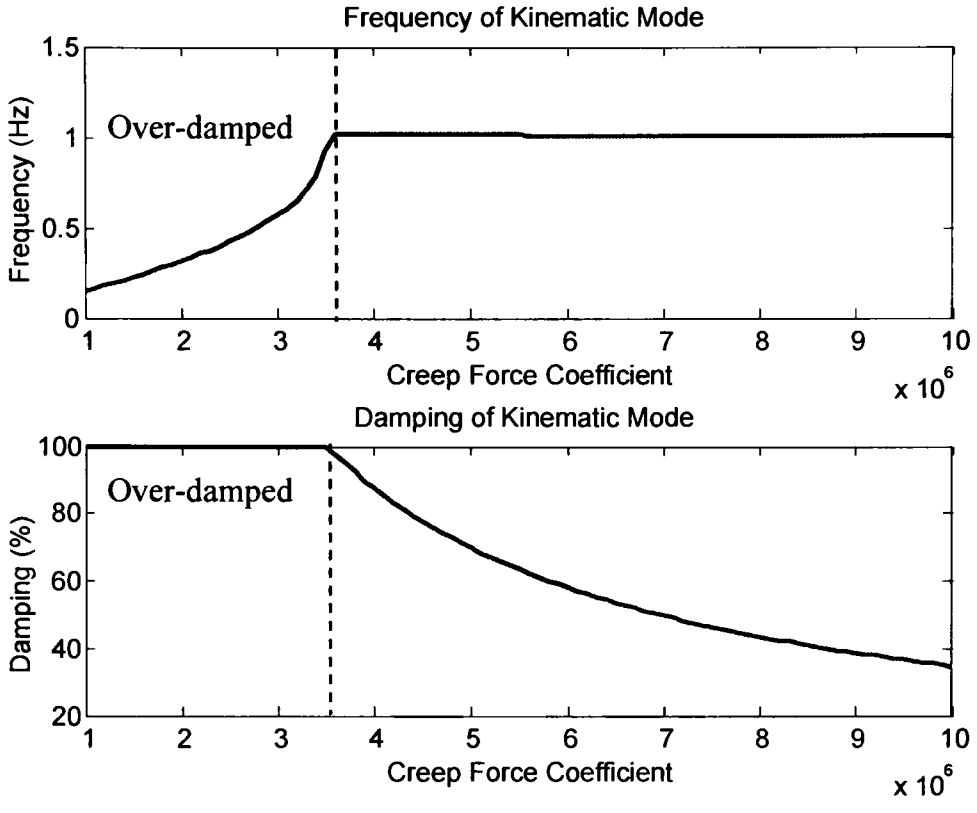

Figure-4.5: Damping and frequency variation of the kinematic mode (v_v=10m/s and K_w=5×10^6 N/rad)

When the forward speed of the vehicle is increased to 60m/sec the natural frequency of the kinematic mode is also increased proportionally (Figure-4.3). Overall damping is lower at higher speeds because the damping terms $\frac{\dot{y}_w}{v_v}$ and $\frac{\dot{\psi}_w}{v_v}$ in the creepage equations are reduced [109] and finally at some value of speed the wheelset becomes unstable. This value of speed is known as the 'critical speed', which can be adjusted by increasing yaw stiffness. The eigenvalues of the kinematic mode migrate from the left half plane to the right half plane as the creep coefficient is increased, as indicated by the arrow in Figure-4.4. A stiffer yaw spring stabilises the kinematic mode at higher speeds. However, the high stiffness values of the yaw spring over-damp the kinematic mode at lower speeds, as shown in Figure-4.5. The damping of the kinematic mode is 100% at lower creep coefficient values when the vehicle is running at lower speeds. Therefore, a suitable value for yaw stiffness should be chosen, keeping in mind the maximum speed of the vehicle, curve radius and various wheel-rail contact conditions.

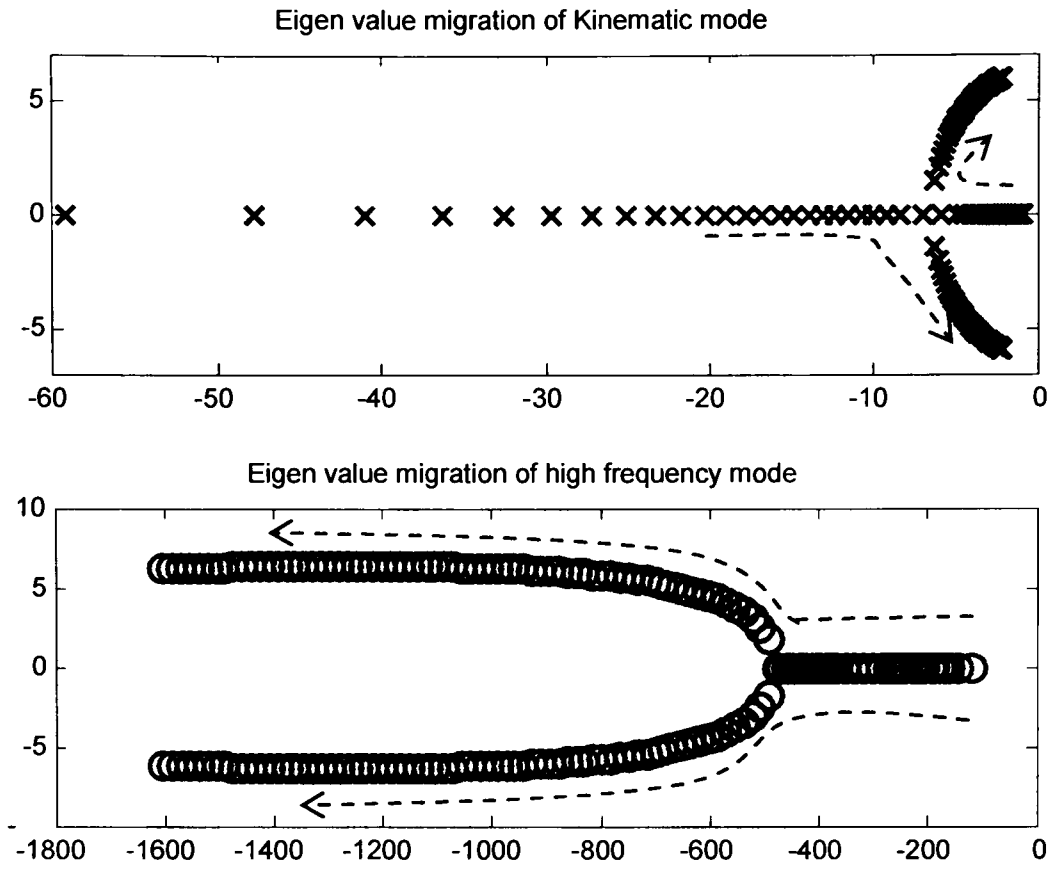

Figure-4.6: Eigen value migration of the kinematic and high frequency modes (v_v=10m/s and K_w=5×10^{6}N/rad)

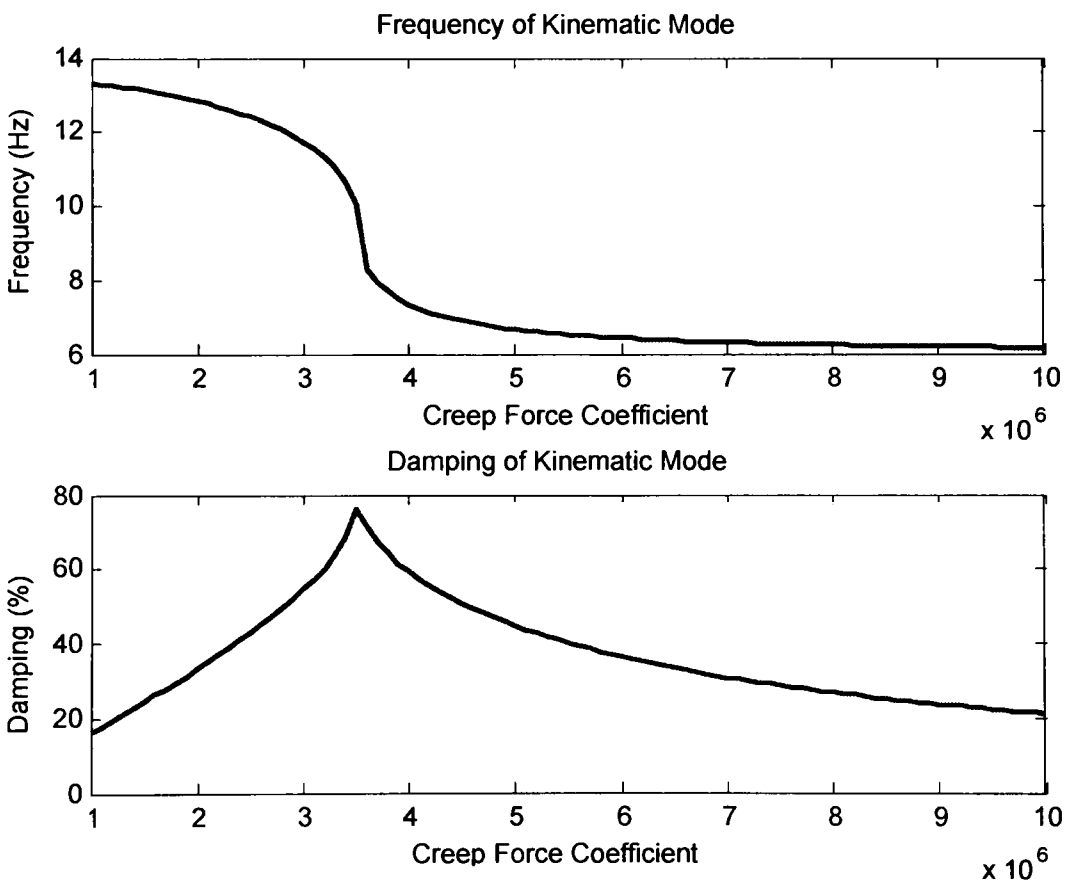

Figure-4.7: Damping and frequency variation of the kinematic mode (v_v=60m/s and K_w=5×10^6 N/rad)

Figure-4.6 shows the migration of eigenvalues for the kinematic and high frequency modes at higher values of yaw stiffness. Both wheelset modes are over-damped at low creep coefficient values, while the eigenvalues of the kinematic mode move towards the unstable region as creep coefficients are increased, whereas high frequency eigenvalues move away. However, the higher yaw stiffness values ensure the dynamic stability of the

wheelset dynamics at higher vehicle speed values, as shown in Figure-4.7. The overall damping of the kinematic mode is higher at a vehicle speed of 60 m/sec when the yaw stiffness is 5×10^6 N/rad.

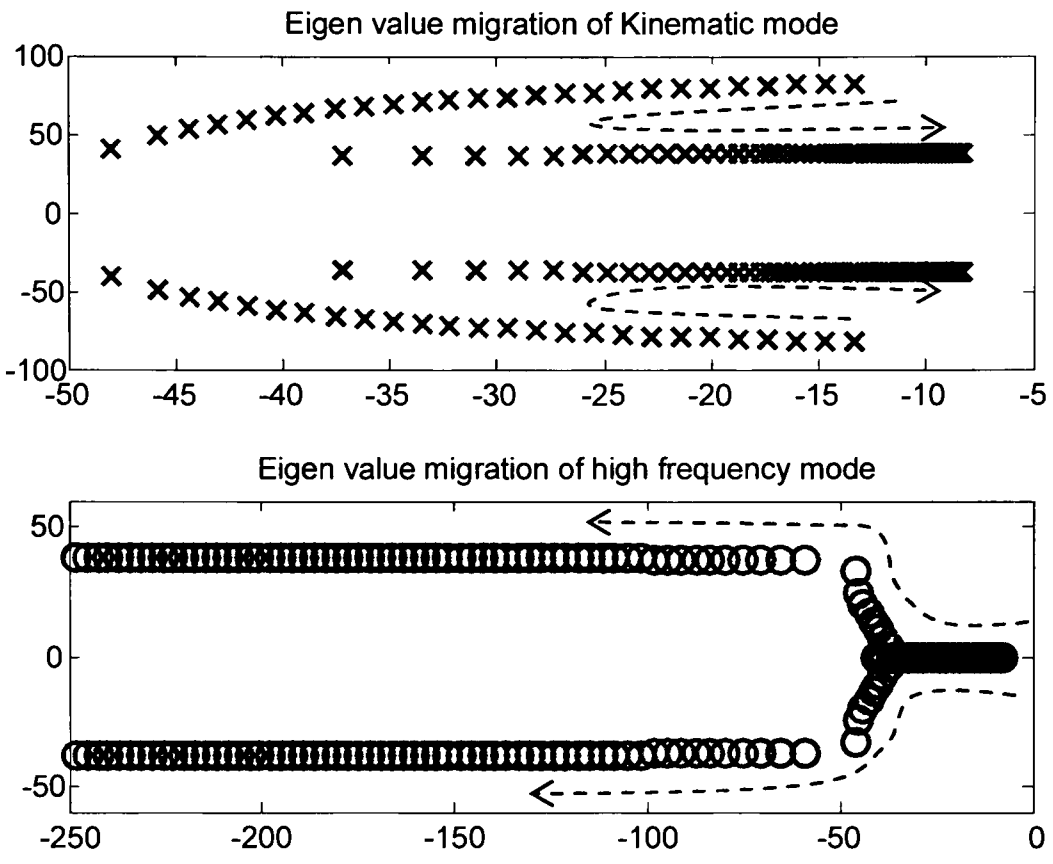

Figure-4.8: Eigen value migration of the kinematic and high frequency modes (v_v=60m/s and K_w=5×10^6 N/rad)

4.5 Kalman filter design

The problem of state estimation concerns the task of estimating the state of a process while only having access to partial and/or noisy measurements from that process. It is a ubiquitous problem encountered in almost every discipline within science and engineering. During the last decades, many research areas (robotics, economic forecasting, etc.) have looked into the matter of how a system can deal online with uncertainty in an optimal way. Optimality is hereby often translated into a minimum mean square error state estimation problem [122].

The most commonly used type of state estimator is the Kalman filter, which is an optimal estimator for linear systems, but unfortunately very few systems in the real world are linear. A common approach to overcoming this problem is to linearise the system first, before using the Kalman filter [123]. The filter has been the subject of extensive research and application, particularly in the area of autonomous or assisted navigation. It consists of a set of mathematical equations and provides an efficient

computational (recursive) means to estimate the state of a process in a way that minimises the mean of the squared error [124]. The Kalman filter was chosen for this research because it gives good results due to its optimality and robustness in the presence of stochastic noises applied by the track, it is convenient for online real-time processing and it is easy to formulate and implement given a basic understanding. A Kalman Bucy filter, which is a continuous time counterpart of the discrete Kalman filter, is used in this research for state estimation. Consider the linearised small signal wheelset model given in equation (4.37), which may be written in the following standard state space form:

$$\dot{x}(t) = Ax(t) + Bu(t) + w(t)$$

Here, *x(t)* is a vector of the actual states, *u(t)* the vector of input and *w(t)* represents process noise applied by the track. Two sensors (a gyro sensor for yaw rate measurement and an accelerometer for lateral acceleration measurement), as indicated in equation (4.39), have been found to be sufficient for the Kalman filter to provide satisfactory estimation results [121, 125-126].

$$z(t) = \begin{bmatrix} 0 & 0 & 0 & 1 \\ 0 & \dfrac{2g_{22}}{m_w} & -\dfrac{2g_{22}}{v_v m_w} & 0 \end{bmatrix} \begin{bmatrix} \Delta y_w \\ \Delta \psi_w \\ \Delta \dot{y}_w \\ \Delta \dot{\psi}_w \end{bmatrix} + v(t) \qquad (4.39)$$

Or, in standard state space form, $z(t) = Cx(t) + Du(t) + v(t)$ where *v(t)* is a vector representing the noise level of the sensors. It is assumed that there is no correlation between process and measurement noises. The equations for the Kalman Bucy filter are then given as follows:

$$\dot{\hat{x}}(t) = A\hat{x}(t) + Bu(t) + K[z(t) - C\hat{x}(t)] \qquad (4.40)$$

$$K = PC^T R^{-1} \qquad (4.41)$$

$$\dot{P} = AP + PA^T - KRK^T + Q \qquad (4.42)$$

In the above equations the *-1* superscript indicates matrix inversion and superscript *T* indicates matrix transposition. In equation (4.40) $\hat{x}$ represents the estimated state vector and K is Kalman filter gain, which is used to weight the measurement innovation $z(t) - Cx(t)$. Kalman filter gain K is calculated using equation (4.41), where P is the estimation error covariance that depends upon the selection of the measurement noise covariance R and the process noise covariance Q calculated using equation (4.42). Process noise covariance Q and measurement noise covariance R are calculated using the following equations:

$$Q = E\left[ww^T\right] \tag{4.43}$$

$$R = E\left[vv^T\right] \tag{4.44}$$

Figure-4.9 shows a block diagram of the Kalman Bucy filter in simple form. A more detailed diagram showing the pictorial view of Kalman Bucy equations is given in Figure-4.10. Knowledge of the system is included in the form of a dynamics model, which has to be detailed sufficiently to include the dynamics of the parts of the system that are to be estimated [9].

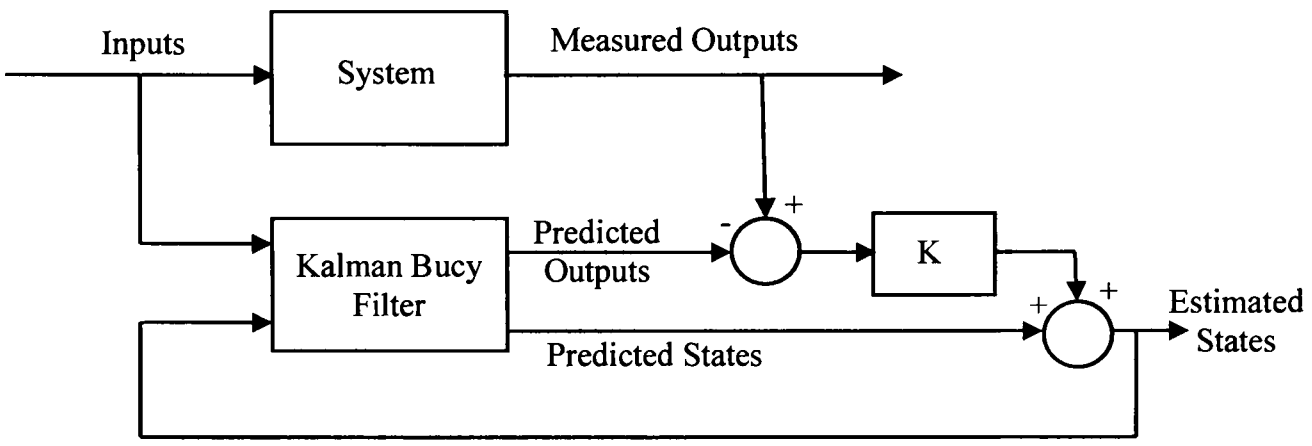

Figure-4.9: Block diagram of a Kalman Bucy filter

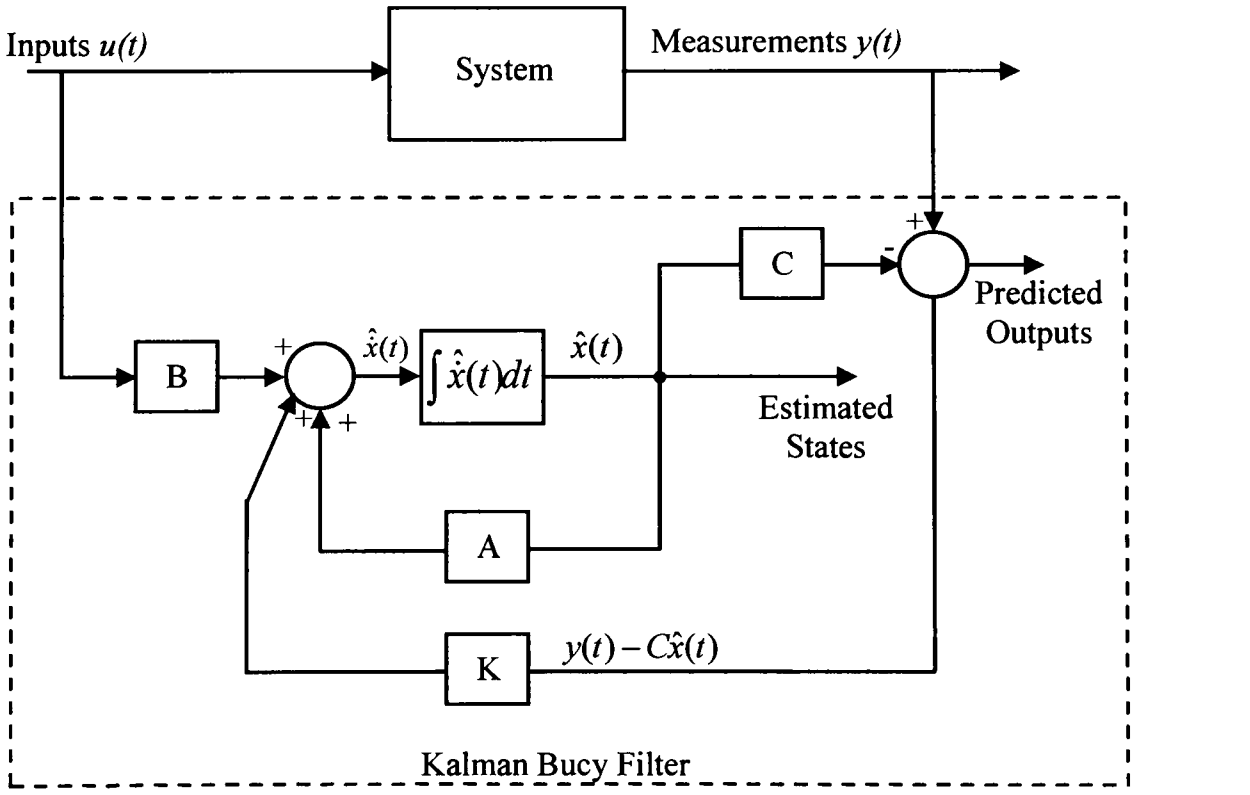

Figure-4.10: Detailed block diagram of the Kalman Bucy filter

A Kalman filter, based on the small signal model in equation (4.37), can be designed to estimate the states of the system at specific points on the creep curve. Nevertheless, this is not a trivial application of the Kalman filter because track irregularities y_t that excite the lateral and yaw dynamics of the railway wheelset are not directly measurable [9] and cannot be neglected either, which makes the design of the Kalman filter more

complex. This problem can be solved by formulating the unknown parameter into state equations as part of the state vector rather than an input, such that the dynamics of the system remain unchanged [118, 127]. Therefore, equation (4.37) is reformulated whereby y_t is treated as part of the state vector by assuming that $\Delta\dot{y}_t = -N\Delta y_t + \dot{y}_t$, where N is a small positive constant added to the system to keep the system matrix fully ranked. The modified state space model and the measurement equation are given in equations (4.43) and (4.44) respectively.

$$\frac{d}{dt}\begin{bmatrix} \Delta\psi_w \\ \Delta\dot{y}_w \\ \Delta\dot{\psi}_w \\ \Delta y_t \\ \Delta y_w - \Delta y_t \end{bmatrix} = \begin{bmatrix} 0 & 0 & 1 & 0 & 0 \\ \frac{2g_{22}}{m_w} & -\frac{2g_{22}}{v_v m_w} & 0 & 0 & 0 \\ -\frac{k_w}{I_w} & 0 & -\frac{2L_g^2 g_{11}}{v_v I_w} & 0 & -\frac{2L_g \lambda_w g_{11}}{r_o I_w} \\ 0 & 0 & 0 & N & 0 \\ 0 & 1 & 0 & 0 & 0 \end{bmatrix} \begin{bmatrix} \Delta\psi_w \\ \Delta\dot{y}_w \\ \Delta\dot{\psi}_w \\ \Delta y_t \\ \Delta y_w - \Delta y_t \end{bmatrix} + \begin{bmatrix} 0 \\ 0 \\ 0 \\ 1 \\ -1 \end{bmatrix} \Delta\dot{y}_t \tag{4.43}$$

In the reformulated equation the lateral displacement of the wheelset is replaced by the estimator state representing the lateral displacement relative to the track, i.e. Δy_w-Δy_t. The value of constant N and the covariance matrix for track noise Q can be adjusted to optimally tune the Kalman filter at different operating points.

$$z(t) = \begin{bmatrix} 0 & 0 & 1 & 0 & 0 \\ \frac{2g_{22}}{m_w} & -\frac{2g_{22}}{v_v m_w} & 0 & 0 & 0 \end{bmatrix} \begin{bmatrix} \Delta\psi_w \\ \Delta\dot{y}_w \\ \Delta\dot{\psi}_w \\ \Delta y_t \\ \Delta y_w - \Delta y_t \end{bmatrix} + v \tag{4.44}$$

4.6 State estimation

The creep curve shown in Figure-4.11 is used in the initial design and assessment of the Kalman filters. State estimation is carried out at two different operating points P_1 and P_2. P_1 is located in the linear region and P_2 in the nonlinear region of the creep curve. Assuming that the correlation between the yaw rate and lateral acceleration is zero, and using gyro sensor (AD22304) and accelerometer (Typical IEPE) data sheets the measurement noise covariance matrix is calculated as

$$R = E\left(\begin{bmatrix} \dot{\psi}_w \\ \ddot{y}_w \end{bmatrix}\begin{bmatrix} \dot{\psi}_w & \ddot{y}_w \end{bmatrix}\right) = E\begin{bmatrix} \dot{\psi}_w^{\,2} & \dot{\psi}_w \ddot{y}_w \\ \ddot{y}_w \dot{\psi}_w & \ddot{y}_w^{\,2} \end{bmatrix} = \begin{bmatrix} 9\times10^{-8} & 0 \\ 0 & 6\times10^{-11} \end{bmatrix}$$

By tuning the process noise covariance matrix Q and selecting a suitable value for constant N, the performance of the Kalman filters can be studied thoroughly. The determination of the process noise covariance is a more difficult process, so a trial and error approach is applied to find an optimal value at any specific operating point. For N any negative value can be selected because the positive value of the N renders the system unobservable (undetectable), which is a preliminary requirement when designing the state estimator.

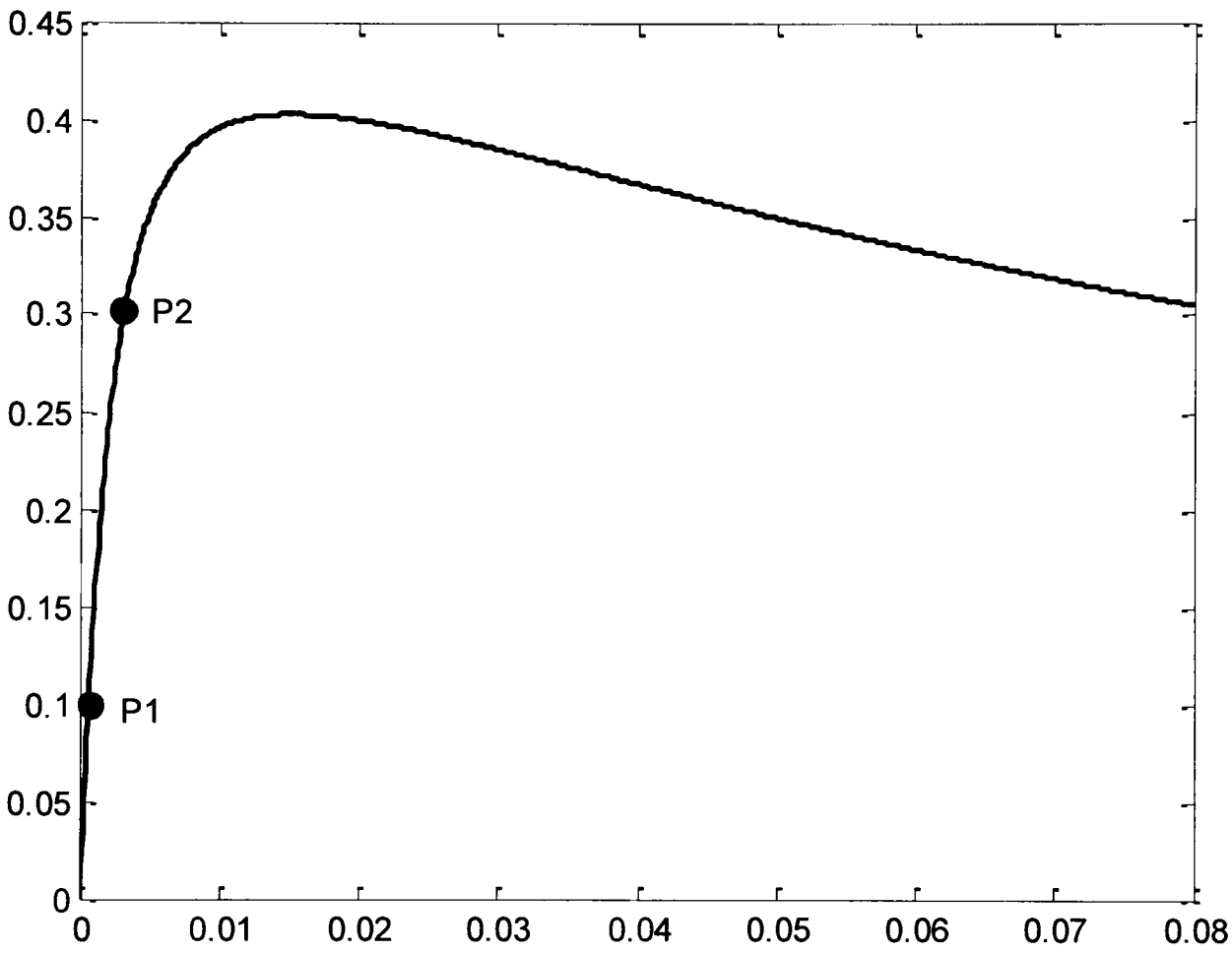

Figure-4.11 Creep curve

First, the estimation is carried out in the linear region of the creep curve (i.e. at operating point P_1). The creep coefficients values at this operating point are calculated as $g_{11}=1.17\times10^{7}$ and $g_{22}=1.1\times10^{7}$. The optimal value of the constant N found through trial and error is -0.13. The process noise covariance matrix Q is set to 6×10^{-9} The results of the state estimation are shown in the following figures (4.12 and 4.13). The design of the filter is based on the small signal mode, so the outputs of the filter show the change in state rather than the actual state.

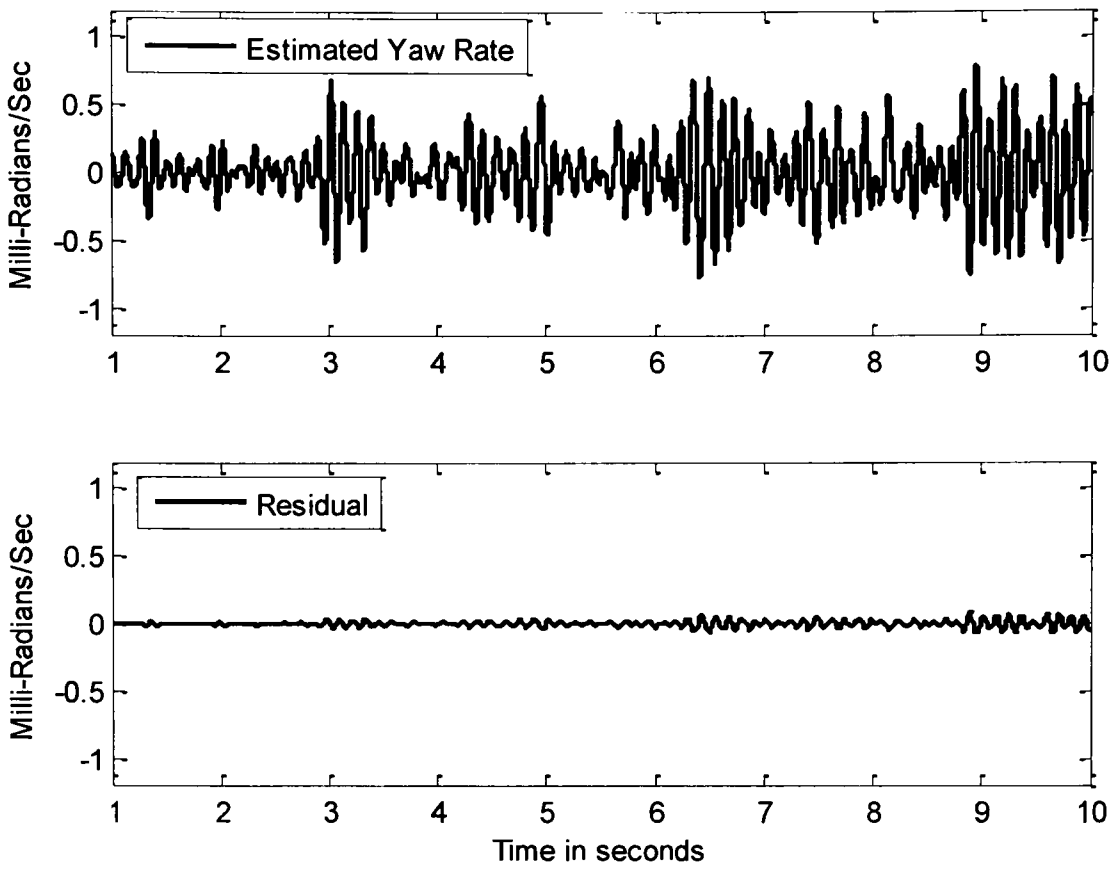

Figure-4.12 Yaw rate ($\Delta\dot{\psi}_w$) estimation at P_1

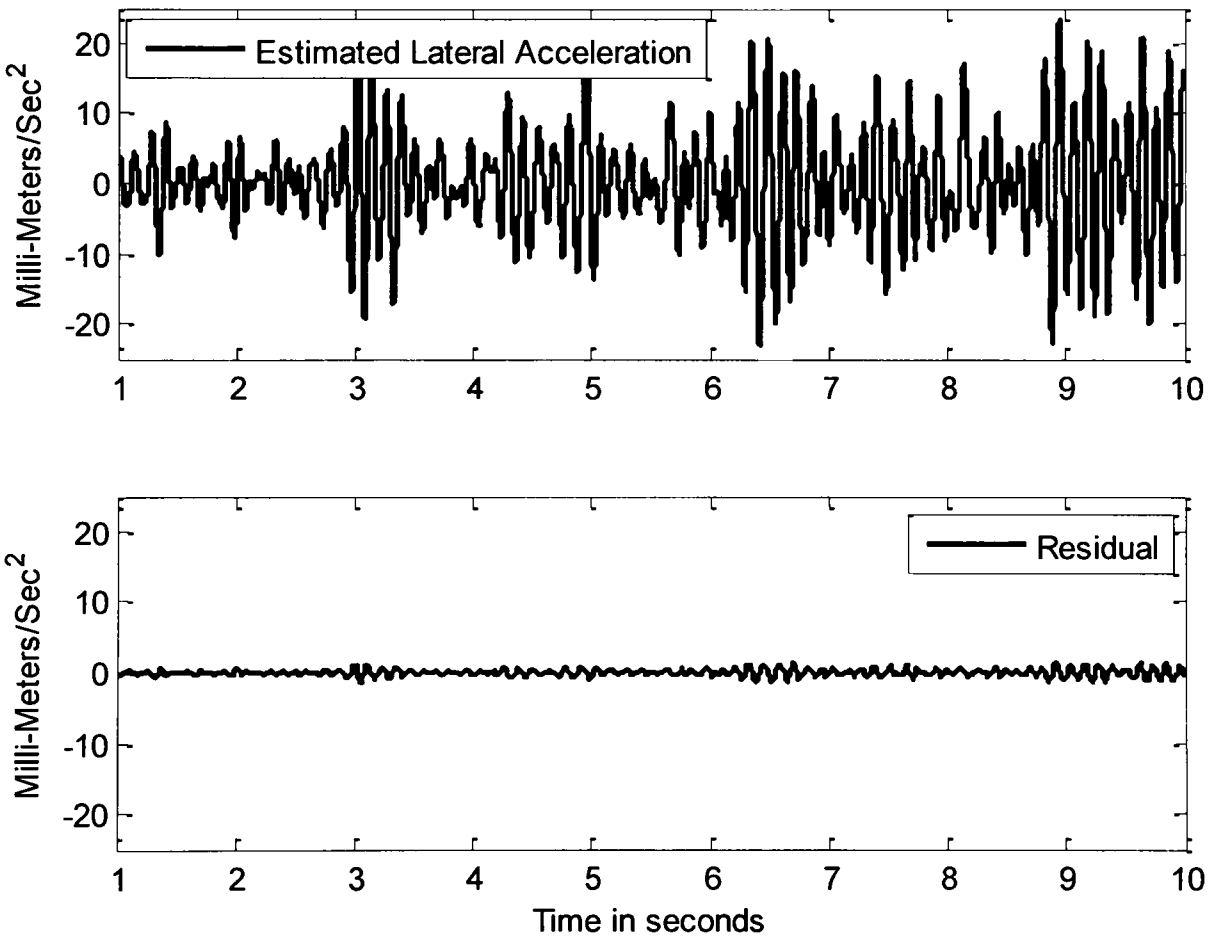

Figure-4.13 Lateral acceleration ($\Delta\ddot{y}_w$) estimation at P_1

The estimation errors for the yaw rate and the lateral acceleration of the wheelset are all very small and hence negligible. At operating point P_2 the values of the creep coefficients are calculated as $g_{11}=2.7\times10^6$ and $g_{22}=6\times10^6$. The best value of N is found as -0.05. The process noise covariance matrix Q is set to 2×10^{-9}

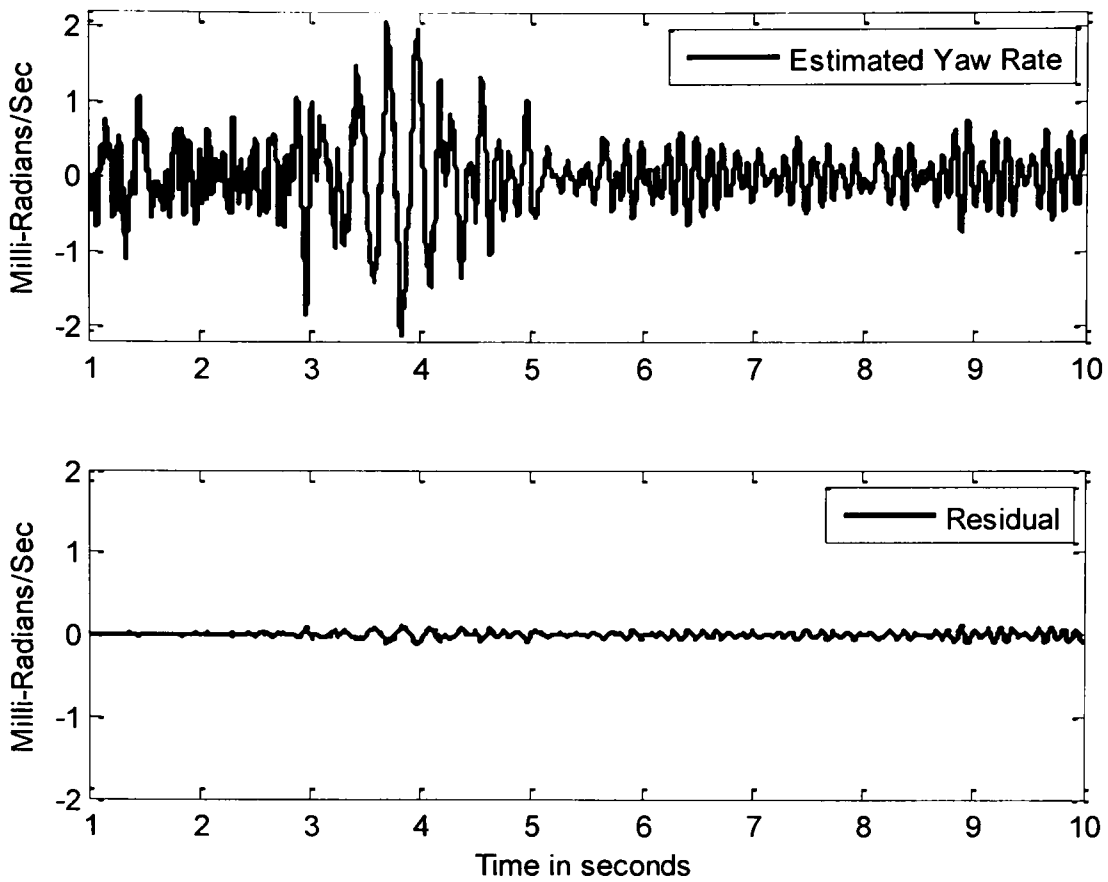

Figure-4.14 Yaw rate ($\Delta\dot{\psi}_w$) estimation at P_2

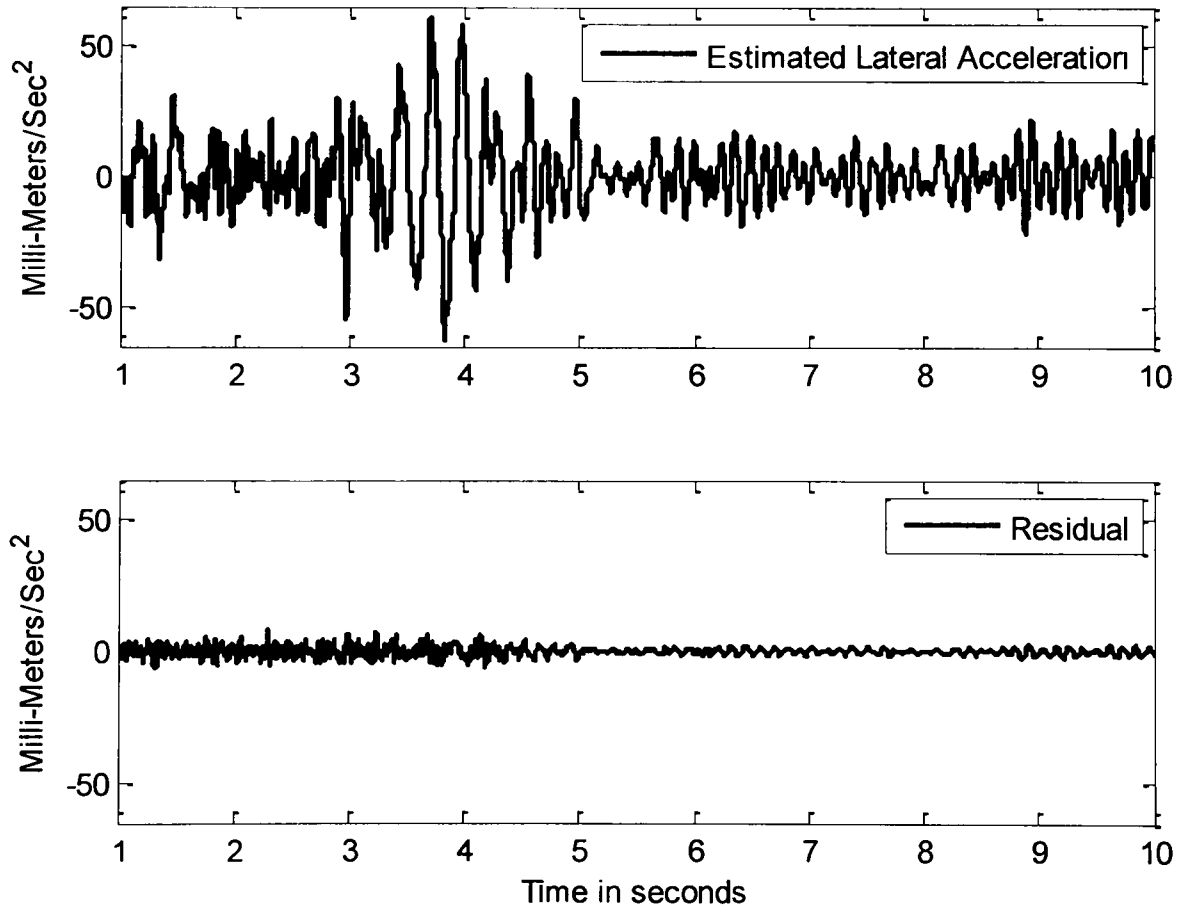

Figure-4.15 Lateral acceleration ($\Delta\ddot{y}_w$) estimation at P_2

Figure-4.14 and 4.15 show the estimation results at operating point P_2. Figure-4.14 shows the yaw rate estimation and the estimation error, which is again very low. The estimated lateral acceleration is shown in Figure-4.15, the estimation error in this case is also small, which proves that a properly tuned Kalman filter can provide a good

estimation of the wheelset states at any specific operating point of the wheelset. As we know, the design of the Kalman filters is based on a small signal model, so a larger error is expected if the Kalman filter tuned at P_1 is operated at P_2 , as shown in the following figure.

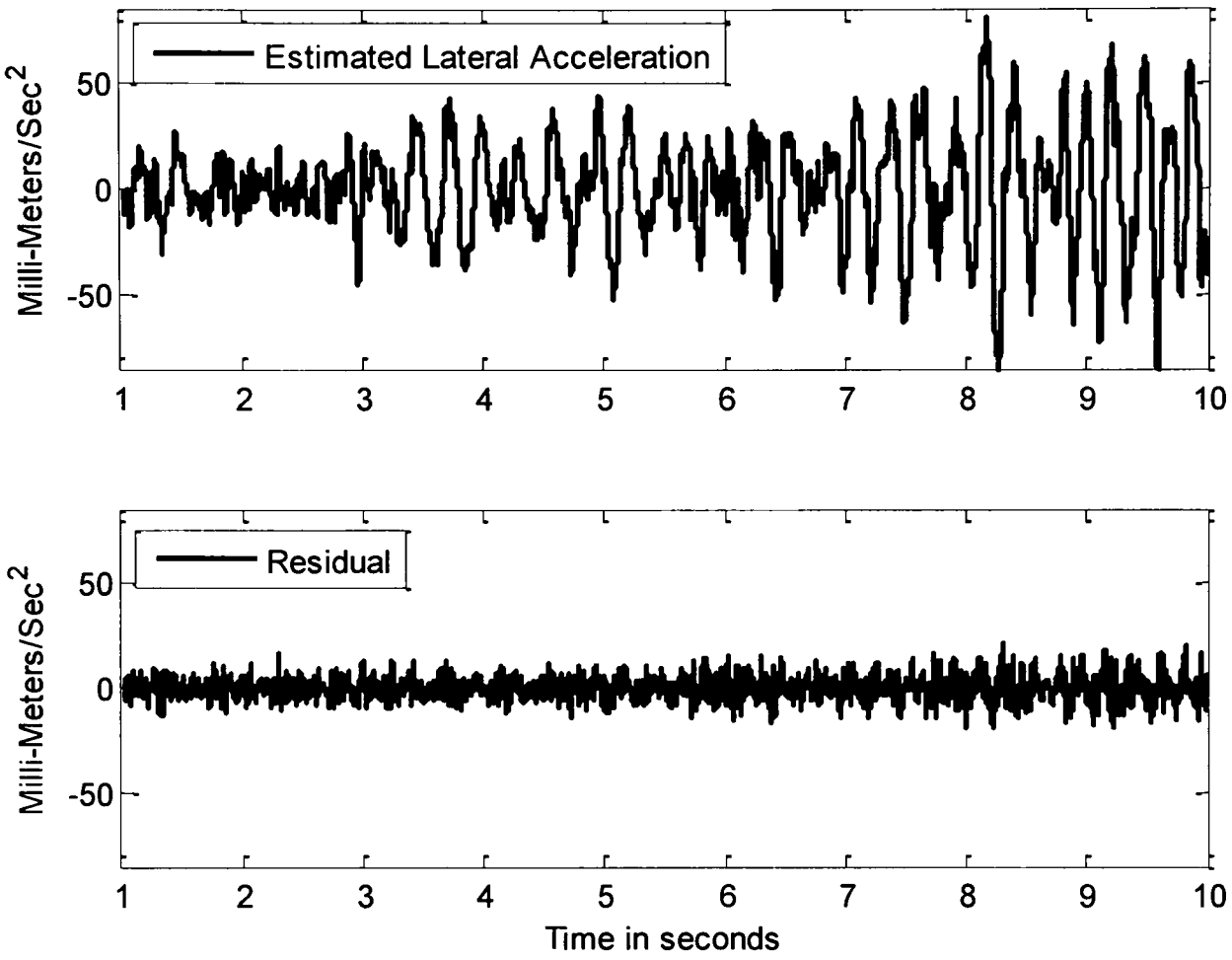

Figure-4.16 Lateral acceleration ($\Delta\ddot{y}_w$) estimation at P_2 by Kalman Filter tuned at P_1

Figure-4.16 shows that the Kalman filter residuals are increased when the operating point of the wheelset is moved away from the point where the Kalman filter is designed to operate. In other words, the operating point of the wheelset is reflected in the values of the residuals.

5. Contact Condition Estimation

Model based estimation uses the knowledge of a system in the form of mathematical model and measured response(s) input to perform real-time estimation of the system parameters of interest [9]. This chapter presents the use of model based detection for estimating wheel rail contact conditions. The detection algorithm is formulated based on the multiple model approach. The multiple model approach has already been applied for detecting faults in vehicle suspension systems [21, 83-84] and other condition monitoring schemes. The proposed scheme is shown in the Figure 5.1.

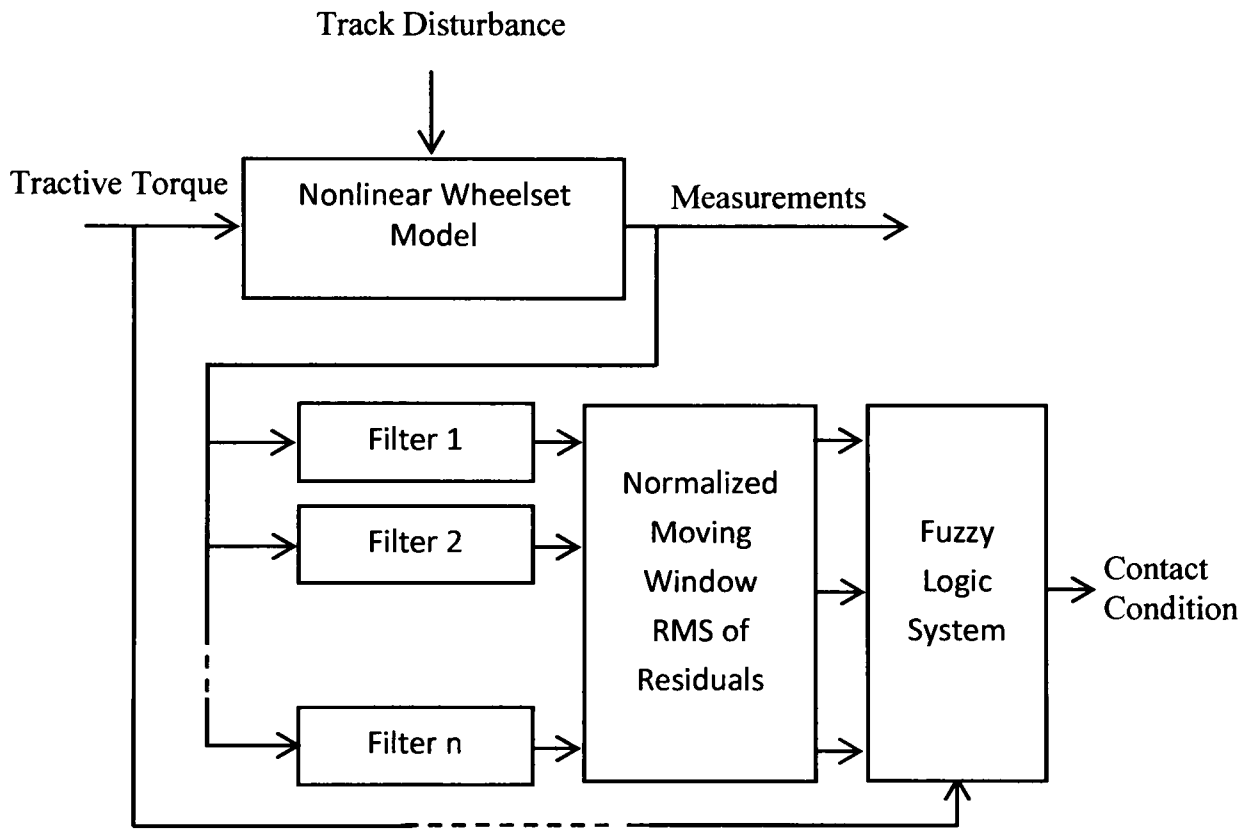

Figure 5.1 Multiple Model Based Estimator

This scheme identifies the contact conditions based on residual signals, which are the differences generated between the observations and the system's mathematical model. In order to simulate the behaviour of an actual wheelset the nonlinear wheelset model introduced in Chapter 3 is used, consisting of the dynamics of the rotational, torsional, lateral, and yaw motions of the wheelset in the presence of an unknown track disturbance in the lateral direction with two sensors measuring the yaw rate and the lateral acceleration. The states of wheelset dynamics in different contact conditions are estimated using different Kalman filters. Each Kaman filter in the filter bank is designed and optimally tuned to operate in a specific contact condition. All the Kalman filters are run in parallel, and the normalized rms values of the residuals with moving time window

(Equation 5.1) are calculated. The rms values of the residuals are then fed into a fuzzy logic system that examines the rms values to identify the contact condition. The design detail and the operation of the fuzzy logic system are discussed in the next chapter.

$$E_{1\_Normalized} = \frac{\frac{1}{\Delta T}\int_{t-\Delta T}^{t}(E_1^2(t)dt}{\sqrt{\left(\frac{1}{\Delta T}\int_{t-\Delta T}^{t}(E_1^2(t)dt\right)^2+\left(\frac{1}{\Delta T}\int_{t-\Delta T}^{t}(E_2^2(t)dt\right)^2+...+\left(\frac{1}{\Delta T}\int_{t-\Delta T}^{t}E_n^2(t)dt\right)^2}} \quad (5.1)$$

where E_1, E_2, and E_3, etc., are residuals of respective filter ΔT is the time window for which the rms value is calculated.

5.1 Basic Idea of the Scheme

This chapter discusses two different designs employed to detect the wheel rail contact conditions using the same basic principle as illustrated in Figure 5.1. One is focussed on the saturation conditions of the creep curves and the other on the different creep coefficient values, as covered in the next two sections. The design aim of the scheme is to not only determine the available adhesion level but also indicate how far the wheelset operating point is from the saturation region. Each creep curve in this design is divided into four sections: linear (P_1), nonlinear away from saturation (P_2), nonlinear near saturation (P_3), and the saturation region (P_4), as shown in Figure 5.3.

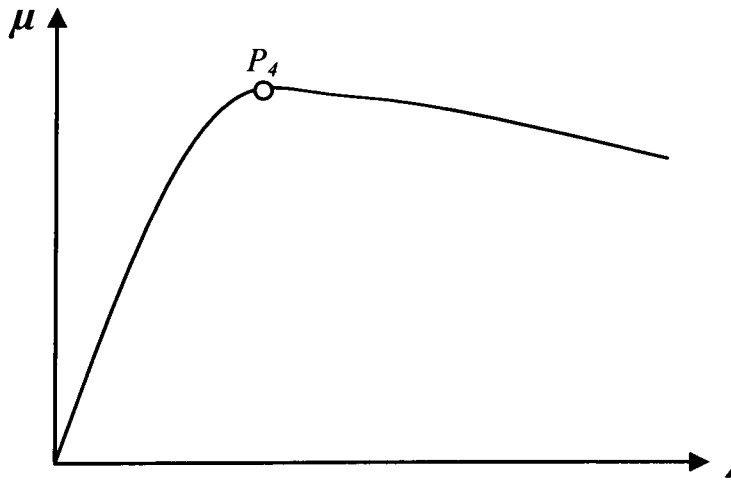

Figure 5.2 Basic Idea of Design I

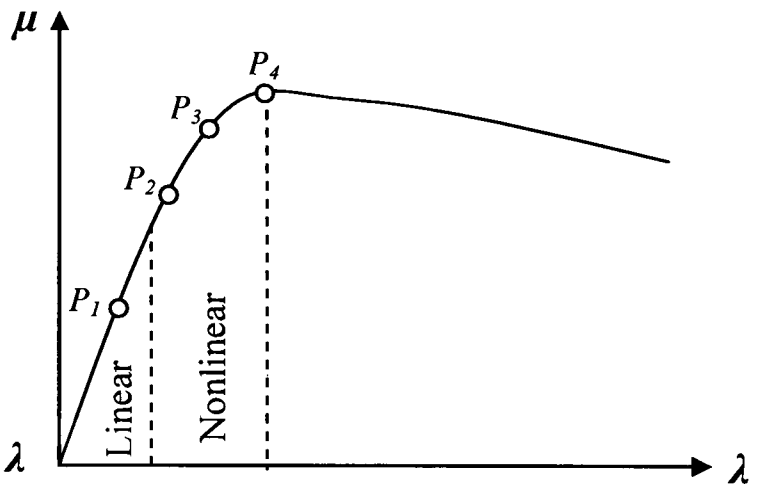

Figure 5.3 Basic Idea of Design II

Figure 5.4 shows the creep curves used for the design and simulation of adhesion detection system. The creep curves are created using a contact force model developed by Polach [136]. This is effectively a curve fitting formula based on experimental results, rather than any physical mechanism [136]. It is described by

$$F = \frac{2Q\mu}{\pi}\left(\frac{k_A\varepsilon}{1+k_A\varepsilon} + \arctan k_S\varepsilon\right)$$

$$\varepsilon = \frac{2}{3}\frac{C\pi a^2 b}{Q\mu}\gamma$$

where Q is the wheel load, C is proportionality coefficient characterising the contact shear stiffness and can be derived from Kalker's linear theory [136] , a and b are the semi-axes of the elliptic contact patch and k_A and k_S are curve tuning parameters.

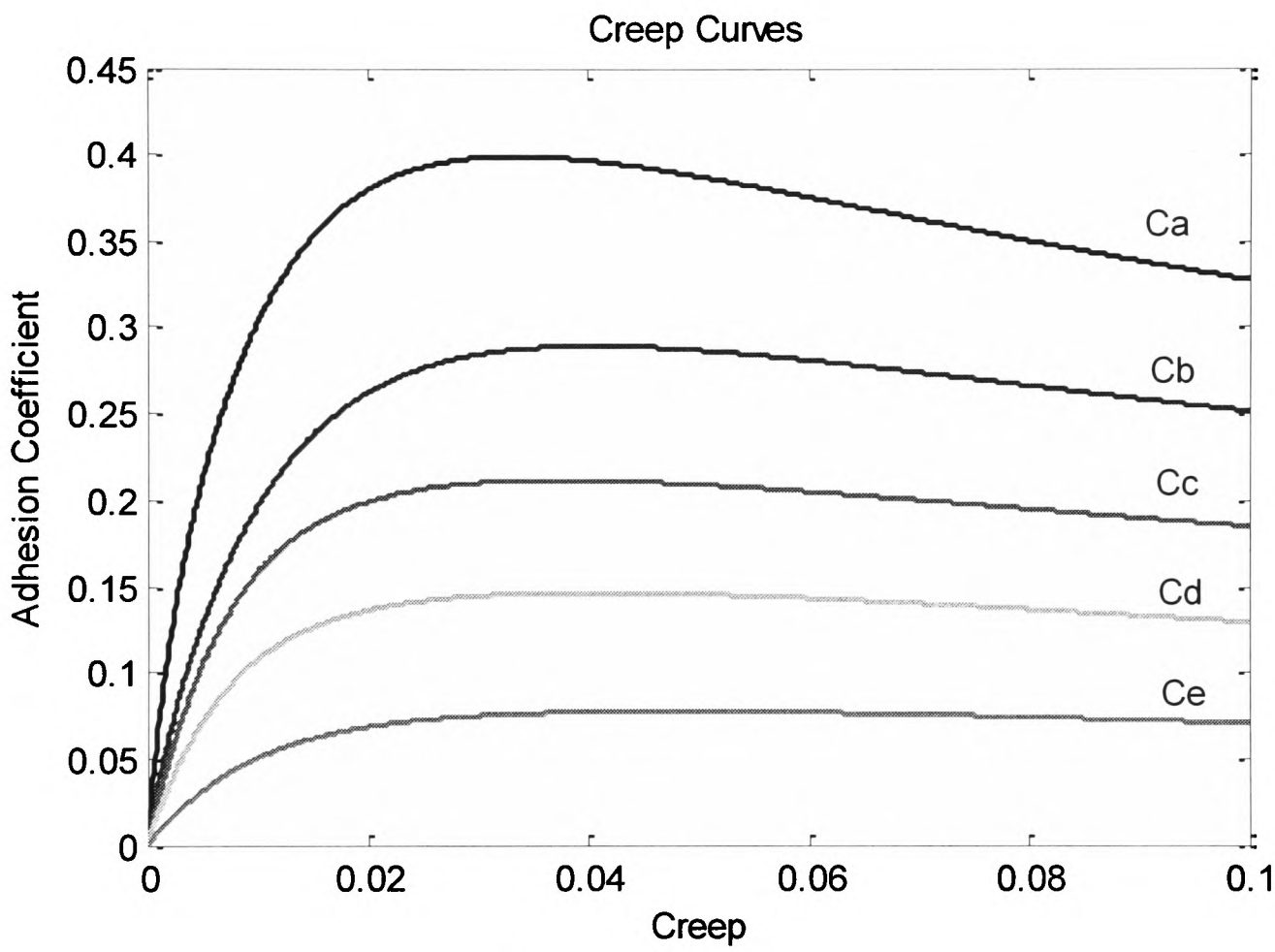

Figure 5.4 Creep Curves

In practice, the creep force decreases with the increase in slip beyond the adhesion limit. This is thought to be the result of the build-up of heat at the contact patch as the creepage increases. This variation is modelled in the Polach model by expressing the μ in terms of the creep velocity, V_c

$$\mu = \mu_o[(1-A)e^{-BV_C} + A$$

where μ_o is the limiting friction coefficient; A and B are curve tuning parameters ($A=\mu_\infty/\mu_o$ is the ratio of the limit friction coefficient at infinite slip velocity to the maximum friction coefficient). The curve shape is tuned using the terms k_A, k_S, μ_o, A and B. Table 5.1 contains the values used to tune the creep curves shown in figure 5.4.

Parameter	Dry (C_a)	Wet (C_b)	Low (C_c)	Very low (C_d)	Very Low (C_e)
k_A	0.7	1	1	0.9	0.8
k_S	0.18	0.4	1	0.7	1
μ_o	0.55	0.4	0.27	0.18	0.1
A	0.4	0.4	0.4	0.1	0.1
B	0.6	0.5	0.4	0.2	0.2

Table 5.1: Curve tuning Parameters

5.2 Contact Condition Estimation (Design I)

In Design I, four Kalman filters are found to be sufficient to detect changes in the contact conditions. The creep curves shown in the figure 5.4 are used as the basis of the study. The Kalman filters are tuned to focus on the saturation region of each creep curve.

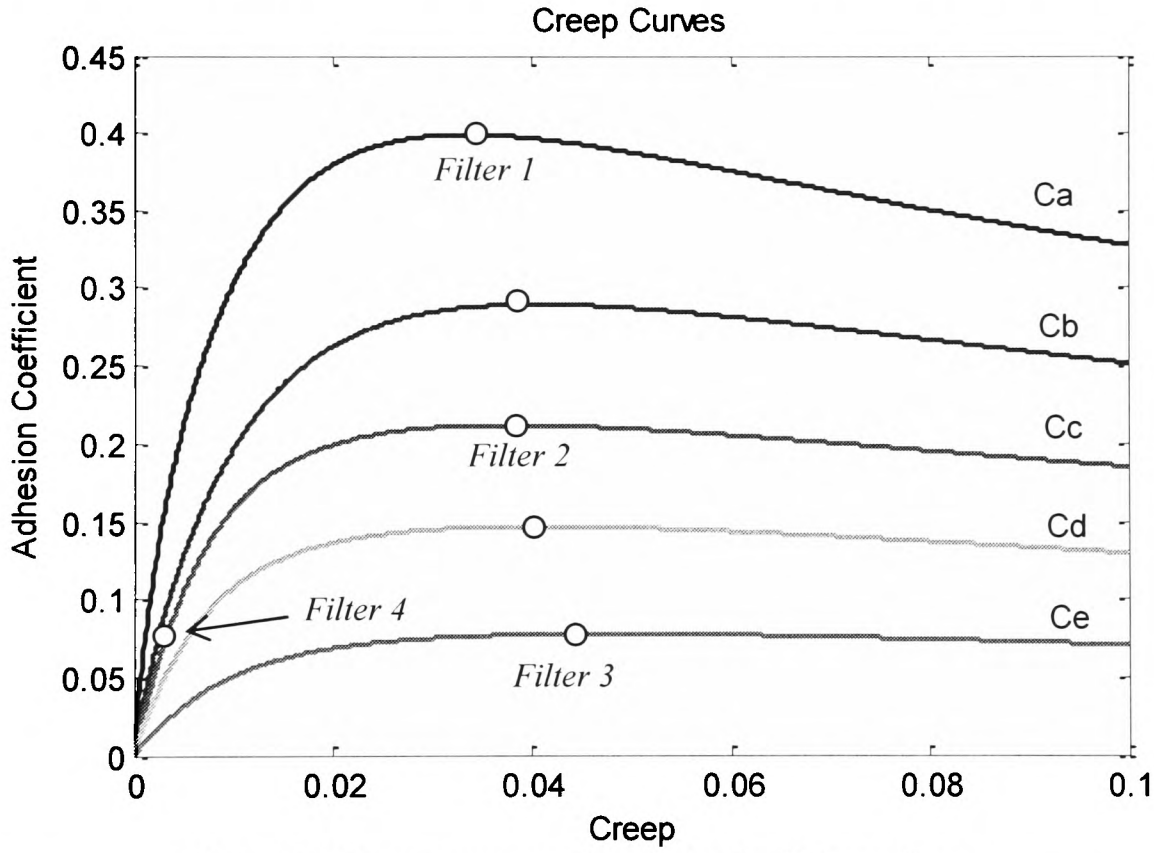

Figure 5.5 Creep curves used to design the Kalman filters

Operating Point	*Slope* $(\frac{d\mu}{d\gamma})$	*Traction Ratio* $(\frac{\mu}{\gamma})$	g_{11}	g_{22}
$\mathbf{P_a}$	0	13	8759	8.67×10^5
$\mathbf{P_b}$	0	7	5320	5.2×10^5
$\mathbf{P_c}$	0	5	4097	4×10^5
$\mathbf{P_d}$	0	3.5	2693	2.6×10^5
$\mathbf{P_e}$	0	1.5	1240	1.2×10^5

Table 5.2: Filter Design Parameters

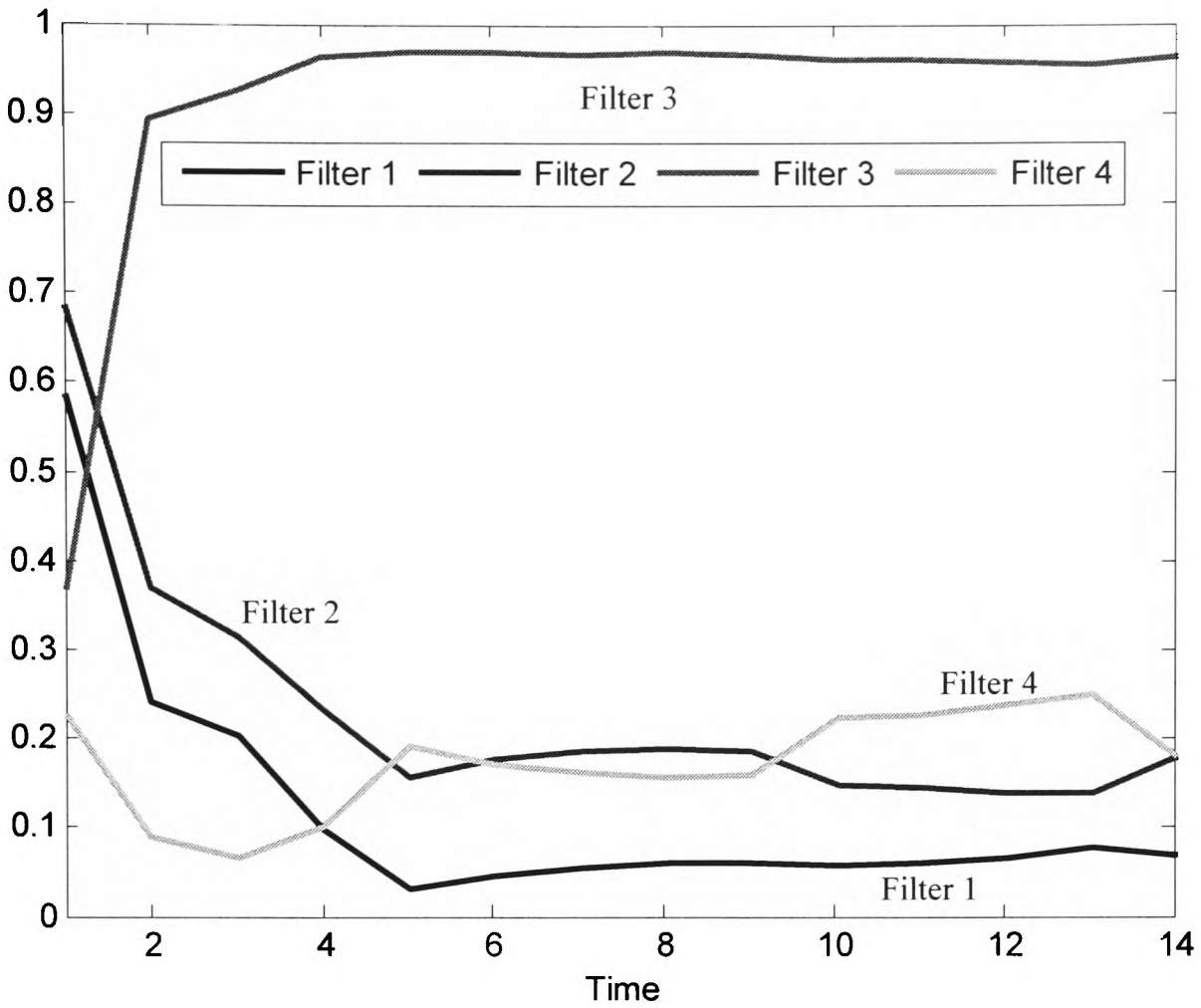

Figure 5.6 Residuals of filters at saturation region of C_a

A filter is tuned at any specific operating point by varying the tuning parameters (Constant N and process noise covariance Q) until the error produced by filter at that point is at lowest. Filter 1 is tuned in such a way that it can operate at the saturation region of creep curve C_a and C_b. Because filter-1 is designed using higher traction ratio therefore, it works well when the adhesion level is more than 30%. Similarly, Filter 2 is designed to operate on the saturation region of creep curve C_c. The design of filter-2 is based on moderate traction ratio values therefore it works well when the adhesion level is between 30% and 15%. Filter 3 is designed to operate on the saturation region of creep curve C_d. It is designed using small values of traction ratio therefore, works well when the adhesion level is less than 15%. Filter 4 is designed to operate in the linear region of creep curve C_b. The purpose of Filter 4 is to identify whether the wheelset is operating in the saturation region of the creep curve. In railway research, it is a normal practice to use computer simulation to study new concepts and/or vehicle designs because of the difficulty and high costs associated with real track testing. Therefore, a Simulink model of the proposed estimation scheme is used for performance assessment. The results of the simulation are presented in the following figures.

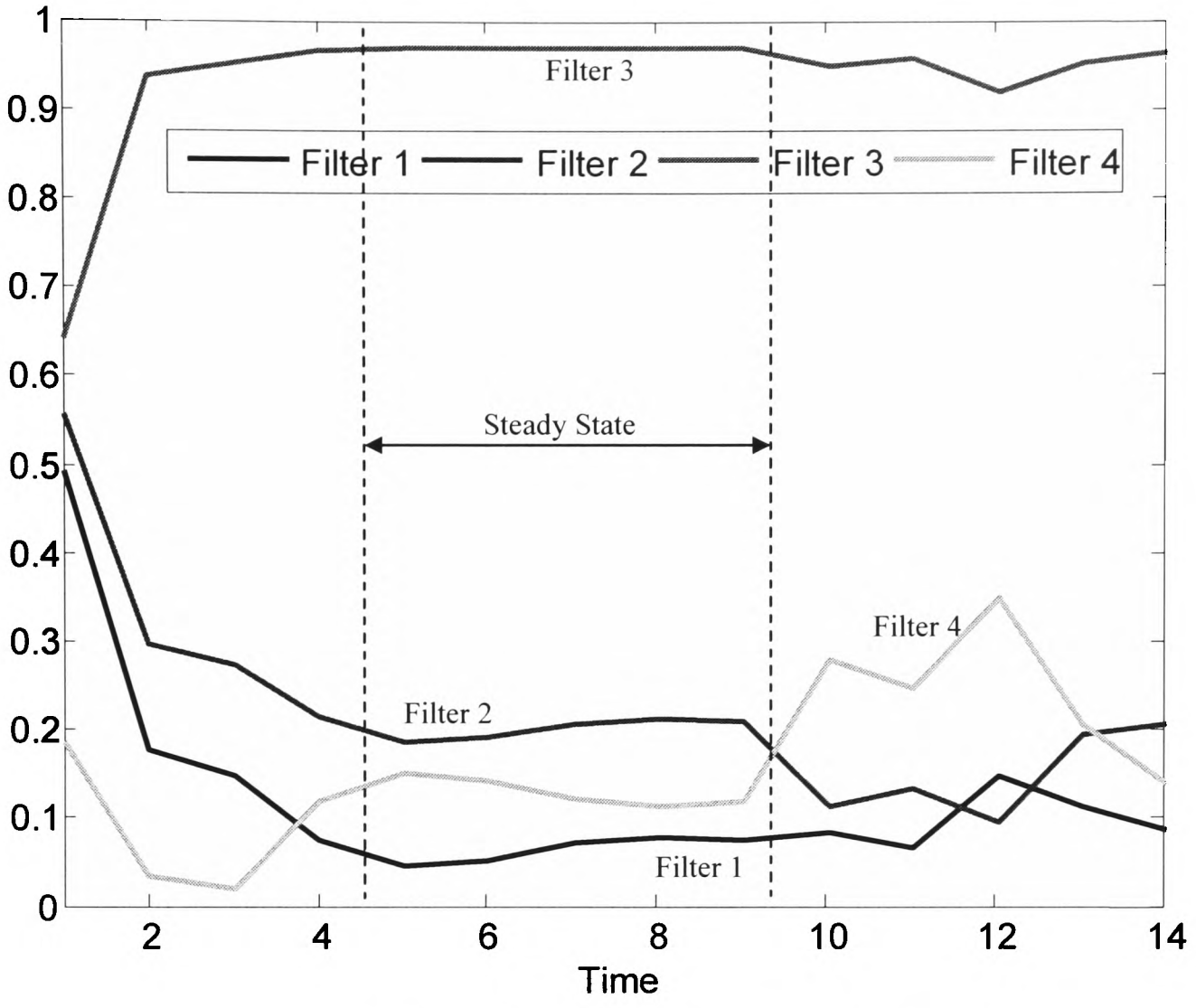

Figure 5.7 Residuals of filters at saturation region of C_b

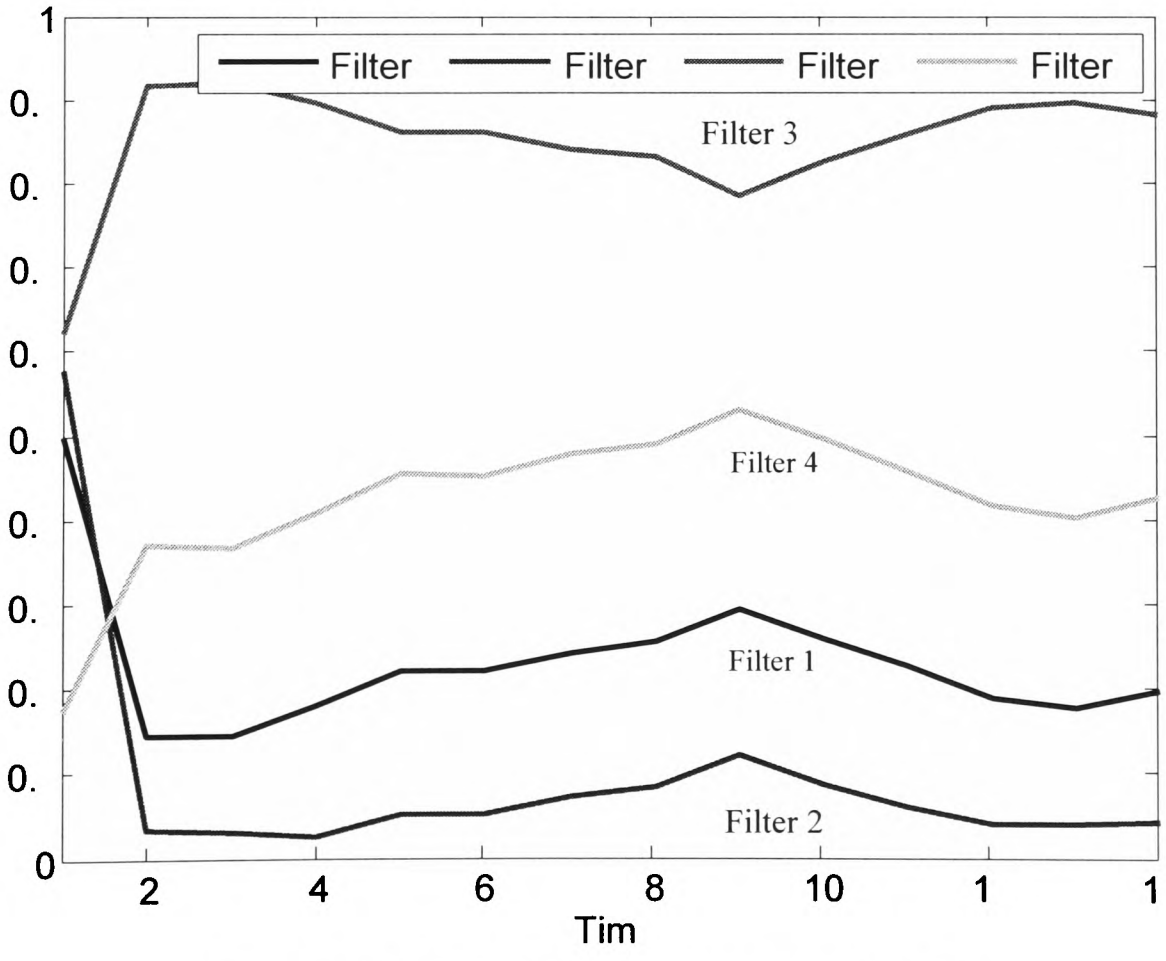

Figure 5.8 Residuals of filters at saturation region of C_C

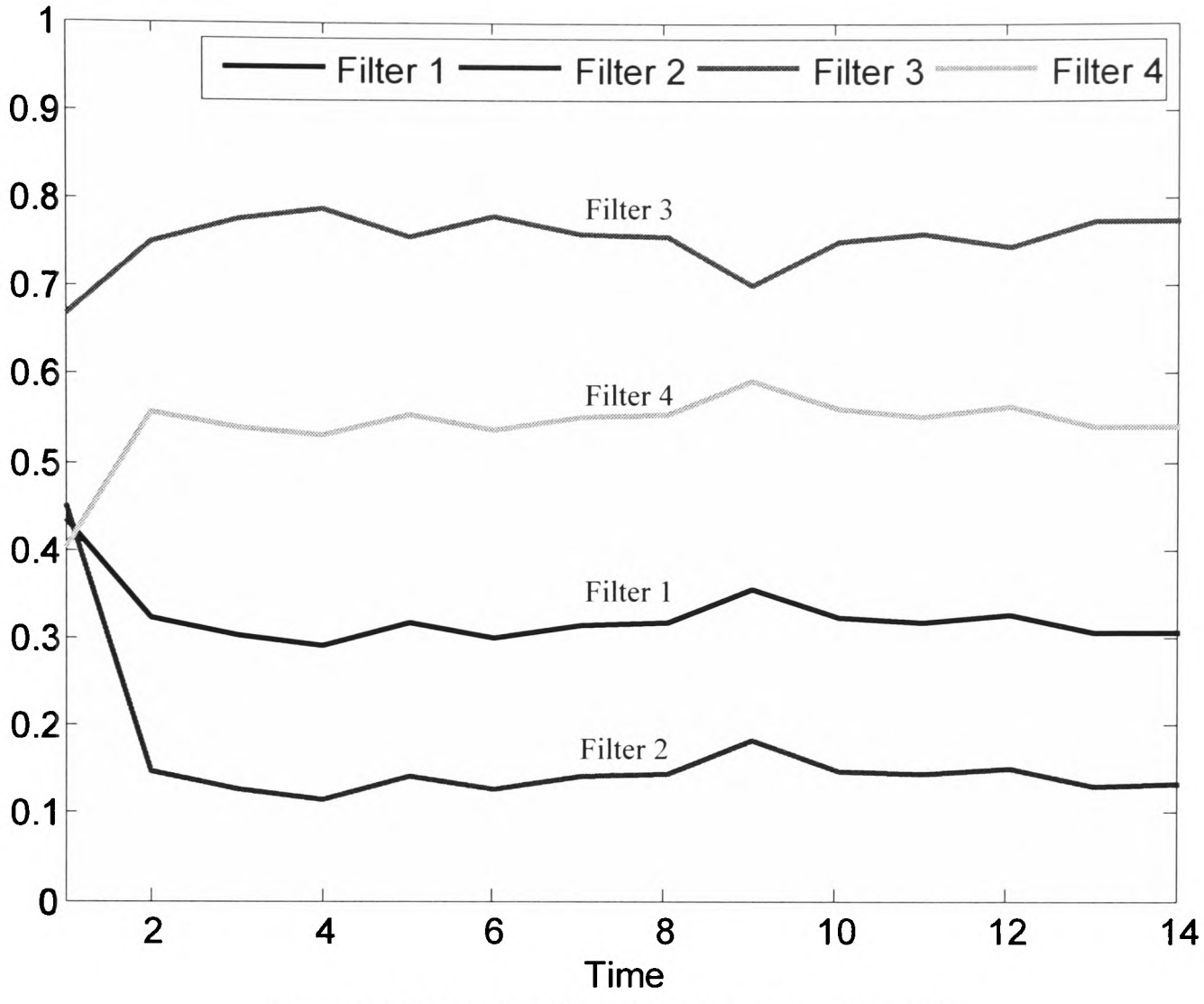

Figure 5.9 Residuals of filters at saturation region of C_d

Figure 5.6 shows the residuals of filters when the wheelset is operated at the saturation region of creep curve C_a. The residual of Filter 1 is minimal, as expected, indicating that the wheelset is operating at the saturation region of creep curve C_a. Similarly, at the saturation of creep curve C_b, the residual of Filter 1 is again minimal but slightly greater than the previous case, as shown in Figure 5.7.

When the wheelset is operated at the saturation point of creep curve C_c, the residual of Filter 2 is minimal, and the residual of Filter 1 is increased, as shown in Figure 5.8. Figure 5.9 shows the residuals of the filters when the wheelset is operated at the saturation region of creep curve C_d. If the wheelset is not operated on the saturation points of the creep curves, the residual of Filter 4 should be minimal. For instance, when the wheelset is operated in the linear region of creep curve C_a, the residual of Filter 4 is minimal, as shown in Figure 5.10. In this way, Filter 4 provides the information to ensure that the wheelset operating point is reached to the saturation point, thus providing a correct determination.

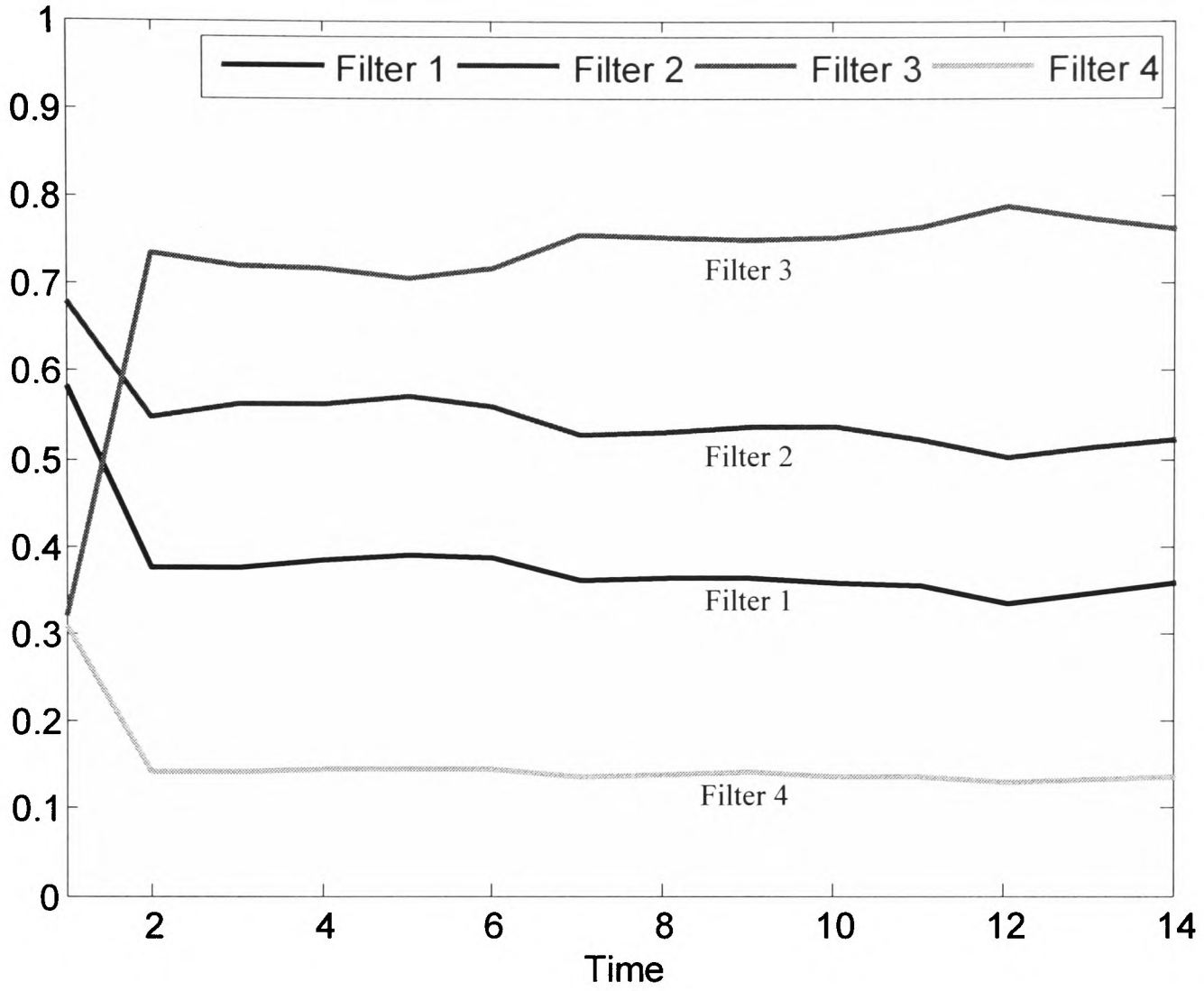

Figure 5.10 Residuals of filters when the wheelset is operated in the linear region of C_a

An analysis of the figures quite clearly presents that each creep curve residual has a different value. In addition, if a generalisation is developed between residual values and creep curves (adhesion level), it would be possible to determine the adhesion level from residual values for verity of other contact conditions that are not included in the Kalman filter design. In order to do so, the model is simulated in various other contact conditions shown by the dotted lines in Figure 5.11, and table 5.3 is developed.

No.	Adhesion (μ%)	Filter 1	Filter 2	Filter 3	Filter 4	Filter with lowest Residual
1	C_a (40%)	0.08	0.2	0.95	0.2-0.3	Filter-1
2	C_f (35%)	0.09	0.2	0.95	0.25-0.35	Filter-1
3	C_b (30%)	0.08	0.2	0.9	0.2-0.4	Filter-1
4	C_c (20%)	0.25	0.1	0.8	0.2-0.6	Filter-2
5	C_d (15%)	0.32	0.12	0. 8	0.6-0.65	Filter-2
6	C_e (10%)	0.48	0.37	0.15	0.7	Filter-3
7	C_g (3%)	0.5	0.4	0.12	0.72	Filter-3

Table 5.3 Residual Values for Design I

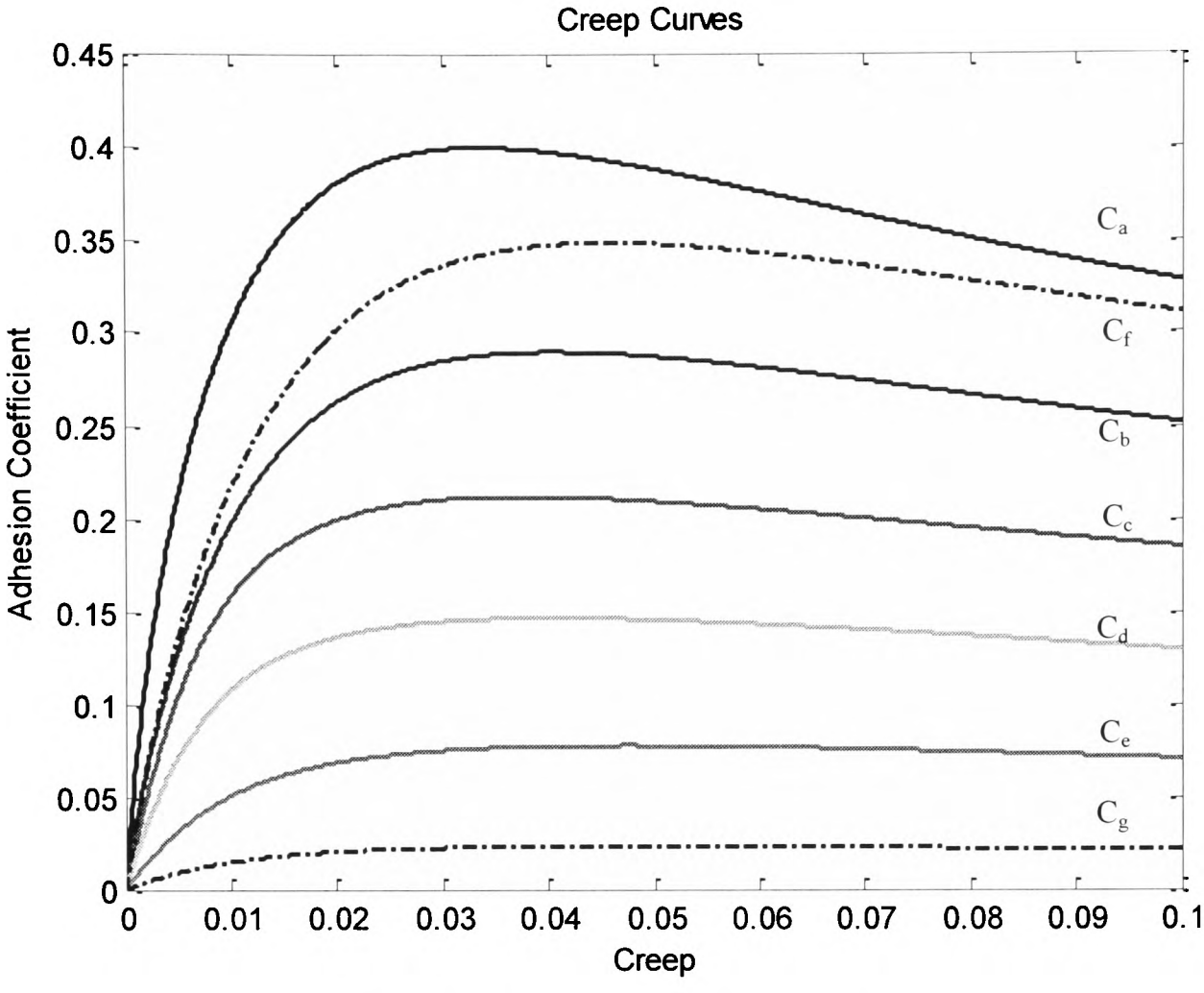

Figure 5.11 Creep Curves to validate proposed idea

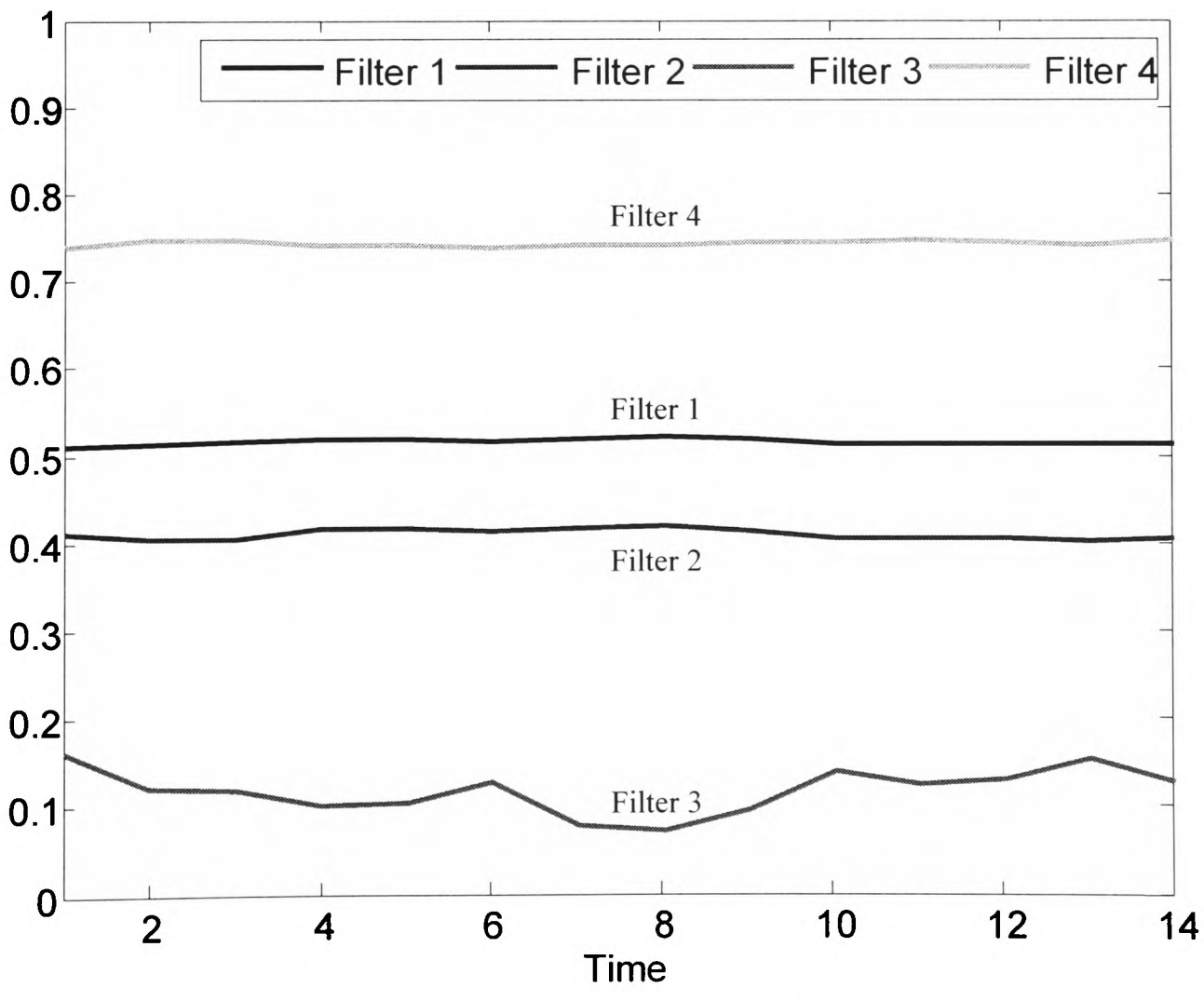

Figure 5.12 Residuals of filters at saturation region of C_g

Figure 5.12 shows the residuals of the filters when the wheelset is operated in the saturation condition of creep curve C_g. At this operating point, the residual of Filter 3 is minimal, which indicates that the wheelset is operated in the contact condition where overall adhesion is less than 5%. The residual values in different contact conditions are summarised in Table 5.3. Which shows when the adhesion level is more than 30% the residual of the filter-1 is at lowest, when the adhesion level is between 30% and 15%, residual of filter-2 is at lowest and when the adhesion level is less than 15% residual of filter-3 is at lowest. The residuals of the Kalman filters vary consistently, as expected. That makes it easier to develop a decision-making system to identify the contact condition by analysing the residuals.

5.3 Contact Condition Estimation (Design II)

In Design II, five different creep curves, shown in figure 5.13, are used as a basis of various levels of contact conditions. Five Kalman filters are used in this design, and each of the estimators is tuned to match one particular track condition to provide the best results at each specific design point. Increased estimation errors are expected if the contact condition is not at or near the chosen operating point. The level of matches/mismatches is reflected in the residuals of the models concerned when compared with the measured wheelset response.

The design of each of the Kalman filters is based on the coefficient values (g_{11} and g_{22}). Therefore, a Kalman filter works well whenever the coefficient values are the same as the linearised model or close to those at the specific operating point it is designed for. In general, coefficients (g_{11} and g_{22}) are high in the linear region of creep curves and are decreased with the slope of the creep curve in the nonlinear region; at the saturation region, g_{11} is nearly zero and g_{22} is also comparatively low. If the design of the Kalman filters is arranged in such a way that some of the Kalman filters are designed in a linear region, some in nonlinear, and some in the saturation region, than it is possible to determine the operating point of the wheelset as well as the contact condition between wheel and rail. It is very important to keep in mind the practical aspects of such design (while choosing number of Kalman filters), otherwise the entirety of the design is useless if it cannot be implemented easily. For this purpose, the behaviour of the Kalman filters is studied thoroughly in different contact conditions while maintaining a view of the practical aspects; thus, only five Kalman filters are used to identify the contact condition.

A table containing the creep coefficients values at different operating points is created and is given below.

Creep Curve	Operating Point	g_{11}	g_{22}
C_a	P_1	7.3×10^6	4.6×10^6
	P_2	8.3×10^5	2.2×10^6
	P_3	6.2×10^5	1.7×10^6
	P_4	8814	8.67×10^5
C_b	P_1	2.2×10^6	2.2×10^6
	P_2	1×10^6	1.4×10^6
	P_3	4×10^5	1×10^6
	P_4	5320	5.2×10^5
C_c	P_1	1.8×10^6	1.8×10^6
	P_2	9.2×10^5	1.2×10^6
	P_3	8×10^5	9×10^5
	P_4	4097	4×10^5
C_d	P_1	1.2×10^6	1.2×10^6
	P_2	4.7×10^5	8.4×10^5
	P_3	2×10^5	6×10^5
	P_4	2693	1.2×10^5
C_e	P_1	5×10^5	5×10^5
	P_2	2.5×10^5	3.7×10^5
	P_3	1×10^5	2.7×10^5
	P_4	1240	1.2×10^5

Table 5.4: Creep Coefficients at different points on creep curves

It can be seen from the table 5.4 that the filter designed at any operating would work at multiple curves if the creep coefficient values are similar. Therefore after a thorough study of table 5.4, Filter 1 is tuned in the linear region of creep curve C_a ($g_{11}=7.3\times10^6$, $g_{22}=4.6\times10^6$), the coefficient values for the design of Kalman Filter 2 are $g_{11}=8.3\times10^5$ and $g_{22}=2.2\times10^6$. Filter 3 is designed to operate in the linear region of creep curves C_b and C_c ($g_{11}=2.2\times10^6$, $g_{22}=2.2\times10^6$); Filter 4 is designed to operate on the saturation region of creep curves C_a and C_b ($g_{11}=8814$, $g_{22}=8.67\times10^5$); and Filter 5 is designed to operate in the nonlinear region of creep curve C_e ($g_{11}=2.5\times10^5$, $g_{22}=3.7\times10^5$). Any other combination of the points can also be chosen to design filters that will change the tuning parameters and the structure of the fuzzy logic system accordingly. Simulations are carried out using a variety of different contact conditions, as represented by the creep curves shown in Figure 5.12. The results of the simulation are discussed in following sections.

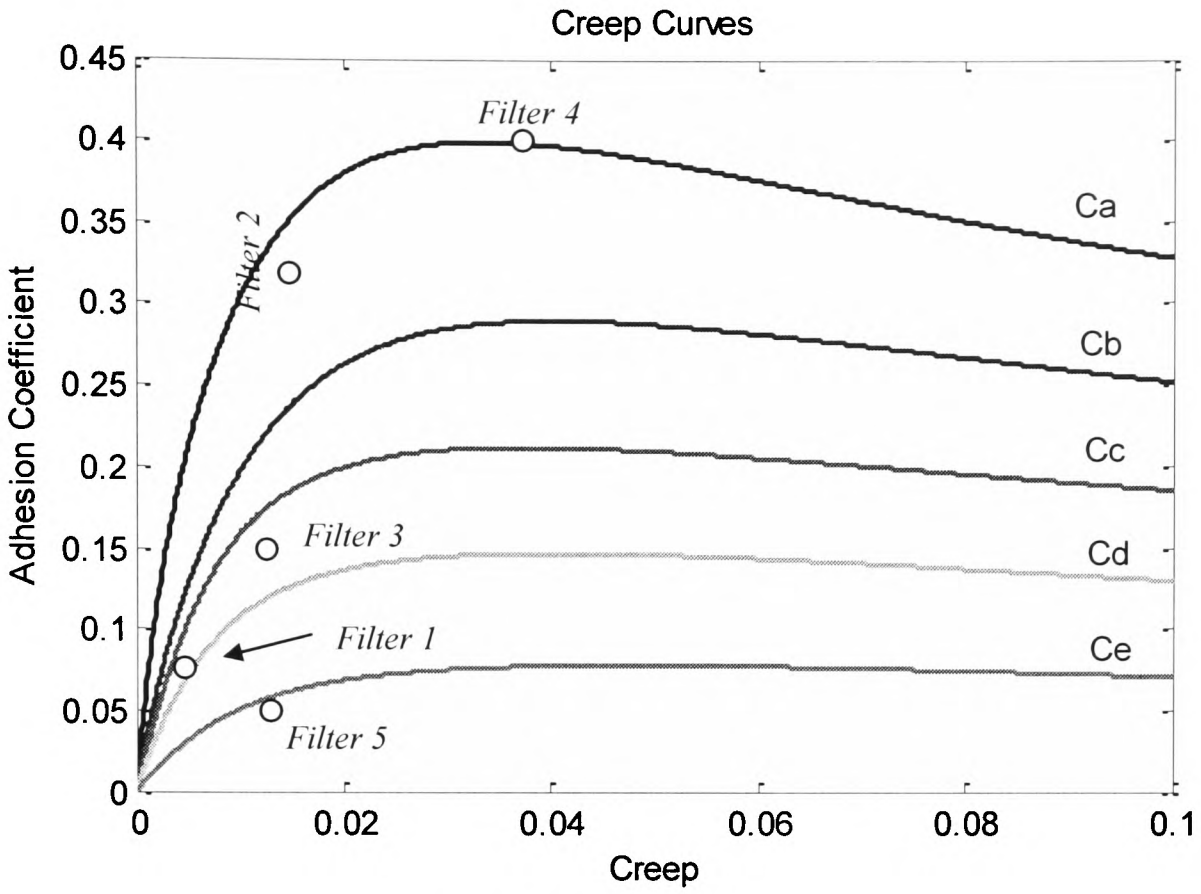

Figure 5.13 Creep Curves

5.3.1 Case 1 (Simulation Using Creep Curve C_a)

As discussed earlier, linear region, nonlinear region away from saturation, nonlinear region near saturation, and the saturation region on any creep curve would be regarded as P_1, P_2, P_3, and P_4, respectively. In Case 1, creep curve C_a is used for simulation, and the wheelset is operated on different operating points to assess the variation in the residuals.

In Figure 5.14, the wheelset is operated in the linear region; therefore, the residual of Filter 1 is minimal because the filter is optimally tuned to operate at this point. Similarly, in Figure 5.15, when the operating point of the wheelset is moved up on the creep curve by application of the tractive torque, the residual of Filter 1 starts to increase and the residuals of Filter 2, Filter 3, and Filter 4 start to decrease, indicating that the operating point is moving away from P_1 and progressing towards the nonlinear region. As the tractive torque is increased further, the operating point of the wheelset is moved further away from P_1, and it reaches the nonlinear region where the residual of Filter 3 is minimal, the residual of Filter 4 is decreasing, and the residuals of Filter 1 and Filter 2 are increasing, indicating that the wheelset is operating in the nonlinear region of the creep curve and is near the saturation point. The residuals are shown in Figure 5.16.

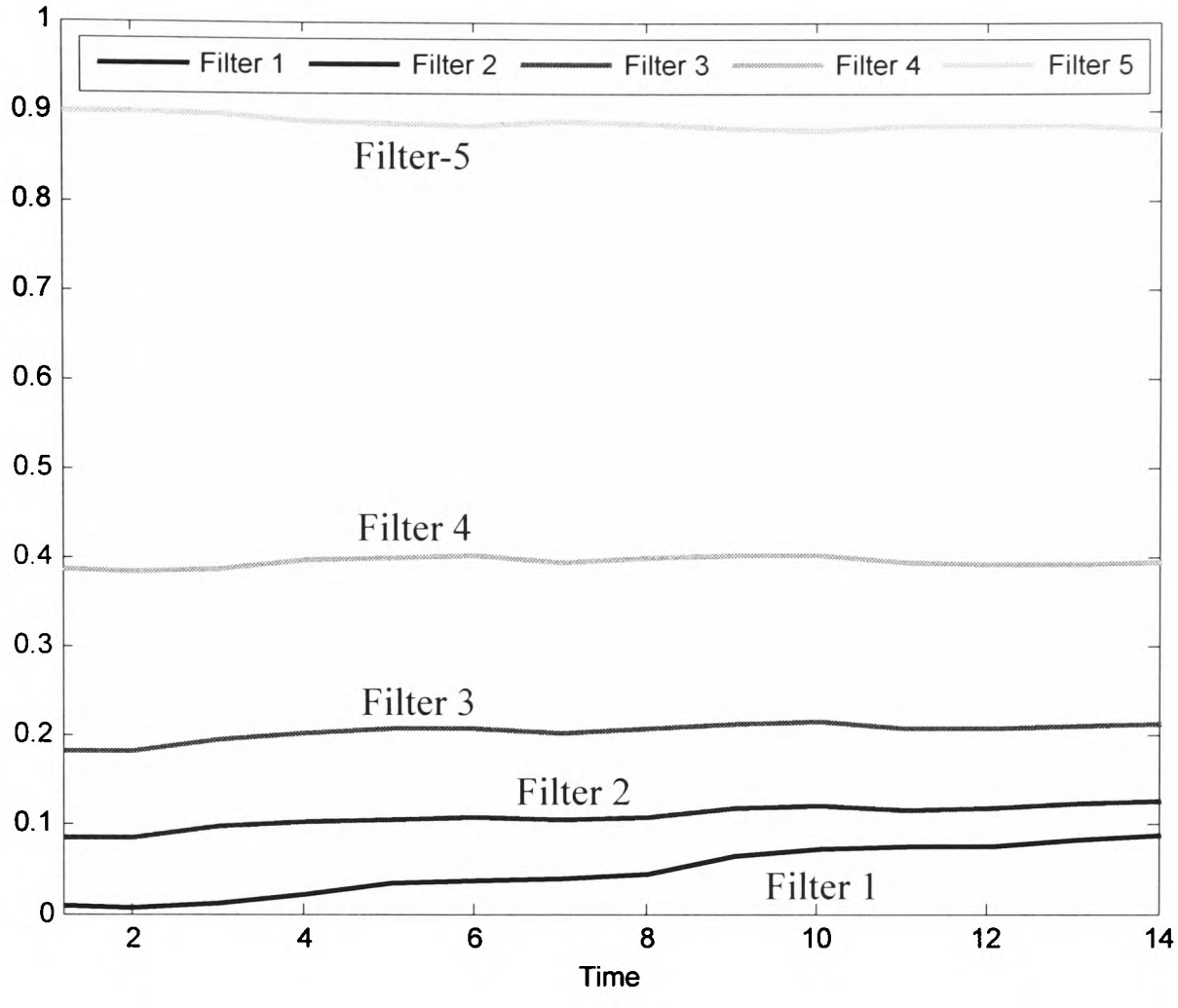

Figure 5.14 Residuals of the filters at P_1 of C_a

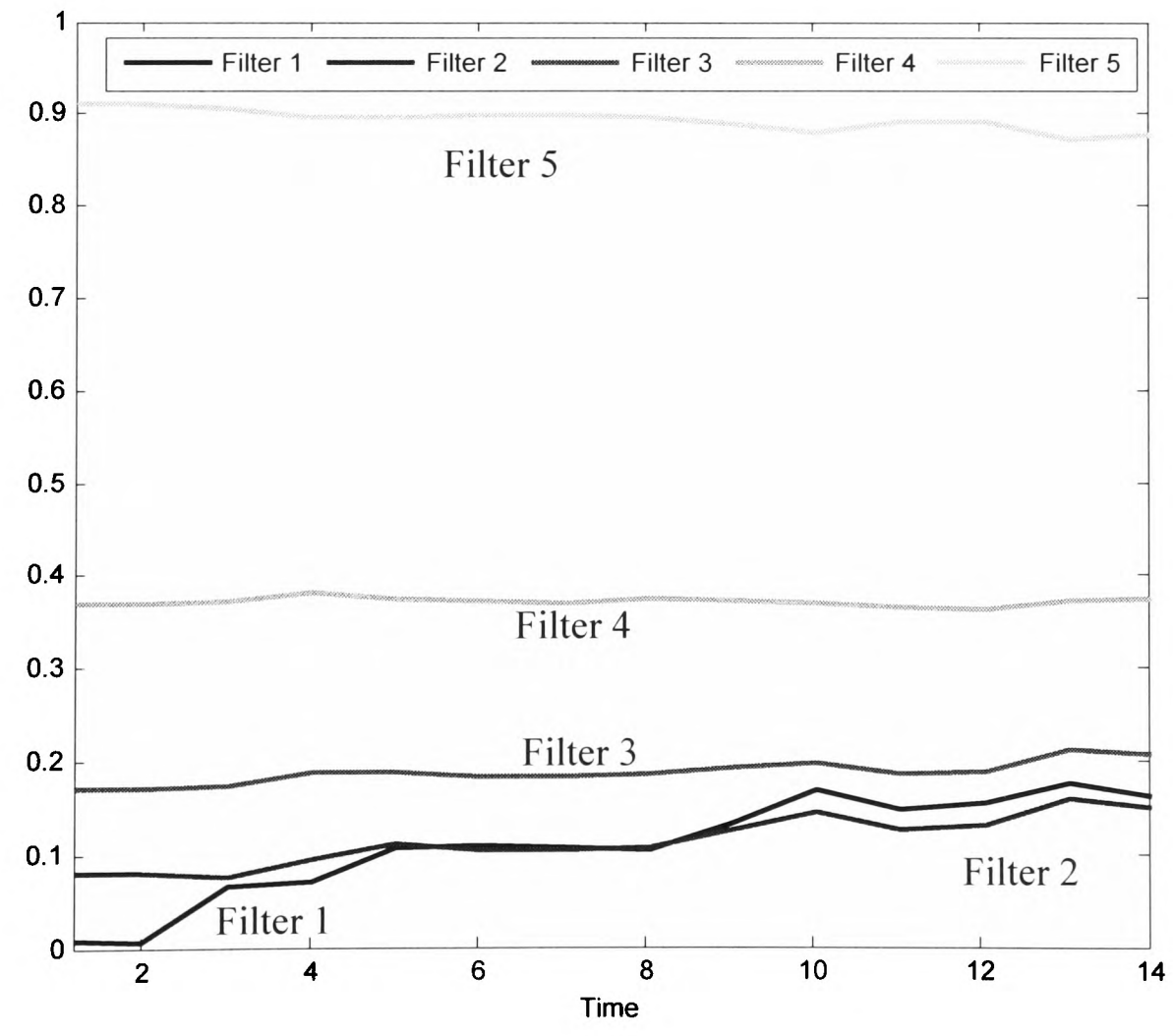

Figure 5.15 Residuals of the filters at P_2 of C_a

Figure 5.17 shows the residuals of filters when the wheelset is operated at the saturation region. However, this time the residuals take some time to settle down because of the time taken in the simulation to drive the wheelset to the desired operating point. It takes approximately five seconds to maintain the steady value of the torque, and the residuals are settled to a steady value after six seconds because of the one-second time window. The residual of Filter 4 is minimal because it is designed to operate at this point; residuals of other filters are also changed accordingly. Conclusively, it is clear that the residual of each filter tends to produce the lowest residual when the wheelset is operated at the point where it is optimally tuned to operate, and it increases gradually when the operating point is moved away from that point.

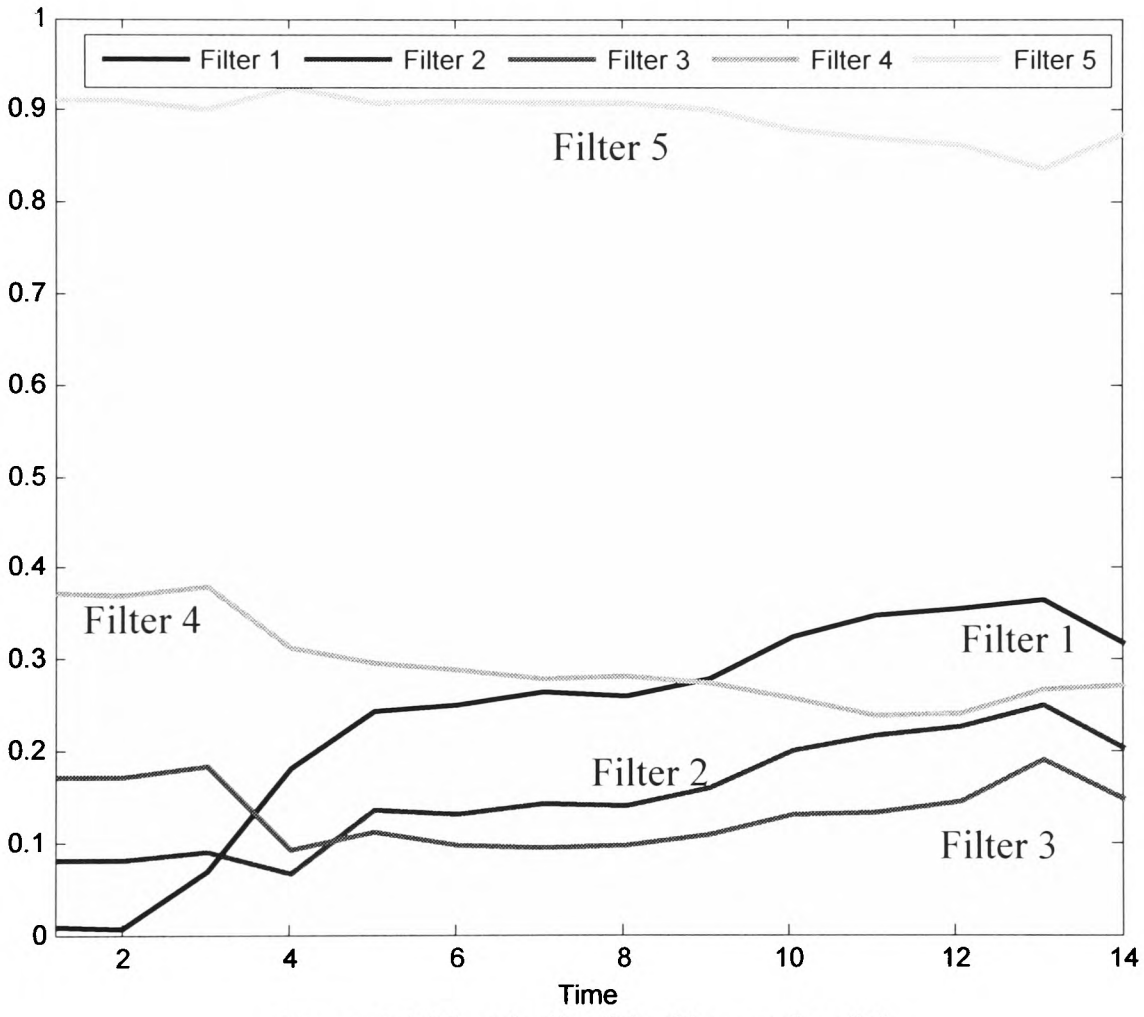

Figure 5.16 Residuals of the filters at P_3 of C_a

When the wheelset is operated on operating points other than these designated four points, then the operating point can be identified by analyzing the combination of the residual values. For instance, Figure 5.18 shows the residual values when the wheelset is operated on a point located between P_3 and P_4. From Figure 5.16 and Figure 5.17, we know that when the wheelset is operated at P_3, the residual of Filter 3 is minimal and when the wheelset is operated at P_4, the residual of Filter 4 is minimal; the similar residual values of Filter 3 and Filter 4 indicate that the wheelset is operating at an operating point located in the middle.

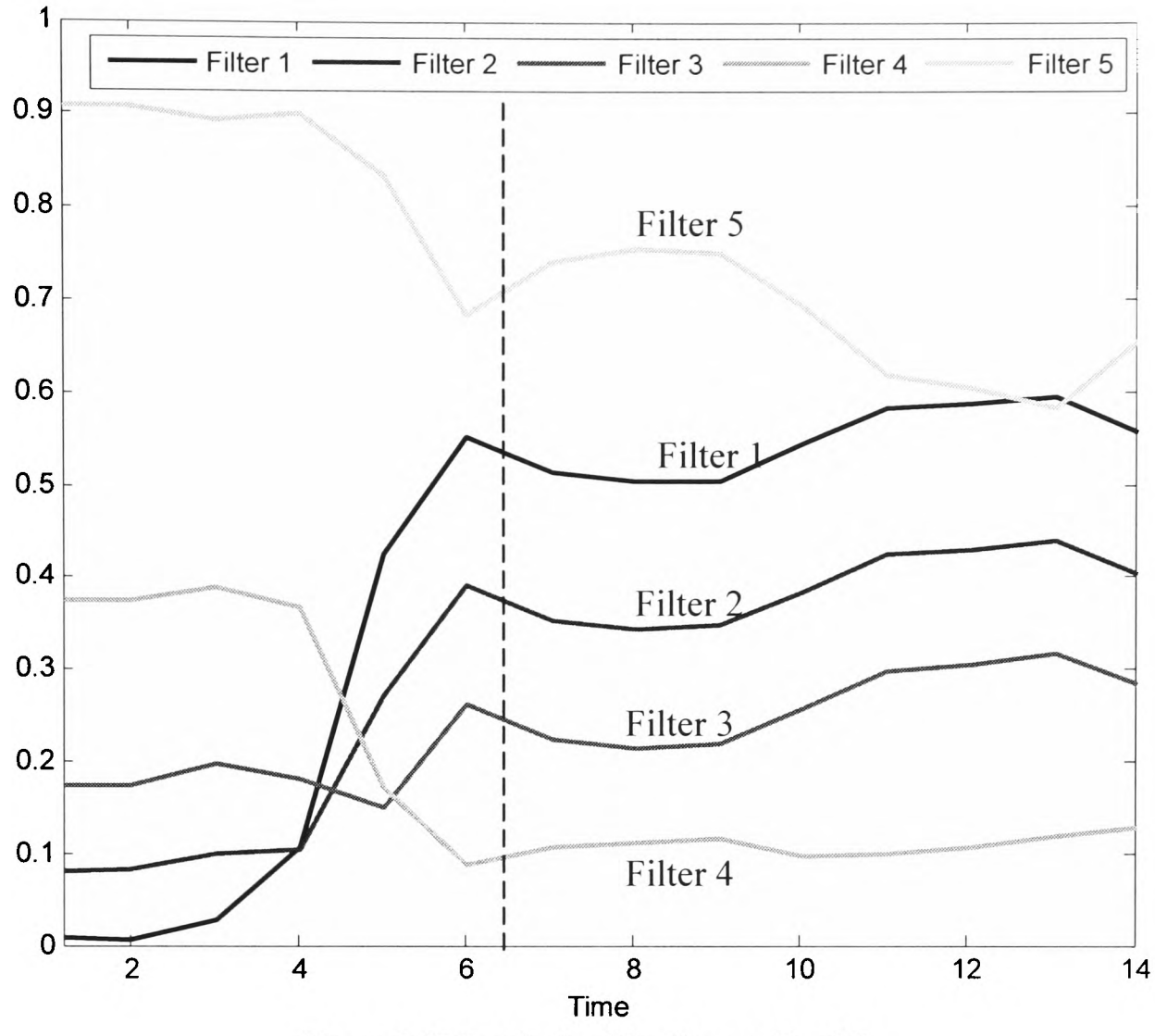

Figure 5.17 Residuals of the filters at P_4 of C_a

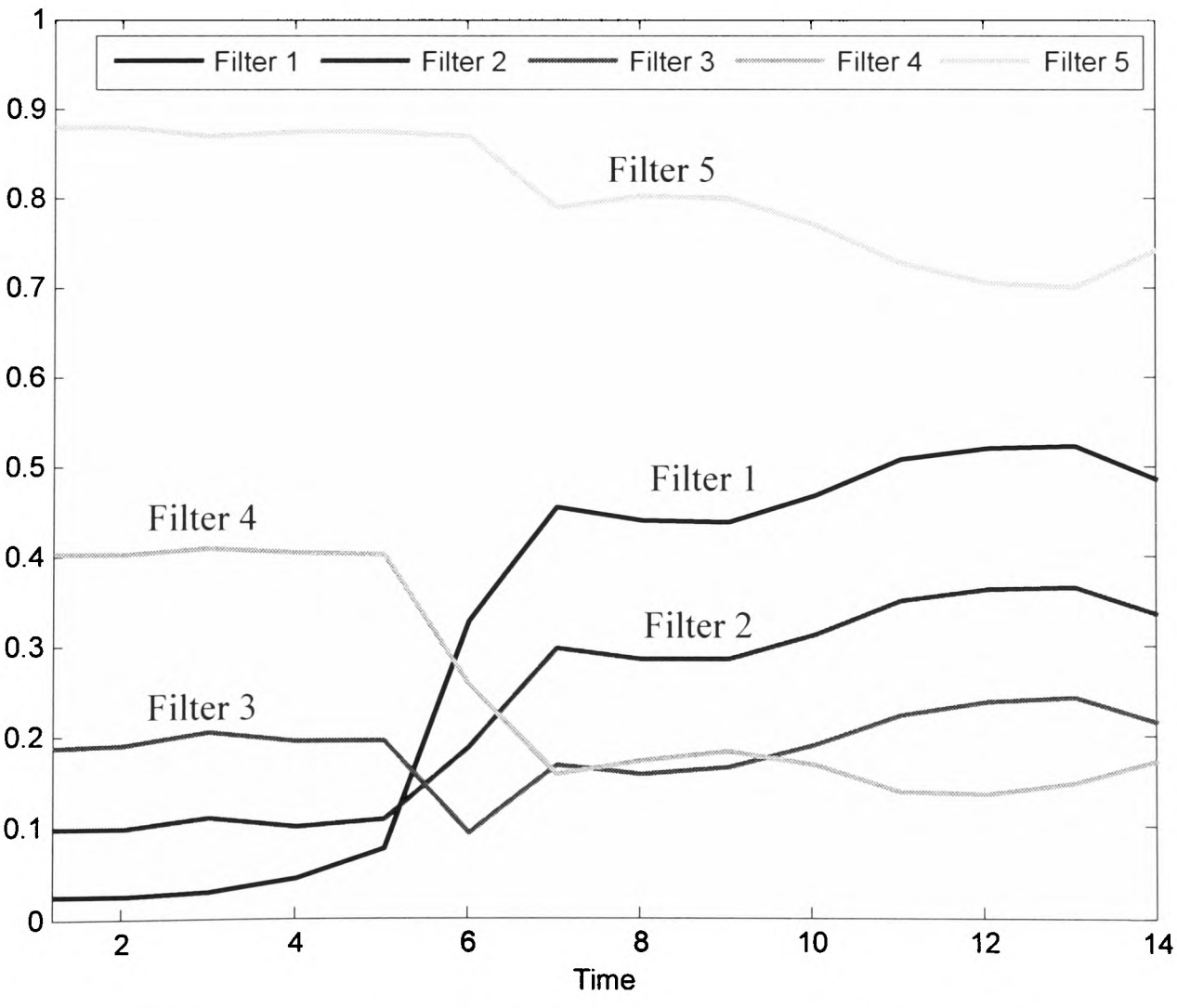

Figure 5.18 Residuals of the filters at point located between P_3 and P_4 on C_a

5.3.2 Case 2 (Simulation using Creep Curve C_c)

In this case, creep curve C_c is used in simulation. The wheelset is simulated on several operating points on C_c, and the results of the simulation are presented below.

Figure 5.19 shows the residuals when the wheelset is operated at P_1. The residual of Filter 3 is minimal because Filter 3 is designed to operate at this point. When the tractive torque is increased to force the operating condition of the wheelset to move to P_2, the residual of Filter 3 is increased (Figure 5.20), indicating that the operating point of the wheelset is moving away from the linear region. With the application of the tractive torque, the residual of Filter 3 continues to increase, and the residual of Filter 4 is decreased; the residuals of the other filters are also affected accordingly. Figure 5.22 shows the residuals of the filters at the saturation point. During the steady state, the residual of Filter 4 is minimal, which indicates that the wheelset is operated at the saturation point. In some cases (e.g., Figure 5.20 and Figure 5.21), it is difficult to differentiate the two operating points because the difference in residual values is very small. This happens when the two operating points located on different creep curves have the similar dynamic responses. In such cases, the tractive torque can be analyzed to distinguish between the two operating points.

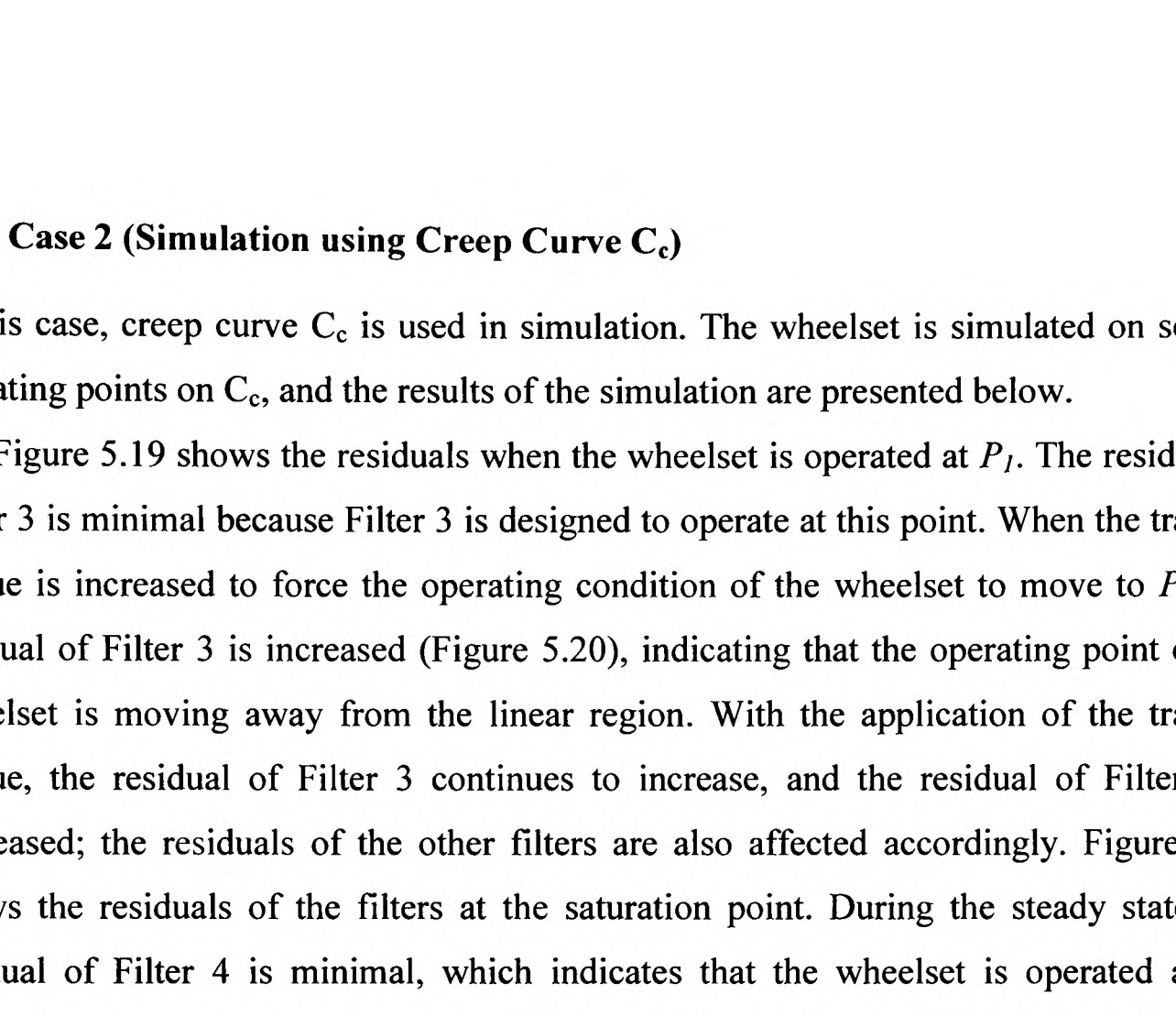

Figure 5.19 Residuals of the filters at P_1 on C_c

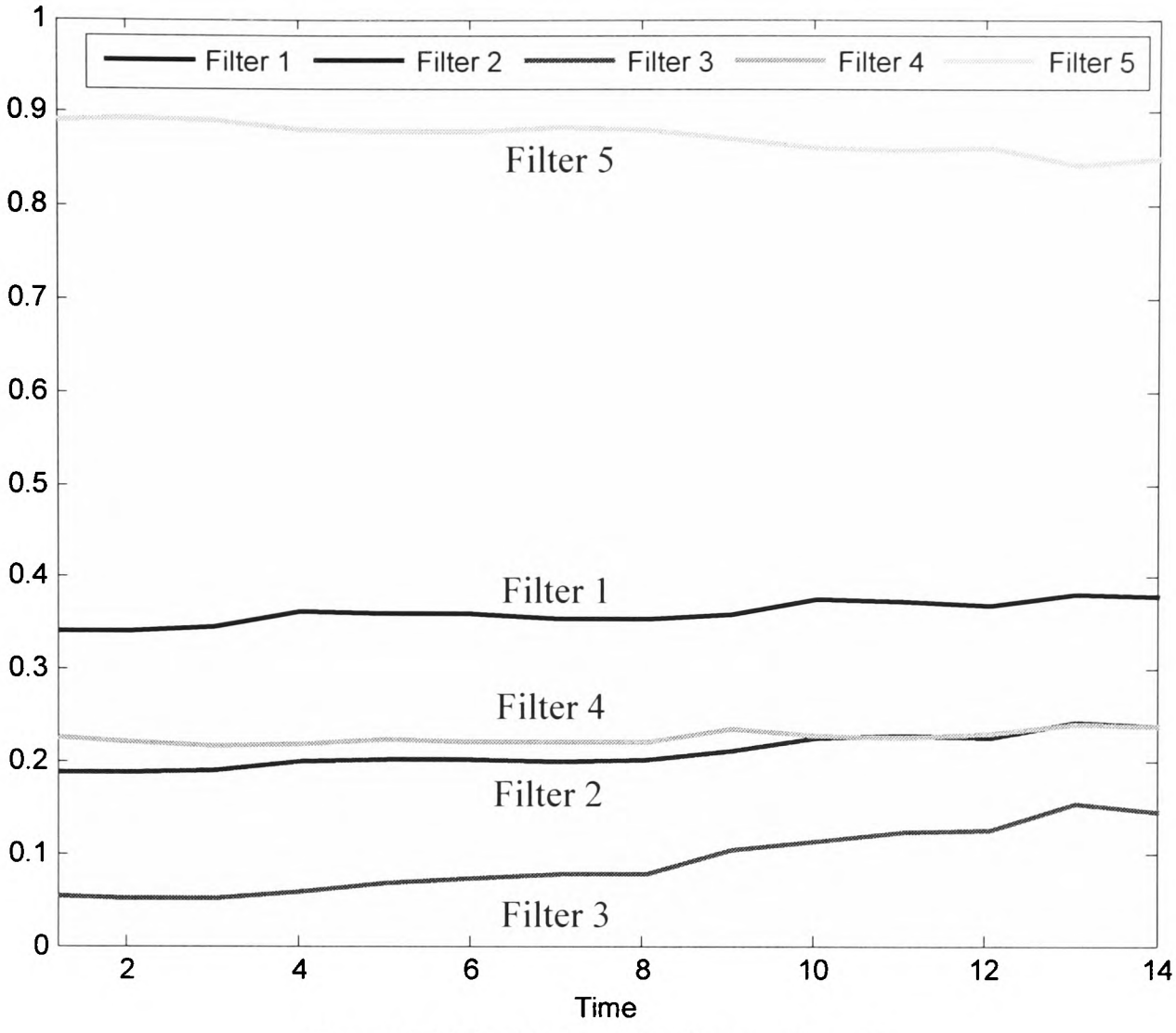

Figure 5.20 Residuals of the filters at P_2 on C_c

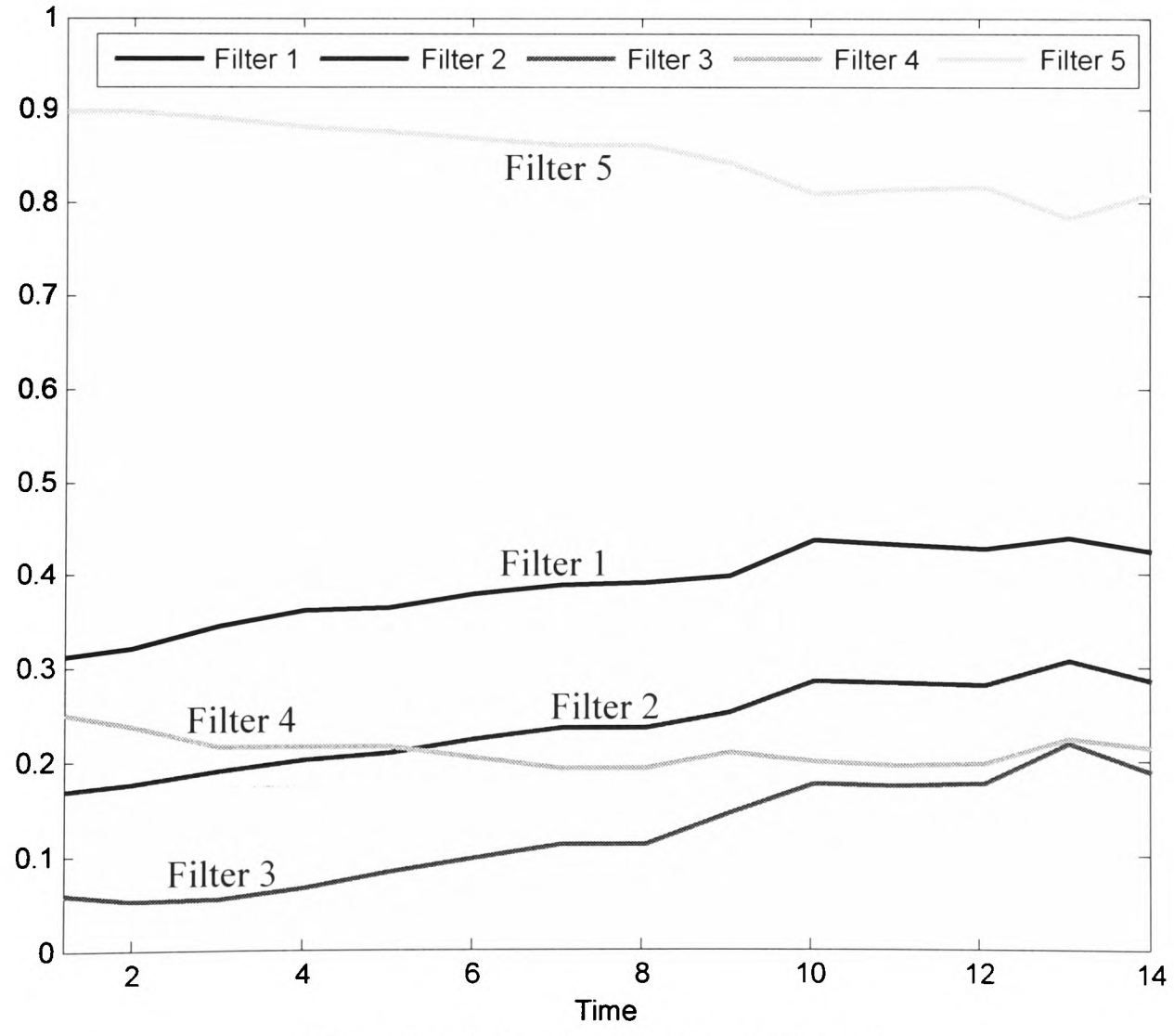

Figure 5.21 Residuals of the filters at P_3 on C_c

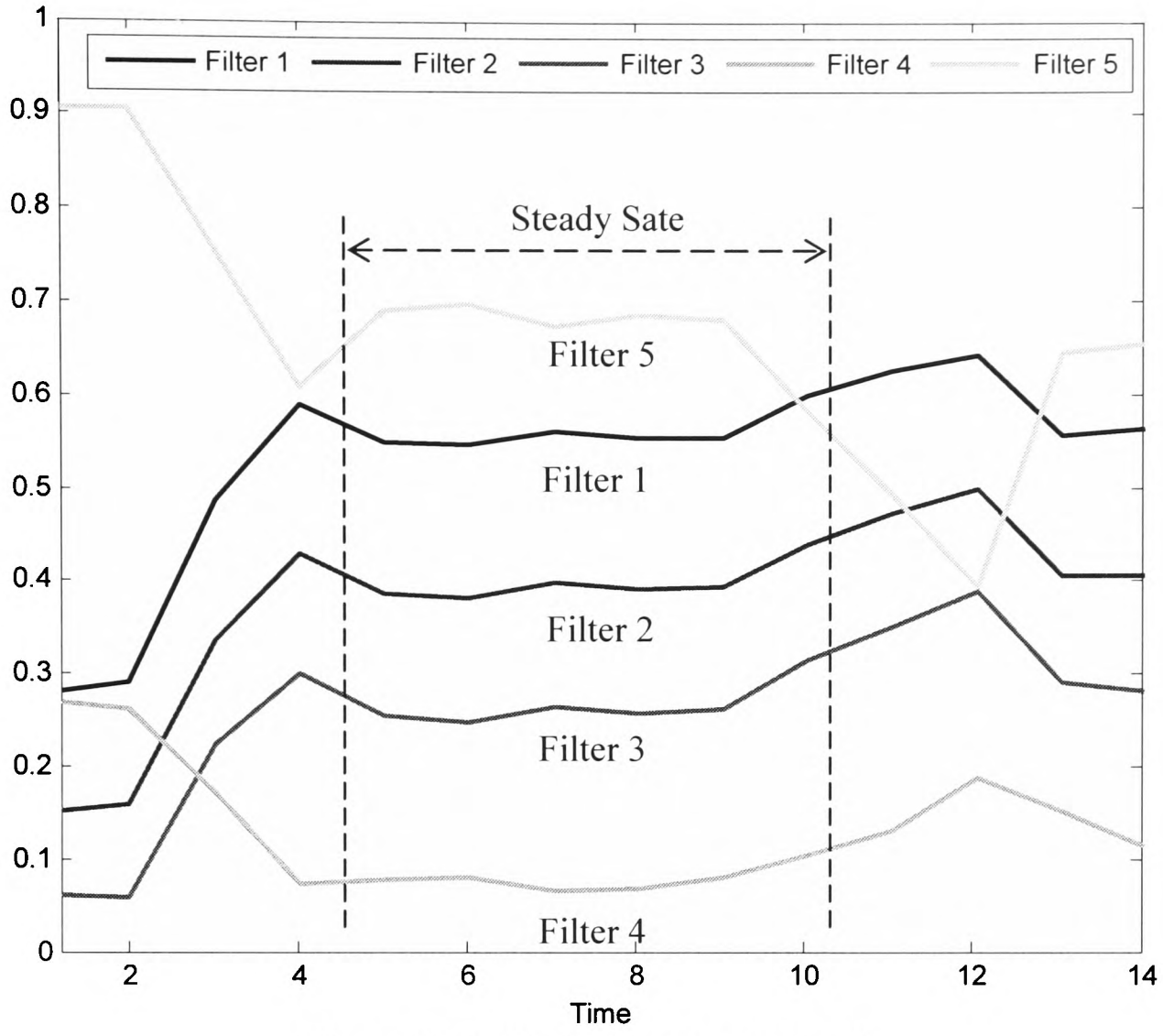

Figure 5.22 Residuals of the filters at P_4 on C_c

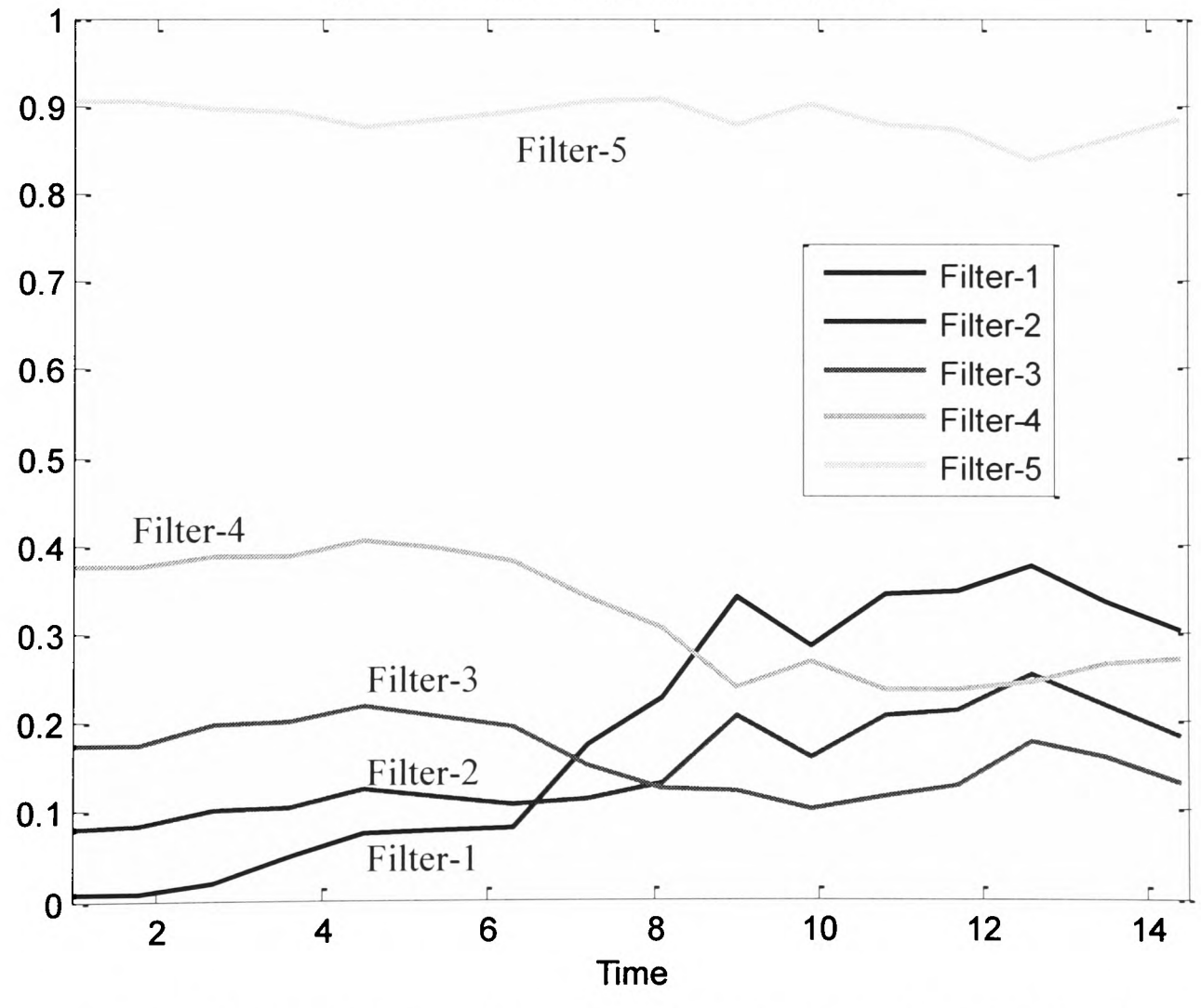

Fig.5.23. Residuals of the filters when the Operating point changed from P_1 to P_3 on C_a

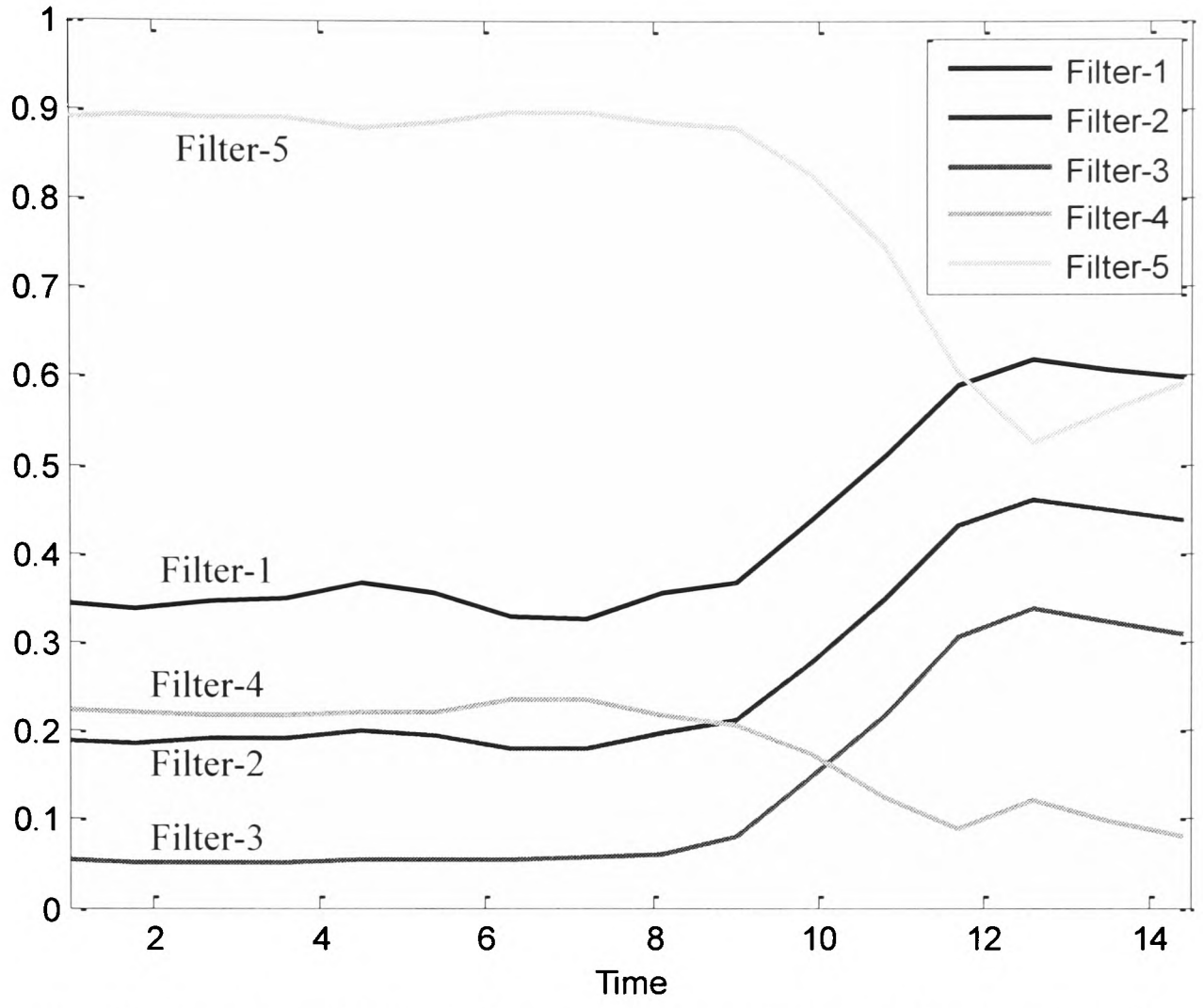

Fig.5.24. Residuals of the filters when the Operating point changed from P_1 to P_4 on C_c

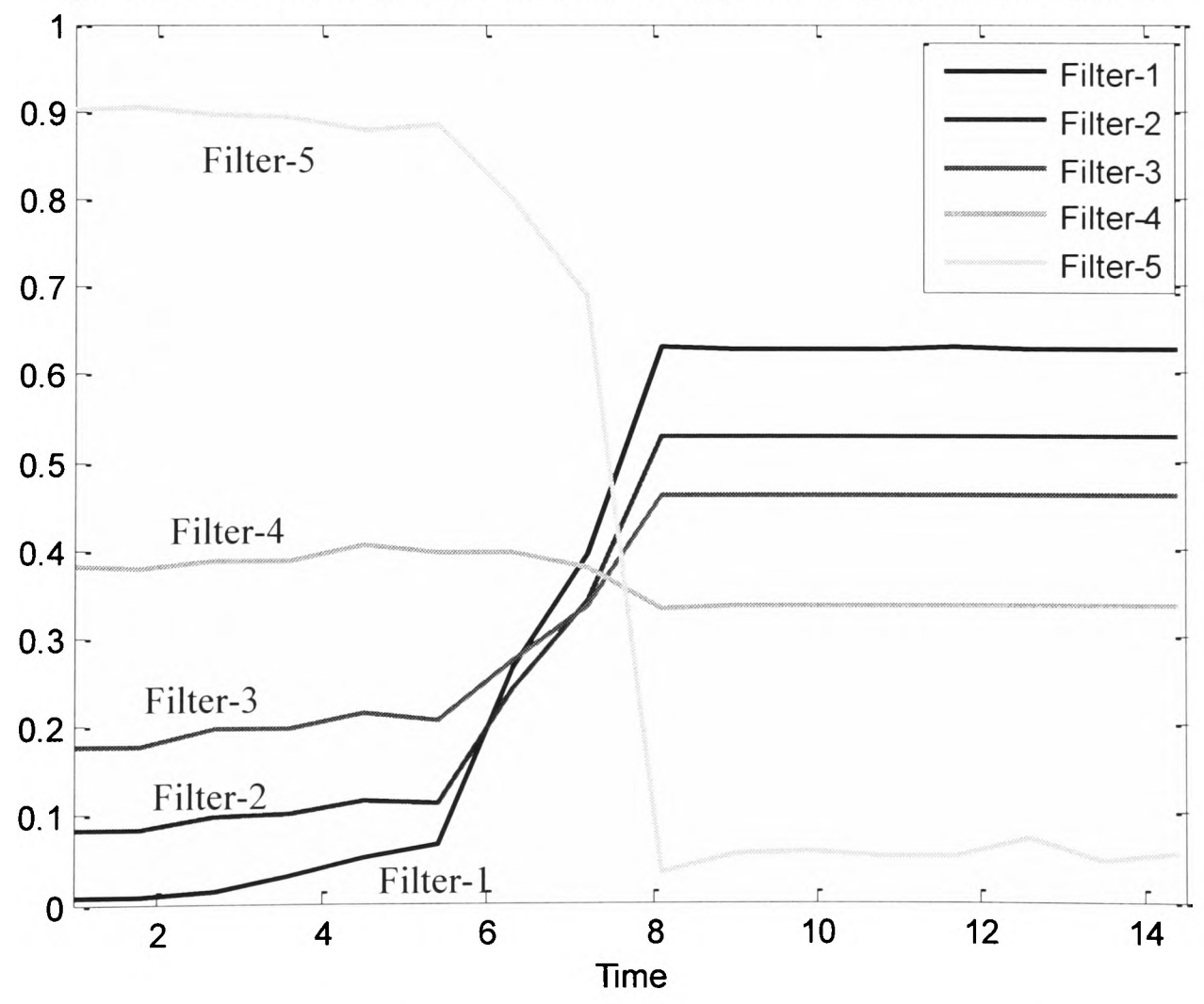

Fig.5.25. Residuals of the filters when the contact condition is changed from C_a to C_e

5.3.3 Case-3 (When the operating condition is changed during the simulation)

Figure 5.23 shows the simulation result when the operating condition changes from P_1 to P_3 while the wheelset is operated in contact condition represented by creep curve C_a. At the start of the simulation the wheelset is operated at P_1 which is quite evident from the figure because the residual of the filter-1 has the lowest value. After six seconds tractive torque is increased to drive the wheelset contact condition to P_3. After another two seconds when the tractive torque reaches to steady state, the residual of filter-3 is at the lowest indicating that the wheelset is now operating at P_3.

In figure 5.25, the wheelset is operated on creep curve C_c and the operating point is changed from P_1 to P_4. At the beginning of the simulation, the wheelset is operated in the linear region and, after six seconds, the operating point is switched to P_3 by the application of a tractive torque. The simulation takes nearly 3 seconds to reach the steady value. At steady output, the residual of the filter-4 is lowest suggesting that the wheelset is operating at the saturation point of the creep curve C_c. Residual values are changed with the changes in operating point (or creep) which if interpreted correctly can be useful for the drivers to adjust traction forces while accelerating the vehicles. In figure 5.25 the operating condition is changed from C_a to C_e during the simulation. At the start of the simulation, the wheelset is operated in the linear region of the creep curve C_a, as indicated by the residuals, after 5 seconds the contact condition is switched to C_e, therefore the residual of the filter-5 has lowest value, whereas the residuals of filters, designed to operate in high adhesion conditions (filter-1, filter-2, filter-3), are increased.

5.3.4 Summary of Design II

The simulations in Design II are carried out at several other creep curves (Figure 5.11), representing different levels of adhesion, and a table is developed summarising residual values at different operating points on each creep curve. It can be seen in the table 5.2, the residual values are gradually changed when the operating condition is changed on any of the creep curves and large variation is observed when the operating condition reaches to saturation point. Therefore it is better to separately analyse the residuals on saturation and non-saturation operating conditions.

Creep Curve	Operating Point	Filter 1	Filter 2	Filter 3	Filter 4	Filter 5	Filter with Lowest Residual
C_a (40%)	P_1	0.1	0.15	0.21	0.41	0.85	*Filter-1*
	P_2	0.15	0.16	0.22	0.41	0.84	*Filter-1*
	P_3	0.15	0.11	0.19	0.39	0.88	*Filter-2*
	P_4	0.55	0.4	0.29	0.13	0.6	*Filter-4*
C_f (30%)	P_1	0.2	0.11	0.12	0.35	0.89	*Filter-2*
	P_2	0.28	0.19	0.18	0.33	0.85	*Filter-3*
	P_3	0.34	0.21	0.19	0.3	0.82	*Filter-3*
	P_4	0.58	0.41	0.3	0.18	0.6	*Filter-4*
C_c (20%)	P_1	0.3	0.16	0.11	0.31	0.87	*Filter-3*
	P_2	0.33	0.21	0.15	0.29	0.84	*Filter-3*
	P_3	0.41	0.29	0.2	0.25	0.8	*Filter-3*
	P_4	0.52	0.35	0.22	0.11	0.5	*Filter-4*
C_g (16%)	P_1	0.39	0.21	0.09	0.21	0.85	*Filter-3*
	P_2	0.42	0.29	0.16	0.2	0.8	*Filter-3*
	P_3	0.51	0.36	0.22	0.15	0.7	*Filter-4*
	P_4	0.61	0.5	0.36	0.12	0.5	*Filter-4*
C_h (7%)	P_1	0.65	0.5	0.38	0.18	0.4	*Filter-4*
	P_2	0.65	0.5	0.39	0.19	0.38	*Filter-4*
	P_3	0.65	0.51	0.41	0.23	0.23	*Filter-4* *Filter-5*
	P_4	0.65	0.53	0.45	0.32	0.04	*Filter-5*
C_i (3%)	P_1	0.6	0.52	0.47	0.39	0.12	*Filter-5*
	P_2	0.6	0.52	0.47	0.39	0.13	*Filter-5*
	P_3	0.58	0.51	0.47	0.41	0.19	*Filter-5*
	P_4	0.58	0.5	0.45	0.41	0.21	*Filter-5*

Table 5.5 Residual Values for Design II

In non-saturation conditions as the adhesion level is decreased the values of the residual of filter-1 are increased and reaches to its maximum value (i.e. 0.65) when the adhesion level is 10% or less. This is because the design of the filter-1 is based on the high coefficient values. The design of the filter-2 is also based on high coefficient values (but not as high as in case of filter-1), that is why when the adhesion level is decreased the residual values are increased and reaches to its maximum value (i.e. 0.52) when the adhesion level 10% or less. The maximum value of residual of filter-1 is higher than the filter-2 because of the same reason (i.e. the design of filter-1 is based on high coefficient values than filter-2), therefore the error produced by filter-2 is slightly less than filter-1.

The design of the filter-3 is based on moderate coefficient values therefore the residual of filter-3 has lower values when the operating condition is not in linear region or the adhesion level is moderate (i.e. 30%-15%). The design of filter-4 is based on the lower coefficient values therefore the residual values are high when the adhesion level is

high and are decreased when the adhesion level is decreased until it drops below 7%. The design of the filter-5 is based on very low coefficient values therefore the residual values are very high for high adhesion values and start decreasing when the adhesion level start to drop below 10%. At the saturation condition the residual of filter-4 has lowest value when the adhesion level is more than 15% and at lower adhesion levels the residual of filter-5 has lowest values. The values of the residuals of the rest of the filters are high at saturation conditions.

The Kalman filters show great agreement with the idea proposed earlier and provide a good consistency even in those adhesion conditions which are not the part of the Kalman filter design. The results also indicate that the residual values provide a unique combination at each operating point. That provides a basis to generalise the idea for all possible contact conditions based on the results summarized in table 5.5.

6. Fuzzy Logic Identification Of Contact Conditions

6.1 Fuzzy Inference System

From the simulation results given in Chapter 5 it is obvious that the variation in residuals can be interpreted into contact condition information by developing a suitable decision-making system. The identification of contact condition from the combination of residual values is a multi-valued logic problem and the fuzzy logic is a suitable and simple solution for such applications. Therefore a fuzzy inference system is proposed to detect the changes in the contact condition which takes into account the residuals and the tractive torque to identify the contact condition. Fuzzy inference systems have been successfully applied in fields such as automatic control, data classification, decision analysis, expert systems and computer vision. Because of their multidisciplinary nature, fuzzy inference systems are associated with a number of names, such as fuzzy-rule-based systems, fuzzy expert systems, fuzzy modeling, fuzzy associative memory, fuzzy logic controllers, and simply fuzzy systems [128].

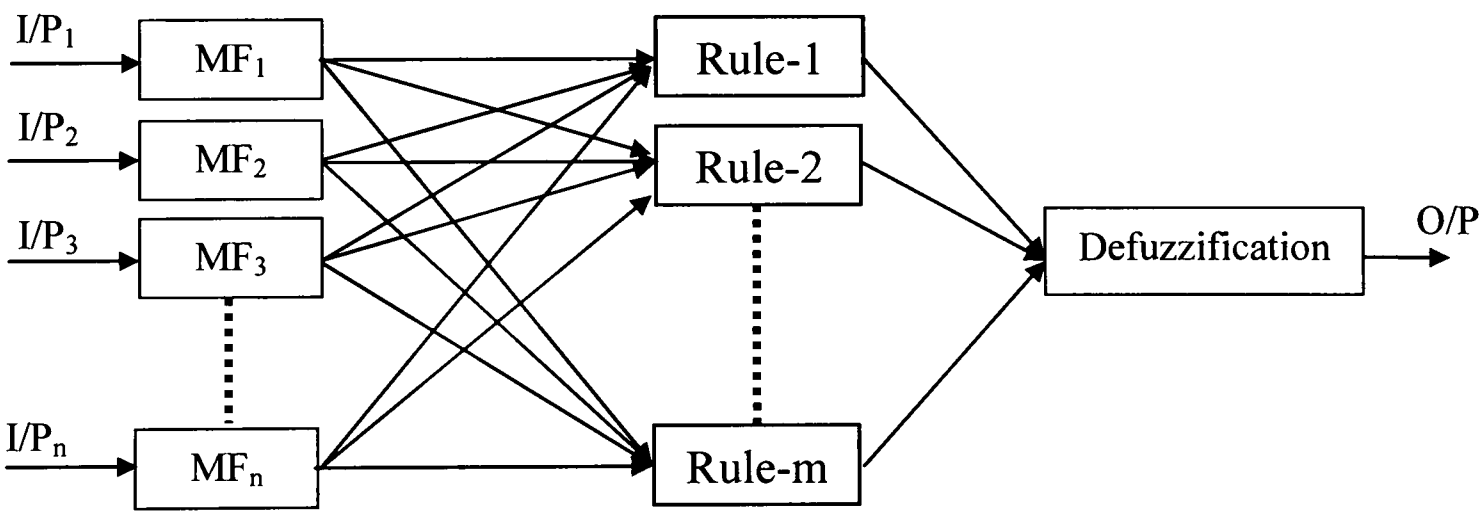

Figure 6.1: General Structure of fuzzy inference system

A generic fuzzy logic system consists of three main parts, as shown in Figure 6.1. The first part is the input fuzzification, which scales the inputs (on a scale of 0 to 1) and determines the magnitude of participation in producing the output. The inputs are then processed according to set rules that are stored in the fuzzy database, and the fuzzified output is produced, which is a combination of all individual rules. Defuzzification is required to determine the single scalar output, usually on a scale of 0 to 100. In order to design a fuzzy reasoning system for any specific application, there are several choices to

be made. They include an appropriate type of fuzzy inference system, appropriate input membership functions and the choice of a defuzzification method.

6.1.1 Types of Fuzzy Inference System

Two types of fuzzy inference systems can be implemented here: Mamdani-type and Sugeno-type. These two types of inference systems vary only in the way in which outputs are determined and therefore the design of the first two steps is the same for either type of fuzzy inference system. Mamdani's fuzzy inference method is the most commonly seen fuzzy methodology. Mamdani's method was among the first control systems built using fuzzy set theory. It was proposed in 1975 by Ebrahim Mamdani [129] as an attempt to control a steam engine and boiler combination by synthesising a set of linguistic control rules obtained from experienced human operators. The main difference between Mamdani and Sugeno is that the Sugeno output membership functions are either linear or constant [130-131], and are therefore not suitable for this application. In Mamdani-type inference the output membership functions is fuzzy set. After the aggregation process, there is a fuzzy set for each output variable that needs defuzzification.

6.1.2 Input Membership Function

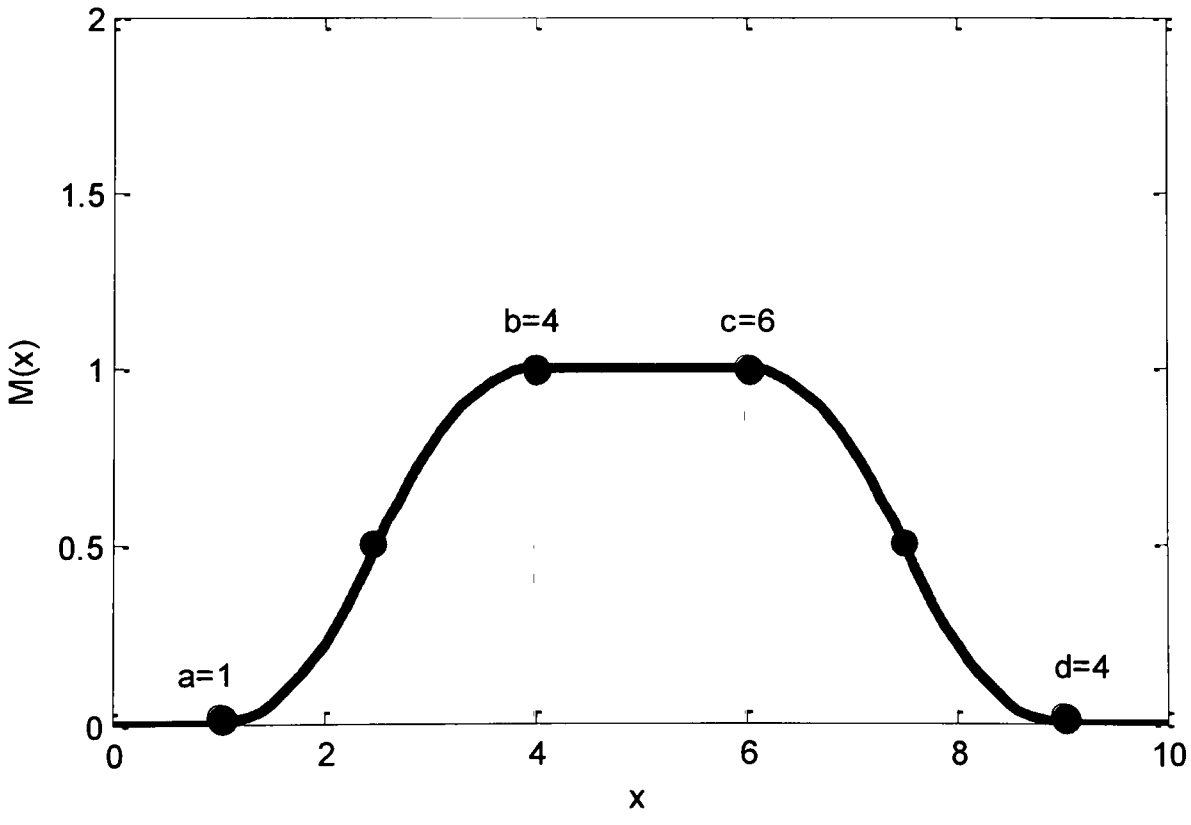

Figure-.6.2. Bell-shaped Membership function

There are several type of representations of membership functions that can be used for specific applications, such as triangular, trapezoidal and bell-shaped. The type of representation of the membership function depends on the transition in the input variable. If the transition in the input variable is abrupt, a rectangular membership function is suitable for such applications [72]. In this particular application the transition in input variables (i.e. residuals) are smooth, as shown in Figure-6.6; therefore a bell-shaped curve is used for the input and output membership functions, which can be created easily in Matlab by using the *pimf* command. The membership function is shown in Figure 6.2 and is defined by Equation (6.1).

$$M(x)=\begin{cases} 0, & x \le a \\ 2\left(\dfrac{x-a}{b.-a}\right)^2, & a \le x \le \dfrac{a+b}{2} \\ 1-2\left(\dfrac{x-b}{b.-a}\right)^2, & \dfrac{a+b}{2} \le x \le b \\ 1, & b \le x \le c \\ 1-2\left(\dfrac{x-c}{d.-c}\right)^2, & c \le x \le \dfrac{c+d}{2} \\ 2\left(\dfrac{x-c}{d.-c}\right)^2, & \dfrac{c+d}{2} \le x \le d \\ 0, & x \ge d \end{cases} \tag{6.1}$$

The membership function is evaluated at the points determined by the vector x. The parameters a and d locate the "feet" of the curve, while b and c locate its "shoulders."

6.1.3 Defuzzification

There are many defuzzification techniques, such as the weighted average defuzzification technique, the maximum defuzzification technique and the centroid defuzzification technique. The centroid defuzzification technique is the most commonly used and a very accurate defuzzification method [132], which determines the centre of the area of the combined membership functions [133-134]. This technique was developed by Sugeno in 1985 and is also known as centre of gravity or centre of area defuzzification. The centroid defuzzification technique can be expressed as

$$n=\frac{\int M_{output}(x)\, x\, dx}{\int M_{output}(x)\; dx} \tag{6.2}$$

where n is the defuzzified output ranging from 0 to 100, $M_{output}(x)$ is the aggregated membership function and x is the output variable. The only disadvantage of this method is that it is computationally difficult for complex membership functions.

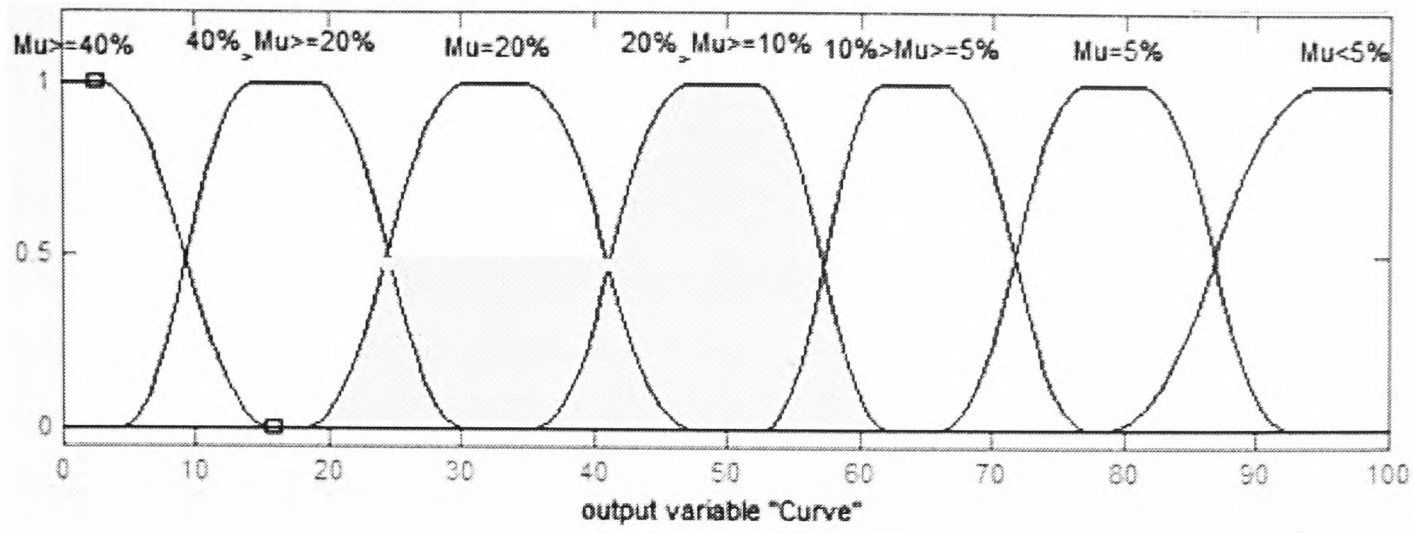

Figure-.6.3. Defuzzification of fuzzy output

Figure 6.3 shows an example output when the wheelset is operated on an adhesion level between 10% and 20%. The final output function $M_{output}(x)$ is shown in Figure-6.4. The centre of gravity of all the outputs, calculated using Equation 6.2, is 45.89.

$$n_1 = \frac{\int_{18.2}^{24.4} 2\left(\frac{x-a_3}{b_3-a_3}\right)^2 x\,dx + \int_{24.4}^{41.37} 0.5x\,dx + \int_{41.37}^{47.2}\left[1-2\left(\frac{x-b_4}{b_4-a_4}\right)^2\right]x\,dx + \int_{47.2}^{51.9} x\,dx}{\int_{18.2}^{24.4} 2\left(\frac{x-a_3}{b_3-a_3}\right)^2 dx + \int_{24.4}^{41.37} 0.5\,dx + \int_{41.37}^{47.2}\left[1-2\left(\frac{x-b_4}{b_4-a_4}\right)^2\right]dx + \int_{47.2}^{51.9} 1\,dx}$$

$$+ \int_{51.9}^{57.1}\left[1-2\left(\frac{x-c_4}{d_4-c_4}\right)^2\right]x\,dx + \int_{57.1}^{62.3} 2\left(\frac{x-c_4}{d_4-c_4}\right)^2 x\,dx$$

$$+ \int_{51.9}^{57.1}\left[1-2\left(\frac{x-c_4}{d_4-c_4}\right)^2\right]dx + \int_{57.1}^{62.3} 2\left(\frac{x-c_4}{d_4-c_4}\right)^2 dx = 45.89$$

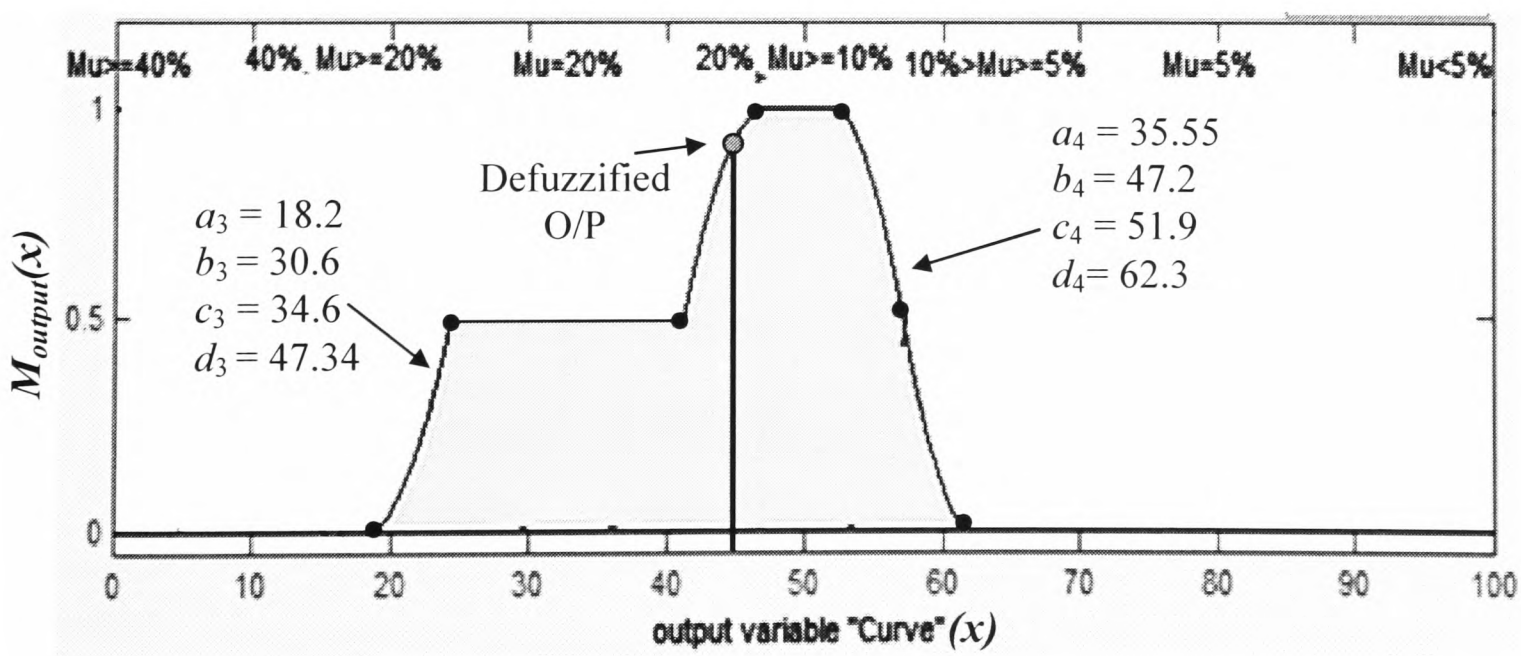

Figure-.6.4.Centroid defuzzification of fuzzy output

6.1.4 Output Conversion

After the defuzzification process, the output is converted to percentage adhesion by developing a relationship between fuzzy logic output and percentage adhesion. This conversion process is not part of the fuzzy inference system. In this thesis two different designs are used for the detection of contact condition between the wheel and the rail. For each of the approaches the design of the fuzzy logic is different. The design and the effectiveness of each of these approaches are covered in the following sections.

6.2 Fuzzy Logic System (Design-I)

The basic idea of this approach is that, if the wheelset operating point is at the saturation region of the creep curve, the residual information together with the tractive torque can easily be used to determine the adhesion level. The fuzzy inference system (FIS) that analyses the residuals and the tractive torque is shown in Figure 6.5. Design details of each of the divisions are given in the following sections.

6.2.1 Input Membership Functions

Using Table-5.3, residuals are plotted against adhesion level in order to develop the membership functions. The variation of residuals with respect to adhesion is shown in Figure 6.7. The total span of each residual is divided into three categories: 'Low', 'Moderate' and 'High'. There is the possibility to divide the total span into fewer or more categories, Membership functions with four categories were also used but after simulating the system several times at various different creep curves, three categories seem to be the best option.

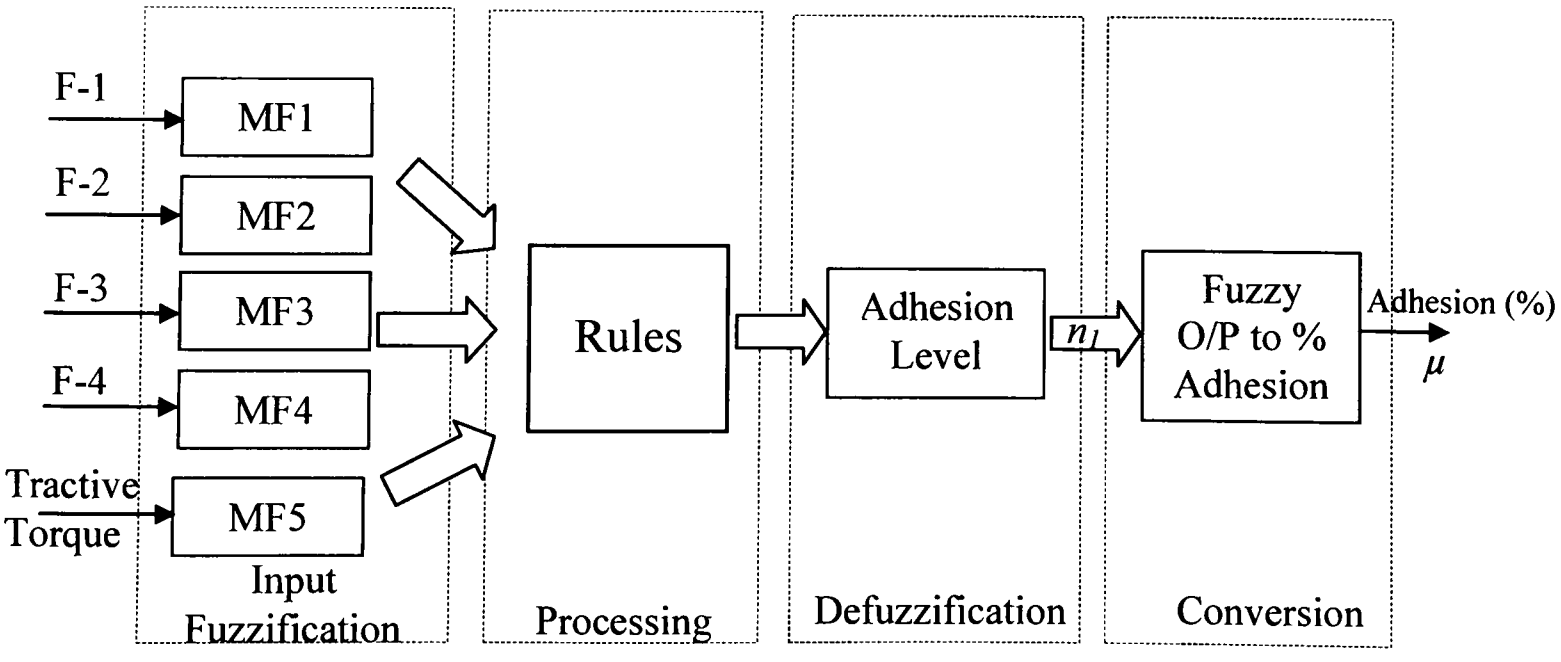

Figure-6.5. Proposed Fuzzy Logic System (Design-I)

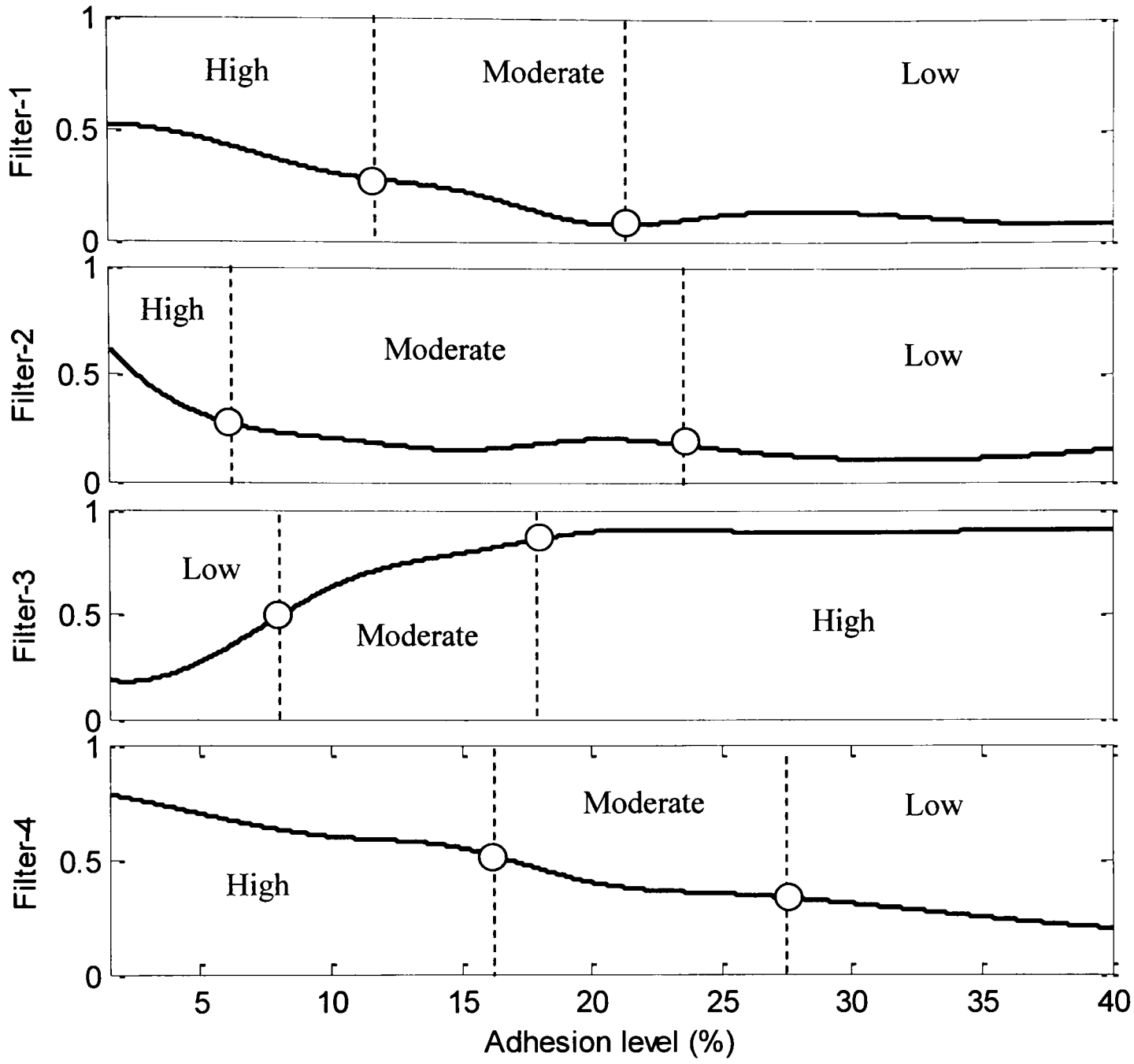

Figure-.6.6. Variation in Residuals with the change in adhesion level

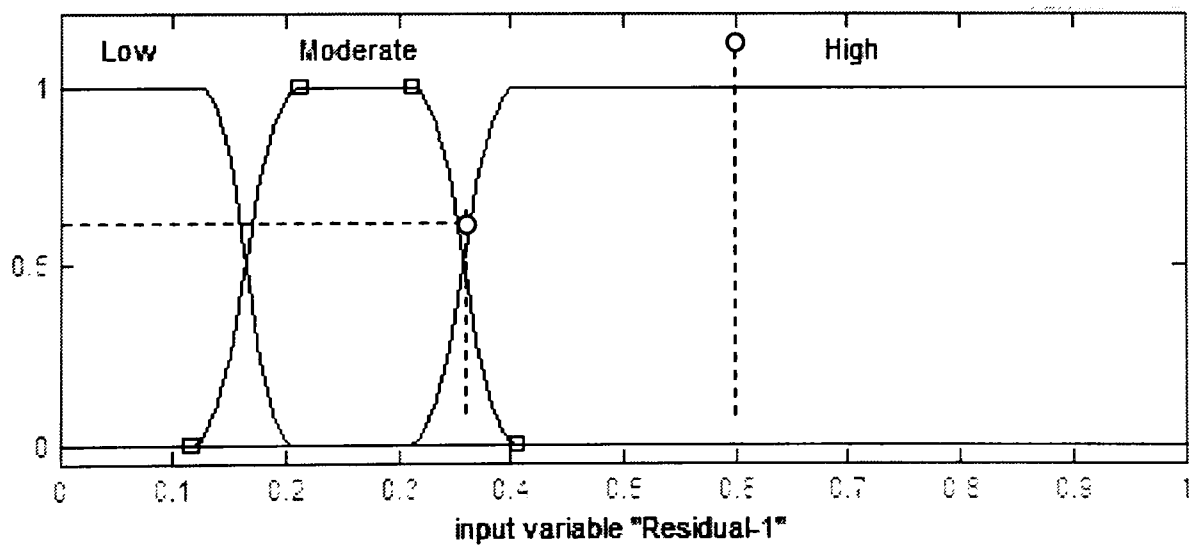

Figure-.6.7 Membership function for the residual of filter-1

From the residual of filter-1 in Figure-6.6, it is clear that when the adhesion level is 20% or more, the residual of filter-1 falls in the category of 'Low'. When the adhesion level is between 10% and 20%, it falls in the category of 'Moderate' and when the

adhesion level is less than 10%, the residual belongs to the 'High' category. This is because filter-1 is tuned to operate on creep curves with maximum adhesion level 20% or more (table-5.). Similarly, the categorisation of the residual of filter-3 is also obvious. When the adhesion level is 15% or more, the residual belongs to category 'High'. When the adhesion level is around 10%, the residual belongs to 'Moderate' and when the adhesion level is less than 10% it belongs to the category 'Low'. In the same way, the residuals of the other filters are divided and the membership functions are formed. Figure-6.7 shows the membership function of the normalised rms value of the residual of filter-1. The horizontal axis represents the normalised value of the residual. The value of the residual then determines the magnitude of participation of the input and the category it belongs to (e.g. 'Large' if the residual value is 0.6 and the degree of membership is 1 and 'Moderate' and 'High' if the residual value is 0.35 and the degree of membership is 0.5 in this case).

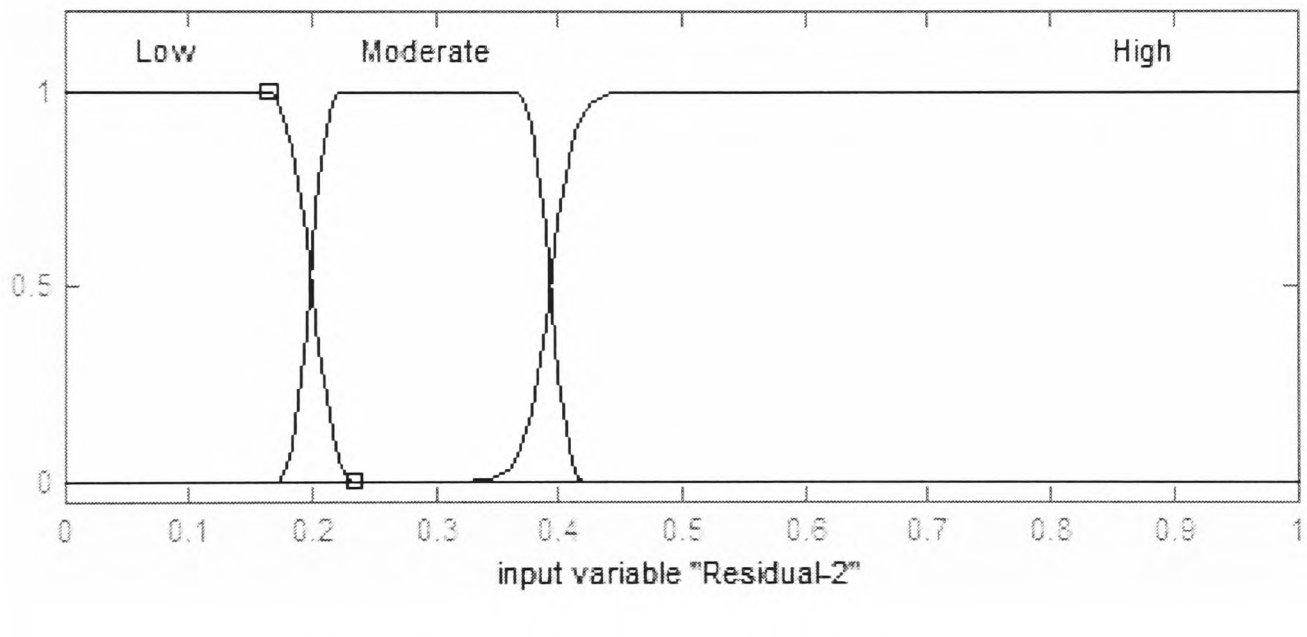

Figure-.6.8. Membership function for the Residual of filter-2

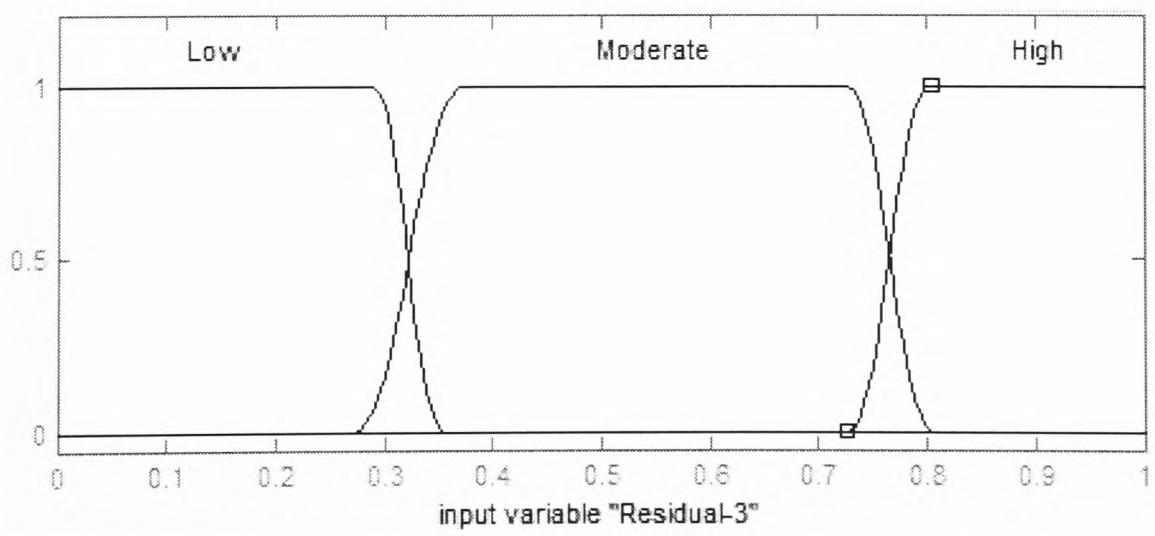

Figure-.6.9. Membership function for the Residual of filter-3

The membership functions for the residuals of filter-2 and filter-3 are shown in Figure-6.8 and Figure-6.9 respectively. The shape and the boundaries of the membership functions are fine-tuned with the help of simulations, to ensure the best possible consistency.

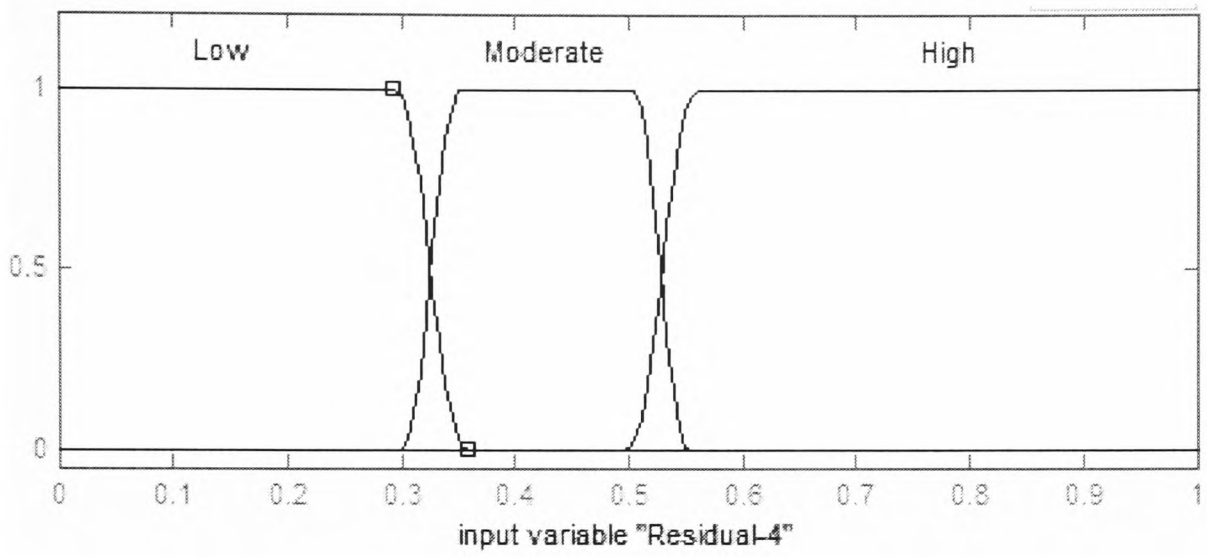

Figure-.6.10. Membership function for the Residual of filter-4

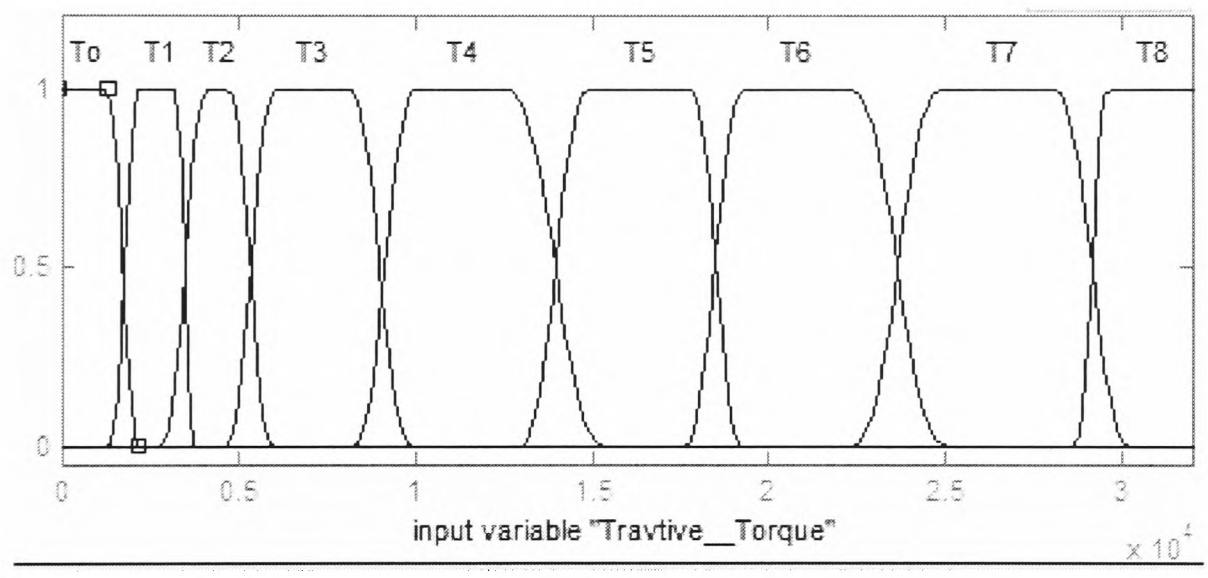

Figure-.6.11. Membership function for the Measured Tractive Torque

In addition to the residuals of the filters, the tractive torque information is also assured to be available and provided as an input to the fuzzy logic system. Figure 6.11 shows the membership function of the tractive torque. It is divided into 9 categories, T0 to T8, which are evolved from trial and error after simulating the system several times. For instance, if adhesion is 40% (μ=0.4), the tractive torque required to drive the wheelset at the saturation region is 29400 N-m (i.e. T_8 in Figure 6.11)

6.2.2 Fuzzy Logic Rules

Once all the inputs are scaled and combined, they are processed according to the rules. Once again Table 5.3 is used to derive the fuzzy logic rules. In fact, in Table 5.3 the

numeric values are replaced by 'linguistic' variables and the new table is formed containing the fuzzy logic rules (Table 6.1).

No.	F-1	F-2	F-3	F-4	T	O/P
1	Low	Low High	High	Low	T8	μ≥40%
2	Low	Low High	High	Low Moderate	T7	40%>μ>20% μ≥40%
3	Low	Low Moderate	High	Low	T6	40%>μ>20% μ=20%
4	Low	Low Moderate	High	Low Moderate	T5	μ=20%
5	Low	Low	High	Low Moderate High	T4	20%>μ≥10% μ=20%
6	Low Moderate	Low	Moderate High	Low Moderate High	T3	20%>μ≥10%
7	Moderate	Low	High	Low Moderate High	T4	20%>μ≥10% μ=20%
8	Moderate High	Low	Low Moderate	High	T2	μ=5%
9	Moderate	Low	Moderate High	High	T2	μ=5% 10%>μ>5%
10	High	Moderate High	Low	High	T1	μ<5% μ=5%
11	High	Moderate High	Low	High	To	μ<5%

Table-6.1. Fuzzy Logic Rules for Design-I

6.2.3 Output membership functions

The output variable (i.e. adhesion level) with the fuzzy set is shown in Figure-6.12. The fuzzy logic outputs a numeric value after the defuzzification process, which indicates the adhesion level. For example, fuzzy logic output 32.8 suggests that the adhesion level is 20%.

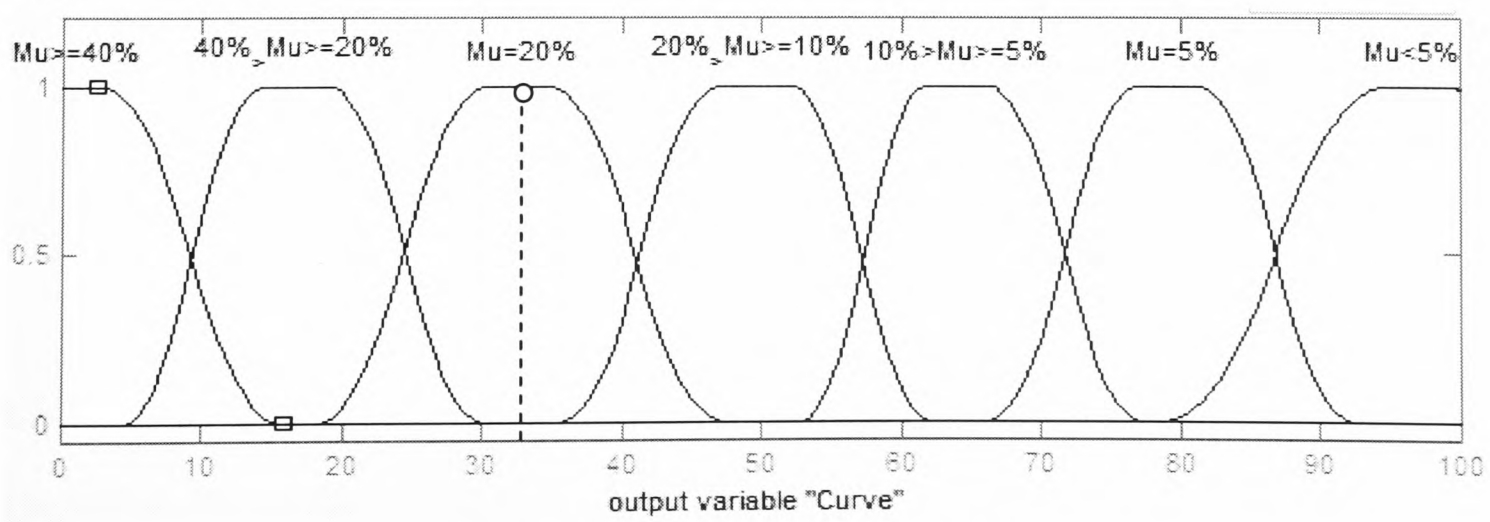

Figure-6.12. Output Membership function

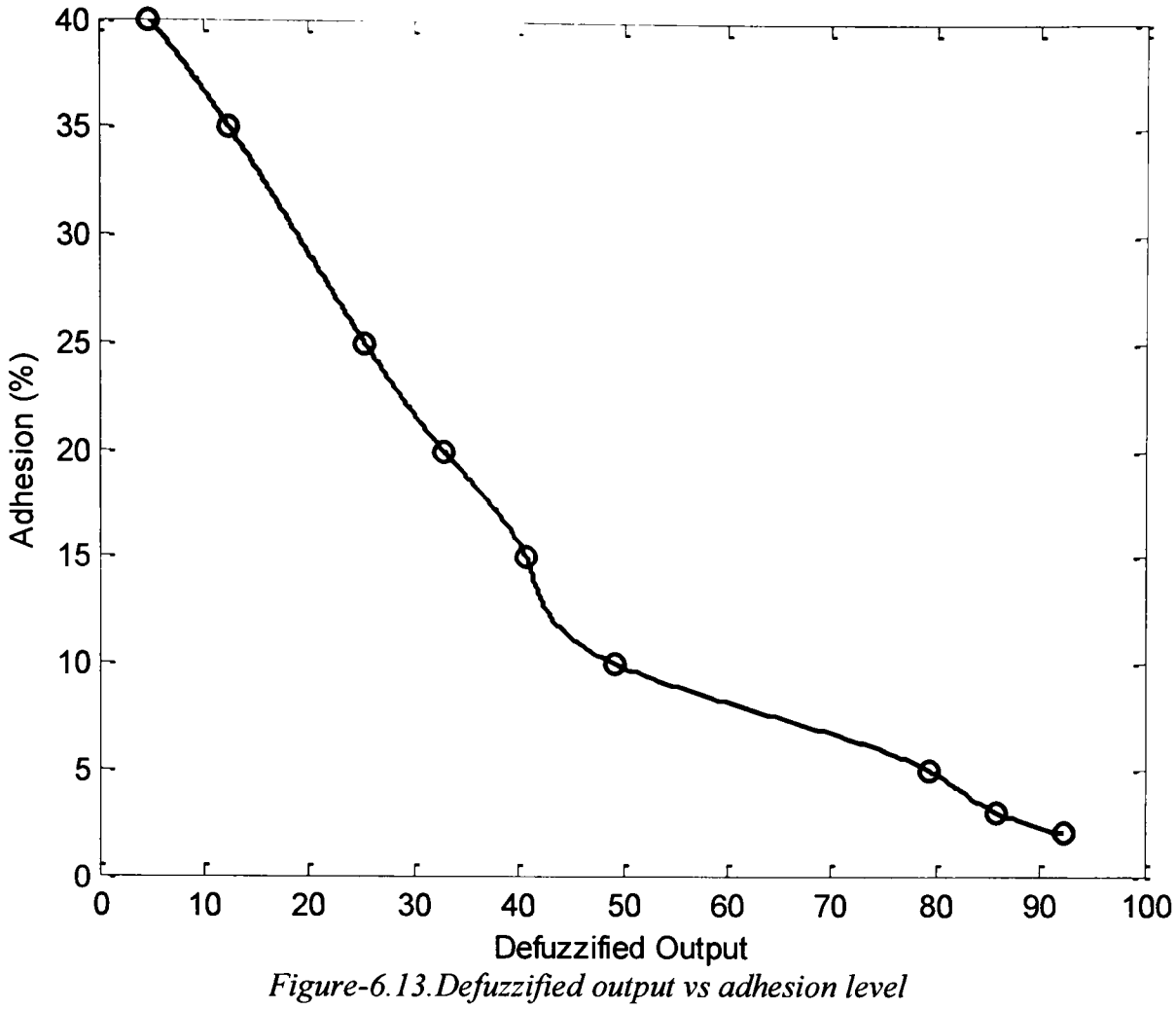

Figure-6.13.Defuzzified output vs adhesion level

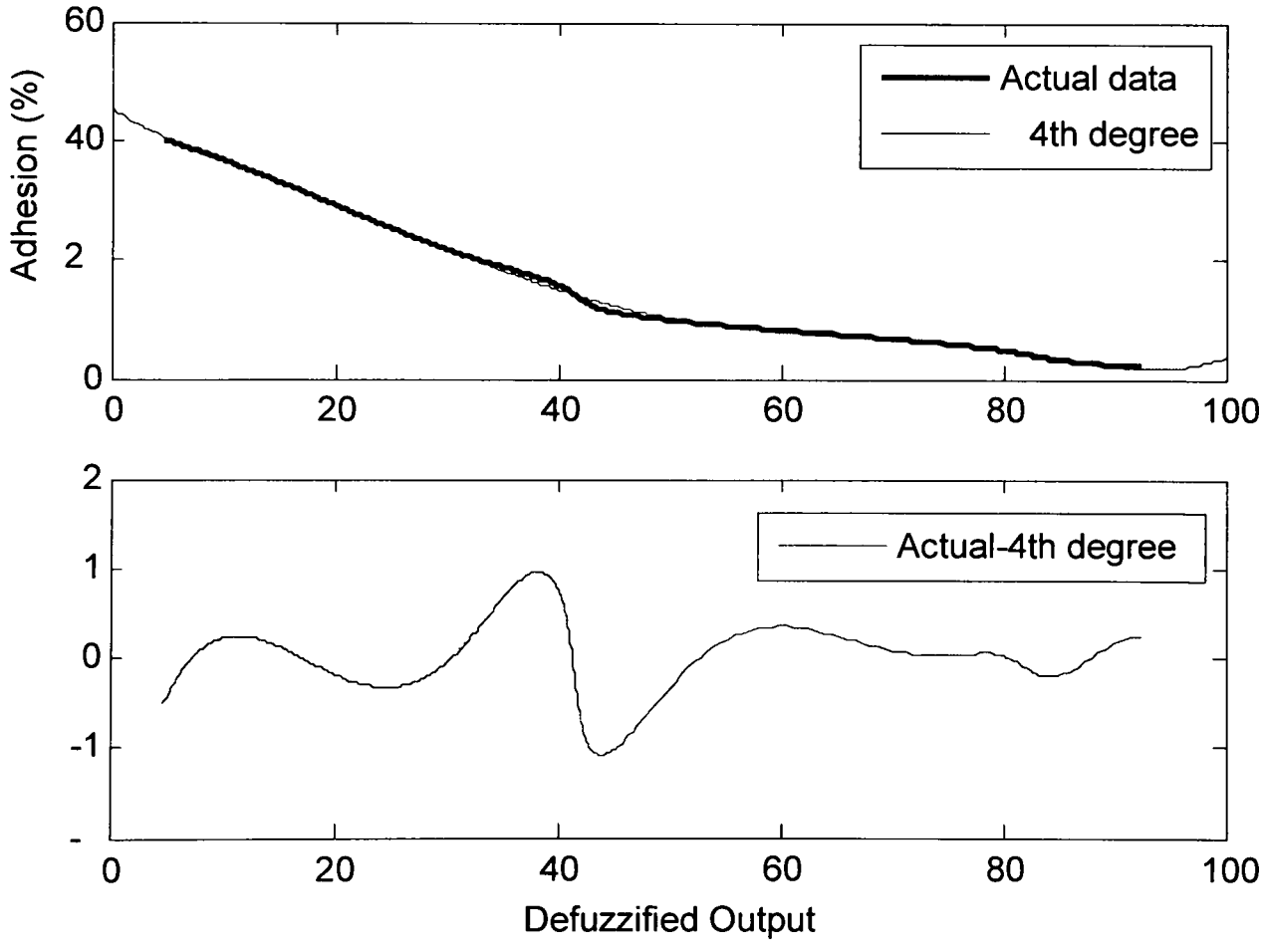

Figure-6.15.Data fitting process

6.2.4 Output conversion

The defuzzified output indicates the adhesion level by producing a numeric value (such as n_1) at the output. In order to develop a relationship between the defuzzified output (n_1)

and percentage adhesion (μ), the adhesion values are plotted against associated defuzzified values, as shown in Figure-6.13. Different polynomials are fitted on the actual data using the *polyfit* function of matlab, and a fourth-order polynomial given in Equation (6.3) is found to be the better choice, with a ±1.2% fitting error as shown in Figure-6.14. Using Equation (6.3) the percentage adhesion for the defuzzified output = 32.8 is calculated as 19.74%.

$$\mu = -2.213\times10^{-6} n_1^{\,4} + 0.00042 n_1^{\,3} - 0.0205 n_1^{\,2} - 0.38 n_1 + 42 \qquad (6.3)$$

6.2.5 Simulation Results

After designing the fuzzy inference system based on the results given in Chapter 5, it is time to test the system on a variety of different creep curves representing various different contact conditions. The creep curves are shown in Figure 6.15. The creep curves with bold solid lines are the one used for the Kalman filter design and the creep curves shown by dotted lines are used to test the detection system.

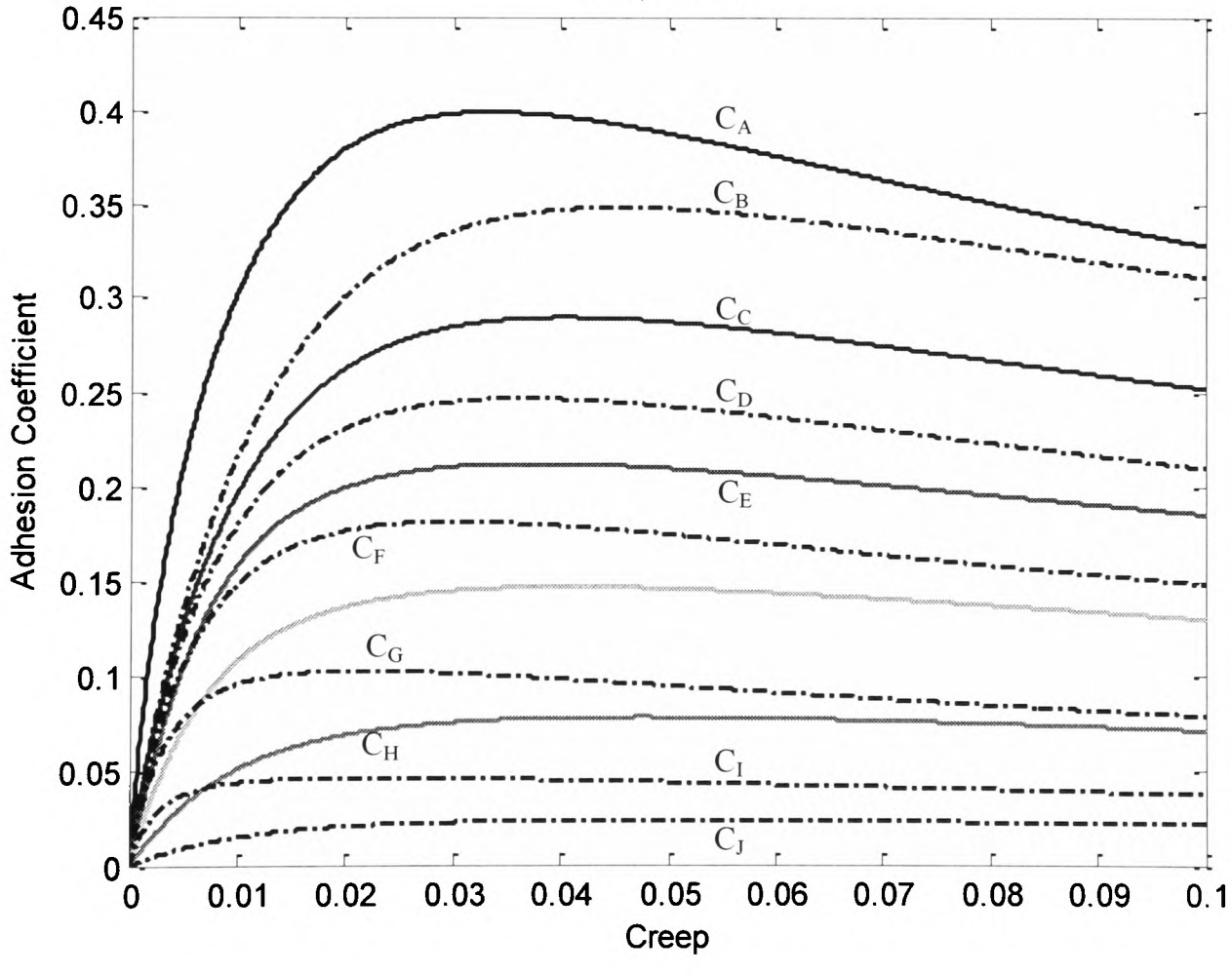

Figure-6.15. Creep Curves

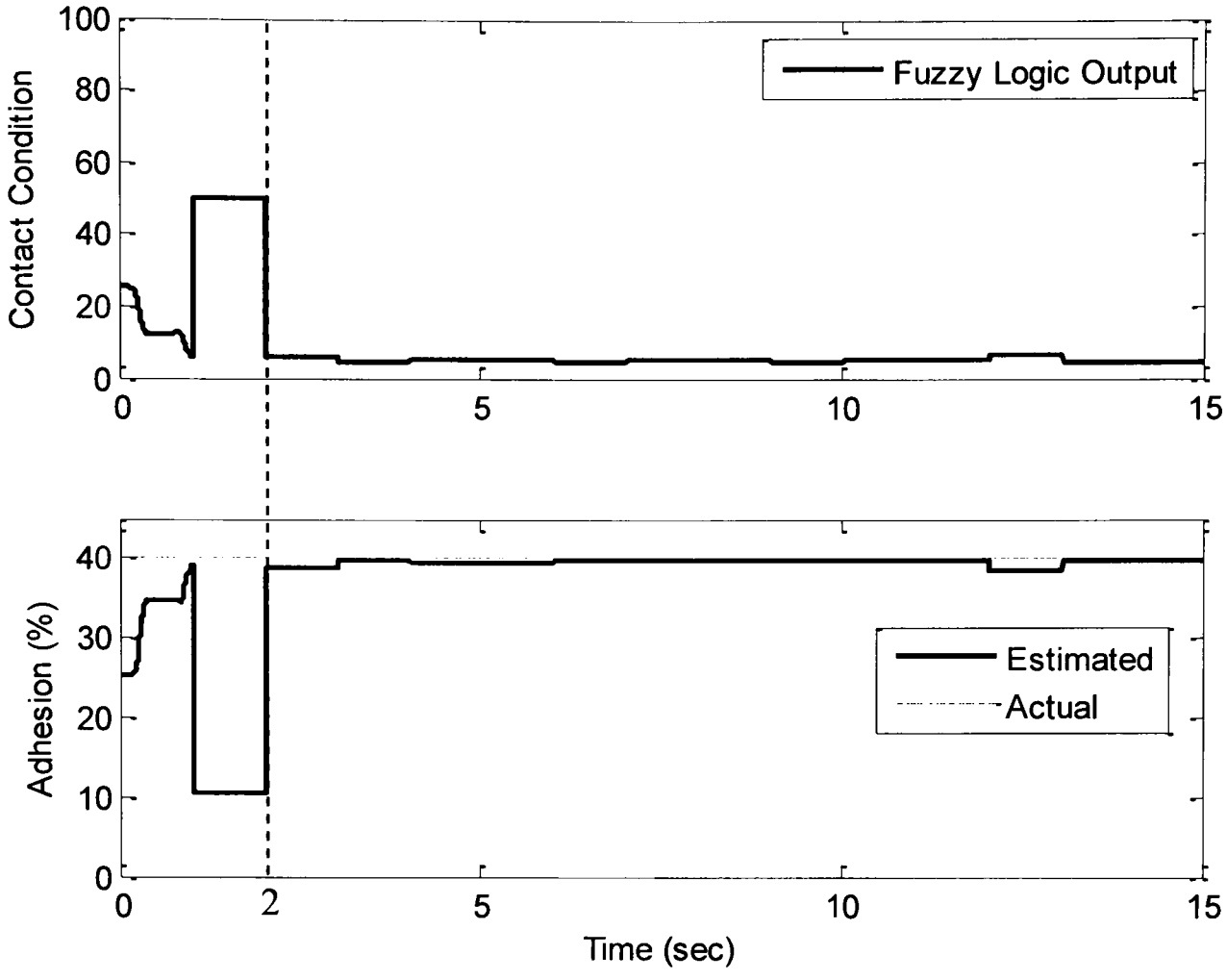

Figure-6.16. Fuzzy Logic output on creep curve C_A

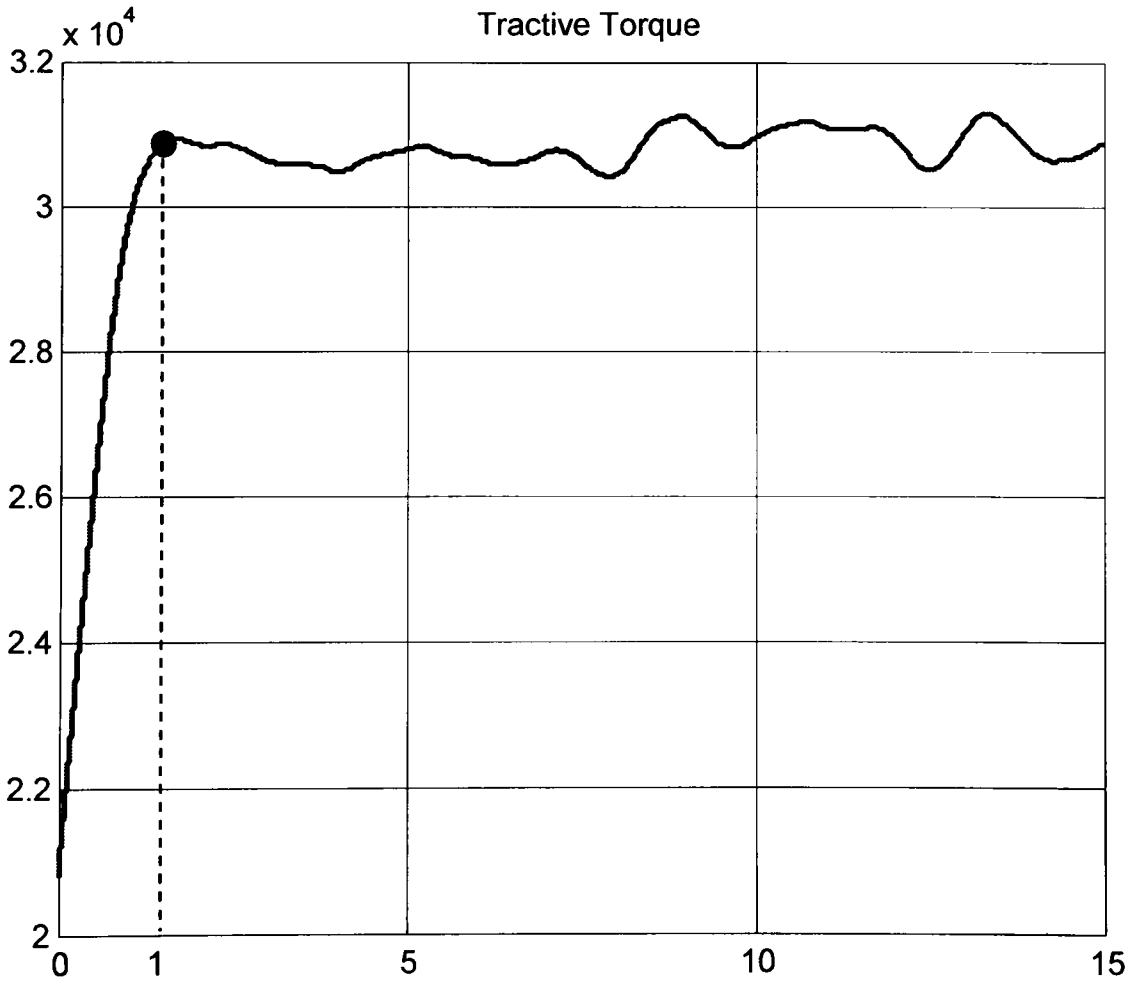

Figure-6.17. Tractive Torque Controlled by PI controller

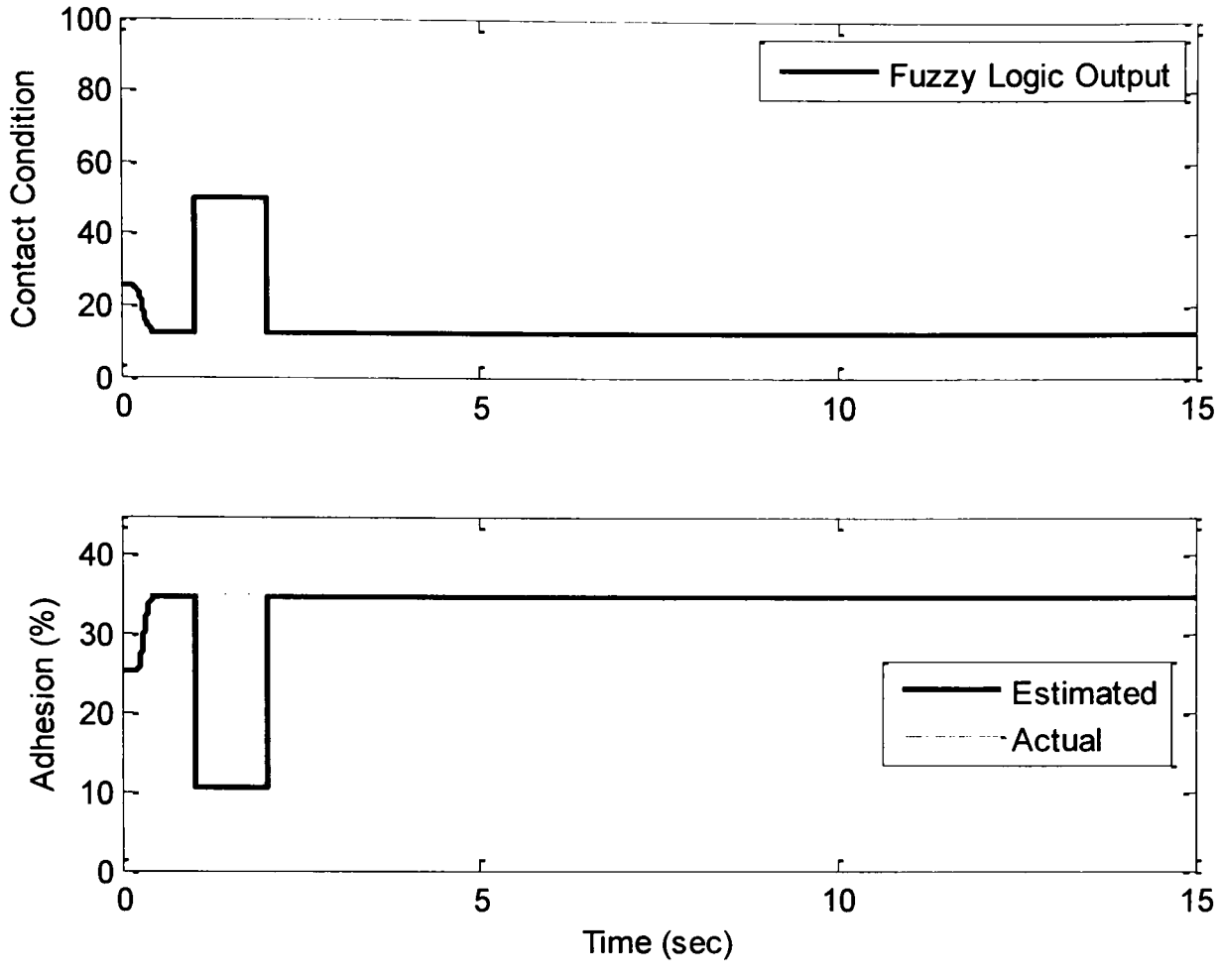

Figure-6.18. Fuzzy Logic output on creep curve C_B

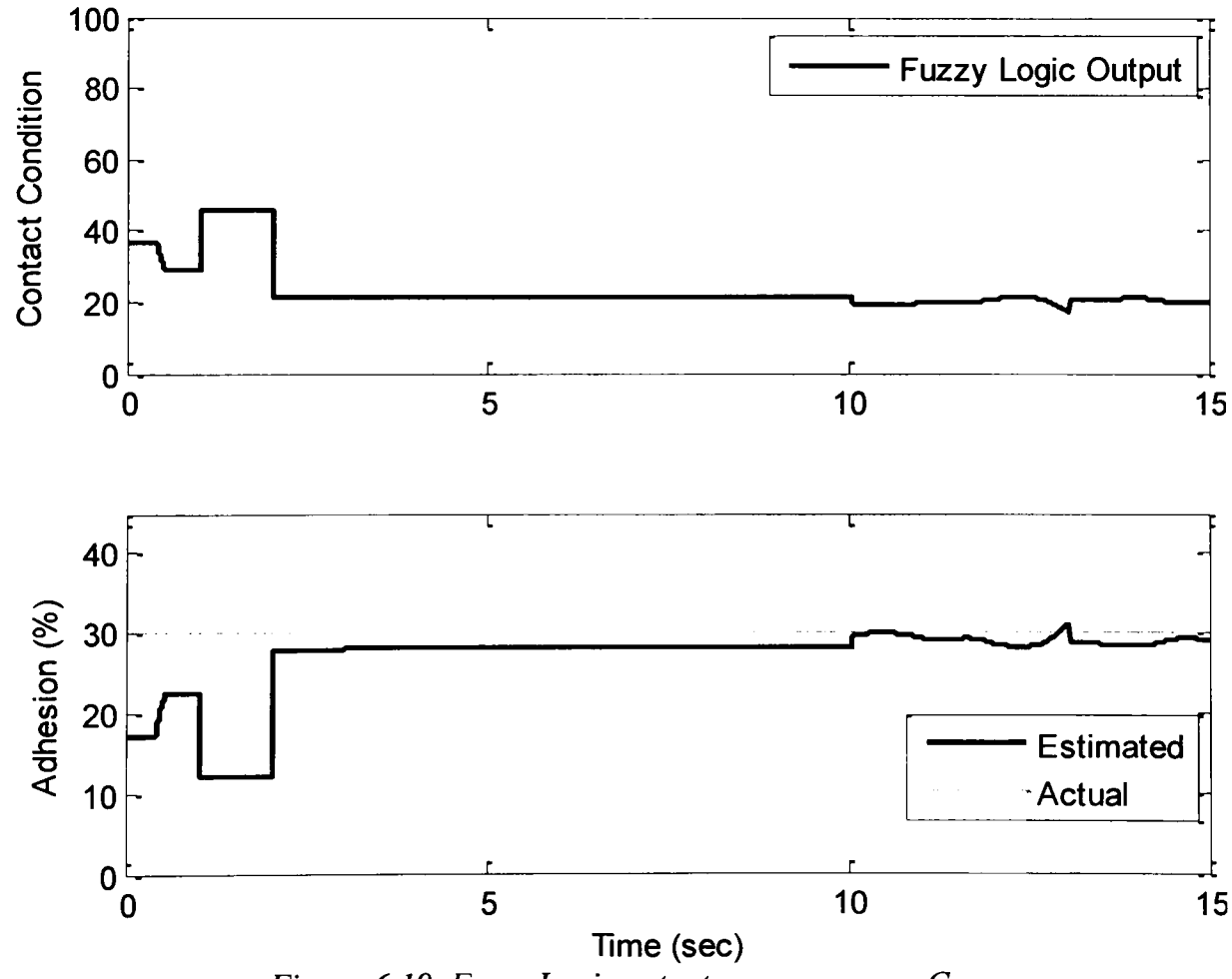

Figure-6.19. Fuzzy Logic output on creep curve C_C

Figure 6.16 shows the output of the fuzzy inference system when the system is operated on creep curve C_A. The fuzzy logic output is converted to adhesion information

using Equation (6.3). The system takes approximately two seconds to react and produce correct output. The delay in this case is the result of the time needed in the simulation to reach a steady condition for the tractive torque (Figure 6.17) and the time (1sec) is required to calculate the moving window rms of residuals. After 2 seconds, the output of the fuzzy logic system is steady and the estimated adhesion level is almost equal to the actual adhesion level. Figure 6.18 shows the result obtained by simulating the Simulink model using creep curve C_B. Again the steady output is produced after a delay of approximately 2 seconds. It is worth noting that almost half of the delay is due to the simulation conditions, which would not be present in practice.

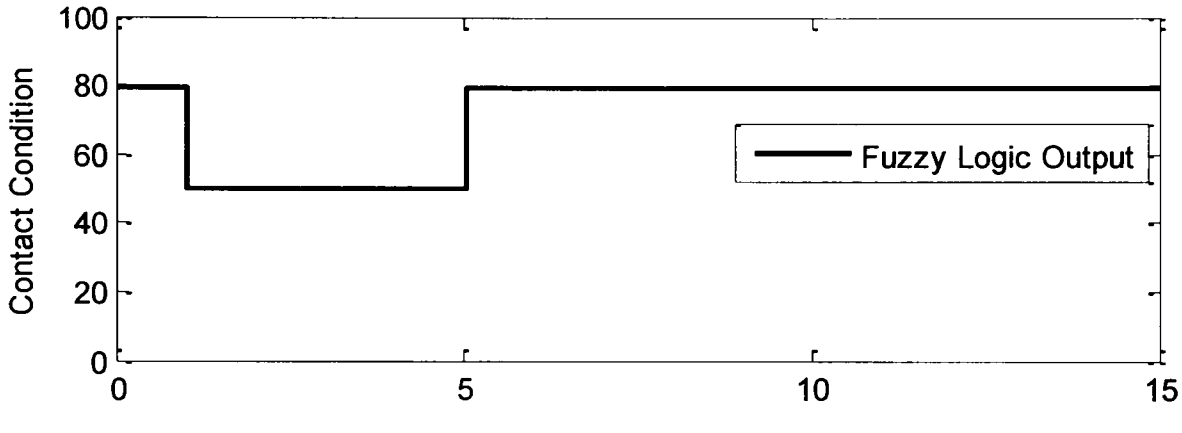

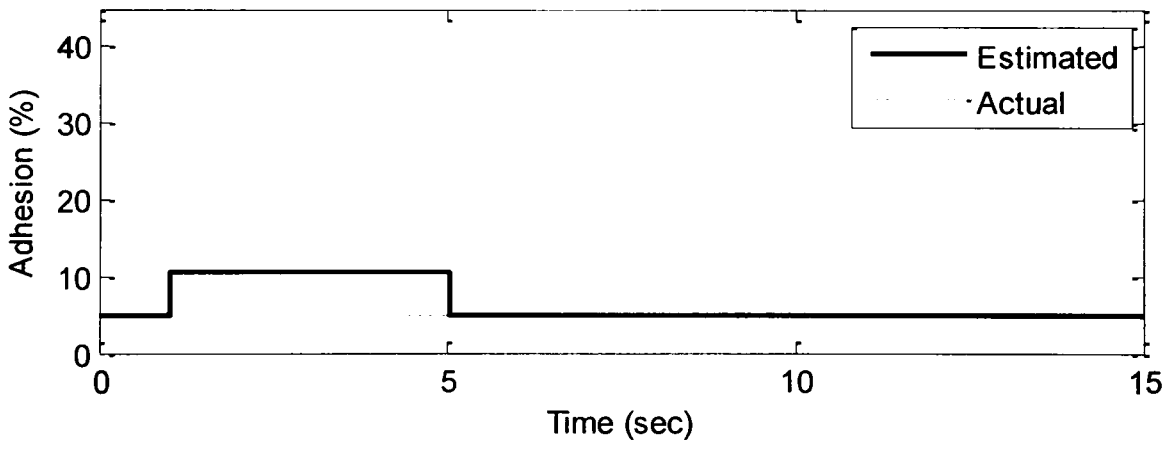

Figure-6.20. Fuzzy Logic output on creep curve C_I

Figure 6.19 shows the output of the fuzzy inference system when it is operated on the creep curve C_C. After a similar delay, the estimated adhesion level is approximately equal to the actual adhesion level. The difference in the actual output and the estimated output is caused by several reasons that include inaccuracy in fuzzy interpretation and the error due to the curve-fitting formula.

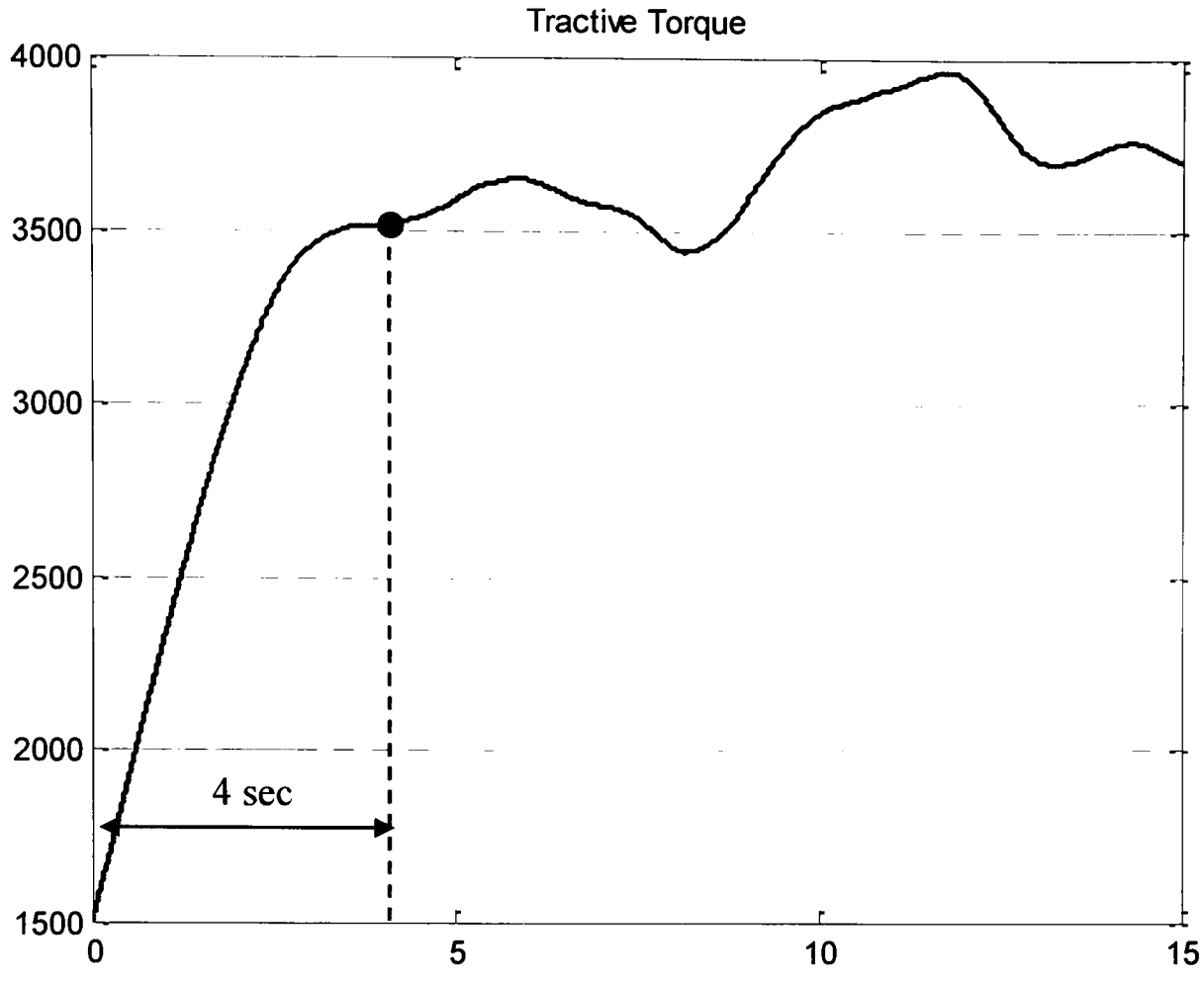

Figure-6.21. Tractive torque to drive wheelset on C_I

Figure 6.20 shows the simulation results when the system is operated on creep curve C_J. The estimated output is again equal to the actual adhesion level but this time a delay of 5 seconds is observed. This is because it is a low adhesion condition with adhesion level 5%, so the tractive torque adjustment in the simulations has to be relatively slow to prevent the operating point from jumping to the unstable region of the curve. The tractive torque is shown in Figure 6.21. Figure 6.22 shows the output when the system is operated on the creep curve C_I. Even though this creep curve was not used in the Kalman filter design or the fuzzy inference system design, the estimated adhesion level is nearly equal to the actual adhesion level. In Figure 6.22 at the 13^{th} second, the adhesion level is momentarily increased; this is because of the overshoot in the tractive torque shown in Figure 6.23. If the tractive torque is controlled smoothly the output of the fuzzy logic system would be more accurate, because a smooth control of the tractive torques allows the residuals of the filters to settle down. In the case of tractive torque with ripples the operating point fluctuates, which eventually results in a false output, as in Figure 6.22.

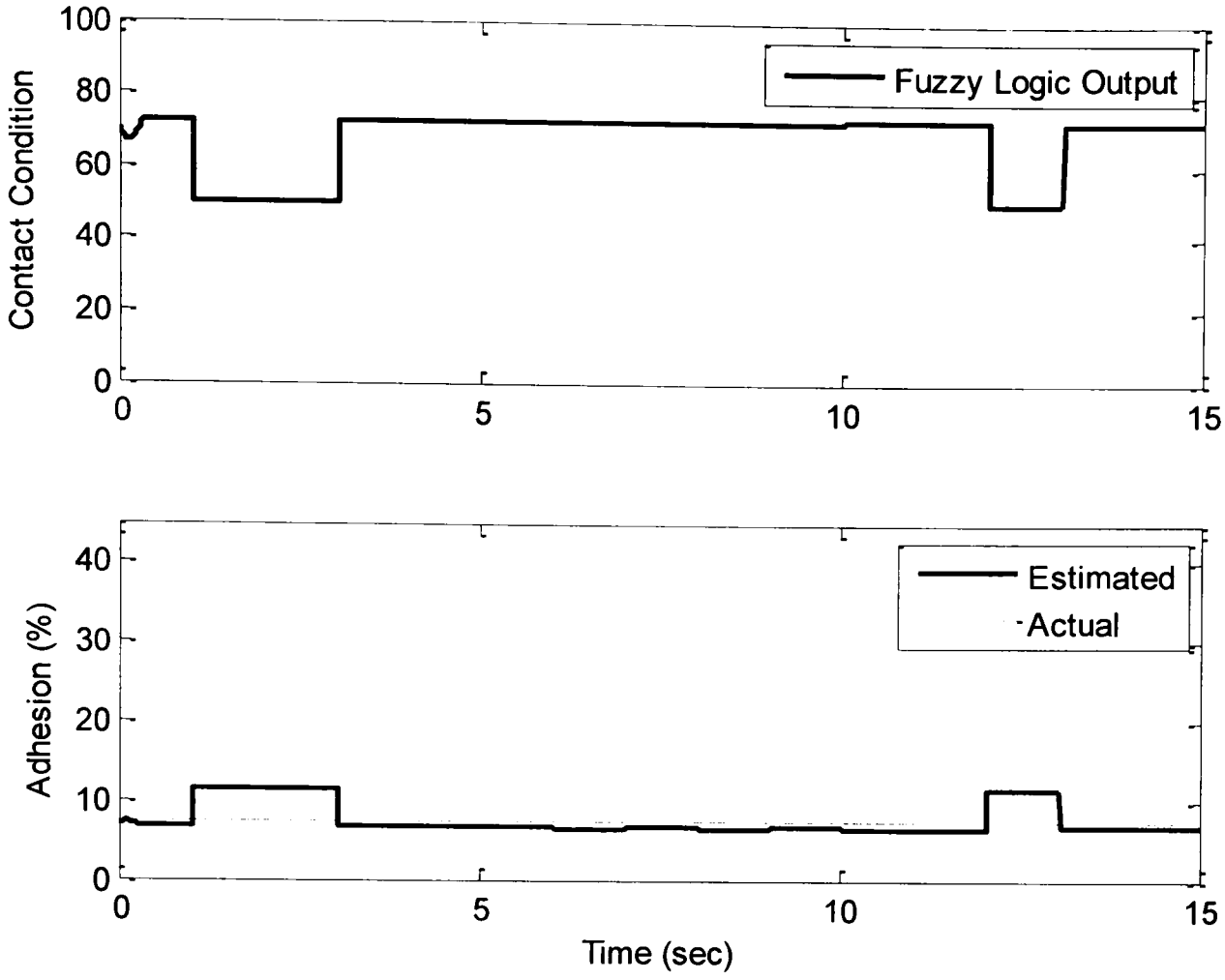

Figure-6.22 Fuzzy Logic output on creep curve C_H

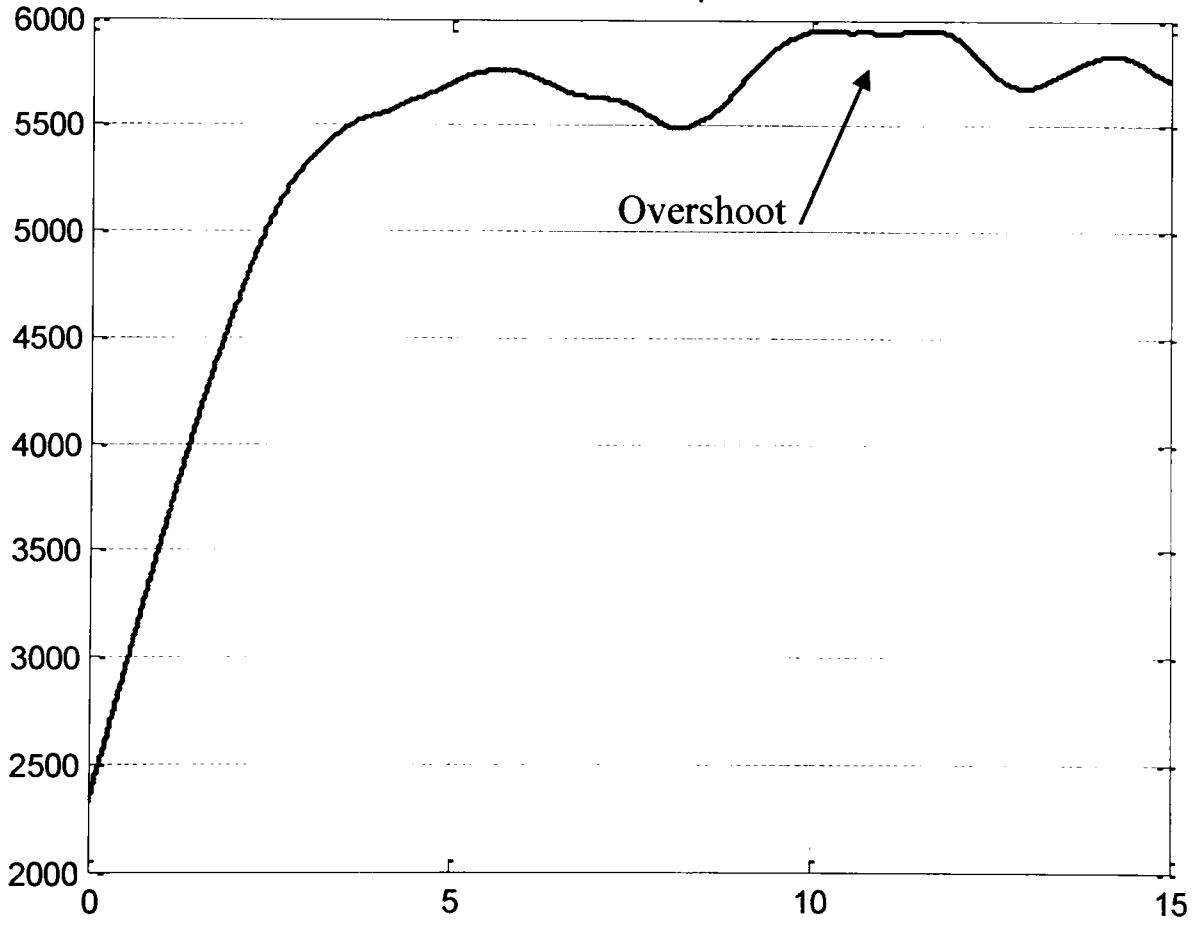

Figure-6.23. Tractive torque to drive wheelset on C_H

6.3 Fuzzy Logic System (Design-II)

This approach attempts to identify the adhesion level as well as the operating point of the wheelset. Therefore the structure of the fuzzy inference system is more complex, as shown in Figure 6.24. The whole fuzzy logic system consists of two fuzzy inference systems, one to detect the adhesion level (FIS-1) and the other to detect the operating point (FIS-2). The same inputs are applied to each system, which is assessed according to assigned membership functions. Different sets of rules are used to identify the operating point of the wheelset and the overall adhesion level. After the final fuzzy logic output is produced it is converted to percentage adhesion level and operating point information.

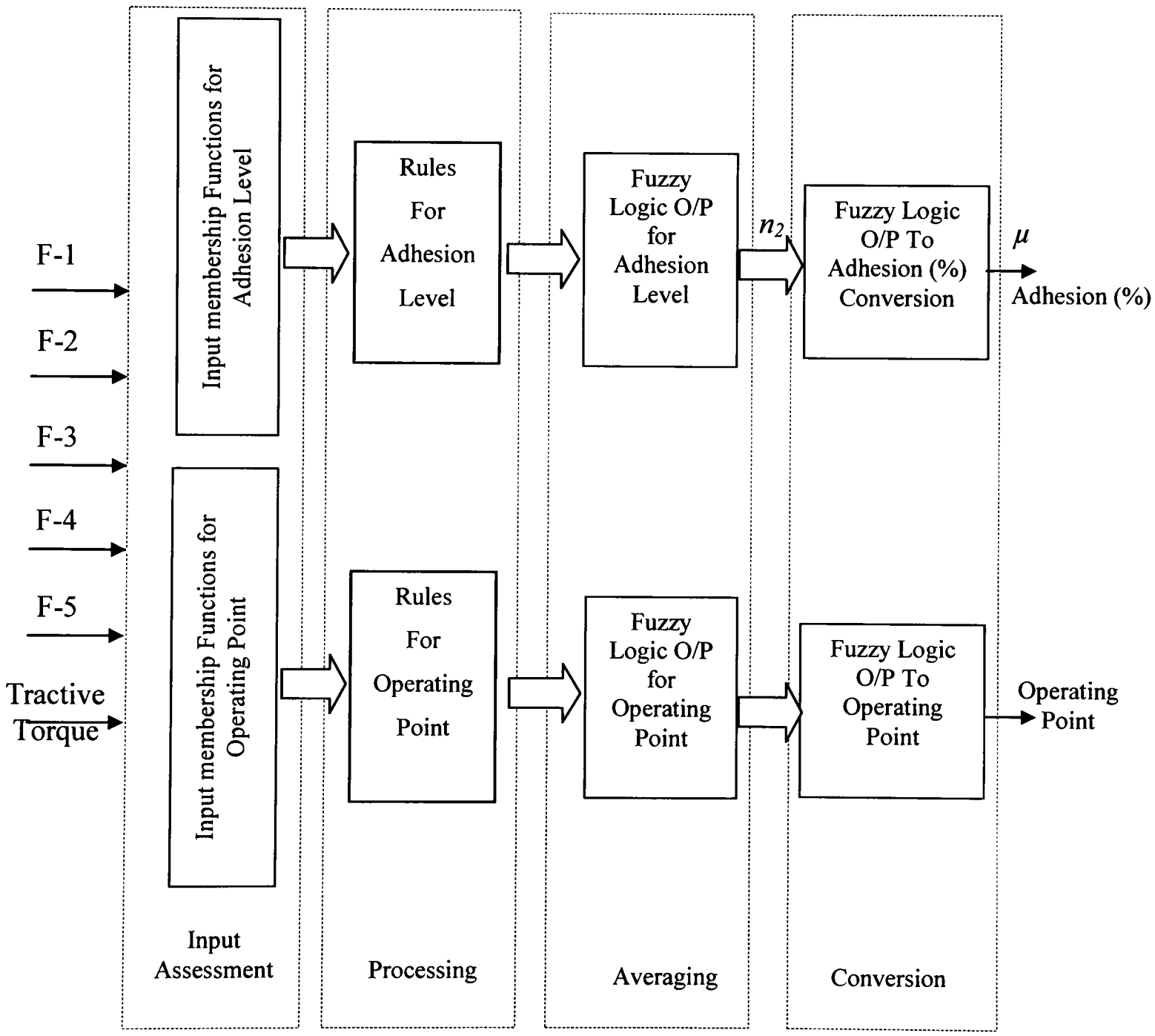

Figure-6.24. Fuzzy Inference System (Design-II)

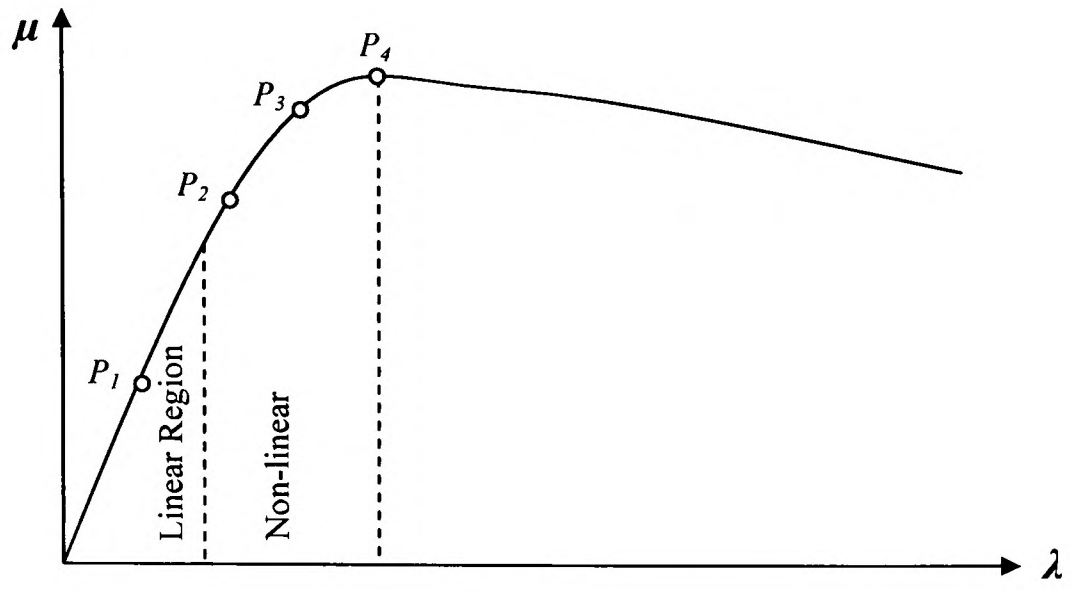

Figure-6.25. Basic Idea of Approach-II

The basic idea of approach-II is that each creep curve is divided into four regions: the linear region, the non-linear region away from saturation, the non-linear region near to saturation and the saturation region, as shown in Figure 6.25 with the help of a generic creep curve. The final outputs of the Fuzzy logic system after analysing the residuals of all filters and the tractive torque produces the estimated adhesion level in percentage and the operating point as P_1(Linear Region), P_2 (Non-linear region away from saturation), P_3 (Non-linear region near to saturation) or P_4 (Saturation Region).

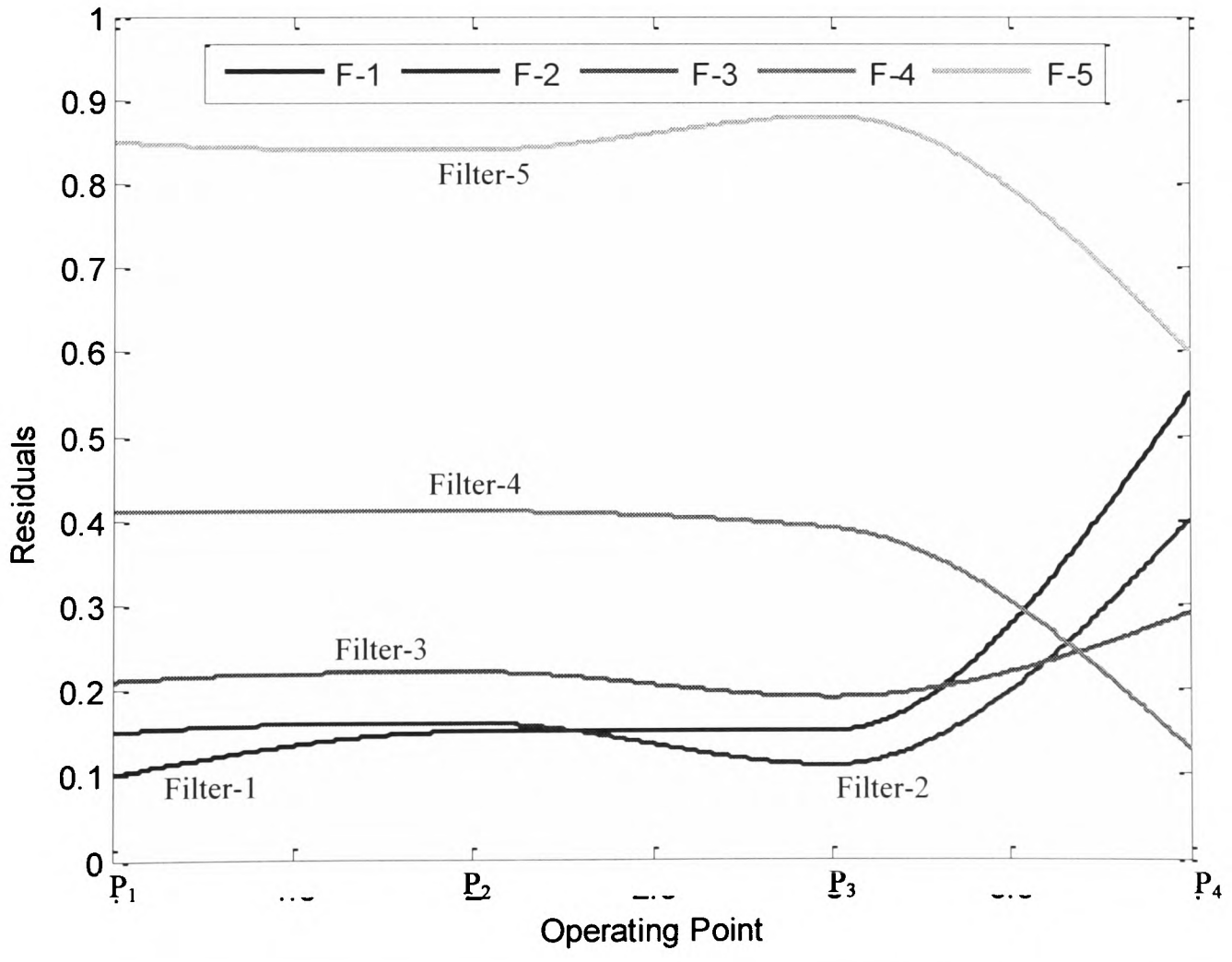

Figure-6.26. Variation of Residuals of all filters on C_a

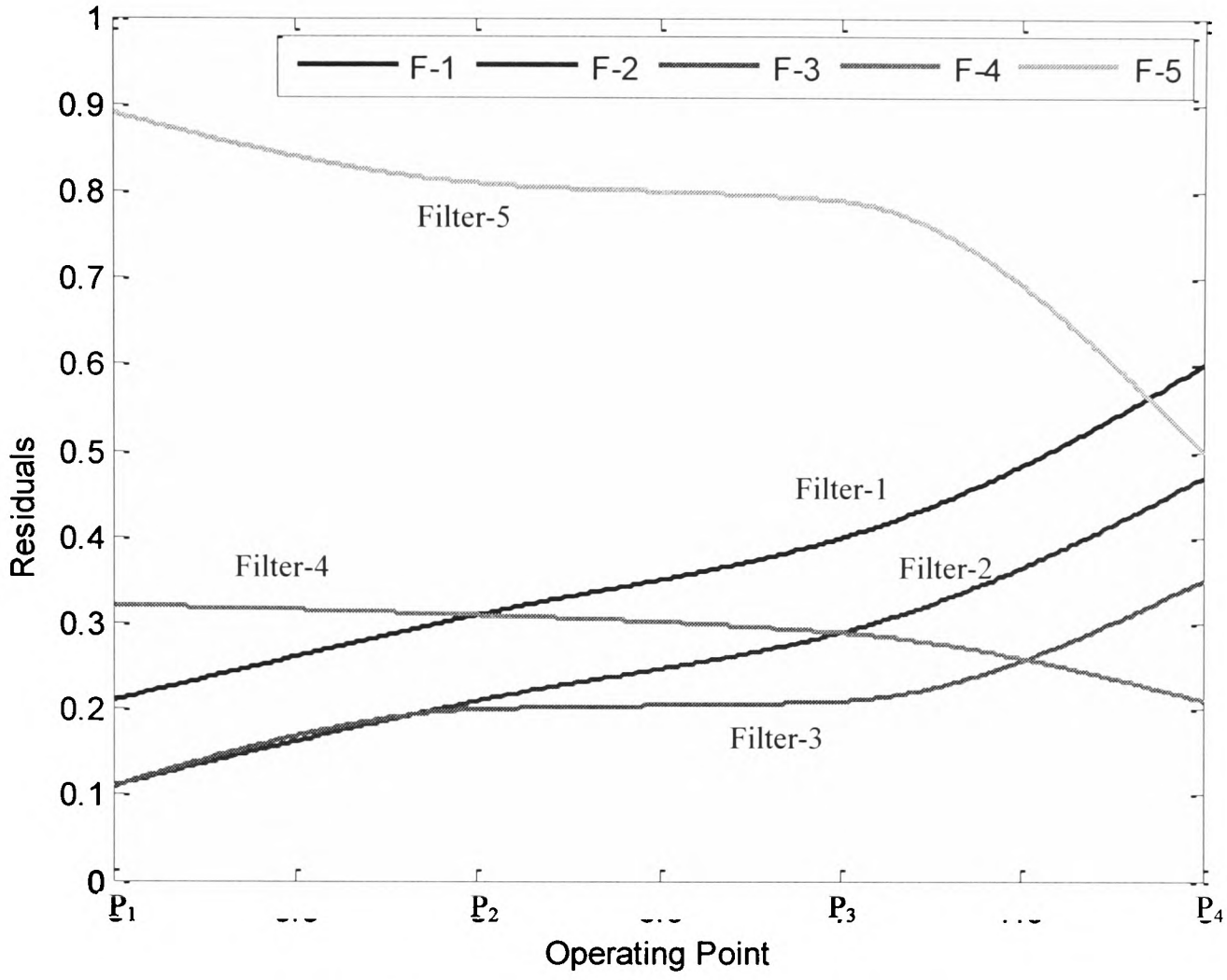

Figure.6.27. Variation of Residuals of all filters on C_b

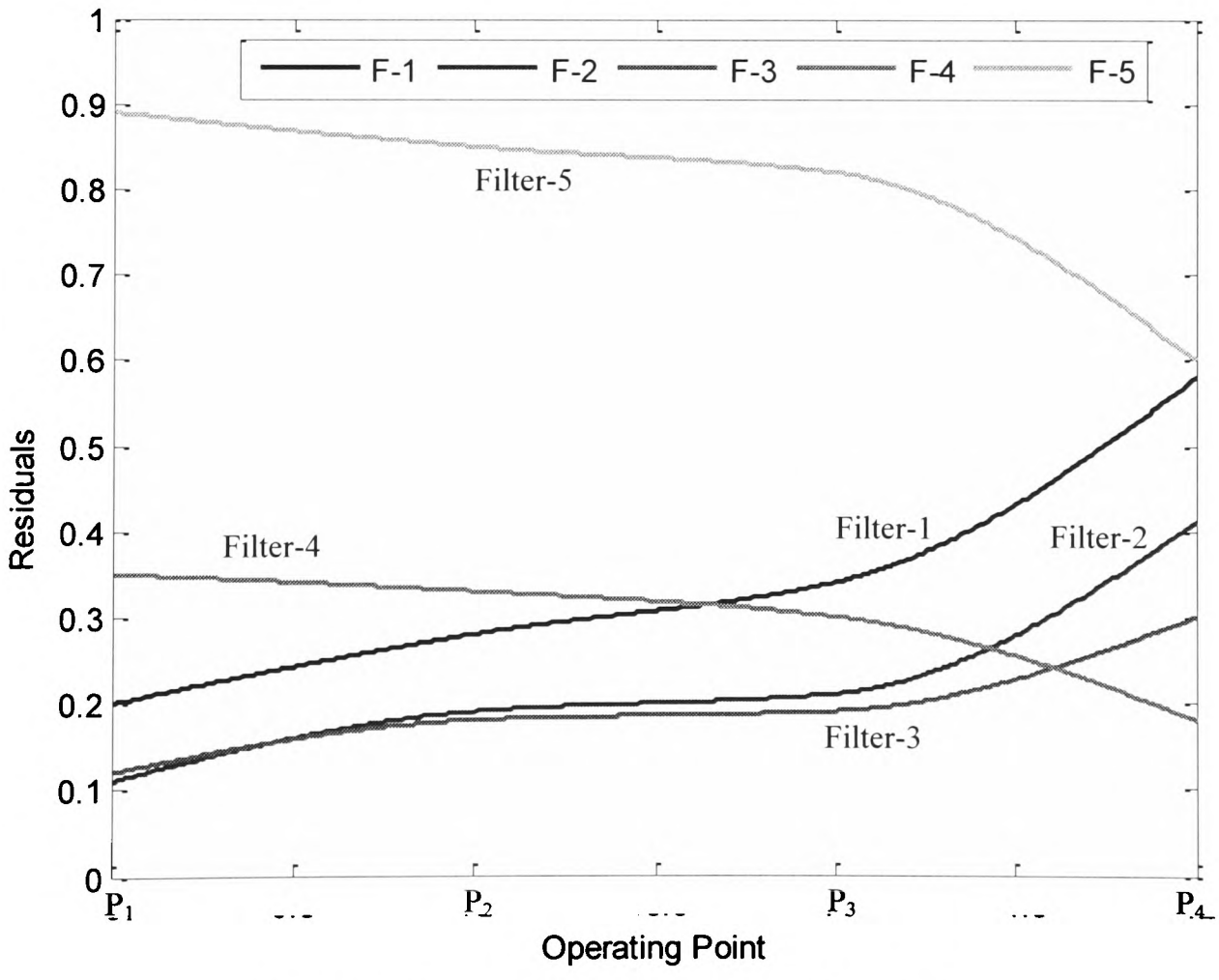

Figure.6.28. Variation of Residuals of all filters on C_c

6.3.1 Input membership functions

Table 5.5 provides a comprehensive analysis of the residuals in a variety of contact conditions and operating points. The design of the input membership function is more complex compared to the previous approach and it requires the analysis of the residuals at each curve separately. Therefore, in order to design the input membership functions for the adhesion condition, the variation in residuals is analysed at different operating points on each creep curve. A large variation in residuals is observed as the operating point reaches the saturation region (after P_3), as shown in Figures 6.26 to 6.34. The total span of the variation of residuals is divided into three categories 'Low', 'Moderate' and 'High,' similar to Design-I.

6.3.1.*a* Input membership functions (FIS-1)

In Figures 6.26, it can be seen that the residual of filter-1 is less than 0.2 if the level adhesion is 40% or more and the wheelset is not operating on the saturation region. Therefore the values of the residual from 0 to 0.2 are categorised as 'Low'. The value of the residual of the filter-1 is between 0.2 and 0.4, if the adhesion level is 20% to 40%. Therefore these values of the residual are categorised as 'Moderate' and rest of the values as 'High'. The membership function of the filter-1 is shown in Figure 6.35.

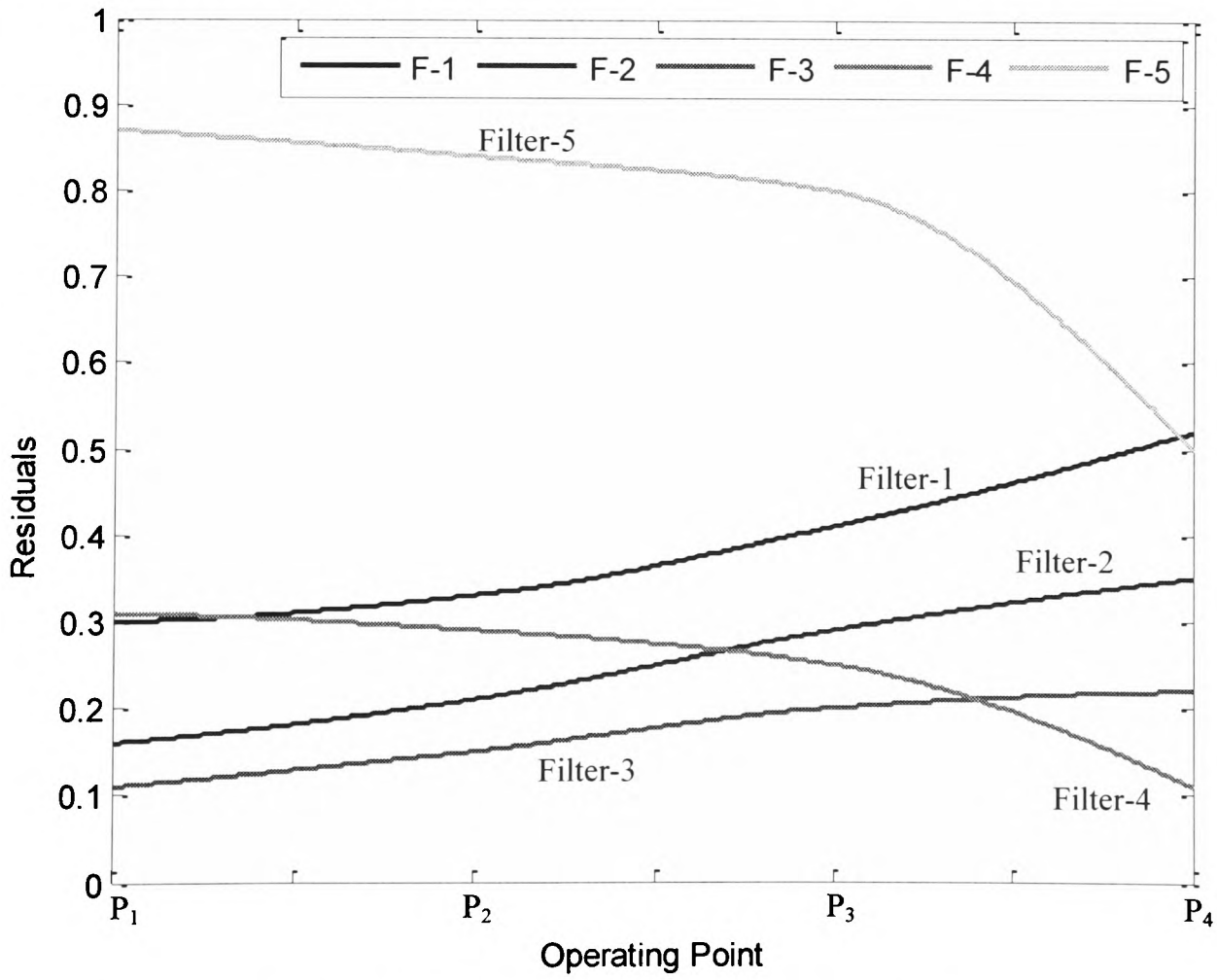

Figure.6.29. Variation of Residuals of all filters on C_d

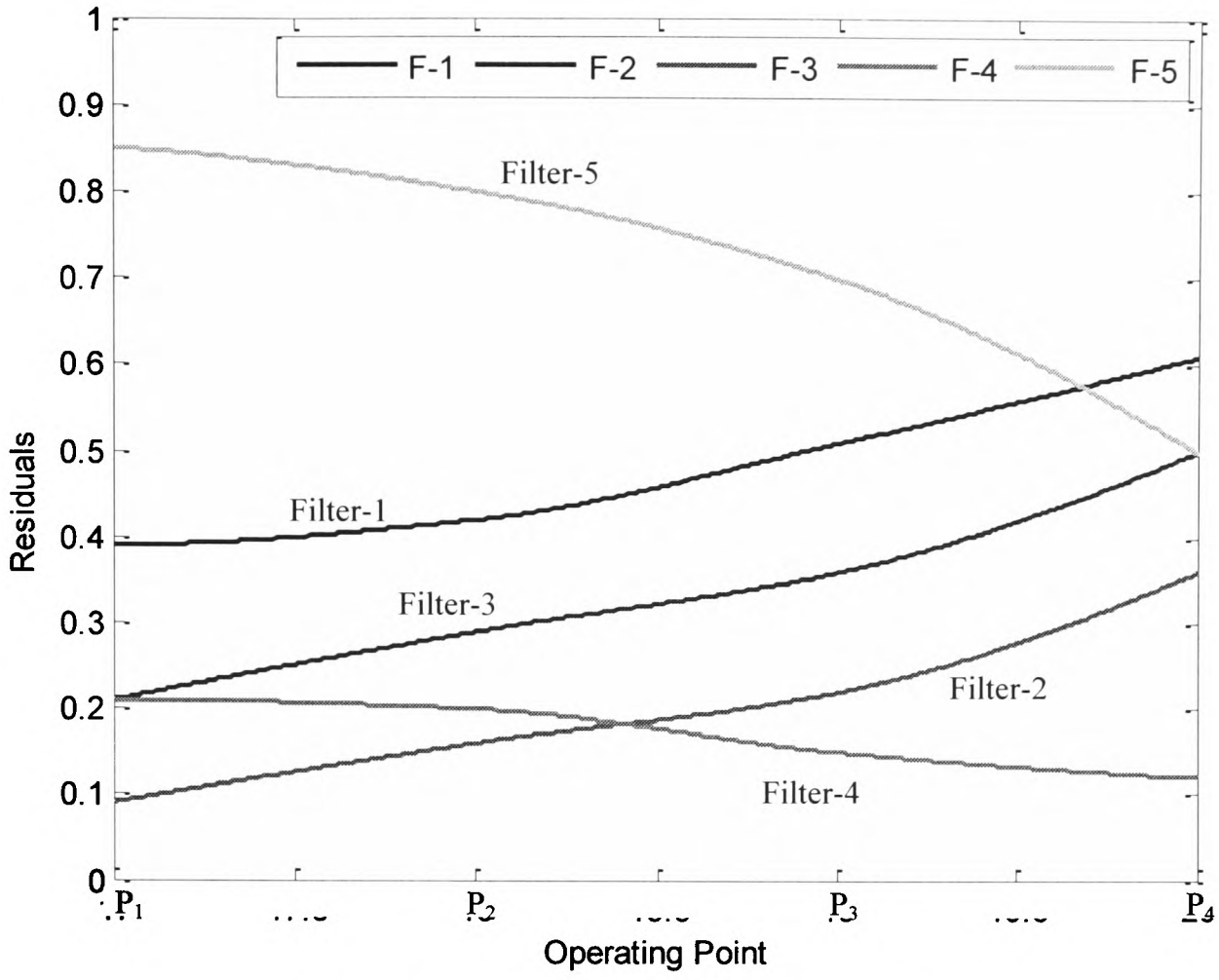

Fig.6.30. Variation of Residuals of all filters on C_e

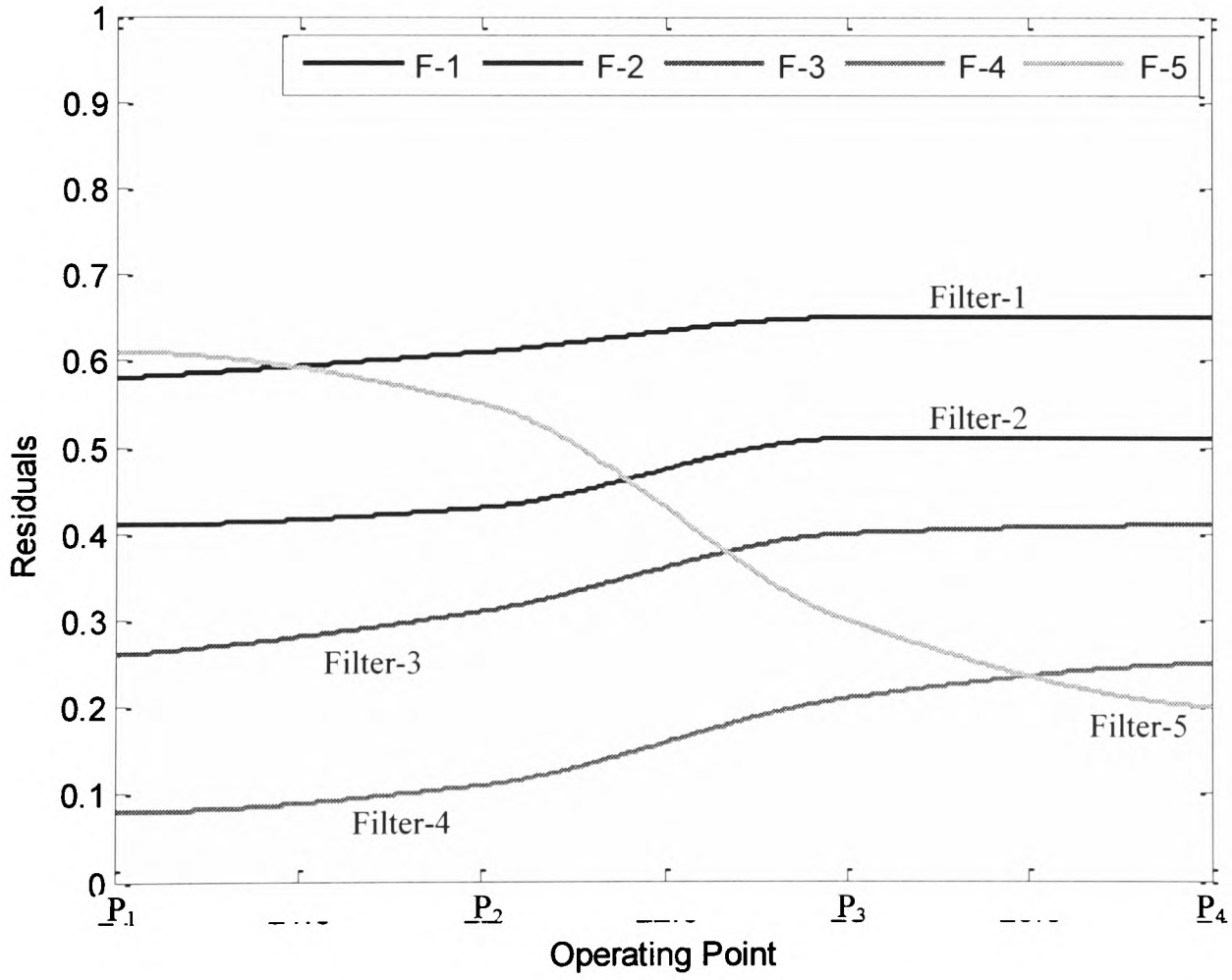

Fig.6.31. Variation of Residuals of all filters on C_f

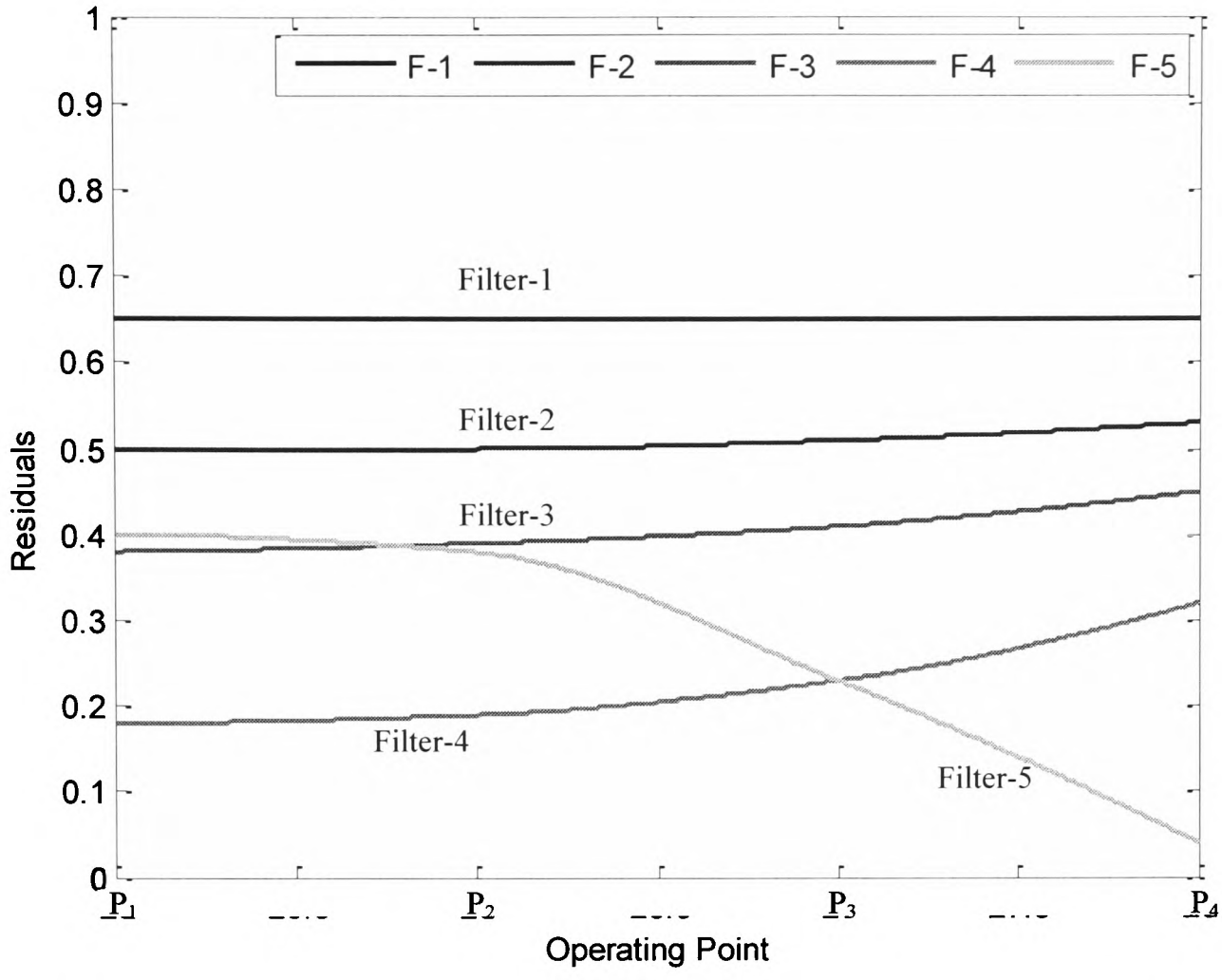

Fig.6.32. Variation of Residuals of all filters on C_g

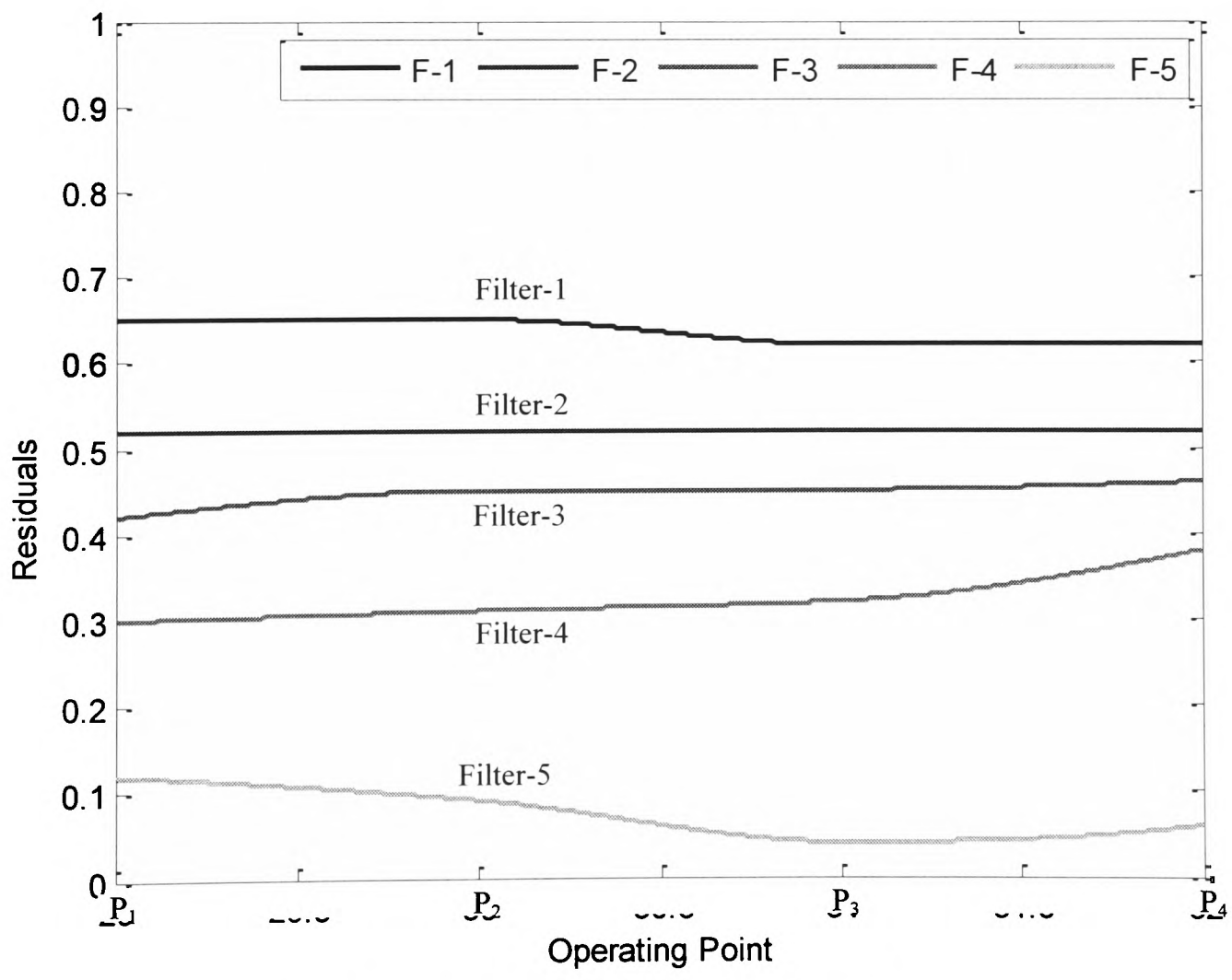

Fig.6.33. Variation of Residuals of all filters on C_h

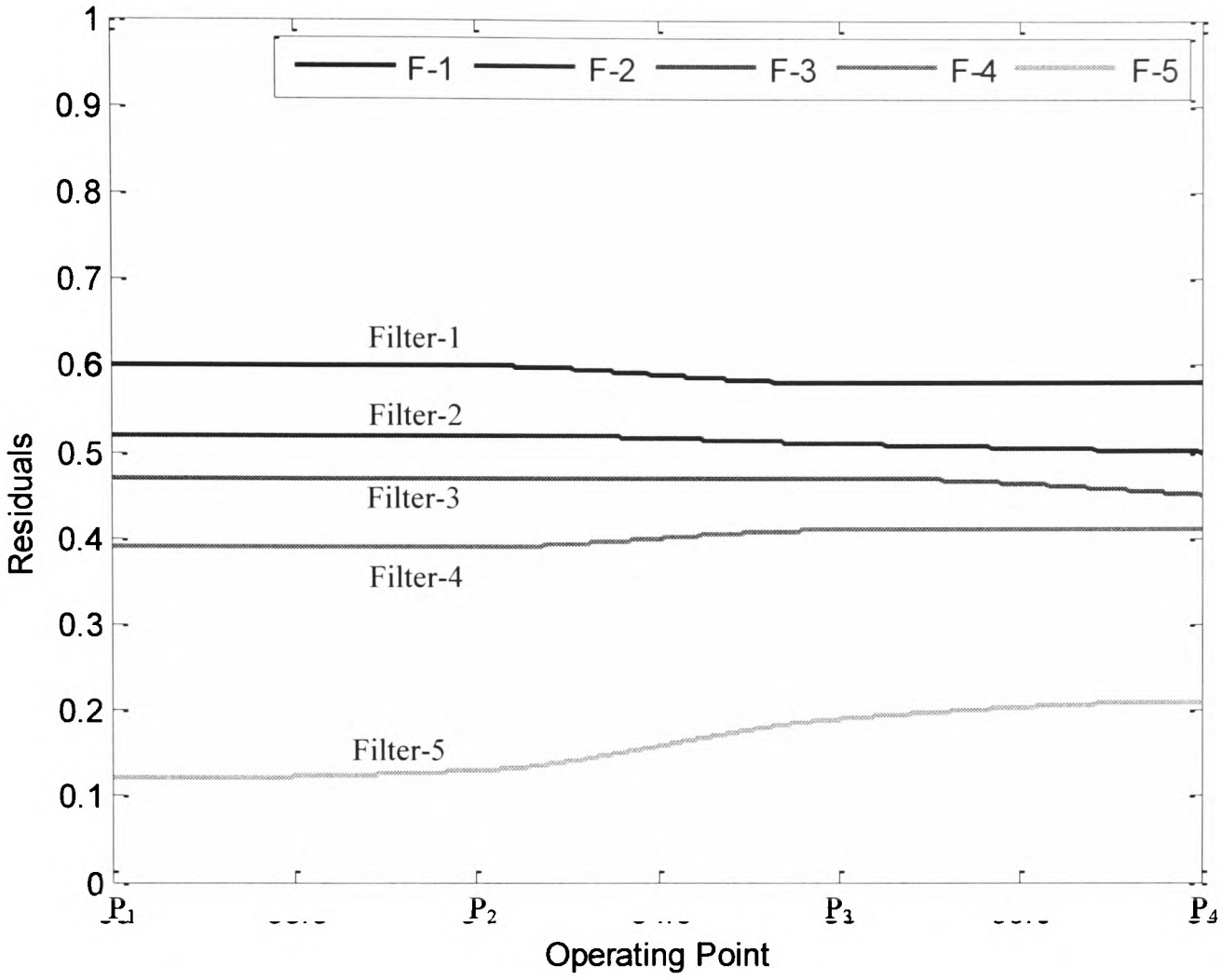

Fig.6.34. Variation of Residuals of all filters on C_i

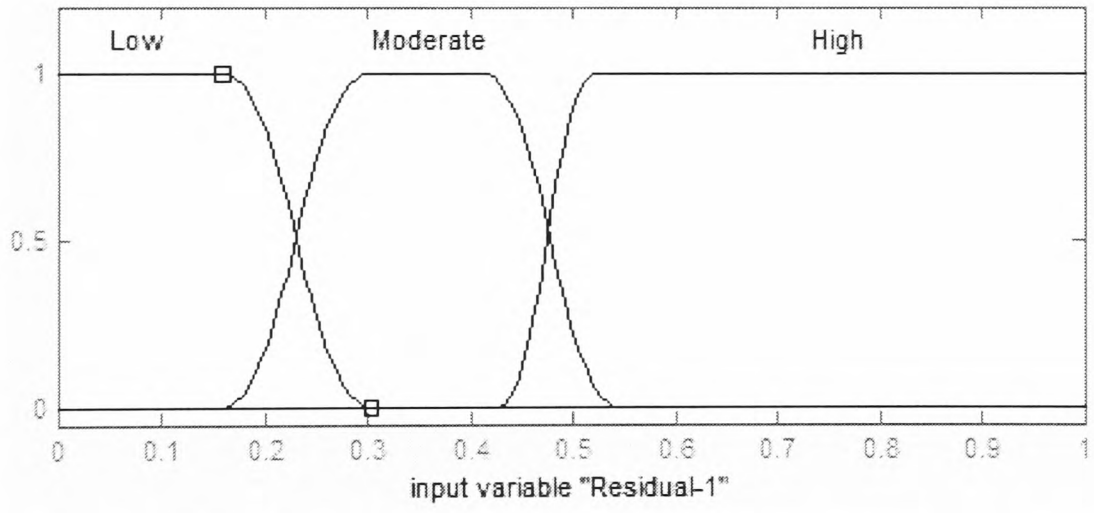

Figure-6.35. Membership function of residual of filter-1

The value of the residual of filter-2 is less than 0.2 when the adhesion is 40% or more and the operating point of the wheelset is not near the saturation region (before P_3), so this span is marked as 'Low'. When the adhesion values are between 20% and 40% and the operating point is not near saturation, the residual values are between 0.2 and 0.4 and are labeled as 'Moderate'. When the adhesion level is less than 20%, the residual values are greater than 0.4 and are categorised as 'High,' as shown in Figure 6.36.

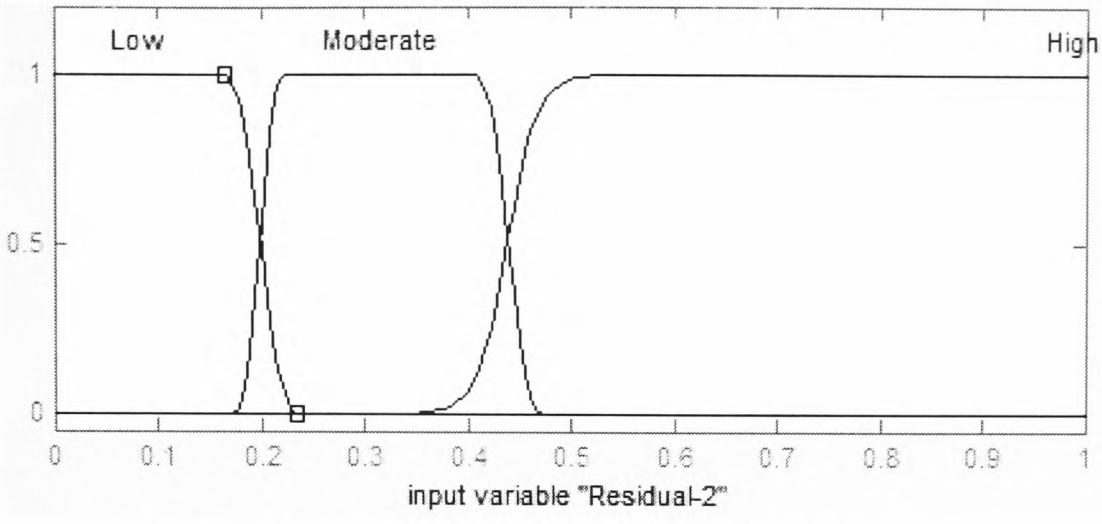

Figure-6.36. Membership function of residual of filter-2

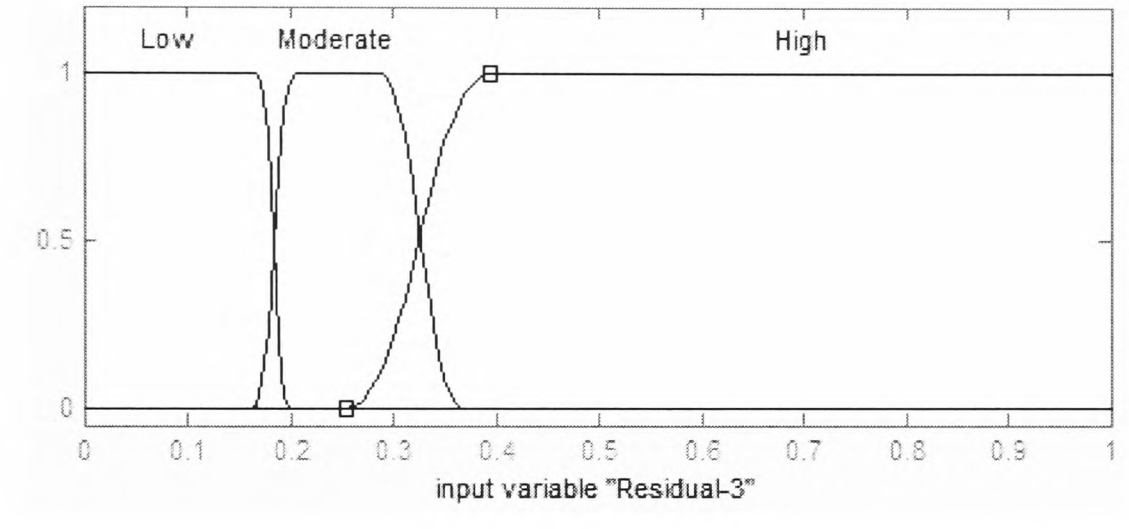

Figure-.6.37. Membership function of residual of filter-3

Similarly, the rest of the membership functions are designed for the adhesion output and are given in the following Figures. The shape and boundaries of the membership functions are also fine-tuned with the help of simulations to ensure the best possible consistency.

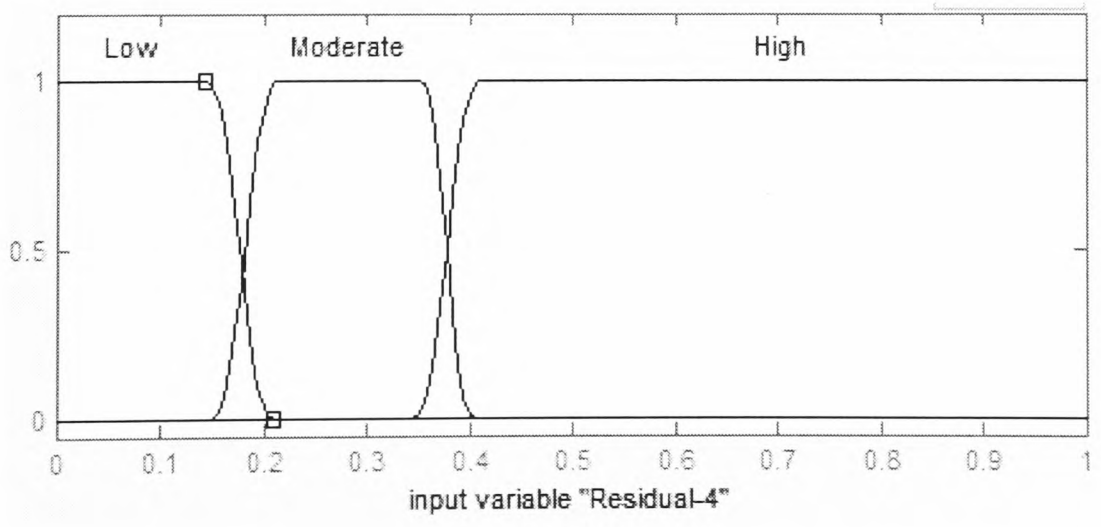

Figure-6.38. Membership function of residual of filter-4

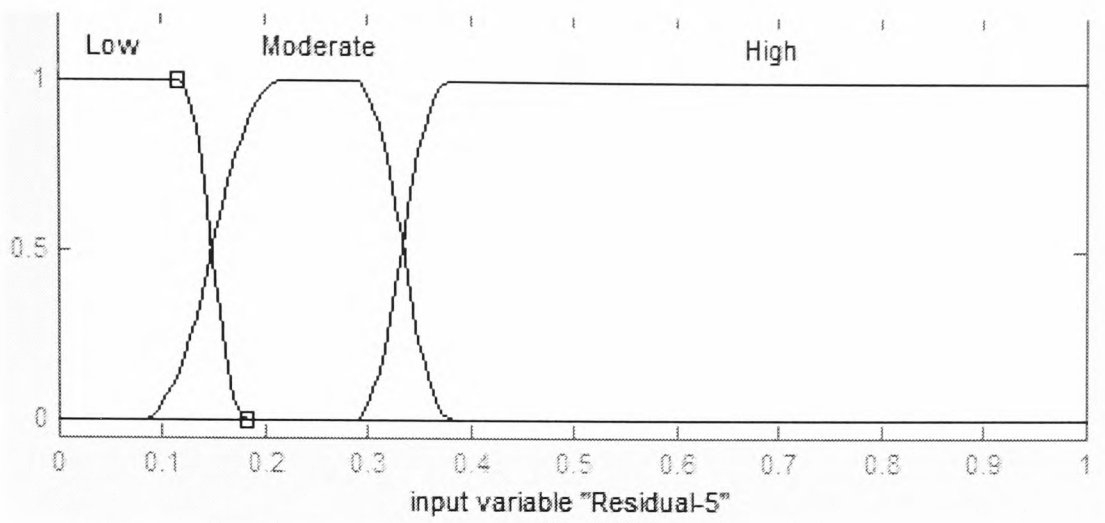

Figure-6.39. Membership function of residual of filter-5

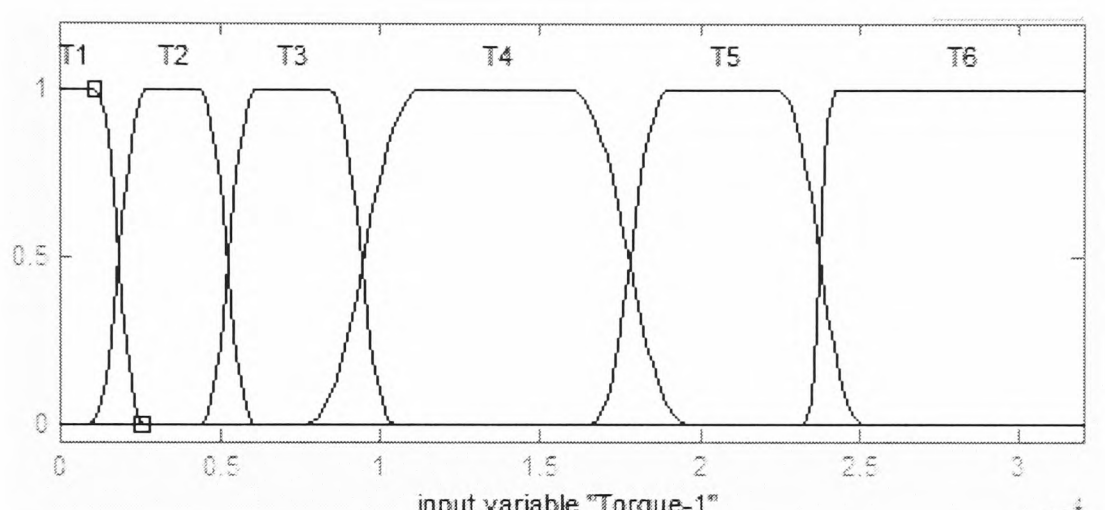

Figure-6.40. Membership function of Tractive Torque

The tractive torque is an important input to the fuzzy logic system to determine the location of the operating point and sometimes to distinguish two operating points that have similar dynamics characteristics. The membership function of the tractive torque is given in Figure 6.40.

6.3.1.*b* Input membership functions (FIS-2)

Filter-1 is designed to operate in the linear region of high adhesion creep curves. Therefore the value of the residual is 'Low' when the adhesion level is 40% or more and the wheelset is operated in the linear region, and 'moderate' if the adhesion level is more than 20%. For low adhesion curves the residual of filter-1 is 'High' as shown in Figure 6.41. From Table 5.5 it can be seen that the minimum to maximum value of the residual of filter-2 is 0.1 to 0.5. It has the lowest value when the adhesion level is between 30% and 40%. This value is marked as 'Low'. Values between 0.1 and 0.4 are marked as 'Moderate' and rest of the values as 'High,' as shown in Figure 6.42.

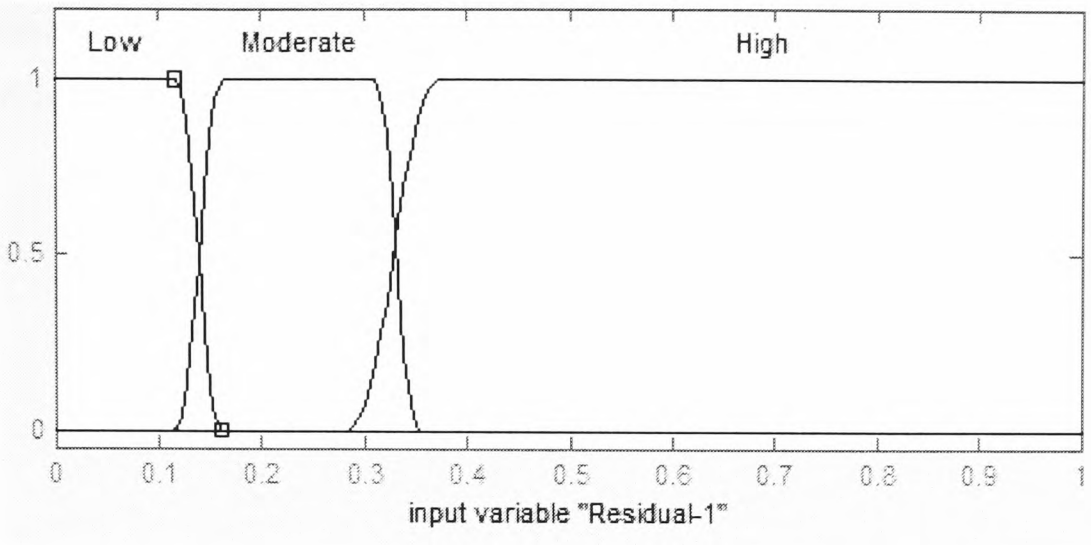

Figure-6.41. Membership function of Residual of filter-1

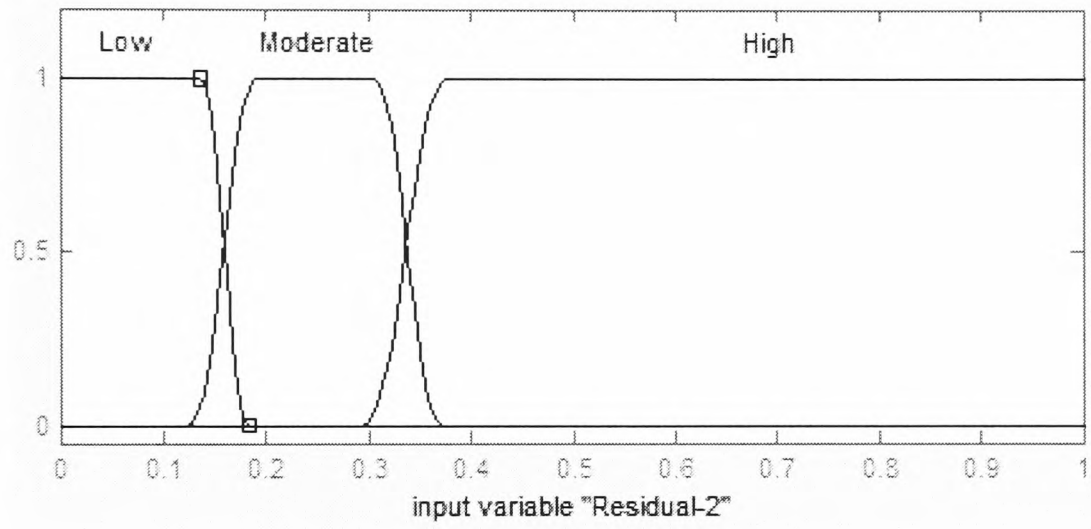

Figure-6.42. Membership function of Residual of filter-2

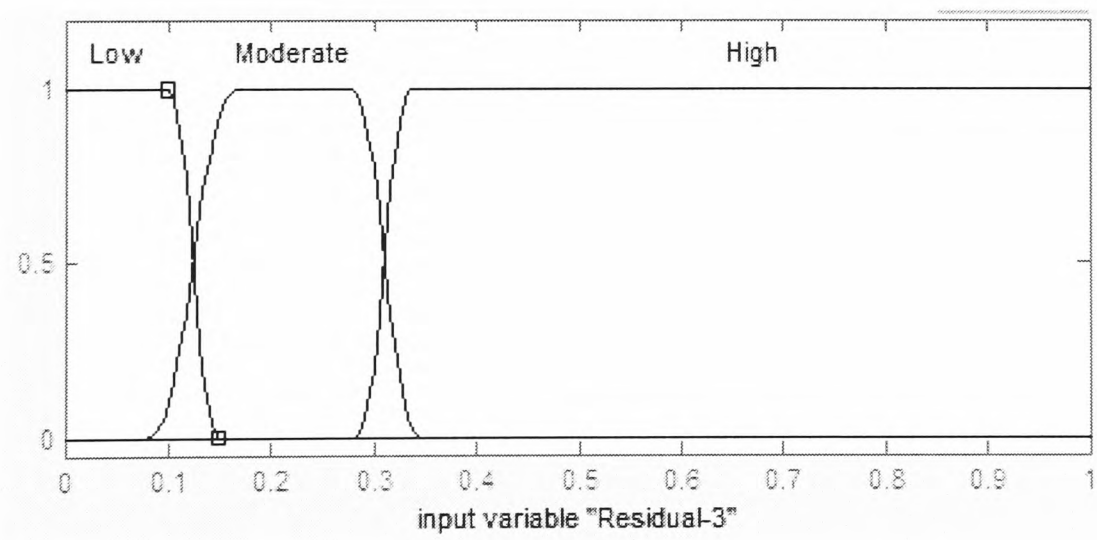

Figure-6.43. Membership function of Residual of filter-3

All other membership functions are also formed by thoroughly analysing the residual values given in Table 5.5. Again during the simulation, the membership function shapes and boundaries are fine-tuned to ensure the best possible results. Fine-tuning is

necessary because the residual values, in most of the cases, are not constant, as they fluctuate around the wheelset operating point.

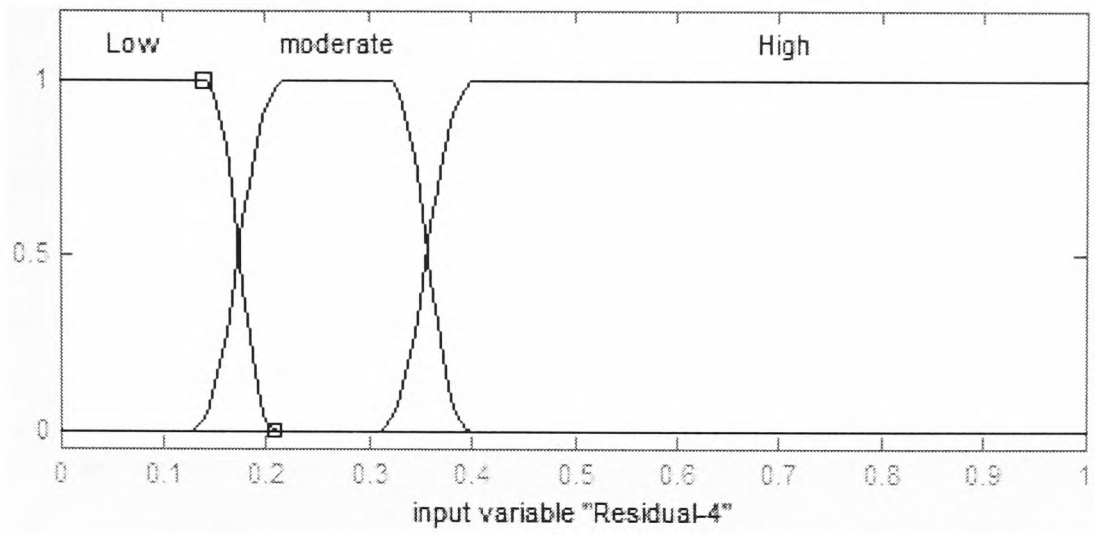

Figure-6.44. Membership function of Residual of filter-4

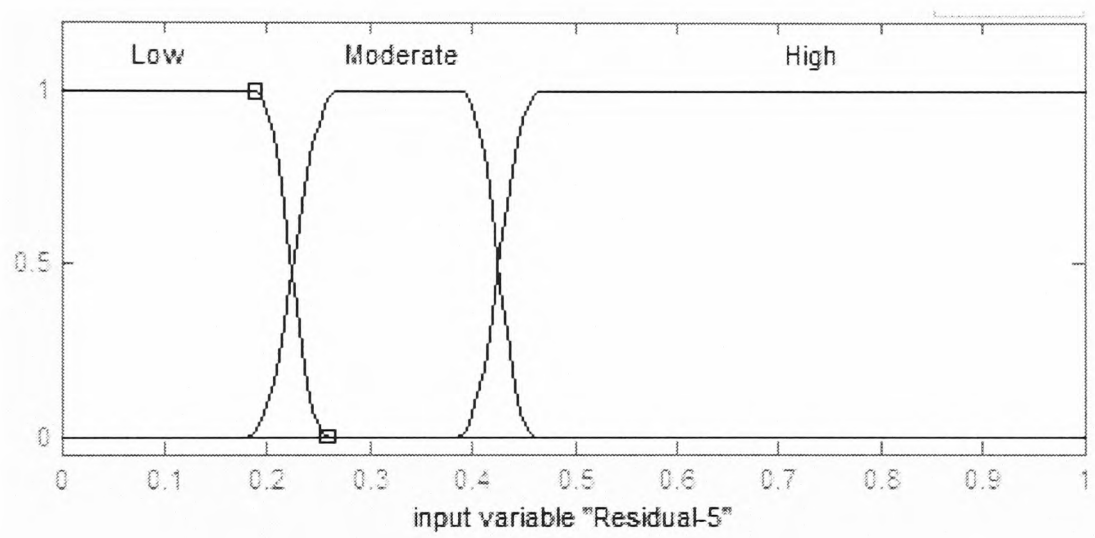

Figure-6.45. Membership function of Residual of filter-5

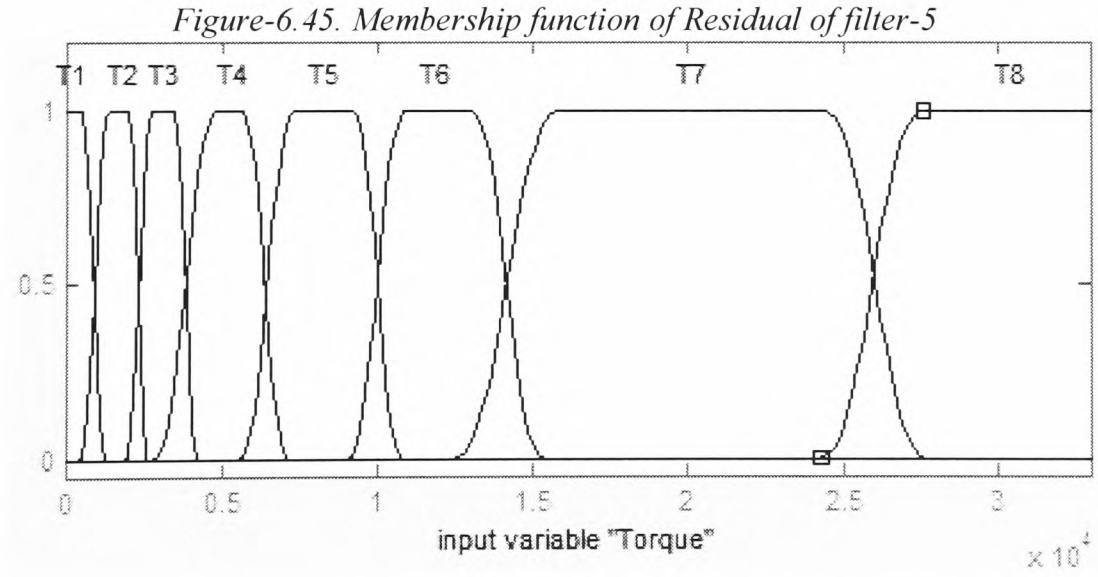

Figure-6.46. Membership function of Tractive Torque

The total span from 0 to 32k N-m of tractive torque in divided into eight sections. From the residual variations it can be seen that, when the adhesion level is more than 15%, the combination of residuals alone is sufficient in most of the cases to distinguish wheelset operating points. When the adhesion is low the tractive torque is more

important; that is why lower values of tractive torque are more finely divided compared to the higher values.

6.3.2 Fuzzy Logic Rules

After the input membership functions are defined, the next part is to develop fuzzy logic rules to process input data. Theoretically six inputs (with five inputs divided into three categories and torque divided into 8 categories) produces 1936 combinations, but in practice many of them are not possible. For example, the residuals of all filters 'Low' or the residuals of all filters 'High' are not possible, as the filters are designed to operate at different operating points and they cannot have equal residual values at the same operating point.

6.3.2.*a* Fuzzy Logic Rules (FIS-1)

Table 6.2 summarises the rules to detect the adhesion level. There are several rules for the same output because in this design the wheelset operating point could be anywhere on the entire creep curve excluding the region after the saturation point. Tractive torque information is not necessary for all the rules, and that is why it is left blank wherever it does not apply.

No.	F-1	F-2	F-3	F-4	F-5	T	Output
1	Low	Low	Moderate	High	High		μ≥40%
2	High	Moderate	Moderate	Low	High	T6	μ≥40%
3	Low	Low	Low	Moderate	High	T6	μ≥40%
4	Moderate	Low	Low	Moderate	High	T6	μ≥40%
5	Moderate	Moderate	Low	Moderate	High	T6	μ≥40%
6	Moderate	Moderate	Low	Low	High	T6	μ≥40%
7	Moderate	Low	Low	Moderate	High	T2	μ=20%
8	High	Moderate	Moderate	Low	High	T4	μ=20%
9	High	Moderate	Moderate	Low	High	T1	10%≥μ≥5%
10	High	High	Moderate	Low	High		10%≥μ≥5%
11	High	High	High	Low	High	T3	10%≥μ≥5%
12	High	High	High	Moderate	Low		μ=5%
13	High	Moderate	Moderate	Low	High	T5	40%>μ≥20%
14	Low	Low	Low	Moderate	High	T4	40%>μ≥20%
15	Moderate	Low	Low	Moderate	High	T5	40%>μ≥20%
16	Moderate	Low	Low	Moderate	High	T3	μ=20%
17	Moderate	Moderate	Low	Moderate	High	T4	μ=20%

18	High	High	High	Moderate	Moderate	T3	10%≥μ≥5%
19	Moderate	Moderate	Low	Moderate	High	T2	20%>μ≥10%
20	Moderate	Moderate	Low	Moderate	High	T3	20%>μ≥10%
21	High	Moderate	Moderate	Low	High	T4	20%>μ≥10%
22	High	High	High	High	Moderate	T1	μ<5%
23	High	High	High	Low	High	T1	10%≥μ>5%
24	High	High	High	Low	High	T1	μ =5%

Table.6.2. Fuzzy Logic Rules for adhesion level

6.2.2.*b* Fuzzy Logic Rules (FIS-2)

Table 6.3 summarises the fuzzy logic rules for FIS-2 developed using Table 5.5. In some of the rules information about tractive torque is not required, so it is left empty.

6.3.3 Output membership functions

Figures 6.47 and 6.48 show the output fuzzy set for adhesion level output and operating point respectively. In Figure 6.47 each adhesion level is associated with a particular number on the horizontal axis. For example, 5% adhesion level is represented by 80 at the fuzzy logic output. If more than one rule is wholly or partially true, the centre of gravity of the combined output is calculated using Equation (6.2).

No.	F-1	F-2	F-3	F-4	F-5	T	Output
1	Low	Moderate	Moderate	High	High		P1
2	Moderate	Low	Low	Moderate	High		P1
3	High	Moderate	Low	Moderate	High		P1
4	High	High	Moderate	Low	High	T1	P1
5	High	High	High	Low	Moderate		P1
6	High	High	High	Moderate	Low	T1	P1
7	High	High	High	High	Low	T1	P1
8	Low	Low	Moderate	High	High		P1
9	Moderate	Moderate	Moderate	High	High		P2
10	Moderate	Moderate	Moderate	Moderate	High		P2
11	High	High	High	Low	High	T4	P2
12	High	High	High	Moderate	Moderate	T1	P2
13	High	High	High	High	Low	T1	P2
14	High	High	High	Low	High	T5	P2
15	Moderate	Low	Moderate	High	High		P3
16	High	Moderate	Moderate	Moderate	High	T7	P4
17	High	High	Moderate	Low	High	T6	P3
18	High	High	High	Moderate	Moderate	T5	P3
19	High	High	High	High	Low	T1	P3
20	High	High	High	High	Low	T2	P3
21	High	High	Moderate	Low	High	T8	P4
22	High	Moderate	Moderate	Moderate	High	T8	P3
23	High	High	Moderate	Low	High		P3
24	High	High	Moderate	Low	High		P3/P4

25	High	High	Moderate	High	High	T8	P4
26	High	High	High	Moderate	High	T8	P4
27	High	High	Moderate	Moderate	High	T7	P4
28	High	High	High	Low	High	T6	P4
29	High	High	High	Moderate	Low	T4	P4
30	High	High	High	High	Low	T3	P4
31	High	High	High	High	Moderate	T2	P4

Table.6.3. Fuzzy Logic Rules for operating point

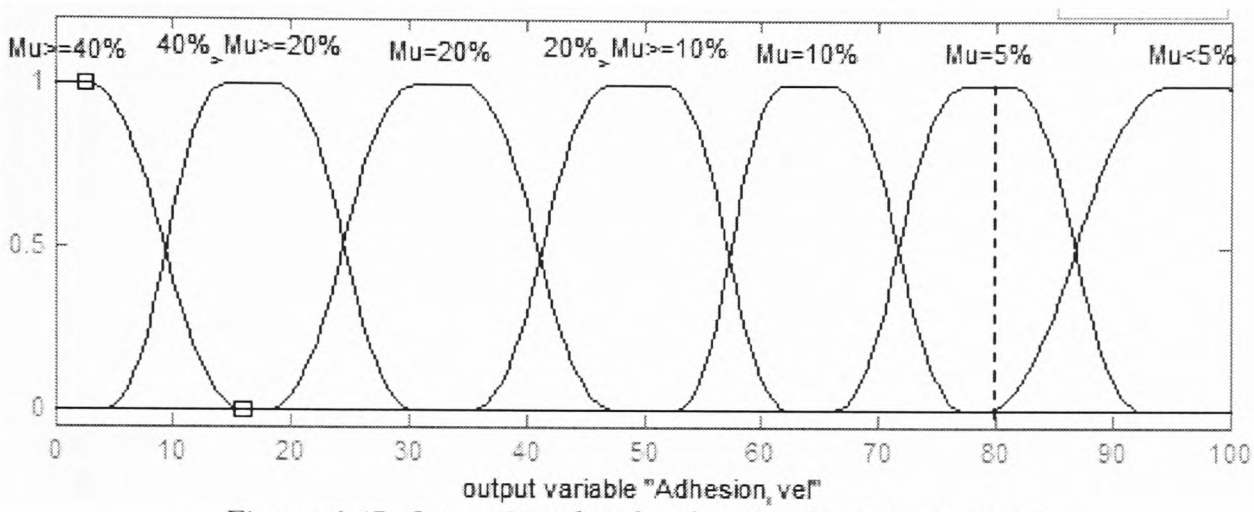

Figure-6.47. Output Membership function for Adhesion level

Similarly, in Figure 6.48 each operating point is represented by a numeric value from 0 to 100. For example, the fuzzy logic output 33.33 indicates that the wheelset operating point is in the non-linear region away from saturation (P_2).

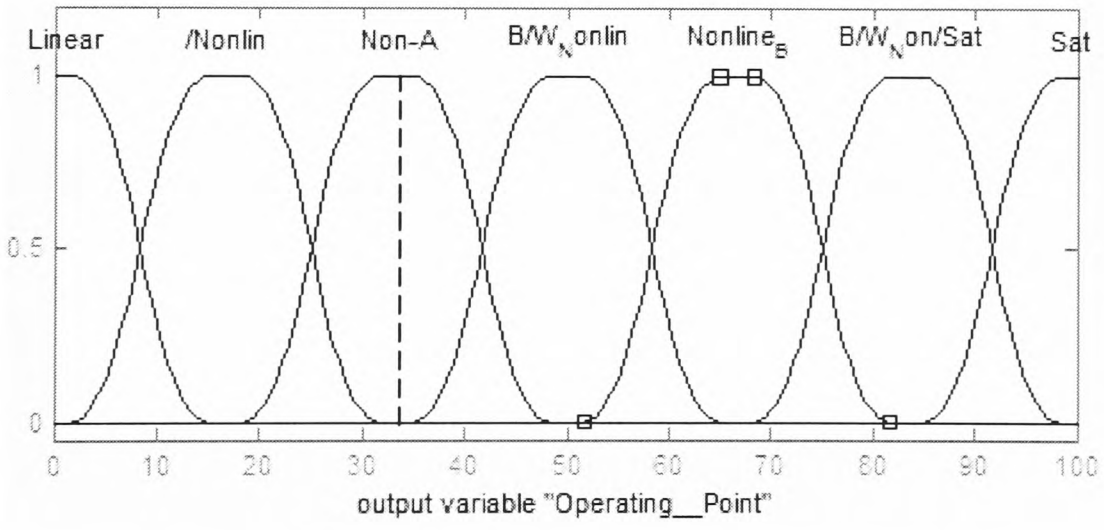

Figure-6.48. Output Membership function for operating point

6.3.4 Output Conversion

The output of FIS-1 is converted to adhesion coefficient using the curve fitting formula given below, where n_2 is the numeric output of FIS-1 as shown in Figure 6.25.

$$\mu = -4.714\times10^{-6} n_2^4 + 0.0011 n_2^3 - 0.08 n_2^2 + 1.8 n_2 + 33 \qquad (6.4)$$

The conversion of the fuzzy logic output to adhesion level using Equation (6.4) is fairly accurate, with a maximum conversion error of 1.5 %.

6.3.5 Simulation Results

Simulations are carried out using the different creep curves shown in Figure 6.15 and the results of the simulation are given below.

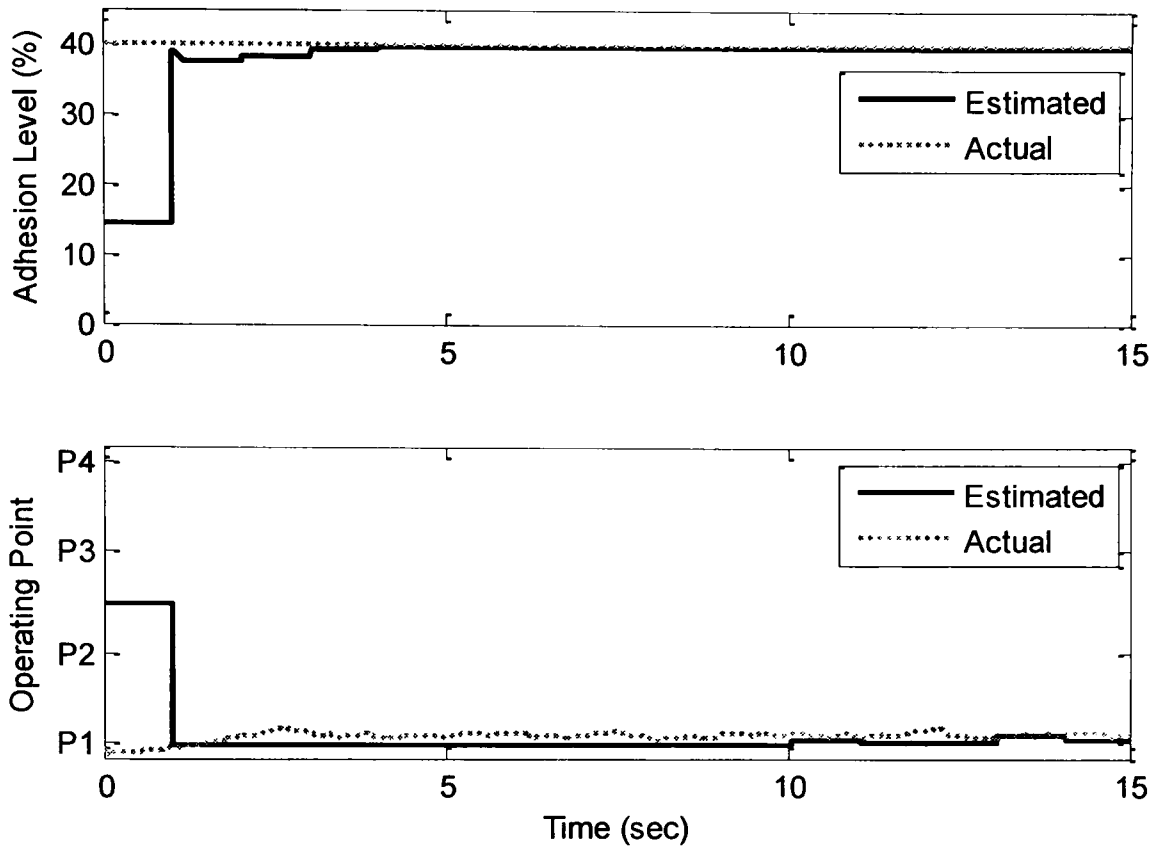

Figure-6.49. Simulation Result when the wheelset is operated on C_A

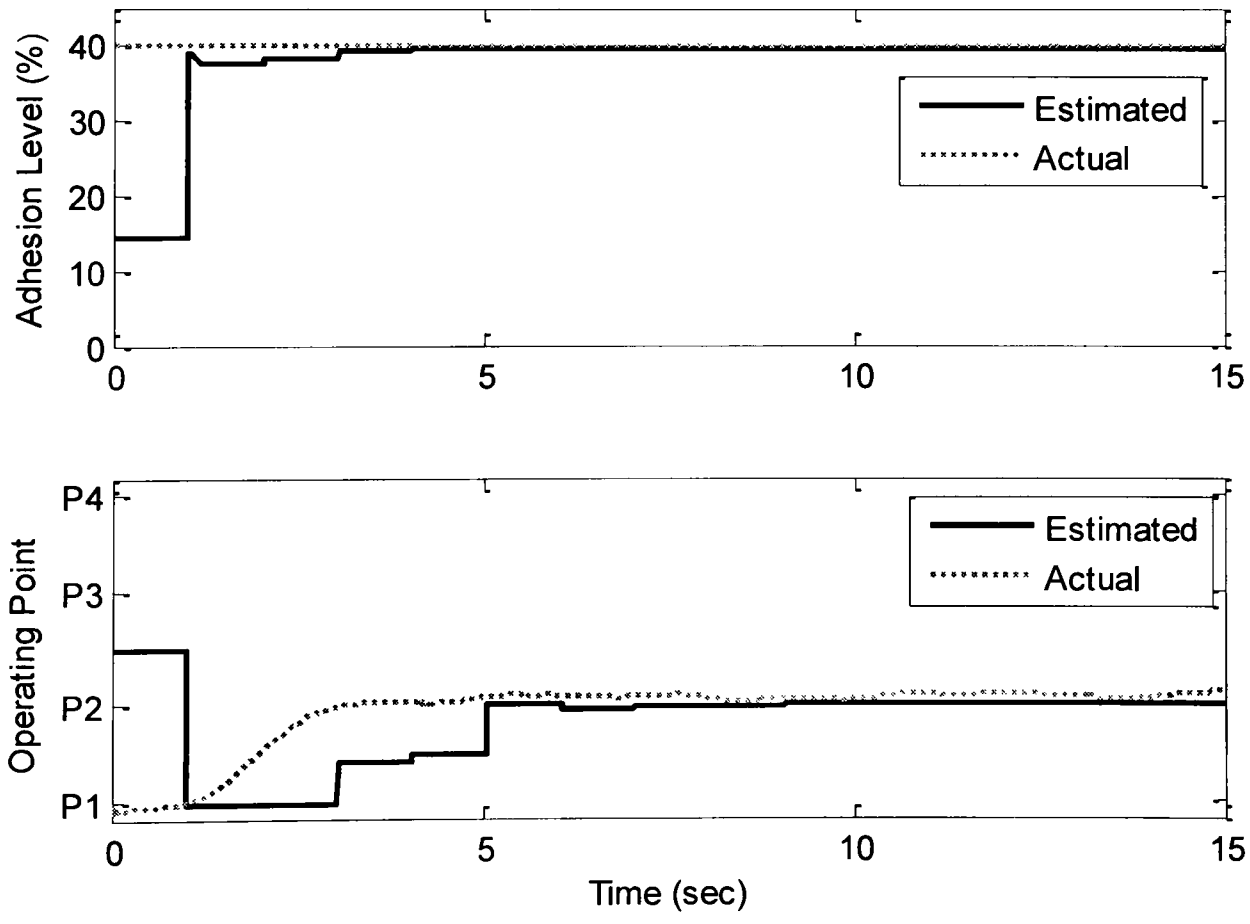

Figure-6.50. Simulation Result when the wheelset is operated on C_A

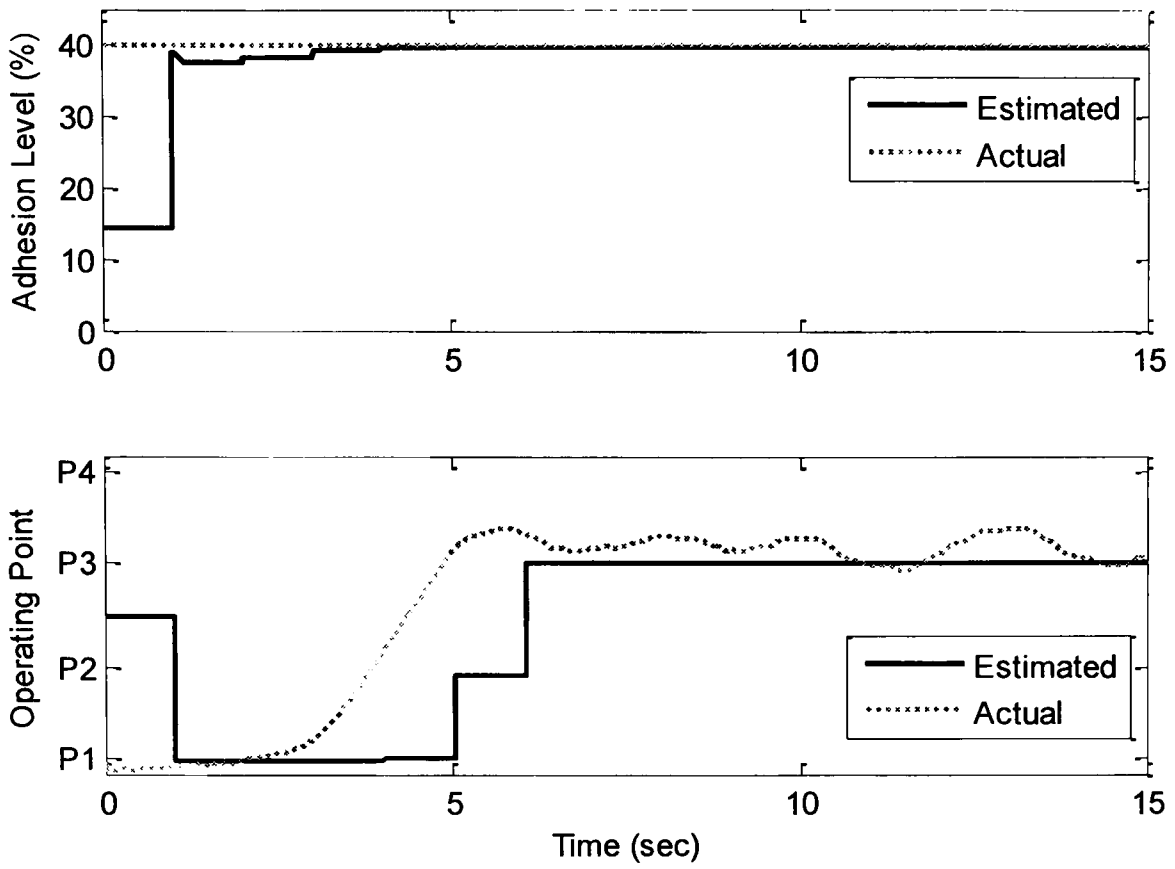

Figure-6.51. Simulation Result when the wheelset is operated on C_A

Figure 6.49 shows the result of the simulation when the wheelset is operated on creep curve C_A. The estimated output is nearly equal to the actual adhesion level. A small amount of tractive effort is applied, so the wheelset operating point is in the linear region. When the tractive torque is increased, the operating point moves up on the creep curve toward the non-linear region, as shown in Figure 6.50. When the tractive torque is further increased the operating point of the wheelset moves towards the slip region, as indicated by the fuzzy logic output in Figures 6.51 and 6.52.

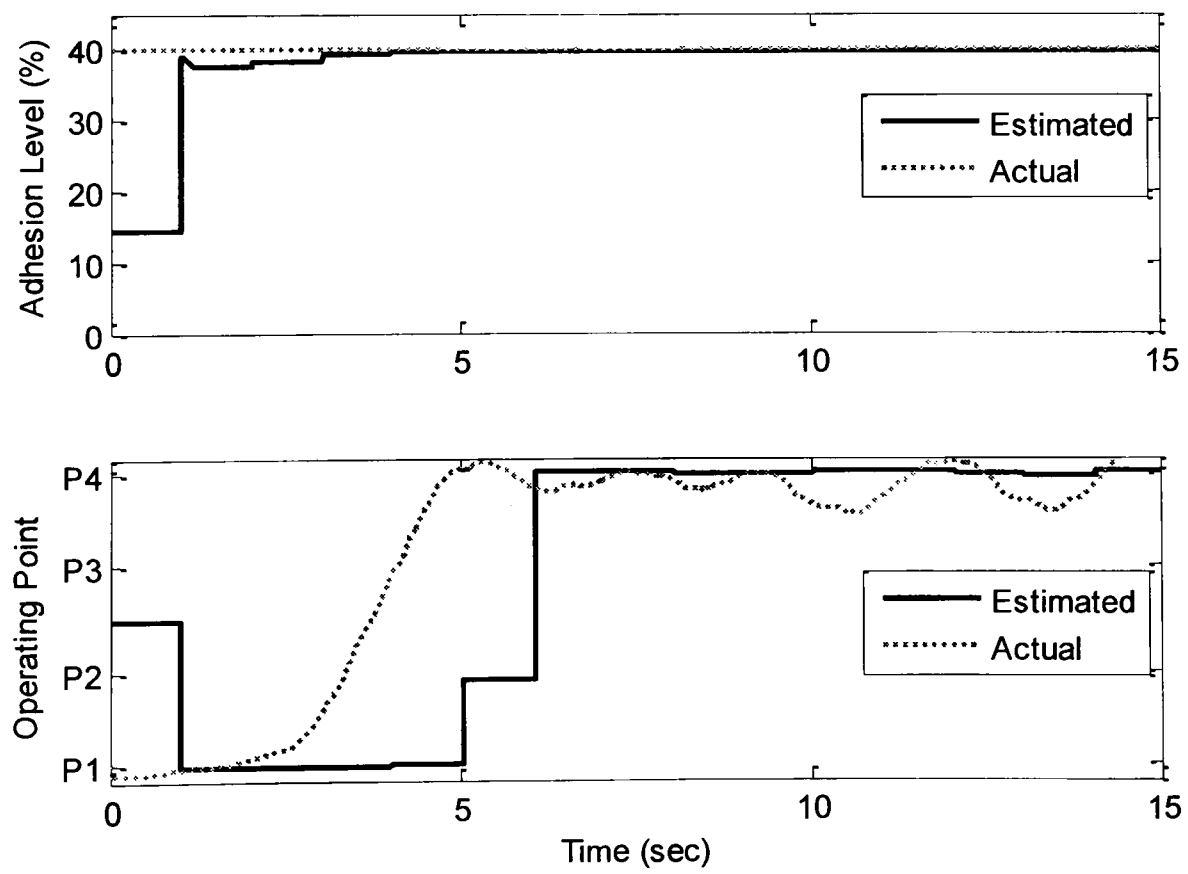

Figure-6.52. Simulation Result when the wheelset is operated on C_A

Figure 6.53 shows the output of the fuzzy logic system when the wheelset is operated on creep curve C_H. In the next simulation result, the wheelset is operated on creep curve C_K. The simulation condition is controlled (by controlling the tractive effort) to keep the operating point in the linear region. Small variations in the tractive torque cause the operating point to fluctuate. The result of the simulation is shown in Figure 6.54.

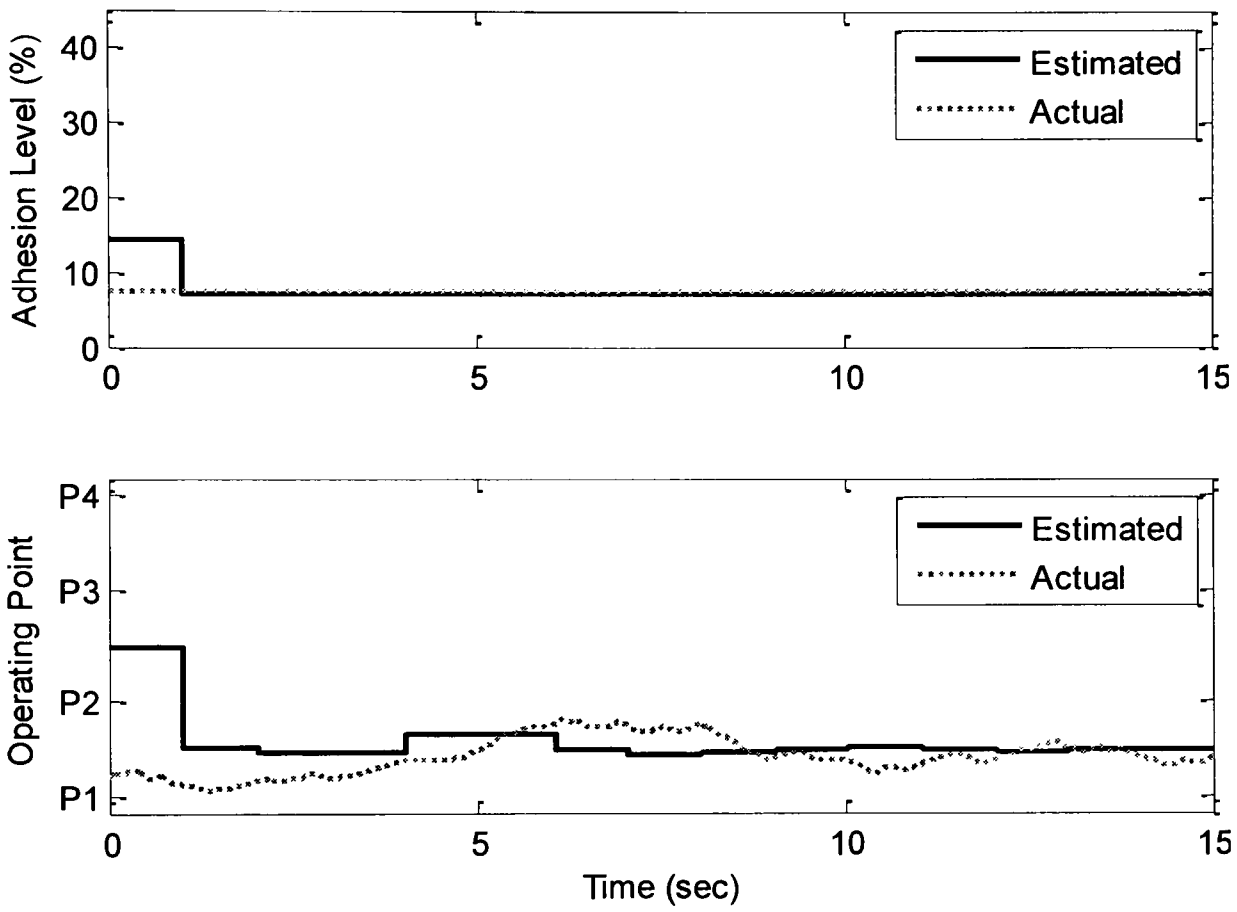

Figure-6.53. Simulation Result when the wheelset is operated on C_H

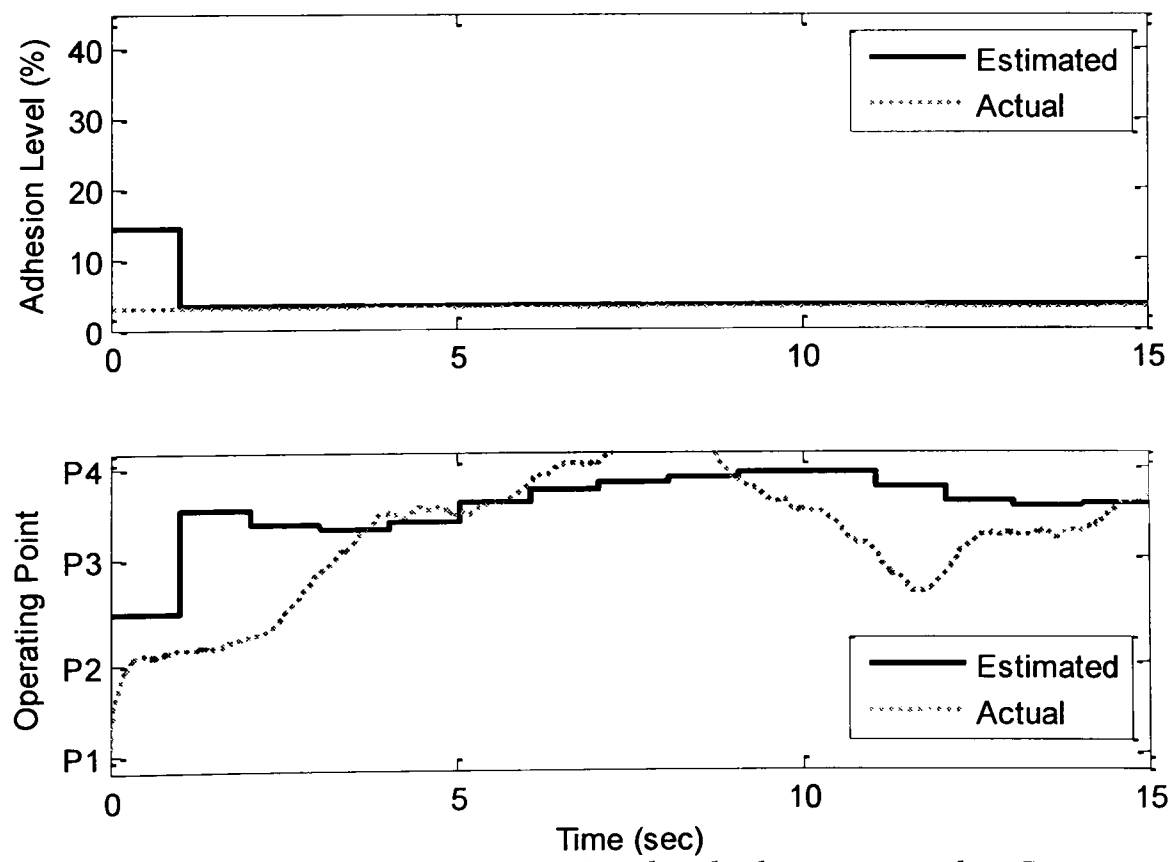

Figure-6.54. Simulation Result when the wheelset is operated on C_K

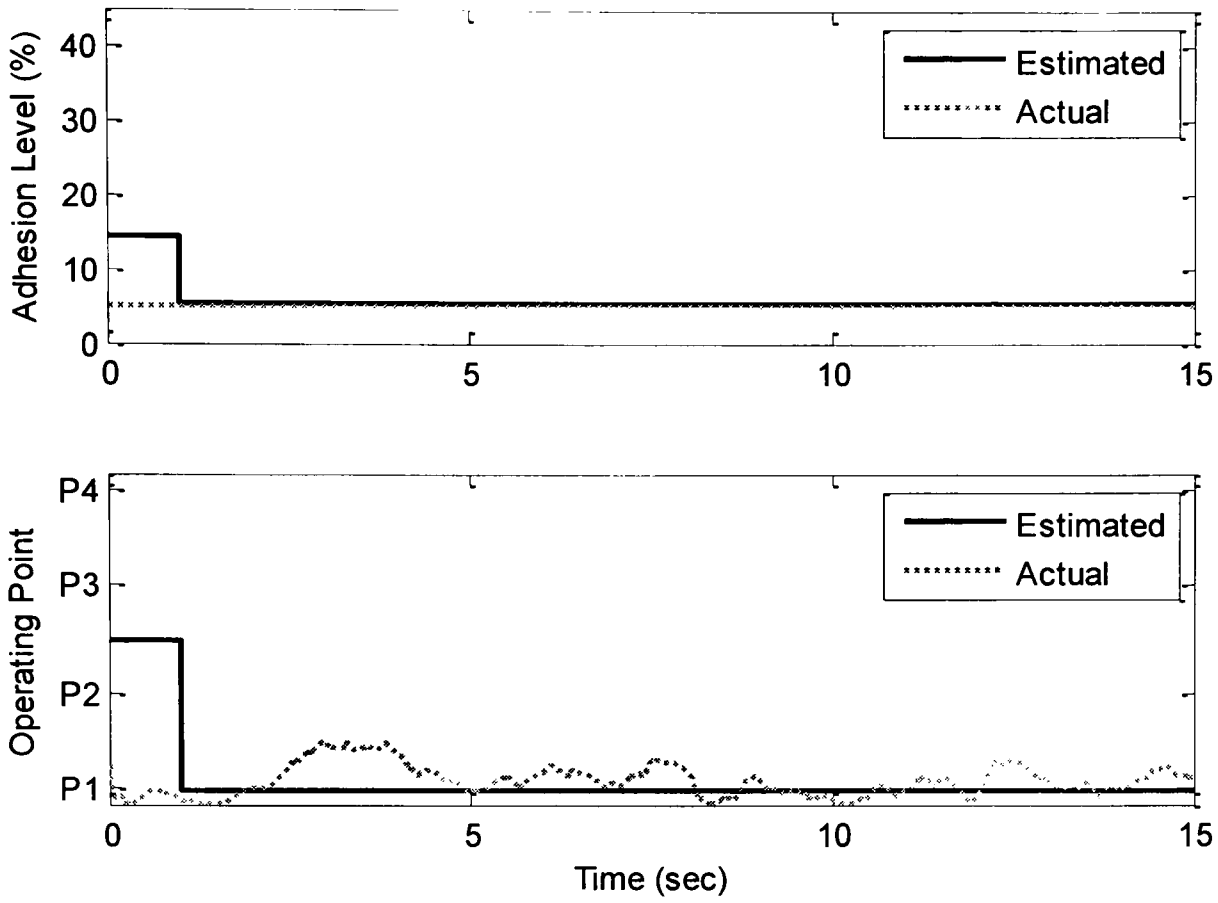

Figure-6.55. Simulation Result when the wheelset is operated on C_J

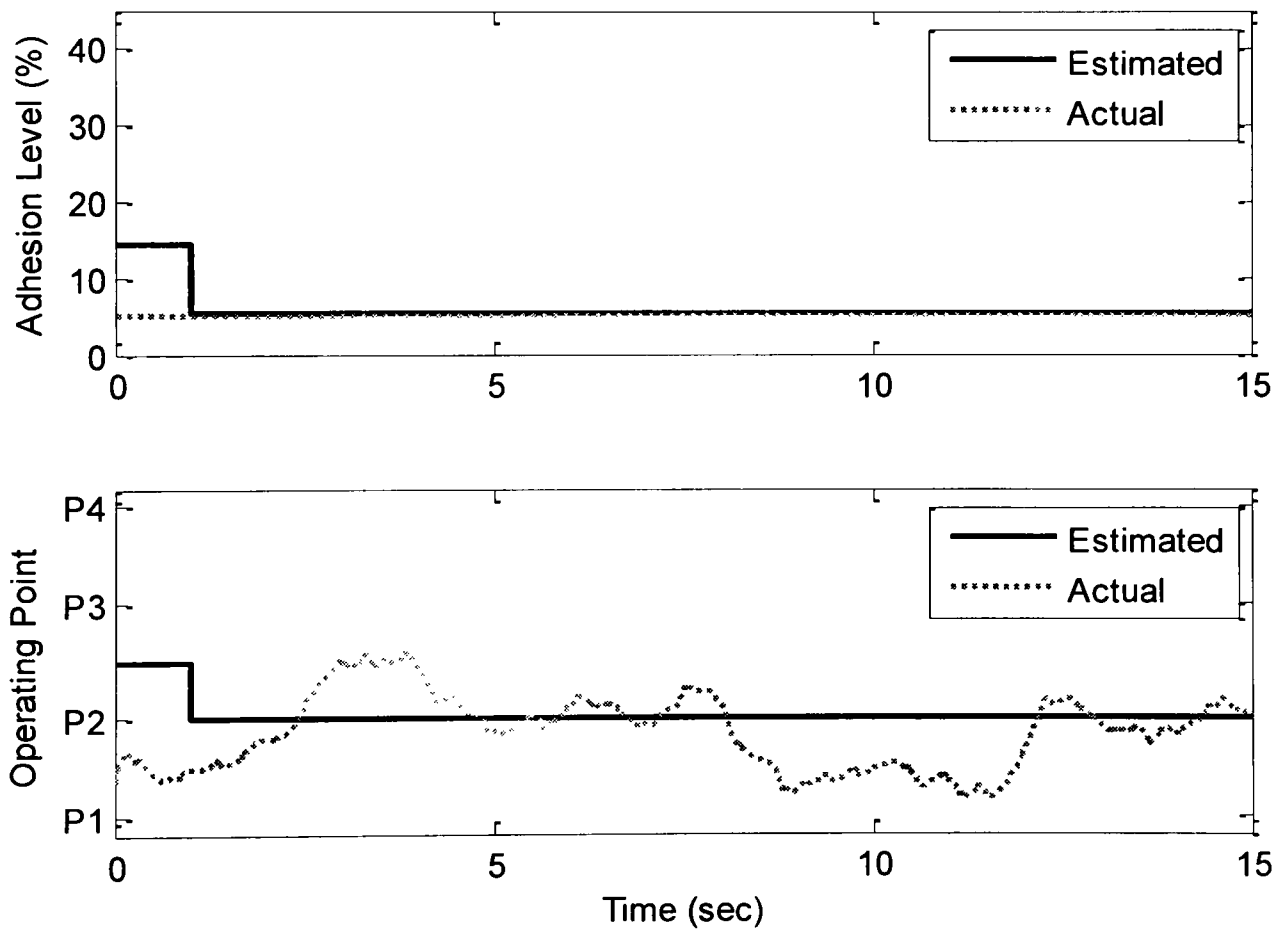

Figure-6.56. Simulation Result when the wheelset is operated on C_J

Figure 6.54 is the result of the simulation of the system using creep curve C_K. Since the adhesion level is exceptionally low in this case, it is very difficult to hold the operating point of the wheelset at the desired location. The same problem is observed when the wheelset is operated using the creep curve representing 5% adhesion level (C_h), as shown in Figure 6.55. However, the estimated value is not affected by these

fluctuations, because the consequent variations in the residuals are not sufficient to change the fuzzy logic output. When the tractive torque is further increased, the wheelset operating point moves to the non-linear region and fluctuates around P_2, as shown in Figure 6.56.

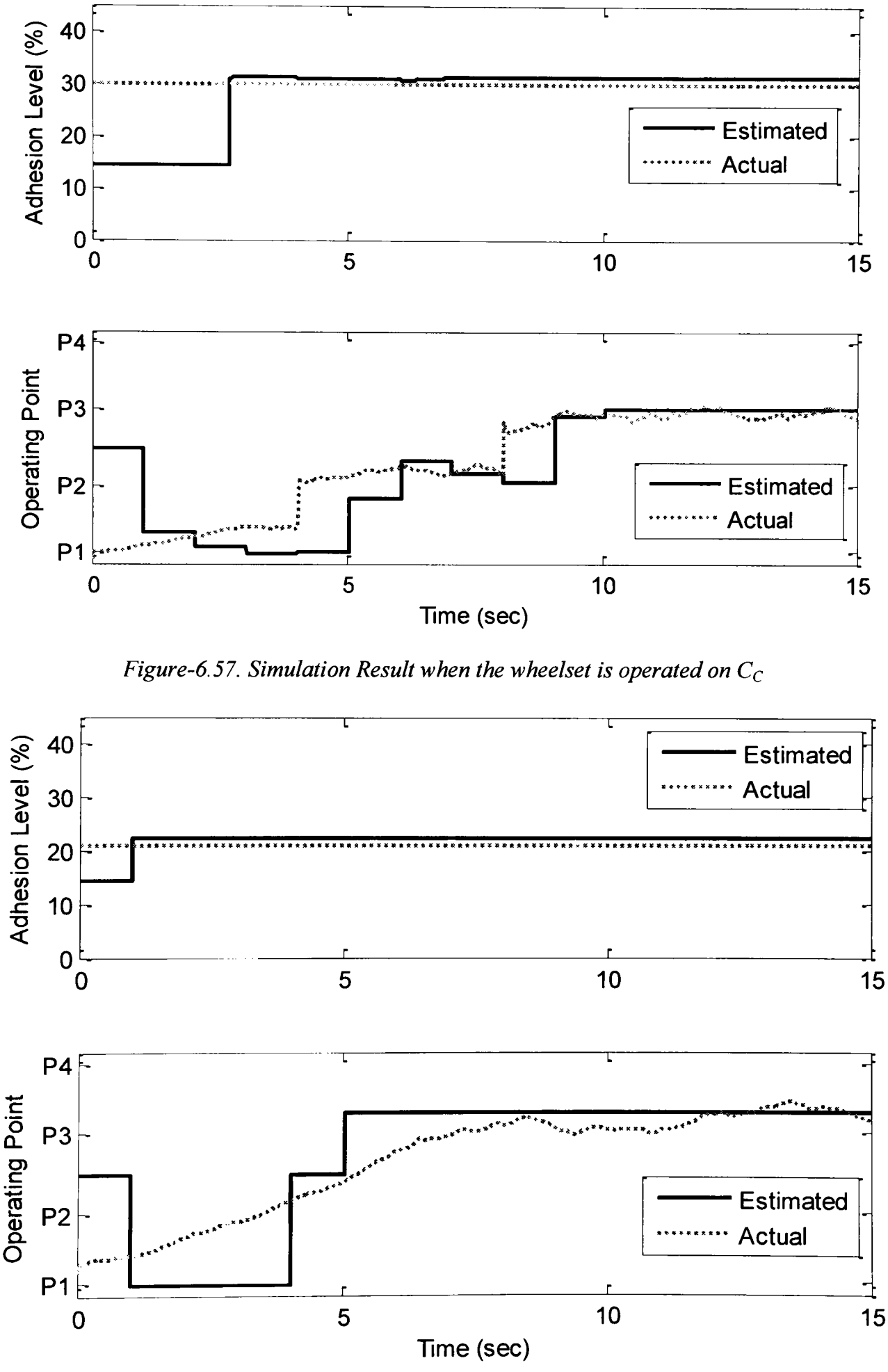

Figure-6.57. Simulation Result when the wheelset is operated on C_C

Figure-6.58. Simulation Result when the wheelset is operated on C_E

Figure 6.57 shows the result when the wheelset is operated on creep curve C_C. The operating point of the wheelset is changed twice during the simulation. At the start of the simulation, the wheelset is operated in the linear region and after 4 seconds the tractive torque is increased, which causes the wheelset operating point to move towards the non-linear region. After 8 seconds, tractive torque is again increased causing the wheelset operating point to move further up towards the saturation region. In Figure 6.58 the wheelset is operated very near to the saturation region of the creep curve C_E. The tractive torque is gradually increased until the wheelset operating point reaches the saturation region. Simulations are also carried out using changing adhesion conditions and the results are presented in the following Figures.

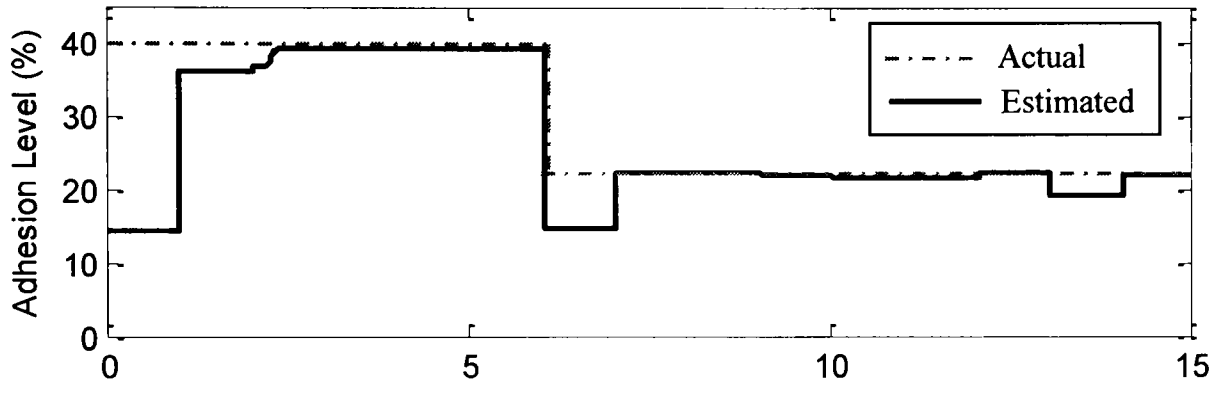

Figure-6.59. Simulation Result when the adhesion level is changed from C_A to C_E

Figure 6.59 shows the result when the adhesion level was changed after 6 seconds of the simulation. At the start of the simulation, the wheelset is operated on creep curve C_A. A small amount of tractive torque is applied to keep the wheelset operating in the linear region. After six seconds, the contact condition is dropped to 30% and the operating point of the wheelset moves a little bit up with the application of the tractive torque. Similarly in Figure 6.60, the wheelset is simulated using low adhesion condition (C_H) and after 6 seconds the adhesion level is changed to 40%. The tractive effort is kept very low throughout the simulation to ensure that the wheelset operates at the bottom of the creep curve.

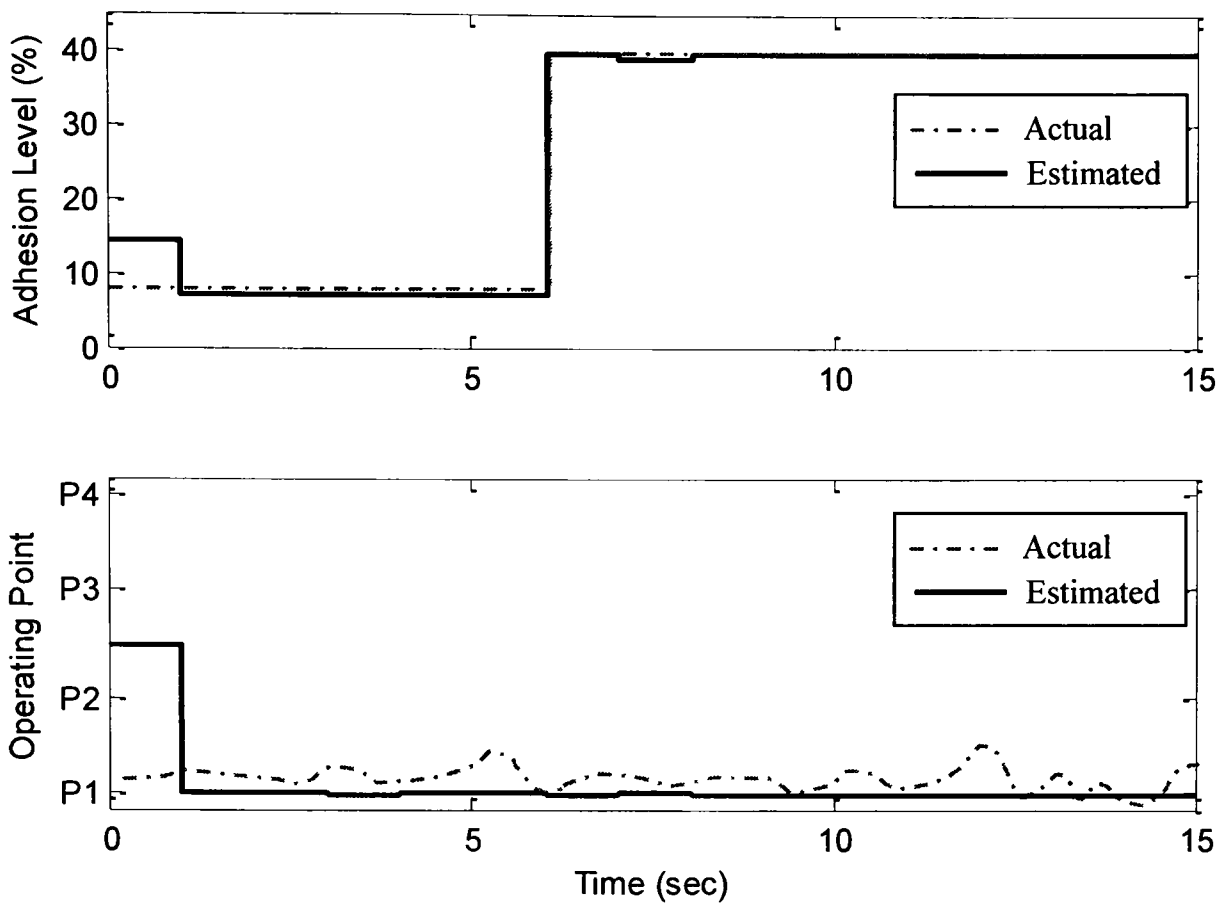

Figure-6.60. Simulation Result when the adhesion level is changed from C_H to C_A

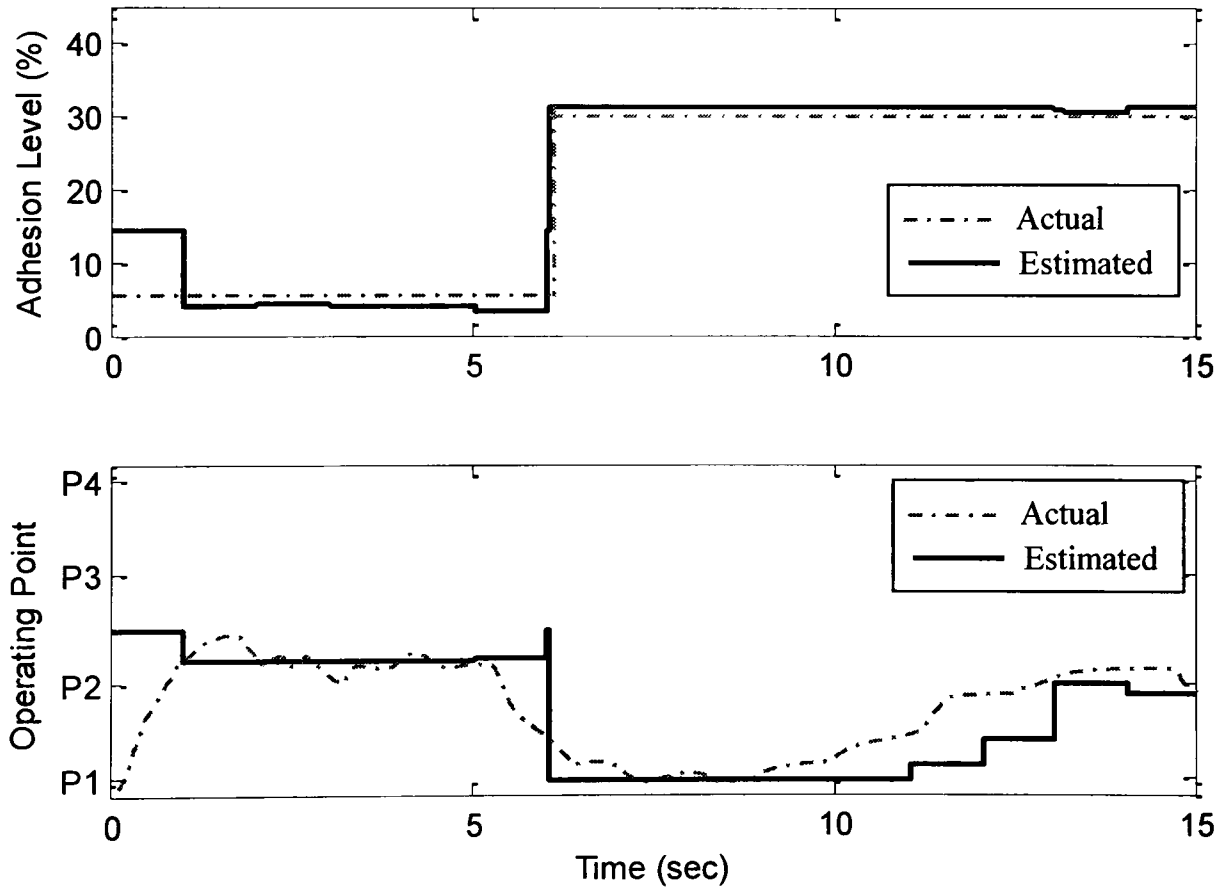

Figure-6.61. Simulation Result when the adhesion level is changed from C_J to C_C

In Figure 6.61 in the beginning of the simulation the wheelset is operated in exceptionally low adhesion conditions (μ=5%), whereby even a small amount of tractive effort causes the operating point to move towards the non-linear region. However, when

the adhesion level is changed after six seconds to 30%, the operating point moves back to the linear region and moves up with further application of tractive torque.

7. Conclusions And Future Work

7.1 Summary

This thesis highlights the challenges faced by the railway industry to improve the adhesion conditions in severe weather conditions. The various different measures taken by the railway organizations (e.g., rail head treatment, sanding, WSPs, etc.) to improve the performance of railway vehicles in low adhesion conditions are discussed in detail. Because of the limitations of the measures taken, a unique idea to detect the wheel-rail adhesion has been proposed with the primary aim of developing a vehicle based technique for the real-time estimation of wheel-rail contact conditions.

This thesis covers the nonlinear contact mechanics and modelling of a single solid axle railway wheelset. An attempt is made to understand the complex wheel-rail mechanics in different contact conditions in order to develop a better understanding of the problem of low adhesion. The results of the eigenvalue analysis are presented, which actually provide a basis to develop an adhesion detection system using the dynamic response of the wheelset. It then covers the design details of the Kalman-Bucy filtering estimation technique. The multiple model based scheme to estimate the wheelset dynamics in different operating conditions is presented, with preliminary simulation results shown. Finally, it discusses the development of a fuzzy logic based decision-making system to interpret these changes in dynamic response of the wheelset into the contact conditions information.

Two different designs based on the same principle are proposed. Design I detects the adhesion level by focusing only on the saturation condition of the creep curves. Conversely, Design II detects the contact conditions by focusing on the entire creep curve, making the structure of this second design comparatively more complex than Design I. As a trade-off, however, the output not only indicates the available adhesion level but it also indicates how far the wheelset is operating from the saturation region.

7.2 Conclusions

In introduction I expressed that the primary aim of this work as providing a solution for the low adhesion problem. Here, I will conclude by describing the progress made towards this goal. Following main conclusions can be drawn from the research:

- Available measures, like sanding, water jetting, WSPs, etc., have resolved the problems caused by low adhesion to some extent. But these measures are not sufficient to eliminate the problem of low adhesion.

- The contact forces generated at the wheel-rail contact patch govern the dynamic behaviour of the railway wheelset. These forces vary nonlinearly with creep, and they are influenced by the unpredictable changes in the adhesion conditions.

- A single Kalman filter is not sufficient to detect the condition changes at the wheel-rail contact.

- The eigenvalue analysis and state estimation results presented in Chapter 4 proved that only yaw and lateral motions of the wheelset are sufficient to detect the changes in the adhesion conditions.

- Although the variations in the residuals of the Kalman filters are not linear, they are predictable and provide great consistency with proposed solution.

- The residuals of the filters provide a unique combination in different contact conditions. Therefore, they can be used as a good first indication to determine the adhesion level.

- The detection system initially designed for a limited number of contact conditions (creep curves) can be extended further for all possible contact conditions using interpolated values of residuals.

- The results in Chapter 6 proved that the detection system works well for all contact conditions.

- The reward for the success of this system has the potential to provide great changes for the rail industry. The information obtained from these systems can be used not only by the drivers to determine the maximum acceleration or braking forces they can apply, but also by rail network operators to optimise the train schedules and make the time tabling adaptive to track conditions in real time.

- The result is that the phenomenon of wheel slip/slide and associated damage and repair costs will be a thing of past. It also saves time because trains can be driven more efficiently in the speeds with the maximum use of adhesion available rather than using the current guidelines.

- The adhesion detection system not only is helpful for conventional railway transport but it also provides a great opportunity for modern driverless trains equipped with ATOs (automated train operations), with the aim of reducing the operational costs and improving the frequency of service.

7.3. Future Work

The problem of low adhesion and its adverse effect on train control systems and rail network operations presents a significant technological challenge to the railway industry; however, this problem provides a great opportunity for the academic community. It is clear that alternative methods are possible and can be achieved through research and innovation. The adhesion detection method presented in this thesis presents a scientific foundation for a new way forward. A number of problems must be solved to allow for the development of a truly practicable inference system. These problems suggest a variety of research directions that need to be pursued to make such a system feasible.

- One such direction would be to improve the simulation conditions (e.g., tractive torque control strategy to reduce the time delays at the output) as close to practical conditions as possible.

- This thesis assumes that the conicity of the wheelset varies linearly. However, in practice it is nonlinear. This provides an opportunity to carry out the research by considering the nonlinear wheel profile.

- The research is carried out assuming the vehicle is moving on a straight track, which can further be extended for the curved tracks as well.

- This study is carried out using the dynamic model of a single solid axle wheelset. Now that the potential of this research is assessed using a single wheelset model,

the research idea can be further extended by taking into account a full vehicle model. Although from various research publications it can be concluded that the model used in this thesis is sufficient to detect the changes at wheel-rail interaction. But in order to simulate the behaviour of an actual vehicle as close as possible effect of the variations in the track gauge on yaw and lateral dynamics can also be considered.

- In this research, three sensors (to measure tractive torque, lateral acceleration of the wheelset, yaw rate of the wheelset) are used. In order to make the implementation cost effective, further work can be carried out to perform the task using fewer sensors.

- Finally, real track testing and experimental validation of the system will be needed before it can be put into practice.

REFERENCES

1. Vasic, G., F. Franklin, and A. Kapoor, "New rail materials and coatings". University of Sheffield, Report: RRUK/A2/1, July 2003.

2. Popovici, R., "Friction in wheel-rail contacts". PhD thesis, University of Twente, Enscheda, Netherlands, 2010.

3. Rail Accident Report by Rail Accident Investigation Branch (RAIB), "Autumn Adhesion Inestigation Part3: Review of adhesion related inidents autumn 2005". January 2007.

4. AWG Adhesion Working Group Report, "Managing low adhesion", 2009.

5. Steenis, N.V, "Monitoring Train Performance In Case Of Low Adhesion". PhD Thesis, Faculty of Engineering Technology, University of Twente, Enschede, Netherlands, May 2010.

6. C. P. Ward, R. M. Goodall and R. Dixon, **"Creep Force Estimation at the Wheel-Rail Interface"**, Proceedings of the 22nd International Symposium on Dynamics of Vehicles on Roads and Tracks Manchester, August 14 - 19, 2011,

7. Bombardier, ORBITA – predictive asset management, the future of fleet maintenance, http://www.bombardier.com/en/transportation/, accessed 7th April 2010.

8. Charles, G. and R. Goodall. "Low adhesion estimation". IET International Conference on Railway Condition Monitoring, Birmingham, UK, 29-30 Nov. 2006, ISBN: 0 86341 732 9

9. Charles. G, R. Goodall and R. Dixon. "Model-based condition monitoring at the wheel-rail interface". *Journal of Vehicle System Dynamics*, Volume 46, Supplement 1, pp. 415-430(16), September 2008.

10. C. Ward, P.Weston, E. Stewart, H. Li, R. Goodall, C. Roberts, T.X. Mei, G. Charles and R. Dixon, "Condition monitoring opportunities using vehicle based

sensors". *IMechE proceedings, Part F: Rail and Rapid Transit*, Vol 225, No.2/2011, pp.202-218.

11. C. P. Ward, R. M. Goodall and R. Dixon, "**Contact Force Estimation in the Railway Vehicle Wheel-Rail Interface**", Proceedings of the 18th IFAC World Congress Milano (Italy), August 28 - September 2, 2011, pp.4398-4403,

12. Kokkeler, F.G.M.,Inventarisatie mondiale research gladde sporen 2003, University of Twente en E.Co, May 16, 2003, UT-03018-A01-R01.

13. Brickle. B, "Railway vehicle dynamics". *Physics in Technology*, 17: p. 181, 1986.

14. Yu. J.H, "Re-adhesion control for AC traction system in railway application", PhD thesis, The University of Leeds, 2007.

15. Wickens. A, "Fundamentals of rail vehicle dynamics: guidance and stability". Taylor & Francis. 2003.

16. Wickens. A, "The dynamics of railway vehicles—from Stephenson to Carter. Proceedings of the Institution of Mechanical Engineers", *Part F: Journal of Rail and Rapid Transit*, 212(3): p. 209-217, 2003.

17. Park. K. T, Lee. H. W, Park. C. H, Kim. D. H and Lee. M. H, "The characteristics of driving control of crane", Proceedings of IEEE International Symposium on Industrial Electronics, Pusan, South Korea, 2001, p. 734 – 739.

18. Li. H and R. Goodal, "Modelling and analysis of a railway wheelset for active control", proceedings of the United Kingdom Automatic Control Conferecne, Swansea UK, 1998, p. 1289 – 1293.

19. Iwnicki. S, "Simulation of wheel-rail contact forces". *Journal of Fatigue & Fracture of Engineering Materials & Structures*, vol. 26 No.10, p. 887-900, 2003..

20. Goodall, R., "Tilting trains and beyond. The future for active railwaysuspensions. 2. Improving stability and guidance". *Computing & Control Engineering Journal*, 1999. 10(5): p. 221-230.

21. Hayashi, Y., H. Tsunashima, and Y. Marumo. "Fault detection of railway vehicles using multiple model approach". IEEE international symposium on system integration, Takamatsu Japan, 2007, p. 1540 - 1543

22. Mei. T. X, Goodall .R.M, "Optimal Control Strategies for the Active Steering of Railway Vehicles". IFAC World Congress, vol F, p.251-256, 1999.

23. Goodall, R. and H. Li, "Solid Axle and Independently-Rotating Railway Wheelsets-A Control Engineering Assessment of Stability". *International Journal of Vehicle System Dynamics*, Vol.33(1): p. 57-67, 2000.

24. Mohan, A. and M. Ahmadian. "Nonlinear investigation of the effect of primary suspension on the hunting stability of a rail wheelset". ASME/IEEE joint rail conferecne (RTD2004), Baltimore USA, April 6-8 2004, p.53-61.

25. Arias-Cuevas. O, "Low Adhesion in the Contact between Wheel and Rail". Phd thesis, Delft University of Technology, The Netherlans, 2010.

26. Zhang. W, J. Chen, X. Wu and X. Jin, "Wheel/rail adhesion and analysis by using full scale roller rig". *Wear*, Vol.253(1-2): p. 82-88, July 2002.

27. Steenis, N.v., "Monitoring Tain Performance in case of Low Adhesion"; PhD Thesis, Faculty of Engineering Technology (CTW) of the University of Twente, Enschede, the Netherlands. May 2010.

28. Chen. H, T. Ban, M. Ishida and T. Nakahara, "Adhesion between rail/wheel under water lubricated contact". *Wear*, vol. 253(1-2): p. 75-81, 2002.

29. Lewis, R., et al., "Effect of oil and water mixtures on adhesion in the wheel/rail contact". *Proceedings of the Institution of Mechanical Engineers, Part F: Journal of Rail and Rapid Transit*, vol. 223(3): p. 275-283, 2009.

30. Broster, M., C. Pritchard, and D. Smith, "Wheel/rail adhesion: its relation to rail contamination on British railways". *Wear*, Vol. 29(3): p. 309-321, 1974.

31. Beagley, T., I. McEwen, and C. Pritchard, "Wheel/rail adhesion--Boundary lubrication by oily fluids". *Wear*, Vol. 31(1): p. 77-88, 1975.

32. Beagley, T. and C. Pritchard, "Wheel/rail adhesion--the overriding influence of water". *Wear*, vol. 35(2): p. 299-313, 1975.

33. Gallardo-Hernandez, E. and R. Lewis, "Twin disc assessment of wheel/rail adhesion". *Wear*, vol. 265(9-10): p. 1309-1316, 2008.

34. Rail Safety and Standards Board, "Review of Low Adhesion Research", 2004.

35. Beagley. T, "A basic study of wheel-rail adhesion. The rheology of rail contaminants causes low friction". BR research report (ref: TN-TRIB-8), May 1974.

36. Beagley. T, M. Broster, I. J. McEwen and C. Pritchard , "A basic study of wheel-rail adhesion. 8. Laboratory studies of the effects of solid debris". BR research report (ref: TN-TRIB-5), January 1973.

37. T. G. Pearce, D. J. Watkins, "Adhesion and Leaves - A Rview of the problem and potentil solutions". BR research report (ref: TM-VTI-017), October 1987.

38. Charles, G. and R. Goodall. "Low Adhesion Estimation". International conferecne on raulway condition monitoring, Birmingham UK, 2006, p. 96-101.

39. C. Pritchard, M. A. Tanvir, "A Bsic study of wheel-rail adhesion: 9. Further observations on leaves". BR research report (ref: TN-TRIB-6), January 1973.

40. Eleveld. J, Gladde Sporen, "Oplossingsrichtingen voor Adhesieproblemen". Report published by the Dutch Railways Technical Research (NSTO) in Dutch (March 1999).

41. Li, Z. and O. Arias Cuevas, "An investigation on the desired properties of friction modifiers for slippery rails". International symposium on speed up, safety and service technology for railway and maglev systems, Nitgata Japan, 2009.

42. "Managing Low Adhesion". Report published by the Adhesion Working Group, UK (September 2001).

43. Admir Mesalic, Arthur Lee Wheeler, Bret Dwayne Worden, Ajith Kuttannair Kumar, Mirza Aref Ahmed Baig, "Method and apparatus for control of a rail contaminant cleaning system". U.S patent 6276 281 B1, August 2001.

44. Jenks, C. W. "Improved methods for increasing wheel/rail adhesion in the presence of natural contaminants." Transit Co-operative Research Program, Research Results Digest, No. 17, 1997.

45. P. R. Cooper, I. J. McEwen, "The Development of Sandite – A Liquid-Sand adhesion improver". BR research report (ref: TN-TRIB-14(A)), December 1976.

46. Shigeura. J, N. Takahashi and N. Isoda, "Apparatus for improving adhesion of a railway vehicle". U.S Patent 4747627, May 1988.

47. Harinder Singh Lamba, Robert Thomas Scott, Joseph Kalousek, Keping Hou, "Locomotive adhesion enhancing material mixtures." U.S Patent 5919295, July 1999.

48. Harinder Singh Lamba, Robert Thomas Scott, Xiaoying Sean Ma, "Locomotive adhesion enhancing slipping discs". U.S Patent 5775228, July 1998.

49. Ferri. V, "Sanding control system for railway vehicles". U.S Patent 5428538, June 1995.

50. Tunley. J and G. Curtis, "Wheel/rail adhesion enhancement". U.S 6629709 B1, Patent , October 2003.

51. I. J. McEwen, "Adhesion and leaves: Use of Sandite". BR research report (ref: TN-TRIB-22), June 1977.

52. Adhesion Working Group (AWG), "Managing Low Adhesion", 4th Ed, 2009.

53. I. J. McEwen, I. D. Pollicott and A. Strabuck, "Water spray treatment for conditioning wheel-rail adhesion: Part-2 Effect of additives". BR research report (ref: TN-TRIB-16), February 1977.

54. I. J. McEwen, "Adhesion and leaves: Experiments with high pressure water jets". research report (ref: TM-ADH-12), April 1974.

55. I. J. McEwan, R.T., "Adhesion and leaves: Wet abrasive blasting tests on southern region". BR research report (ref: TN-TRIB-7), June 1975.

56. Watkins. D, "Tribometer train assessment of southern region water cannon train". BR research report (ref: TN-TRIB-13), September 1976.

57. Taylor. R, " Track testing of adhesion modifying fluids". BR research report (ref: TN-TRIB-19), May 1978.

58. I. J. McEwan, F. G. R. Zobel "Adhesion remedies- A Summary of recent development work on lineside fluid applicators". BR research report (ref: TN-TRIB-8), June 1975.

59. I. J. McEwen, "Rail Contamination and its Influence on Wheel/Rail Adhesion". BR research report, 1999.

60. Watanabe, T. and A. Yamanaka. "Optimisation of readhesion control of Shinkansen trains with wheel–rail adhesion". Proceedings of the power conversion conferecne, Nagaoka Japan, 1997, p. 47-50.

61. Watanabe. T, A. Yamanaka, T. Hirose, K, Hosh and S. Nakamura, "Optimization of readhesion control of Shinkansen trains with wheel-rail adhesion prediction". Proceedings of the power conversion conferecne, Nagaoka Japan, 1997, p. 47-50

62. Mei, T X & Yu, J H & Wilson, D A, "Mechatronic approach for effective wheel slip control in railway traction", *IMechE Proceedings (Part F) - Rail and Rapid Transit*, Vol. 223(3), p. 295-304, 2009.

63. Yasuoka. I, Henmi. T, Nakazawa. Y. Aoyama. I, "Improvement of re-adhesion for commuter trains with vector controltraction inverter". Proceedings of the power conversion confeecne, Nagaoka Japan, 1997, p. 51-56.

64. W. Zhang, j.C., x. Wu, X. Jin, "Wheel/rail adhesion and analysis by using full scale roler rig". *Wear, vol.* 253, p.82-88, 2002.

65. Covino, M., M. Grassi, and E. Pagano. "Traction electric drives: an indirect identification method offriction forces". IEEE international conference on Electric machines and drives, Milwaukee USA, May 1997, p. TA2/5.1 - TA2/5.3.

66. Gajdar, T. and S. Yoshihiro. "Neural Network based Estimation of Friction Coefficient of Wheel and Rail". Institute of Electrical & Electronics Engineers (IEEE) international conferecne on intelligent engineering systems, Budapest Hungary, September 1997, p. 315-318.

67. Rizzo, R. and D. Iannuzzi. "Electrical drives for railway traction: observer for friction force estimation". Proceedings of the IEEE international conferecne on power system technology, December 2002, p. 723-726.

68. Iannuzzi, D. and R. Rizzo. "Disturbance observer for dynamic estimation of friction force in railway traction systems". Proceedings of the 29th Annual conferecne of the IEEE industrial electronics society, November 2003, p. 2979-2982.

69. Ohishi.K. Nakano, K. Miyashita, I. Yasukawa, S. Nagaoka, "Anti-slip control of electric motor coach based on disturbance observer". 5th international workshop on advanced motion control, Coimbra, June 1998, p. 580-585.

70. Yu, J. H, T.X. Mei and D.A. Wilson, "Re-Adhesion control based on wheelset dynamics in railway traction system". Proceedings of the United Kingdom automatic control conferecne, 2006, Sheffield UK,

71. Mei, T.X., J.H. Yu, and D.A. Wilson, "A Mechatronic Approach for Anti-slip Control in Railway Traction". Proceedings of the 17th world congress The international federation of automatic control (IFAC), Seoul, Korea, July 2008, p. 8275-8280.

72. Christian Schimid, "Introduction to fuzzy techniques", retrieved from http://www.atp.ruhr-uni-bochum.de/rt1/syscontrol/node117.html on 1st March 2012.

73. Goodall, R. and C. Roberts. "Concepts and techniques for railway condition monitoring". IET international conferecne on railway condition monitoring, Birmingham UK, November 2006, p. 90-95.

74. Bruni. S, R. M. Goodall, T. X. Mei and H. Hitoshi, "Control and monitoring for railway vehicle dynamics". International Journal of Vehicle System Dynamics, vol. 45, Issue 7(8), p. 743-779, 2007.

75. Xia, F. and P.J. Wolfs, "Estimation des forces D'Interaction entre des roues et un rail". WO Patent WO/2006/130,908, 2006.

76. Xia, F. and P.J. Wolfs, "Estimation of wheel rail interaction forces". U.S Patent 7853412 B2, December 2010.

77. *Xia, F, Bleakley, S & Wolfs, P, "The estimation of wheel-rail interaction forces from wagon accelerations", Proceedings of the fourth Australasian Congress on Applied Mechanics, Melbourne, Australia, 16-18 February 2005, pp. 333-338.*

78. Ward, C.P., et al., "Condition monitoring opportunities using vehicle-based sensors". Proceedings of the Institution of Mechanical Engineers, Part F: Journal of Rail and Rapid Transit, 2011. 225(2): p. 202-218.

79. Ward, C.P., R.M. Goodall, and R. Dixon. "Contact force estimation in the railway vehicle wheel-rail interface". Proceedings of the 18th IFAC World Congress, Università Cattolica del Sacro Cuore, Milano, Italy, 2011.

80. Ward, C.P, Goodall, R.M and Dixon, R, "Creep force estimation at the wheel-rail interface". Proceedings of the 22nd International Symposium on Dynamics of Vehicles on Roads and Tracks (IAVSD2011), Manchester, Manchester Metropolitan University, 14-19 August.

81. Ward, C. P., Goodall, R. M. and Dixon, R, "Wheel-rail profile condition monitoring". UKACC International Conference on Control, Coventry, UK, 7-10 September.

82. Tsunashima, H. and H. Mori. "Condition monitoring of railway vehicle suspension using adaptive multiple model approach". International Conference on Control Automation and Systems (ICCAS), p. 584-589, 2010.

83. Hayashi, Y., H. Tsunashima, and Y. Marumo, "Fault detection of railway vehicle suspension systems using multiple-model approach". Journal of Mechanical Systems for Transportation and Logistics, 2008. Vol. 1(1): p. 88-99.

84. Hayashi, Y., H. Tsunashima, and Y. Marumo, "Fault Detection of Railway Vehicles Using Multiple Model Approach". Nippon Kikai Gakkai Kotsu, Butsuryu Bumon Taikai Koen Ronbunshu, 2006. Vol. 15: p. 133-136.

85. Y. Hayashi, T. Kojima, H. Tsunashima, and Y. Marumo, "Real time fault detection of railway vehicles and tracks". Proceedings of the IET international conference on railway condition monitoring, Birmingham UK, 2006, p. 20-25.

86. Erhardt, R., G. Pfaff, and A. Van Zanten, "VDC, The vehicle dynamics control system of Bosch", SAE technial Paper No. 950759, 1995.

87. H. E. Tseng et al. "Development of vehicle stability control at Ford". IEEE/ASME Transactions on Mechatronics, Vol. 4(3), p. 223–234, 1999.

88. Y. Fukada. "Slip-angle estimation for vehicle stability control". International Journal of Vehicle System Dynamics, Vol. 32(4), p. 375–388, 1999.

89. C. R. Carlson and J. C. Gerdes. "Optimal rollover prevention with steer by wire and differential braking". In ASME Dynamic Systems and Control Division (Publication) DSC, volume 72, pages 345–354, Washington, D.C., 2003.

90. A. Nishio et al. "Development of vehicle stability control system based on vehicle sideslip angle estimation", SAE technical Paper No. 2001-01-0137, 2001.

91. Mei, T.X, H. Li, and R. Goodall, "Kalman filters applied to actively controlled railway vehicle suspensions". Transactions of the Institute of Measurement and Control, 2001. Vol. 23(3): p. 163.

92. Magill, D., "Optimal adaptive estimation of sampled stochastic processes". IEEE Transactions on Automatic Control, 2002. Vol. 10(4): p. 434-439.

93. Barshan, B. and H. Durrant-Whyte, "Inertial navigation systems for mobile robots". IEEE Transactions on Robotics and Automation, 1995. Vol. 11(3): p. 328-342.

94. Goel P., Dedeoglu G., Roumeliotis S.I., and Sukhatme G.S, "Fault Detection and Identification in a Mobile Robot Using Multiple Model Estimation and Neural

Network". Proceedings of the IEEE International Conference on Robotics and Automation, San Francisco, California, April 2000, pp. 2302-2309

95. Leung, T.P, Zhou Qi-Jie, Mao Zhong-Yuan; Yu De-Jiang, "A design method for vehicle dynamic systems based on fuzzy logic control". Proceedings of the American Control Conference, Seattle USA, June 1995. P. 3239-3243.

96. Buckholtz, K., "Use of Fuzzy Logic in Wheel Slip Assignment - Part I: Yaw Rate Control". SAE Technical Paper 2002-01-1221, 2002, doi:10.4271/2002-01-1221.

97. Hessburg, T. and M. Tomizuka, "Fuzzy logic control for lateral vehicle guidance". IEEE Control Systems Magazine, 1994. Vol. 14(4): p. 55-63.

98. Boada, B., M. Boada, and V. Diaz, "Fuzzy-logic applied to yaw moment control for vehicle stability". International journal of Vehicle System Dynamics, 2005. Vol. 43(10): p. 753-770.

99. Kobayashi, K., K.C. Cheok, and K. Watanabe. "Estimation of absolute vehicle speed using fuzzy logic rule-based Kalman filter". Proceeding of the IEEE American control conference, Seattle USA, June 1995, p.3086-3090.

100. Kim, M, "Design of the active steering fuzzy controller with the degree of non-uniformity for a scaled railway vehicle". Proceedings of the 9th World Scientific and Engineering Academy and Society (WSEAS) international conference on Robotics, control and manufacturing technology, 2009.

101. De Koker, P., J. Gouws, and L. Pretorius, "Fuzzy control algorithm for automotive traction control systems". Proceedings of the 8th mediterranean electrotechnical conferecne, Bari, Italy, May 1996, p. 226-229

102. Lee, S.H., S.G. Kim, and J.T. Lim, "Fuzzy-logic-based fast gain-scheduling control for nonlinear suspension systems". IEEE Transactions on Industrial Electronics, 1998. Vol. 45(6): p. 953-955.

103. Zhong, H., et al., "An optimal torque distribution strategy for an integrated starter–generator parallel hybrid electric vehicle based on fuzzy logic control".

Proceedings of the Institution of Mechanical Engineers, Part D: Journal of Automobile Engineering, 2008. Vol. 222(1): p. 79-92.

104. Sun-Ku Kwon, Uk-Youl Huh, Hak-Il Kim and Jin-Hwan Kim, "Re-adhesion control with estimated adhesion force coefficient for wheeled robot using fuzzy logic". 30th annual conferecne of IEEE Industrial electronics society, November 2004, p. 2530-2535.

105. Hashmi, K., et al., "Adjustment approach for fuzzy logic model based selection of non-overlapping machining data in the turning operation". Journal of Materials Processing Technology, 2003. Vol. 142(1): p. 152-162.

106. El Baradie, M., "A fuzzy logic model for machining data selection". International Journal of Machine Tools and Manufacture, 1997. Vol. 37(9): p. 1353-1372.

107. Hashmi, K., M. El Baradie, and M. Ryan, "Fuzzy-logic based intelligent selection of machining parameters". Journal of Materials Processing Technology, 1999. Vol. 94(2-3): p. 94-111.

108. Hashmi, K., I. Graham, and B. Mills, "Fuzzy logic based data selection for the drilling process". Journal of Materials Processing Technology, 2000. Vol. 108(1): p. 55-61.

109. Iwnicki, S., "Handbook of Railway Vehicle Dynamics". CRC Press, 2006.

110. Mei, T.X, J. Yu, and D. Wilson, "A mechatronic approach for effective wheel slip control in railway traction". Proceedings of the Institution of Mechanical Engineers, Part F: Journal of Rail and Rapid Transit, 2009. Vol. 223(3): p. 295-304.

111. Mei, T.X. and R.M. Goodall, "Practical Strategies for Controlling Railway Wheelsets Independently Rotating Wheels". Journal of Dynamic Systems, Measurement, and Control, 2003. Vol. 125(3): p. 354-360.

112. Vaughan, A. "Isambard Kingdom Brunel – Engineering Knight Errant". John Murray, London, 1992, p. 102.

113. Klingel, "Uber den Lauf der Eisenbahnwagen auf Gerarder Bahn". Organ Fortsch. Eisenb-wes. 38 (1883), pp. 113-123.

114. Mei, T.X, J. Yu, and D. Wilson, "Wheelset dynamics and wheel slip detection". In the STECH2006, Chengdu, China, 2006.

115. Wickens, A.H., "Fundamentals of Rail Vehicle Dynamics: Guidance and Stability". Taylor & Francis, 2003.

116. I Hussain, Mei.T.X and A. H. Jones, "Modeling and Estimation of Nonlinear Wheel-rail Contact Mechanics". Proceedings of the twentieth Intenational conference on System Engineering, Coventry UK, 2009: p. 219-223.

117. Kalker, J.J., "The computation of three-dimensional rolling contact with dry friction". International Journal for Numerical Methods in Engineering, 1979. Vol. 14(9): p. 1293-1307.

118. Mei, T.X and R. Goodall. "LQG and GA solutions for active steering of railway vehicles". IEEE proceedings on control theory and applications, January 2000, vol. 147(1), p. 111-117.

119. Mei, T.X. and I. Hussain. "Detection of wheel-rail conditions for improved traction control". Proceedings of the IET conferecne on Railway Traction Systems (RTS 2010), Birmingham UK, April 2010, p.30.

120. I. Hussain and T.X.Mei., "Identification of the Wheel Rail Contact Condition for the Traction and Braking Control". Proceedings of the 22nd International Symposium on Dynamics of Vehicles on Roads and Tracks, Manchester Metropolitan University, 14-19 August 2011.

121. I. Hussain, Mei.T.X., "Multi Kalman Filtering Approach for Estimation of Wheel-Rail Contact Conditions". Proceedings of the United kingdom Automatic Control Conferecne 2010, 2010: p. 459-464.

122. Lefebvre, T., H. Bruyninckx, and J. De Schutter, "Kalman filters for non-linear systems: a comparison of performance". International journal of Control, 2004. Vol. 77(7): p. 639-653.

123. F. Orderud, "Comparison of kalman filter estimation approaches for state space models with nonlinear measurements," in Proc. of Scandinavian Conference on Simulation and Modeling, 2005.

124. Welch, G. and G. Bishop, "An Introduction to the Kalman Filter". University of North Carolina at Chapel Hill, Chapel Hill, NC, 1995.

125. I. Hussain, Mei.T.X.and A.H.Jones., "Modeling and Estimation of Nonlinear Wheel-rail Contact Mechanics". Proceedings of the twentieth Intenational conference on System Engineering, 2009: p. 219-223.

126. Hussain, I. and Mei.T. X, "Identification of the Wheel Rail Contact Condition for the Traction and Braking Control". Proceedings of the 22nd International Symposium on Dynamics of Vehicles on Roads and Tracks, Manchester Metropolitan University, 14-19 August 2011.

127. Mei T. X., R.M.Goodall., and H. Li, "Kalman Filter for the State Estimation of a 2-Axle Railway Vehicle". Proceedings of the 5th European Control Conferecne, Karlsruhe, Germany, 1999, CA-10-F812.

128. Fuzzy Inference Systems. Retrieved 10 Feburary, 2012, from http://www.mathworks.co.uk/help/toolbox/fuzzy/fp351dup8.html

129. Mamdani, E.H. and S. Assilian, "An experiment in linguistic synthesis with a fuzzy logic controller,"International Journal of Man-Machine Studies, Vol. 7, No. 1, pp. 1-13, 1975.

130. Sugeno-Type Fuzzy Inference. Retrieved 10 Feburary, 2012, from http://www.mathworks.co.uk/help/toolbox/fuzzy/fp49243.html

131. Sugeno, M., Industrial applications of fuzzy control, Elsevier Science Pub. Co., 1985.

132. Sujit Nath Pant, Keith E. Holbert. "Fuzzy Logic in Decision Making and Signal Processing". From http://enpub.fulton.asu.edu/PowerZone/FuzzyLogic/index.htm on 16th March 2012

133. D. H. Rao, S. S. Saraf, "Study of Defuzzification Methods of Fuzzy Logic Controller for Speed Control of a DC Motor", IEEE Transactions, 1995, pp. 782-787.

134. Nurcahyo, G.W., et al., "Selection of defuzzification method to obtain crisp value for representing uncertain data in a modified sweep algorithm." Journal of Computer Science and Techchnology, 2003. Vol. 3(2): p. 22-28.

135. D. J. Watkins, "Exploring Adhesion With British Rail's Tribometer Train", Railway Engineering Journal, Volume 4 Issue 4, Page 6-13, Nov 18 1975.

136. O.Polach, "Creep forces in simulations of traction vehicles running on adhesion limit." Wear, vol. 258, pp.992-1000, 2005.

APPENDIX-I: LIST OF SYMBOLS

ω_{wL} ..... Left Wheel Angular speed

ω_{wR} ..... Right wheel angular speed

v_v ..... Vehicle speed

M_v ..... Mass of vehicle

m_w ..... Mass of wheelset

I_R ..... Moment of inertia of right wheel

I_L ..... Moment of inertia of left wheel

I_w ..... Moment of inertia of wheelset

ψ_w ..... Yaw movement of wheelset

$\dot{\psi}_w$ ..... Yaw rate of the wheelset

$\ddot{\psi}_w$ ..... Yaw acceleration of the wheelset

y_w ..... Lateral displacement of the wheelset

$\dot{y}_w$ ..... Lateral velocity of the wheelset

$\ddot{y}_w$ ..... Lateral acceleration of the wheelset

λ_L ..... Left wheel creep

λ_R ..... Right wheel creep

λ_{xL} ..... Left wheel creep in longitudinal direction

λ_{xR} ..... Right wheel creep in longitudinal direction

λ_{yL} ..... Left wheel creep in lateral direction

λ_{yR} ..... Right wheel creep in lateral direction

F_L ..... Left wheel creep force

F_R ..... Right wheel creep force

F_{xL} ..... Left wheel creep force in longitudinal direction

F_{xR} ..... Right wheel creep force in longitudinal direction

F_{yL} ..... Left wheel creep force in Lateral direction

F_{yR} ..... Right wheel creep force in Lateral direction

γ_w ..... Wheel conicity

L_g ..... Track half gauge

r_L ..... Left wheel radius

r_R ..... Right wheel radius

r_o ..... Wheel radius at centre position

g_{11} ..... Linearized longitudinal creep force coefficient

g_{22} ..... Linearized lateral creep force coefficient

y_t ..... Track disturbance

T_s ..... Torsional torque

T_t ..... Tractive torque

T_L ..... Left wheel tractive torque

T_R ..... Right wheel tractive torque

f_{11} ..... Longitudinal creep force coefficient

f_{22} ..... Lateral creep force coefficient

f ..... frequency of kinematic oscillations

μ ..... Adhesion coefficient

μ_R ..... Right wheel Adhesion coefficient

μ_L ..... Left wheel Adhesion coefficient

μ_{max} ..... Maximum value of Adhesion coefficient

x_w ..... longitudinal displacement of the wheelset

$\dot{x}_w$ ..... longitudinal velocity of the wheelset

$\ddot{x}_w$ ..... longitudinal acceleration of the wheelset

g ..... Gravitational acceleration

k_w ..... Yaw stiffness of the wheelset

k_s ..... Torsional stiffness of the wheelset axle

ϕ_w ..... Roll angle of the wheelset

θ_s ..... torsional angle between left and right wheels

C_s ..... Damping coefficient of axle

F_c ..... Centrifugal force

F_g ..... Gravitation stiffness force

R_c ..... Curve radius

v_w ..... Equivalent linear speed of the wheel

v_{wL} ..... Equivalent linear speed of the left wheel

v_{wR} ..... Equivalent linear speed of the right wheel

APPENDIX-II: PARAMETER VALUES

Parameter	Description	Value
I_w	Yaw moment of inertia of the wheelset ($kg\ m^2$)	700
r_o	Rolling radius of the wheels at centre position (*meters*)	0.5
γ_w	Conicity of the wheel tread (*radians*)	0.15
L_g	Track half gauge (*meters*)	0.75
m_w	Mass of the wheelset (*kg*)	1250
M_v	Mass of the vehicle (*kg*)	15000
k_s	Torsional stiffness of axle (*N/meter*)	6063260
k_w	Yaw stiffness (*N/rad*)	5×10^6
I_R	Right wheel moment of inertia ($kg\ m^2$)	68.2
I_R	Right wheel moment of inertia ($kg\ m^2$)	133.2
v_v	Vehicle speed (*m/sec*)	40

APPENDIX III: LIST OF PUBLICATIONS

1. I Hussain, Mei T X, and A. H. Jones, "Modeling and Estimation of Nonlinear Wheel-rail Contact Mechanics". Proceedings of the twentieth International conference on System Engineering, 8-10 September 2009, Coventry University UK, p. 219-223.

2. T X Mei, I Hussain, "Detection of wheel-rail contact conditions for improved traction control", The 4th International Conference on Railway Traction Systems (RTS2010) 13-15 April 2010, University of Birmingham UK.

3. I Hussain and Mei T X, "Identification of Wheel-Rail Contact Condition Using Multi Kalman Filtering Approach". Proceedings of the 10th Salford Postgraduate Annual Research Conference 2010, 10-11 July 2010, University of Salford UK, p. 144-155.

4. I Hussain and Mei T X, "Multi Kalman Filtering Approach for Estimation of Wheel-Rail Contact Conditions". Proceedings of the UKACC International Conference on Control 2010, 7-10 September 2010, Coventry University UK, p. 459-464.

5. I Hussain and Mei T X, "Identification of Wheel Rail Contact Condition for Traction and Braking Control". Proceedings of the 1st CSE PG Conference 2010, 17th November 2010, University of Salford UK, ISBN: 978-1-905732-47-0

6. I Hussain and Mei T X, "Fuzzy Logic Based Identification of Wheel-Rail Contact Condition", Proceedings of the 11th Salford Postgraduate Annual Research Conference 2011, 8-9 July 2011, University of Salford UK.

7. I Hussain and Mei T X, "Identification of the Wheel Rail Contact Condition for the Traction and Braking Control", Proceedings of the 22nd International Symposium on Dynamics of Vehicles on Roads and Tracks, Manchester Metropolitan University, 14-19 August 2011.

8. I. Hussain, T X Mei and Mohammad Mirzapour, "Multiple Model Based Identification of the wheel-rail contact condition for traction and braking

control", Proceedings of the 2nd CSE Post Graduate conference, University of Salford, 16thNovember 2011.

9. I. Hussain, T. X. Mei and Mohammad Mirzapour, "Onboard estimation of wheel-rail contact conditions" Proceedings of the 12th Salford Postgraduate Annual Research Conference 2012, 30-31 May 2012, University of Salford UK.

10. I Hussain, Mei T X and Mohammad Mirzapour "Real Time Estimation of the wheel-rail contact conditions using multi-Kalman filtering and fuzzy logic". Proceedings of the UKACC International Conference on Control 2012, 3-5 September 2012.

11. I. Hussain, T. X. Mei and R. T. Ritchings, "Estimation of Wheel-rail Contact Conditions and Adhesion using Multiple Model approach". Manuscript submitted for publication in Journal of Vehicle System Dynamics.

Modelling and Estimation of Non-linear Wheel-Rail Contact Mechanics

I Hussain[1], TX Mei[2] and A Jones[3]
School of Computing, Science and Engineering
Salford University, UK
Emails: [1] I.Hussain@pgr.salford.ac.uk [2]t.x.mei@salford.ac.uk; [3]A.H.Jones@salford.ac.uk

Abstract: This paper presents the development of a model-based approach for the estimation of the complex wheel-rail contact mechanics. A comprehensive non-linear model of a conventional solid-axle wheelset is used as the basis for the study. All main wheelset motions affected by the contact forces are considered including the rotation, forward, lateral, yaw and torsional modes. The non-linearity and changes in the interaction with the rail are modelled by using a set of non-linear creep/slip curves. A multi Kalman filter scheme is proposed, where the estimators are designed using models linearised at selected operating points/conditions and are then run in parallel. The residuals of the estimator outputs are examined to assess the likelihood or closeness of each of the filters to the 'real' contact conditions. This paper mainly covers: (1) the modelling of wheelset dynamics and non-linear contact laws and that of condition changes at the wheel-rail interface; (2) the design detail for the development of the Kalman filters; and (3) simulation results to demonstrate potential effectiveness of the proposed scheme.

Keywords: Wheelset dynamics, creep forces, nonlinear, Kalman filter, multiple model

1. INTRODUCTION

Wheel-rail contact is fundamental to railway operations, but the dynamic properties at the wheel-rail interface are known to be highly non-linear and can be severely affected by often unpredictable external sources of contamination at the contact surfaces which can seriously compromise the provision of basic functions of rail vehicles and even safety. Reliable identification of wheel-rail contact force properties and adhesion limit for traction/braking controls without the need for sophisticated and expensive equipment, to enable the related control systems to adapt to different conditions and optimize the use of adhesion available, has been a difficult technical challenge for rail research.

Studies of dynamic behaviour of railway wheelset affected by nonlinear wheel rail contact mechanics is presented in [1-3]. The rotational and longitudinal dynamics of a wheelset were considered and the influence of the contact condition on relevant modes is assessed thoroughly. In the work a single Kalman filter was used to estimate the changes in contact condition based on torsional vibrations. Another work has been carried out by G Charles and R Goodall to estimate the low adhesion between wheel and rail using the responses of the vehicle to lateral track irregularities [4]. They further carried out this research to estimate the wheel rail profile and adhesion between wheel and rail in [5], using a half vehicle model including the wheelset and secondary suspension for the parameter estimations.

In this research all main motions affected by the contact forces are considered because there are strong interactions between different motions of a wheelset through the creep forces at wheel-rail contact acting in longitudinal and lateral directions. It is therefore essential in the study of wheelset dynamics to use a more comprehensive model that includes all motions of the wheelset related to the contact forces[1]. Multiple Kalman filters are used to estimate the states at different points of creep curve. The proposed scheme offers a number of benefits that are not possible with the current direct measurement based detection/prediction techniques. In particular it would help to improve the safety, reliability and availability for train operations of a railway network. The direct and accurate knowledge of the wheel-rail contact conditions would not only provide a better control in traction/braking but also offer the opportunity for train scheduling and optimisation to be made adaptive to track conditions.

2. WHEELSET MODELLING

The dynamic response of the wheelset is affected by creep forces generated at the wheel-rail contact patch. These contact forces acting in longitudinal and lateral directions have a nonlinear relationship with creep. Creep is the relative speed of the wheels to rail and characterized as lateral and longitudinal creep in accordance with the direction of motion. Total creep at any point on the creep curve is[6]:

$$\lambda = \sqrt{\lambda_x^2 + \lambda_y^2} \tag{1}$$

And respective creep forces for left and right wheels are represented as[6]:

$$F_{ij} = F_j . \frac{\lambda_{ij}}{\lambda_j}, \qquad i = x, y, \quad j = L, R \tag{2}$$

Figure 1 shows the variation of adhesion coefficient with creep for different track conditions. Each curve can be divided into three parts. The first part is approximately linear, the second part is nonlinear and it is known as the high creep section and the third part with negative slope is the unstable portion of the curve[1].

The equations of motion for railway wheelset at any point on the creep curve are represented as[7]:

$$M_v\ddot{x} = F_{xR} + F_{xL} \tag{3}$$

$$m_w\ddot{y} = -F_{yR} - F_{yL} + F_c \tag{4}$$

$$I_w\ddot{\psi} = F_{xR}L_g - F_{xL}L_g - k_w\psi \tag{5}$$

$$T_s = k_s\int(\omega_R - \omega_L)dt + C_s(\omega_R - \omega_L) \tag{6}$$

$$I_L\dot{\omega}_L = T_s - T_L \tag{7}$$

$$I_R\dot{\omega}_R = T_t - T_s - T_R \tag{8}$$

where F_c in equation (4) represents the centrifugal force component and can be neglected when the vehicle is not running on curves and the material damping C_s of shaft in equation (6) is usually very small and therefore also neglected in the further study.

where $\theta_s = \int(\omega_R - \omega_L)dt$

A full model is given in equation 10.

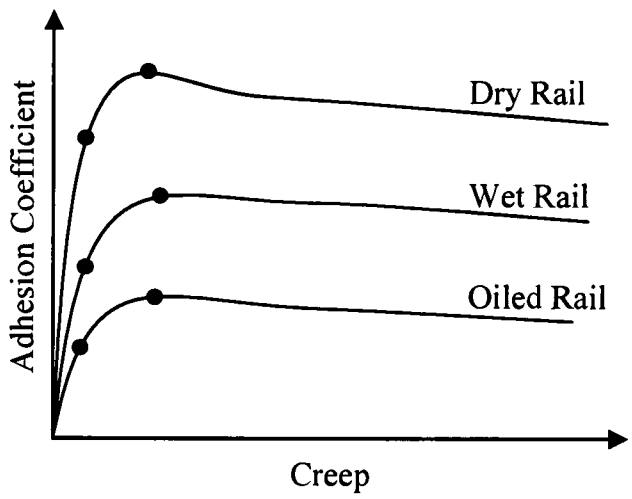

Figure 1: Creep vs adhesion coefficient

$$\begin{bmatrix}\dot{\omega}_R\\ \dot{\omega}_L\\ \dot{\theta}_s\\ \ddot{x}\\ \dot{y}\\ \ddot{\psi}\\ \ddot{y}\\ \dot{\psi}\end{bmatrix} = \begin{bmatrix} 0 & 0 & -\frac{k_s}{I_R} & 0 & 0 & 0 & 0 & 0\\ 0 & 0 & \frac{k_s}{I_R} & 0 & 0 & 0 & 0 & 0\\ 1 & -1 & 0 & 0 & 0 & 0 & 0 & 0\\ 0 & 0 & 0 & 0 & 0 & 0 & 0 & 0\\ 0 & 0 & 0 & 0 & 0 & 0 & 1 & 0\\ 0 & 0 & 0 & 0 & 0 & 0 & 0 & 1\\ 0 & 0 & 0 & 0 & 0 & 0 & 0 & 0\\ 0 & 0 & 0 & 0 & 0 & -\frac{k_w}{I_w} & 0 & 0 \end{bmatrix}\begin{bmatrix}\omega_R\\ \omega_L\\ \theta_s\\ \dot{x}\\ y\\ \psi\\ \dot{y}\\ \dot{\psi}\end{bmatrix} + \begin{bmatrix}\frac{1}{I_R}\\ 0\\ 0\\ 0\\ 0\\ 0\\ 0\\ 0\end{bmatrix} T_t + \begin{bmatrix} -\frac{r_o}{I_R} & 0 & 0 & 0\\ 0 & -\frac{r_o}{I_L} & 0 & 0\\ 0 & 0 & 0 & 0\\ \frac{1}{M_v} & \frac{1}{M_v} & 0 & 0\\ 0 & 0 & 0 & 0\\ 0 & 0 & 0 & 0\\ 0 & 0 & -\frac{1}{m_w} & -\frac{1}{m_w}\\ \frac{L_g}{I_w} & -\frac{L_g}{I_w} & 0 & 0 \end{bmatrix}\begin{bmatrix}F_{xR}\\ F_{xL}\\ F_{yR}\\ F_{yL}\end{bmatrix} \tag{10}$$

In equation (10), the creep forces have nonlinear relationships with the creep. In order to estimate the state variables using linear estimation techniques creep forces are linearized by taking several points along the curve.

2.1. Linearization of Wheelset Model

First order approximations of lateral and longitudinal creep forces around a point (λ_o, μ_o) are shown in equations (11) and (12).

$$F_{xj} = F_{xjo} + \frac{\partial F_{xj}}{\partial \lambda_{xj}}\bigg|_{(\lambda_{xjo},\lambda_{yjo})} \times \Delta\lambda_{xj} + \frac{\partial F_{xj}}{\partial \lambda_{yj}}\bigg|_{(\lambda_{xjo},\lambda_{yjo})} \times \Delta\lambda_{yj} \tag{11}$$

$$F_{yj} = F_{yjo} + \frac{\partial F_{yj}}{\partial \lambda_{yj}}\bigg|_{(\lambda_{xjo},\lambda_{yjo})} \times \Delta\lambda_{yj} + \frac{\partial F_{yj}}{\partial \lambda_{xj}}\bigg|_{(\lambda_{xjo},\lambda_{yjo})} \times \Delta\lambda_{xj} \tag{12}$$

Choosing state variables as

$x = [\omega_R\ \ \omega_L\ \ \theta_s\ \ \dot{x}\ \ y\ \ \psi\ \ \dot{y}\ \ \dot{\psi}]$,

or

$$\Delta F_{xj} = g_{11}\Delta\lambda_{xj} + g_{12}\Delta\lambda_{yj} \tag{13}$$

$$\Delta F_{yj} = g_{22}\Delta\lambda_{yj} + g_{21}\Delta\lambda_{xj} \tag{14}$$

where g_{11}, g_{12}, g_{22} and g_{21} are creep force coefficients and depend upon the operating point on the creep curve.

After substituting equations (13) and (14) in equation (10) a small signal representation of the complete wheelset model is obtained as given in equation (15).

Since the vehicle inertia is much larger than that of the wheels, the vehicle speed may be considered constant[7]. Then it is clear from equation (15) that the dynamic response of the wheelset only depends upon the operating condition determined by creep force coefficients.

Table-1 shows the eigenvalues analyses of the linearised wheelset model as the operating point is moved up on the creep curve of figure 3. In the low creep region, the slope of the curve is high which results in sufficiently high damping of torsional and kinematic modes. As the point is moved towards high creep region damping of kinematic

and torsional mode is decreased and finally become unstable when the slope of creep curve is negative. At this point, the wheelset would produce kinematic oscillations until they are limited by the flanges, torsional vibrations may be observed and wheelset rotational speed will also be increased because of the slip.

3. MULTIPLE MODEL BASED ESTIMATION

The small signal model is only valid at the particular point on the creep curve where linearization is carried out. To provide more precise estimation across entire operating conditions, the use of a bank of filters linearized at different points may be more useful[1].
Figure-2 shows the structure of the proposed multiple model based estimator. The system is excited by irregularities in the track and the yaw rate is the only measurement used in the estimation.

$$\begin{bmatrix} \Delta\dot{\omega}_R \\ \Delta\dot{\omega}_L \\ \Delta\dot{\theta}_s \\ \Delta\dot{x} \\ \Delta\dot{y} \\ \Delta\dot{\psi} \\ \Delta\ddot{y} \\ \Delta\ddot{\psi} \end{bmatrix} = \begin{bmatrix} -\frac{r_o^2 g_{11}}{vI_R} & 0 & -\frac{k_s}{I_R} & 0 & \frac{\gamma g_{11}}{I_R} & \frac{r_o g_{12}}{I_R} & -\frac{r_o g_{12}}{vI_R} & \frac{r_o L_g f_{11}}{vI_R} \\ 0 & -\frac{r_o^2 g_{11}}{vI_L} & \frac{k_s}{I_L} & 0 & -\frac{\gamma g_{11}}{I_L} & \frac{r_o g_{12}}{I_L} & -\frac{r_o g_{12}}{vI_L} & -\frac{r_o L_g g_{11}}{vI_L} \\ 1 & -1 & 0 & 0 & 0 & 0 & 0 & 0 \\ \frac{r_o g_{11}}{M_v v} & \frac{r_o g_{11}}{M_v v} & 0 & 0 & 0 & 0 & \frac{2g_{12}}{M_v v} & -\frac{2g_{12}}{M_v} \\ 0 & 0 & 0 & 0 & 0 & 0 & 1 & 0 \\ 0 & 0 & 0 & 0 & 0 & 0 & 0 & 1 \\ -\frac{r_o g_{21}}{vm_w} & -\frac{r_o g_{21}}{vm_w} & 0 & 0 & 0 & \frac{2g_{22}}{m_w} & -\frac{2g_{22}}{vm_w} & 0 \\ \frac{r_o L_g g_{11}}{vI_w} & -\frac{r_o L_g g_{11}}{vI_w} & 0 & 0 & -\frac{2L_g \gamma g_{11}}{r_o I_w} & -\frac{k_w}{I_w} & 0 & -\frac{2L_g^2 g_{11}}{vI_w} \end{bmatrix} \begin{bmatrix} \Delta\omega_R \\ \Delta\omega_L \\ \Delta\theta_s \\ \Delta\dot{x} \\ \Delta y \\ \Delta\psi \\ \Delta\dot{y} \\ \Delta\dot{\psi} \end{bmatrix} + \begin{bmatrix} \frac{1}{I_R} & -\frac{\gamma g_{11}}{I_R} \\ 0 & \frac{\gamma g_{11}}{I_L} \\ 0 & 0 \\ 0 & 0 \\ 0 & 0 \\ 0 & 0 \\ 0 & 0 \\ 0 & \frac{2L_g \gamma g_{11}}{r_o I_w} \end{bmatrix} \begin{bmatrix} \Delta T_t \\ \Delta y_t \end{bmatrix} \quad (15)$$

Point on Creep Curve (λ_o, μ_o)	**Wheelset Dynamics** (Speed=20m/s K_s= 6063260 N/m K_w=2.5 x10^6 N/rad)							
	Torsional Mode		**Kinematic Mode**		**High Frequency Mode**		**Common Rotation Mode**	
	Frequency (Hz)	**Damping (%)**	**Frequency (Hz)**	**Damping (%)**	**Frequency (Hz)**	**Damping (%)**	**Frequency (Hz)**	**Damping (%)**
(0.00075, 0.025)	40.91	31.6	2.05	66.5	43.61 31.67	100 100	0 72.74	0 100
(0.003, 0.15)	36.29	14.5	1.98	28.5	116.5 55.39	100 100	0 213.3	0 100
(0.0045, 0.3)	36.13	13.0	1.98	25.8	122.25 70.99	100 100	0 237.18	0 100
(0.0337, 0.39)	60	-0.8	2.34 2.61	-100 100	9.51	-2.75	0 3.94	0 -100

Table 1: Eigenvalue analysis of linearized wheelset model

A Kalman filter is used for estimation here because it is a well understood technique that has been applied to a wide variety of parameter estimation applications[5]. The equations of Kalman filter can be found in [8] an are given by

$$K = P_{k+1}C^T(CP_{k+1}C^T + R)^{-1} \quad (16)$$

$$\tilde{x}_{k+1} = \tilde{x}_k + K(z - C\tilde{x}) \quad (17)$$

$$P_{k+1} = AP_kA^T + R - AP_kC^TR^{-1}CP_kA^T \quad (18)$$

In equation (16) K is the Kalman gain used to weight the measurement innovation in equation (17). Equation (18) is used to update the estimated state vector. This set of mathematical equations provides an efficient computational (recursive) means to estimate the state of a process in a way that minimizes the means to the squared error[8].

Numbers of localized Kalman filters can be used here to estimate the parameters in all possible operating conditions. In this preliminary study, only two Kalman filters are used.

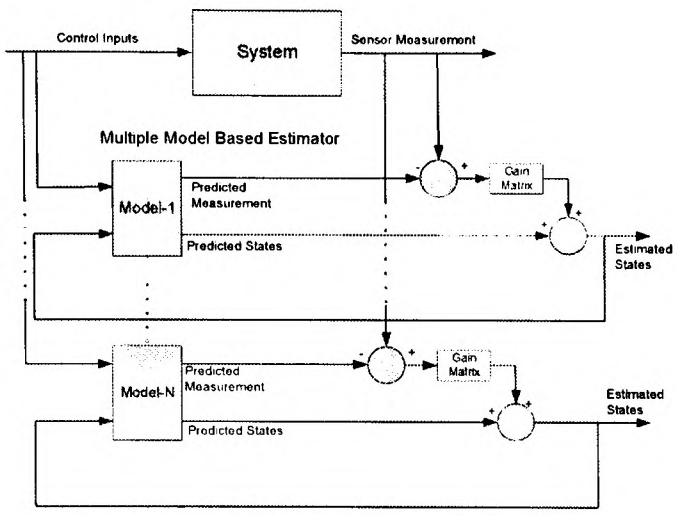

Figure 2: Multiple model based estimator

3.1. Parameter Estimation

Parameter	Value
Mass of Vehicle (M_v)	15000 kg
Right wheel moment of inertia (I_R)	133.2 Kgm^2
Left wheel moment of inertia (I_L)	62.8 Kgm^2
Wheels radius (r_o)	0.5 m
Torsional Stiffness (k_s)	6063260 N/m
Conicity of Wheel(γ)	0.15
Mass of Wheelset (m_w)	1250 kg
Yaw Moment of Inertia (I_w)	600 kg rad^2
Yaw Stiffness (k_w)	2.5x10^6 N/rad
Speed of Vehicle (v)	20 m/s

Table 2: Parameters used in simulation

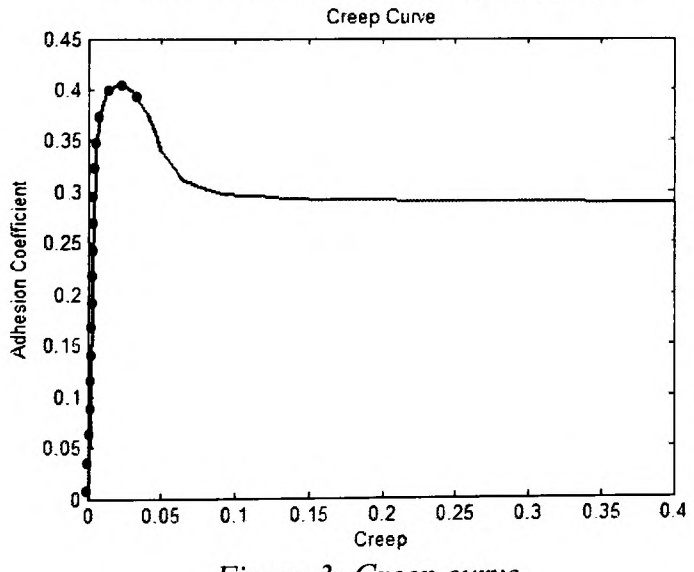

Figure 3: Creep curve

Table 2 summarizes the values of wheelset parameters used in the study. Multiple Kalman filters run in parallel and the output is switched by examining the residuals of the estimator outputs. Creep curve used in simulation is shown in figure 3. The dynamic response of the wheelset is changed as the operating point on the creep curve is changed. If the points on the creep curves are chosen close to each other then the multiple Kalman filter approach can provide estimation in all possible operating conditions.

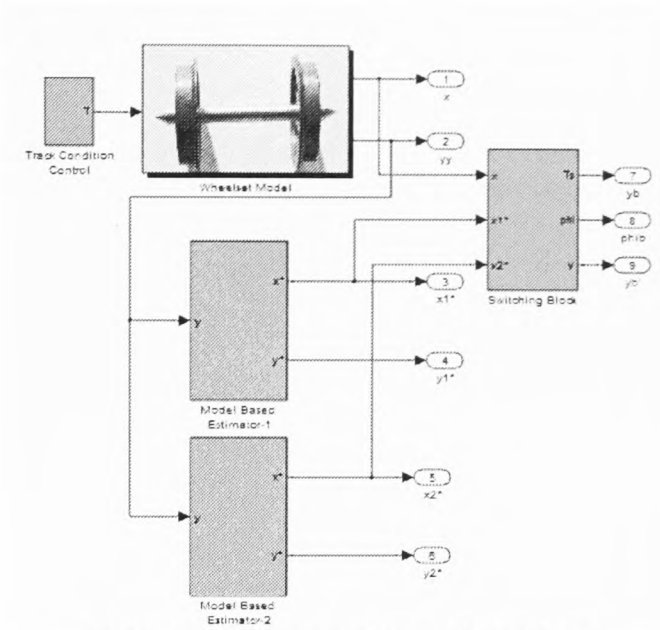

Figure 4: Simulink model of proposed scheme

In this research the outcome of the proposed scheme is demonstrated by using two points on the creep curve. This can be implemented easily for more than two points by simply adding more localized model based filters in the system. Figure 4 shows the Simulink model of the proposed scheme. Simulation is carried out for five seconds and the track condition control block switches the operating point after 2.5 seconds. The switching block selects the estimated output of one of the estimators by comparing the residuals.

Figures 5 and figure 6 show the estimated yaw motion by both estimators. In the beginning of the simulation the estimated yaw motion by estimator-1 is close to the actual state and, after 2.5 seconds when the operating condition is switched, the output of estimator-1 is close to the actual yaw motion. This shows that it is not possible for a single estimator to estimate states in both operating conditions.

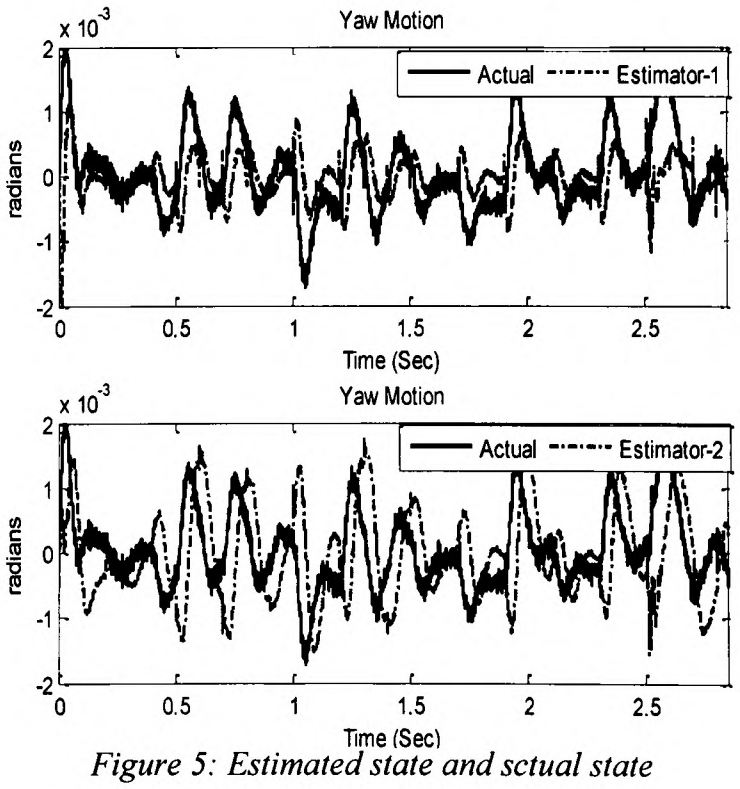

Figure 5: Estimated state and sctual state

The estimation error produced by a Kalman filter is small if the wheelset operating condition is in the vicinity of the point where the estimator is tuned to.

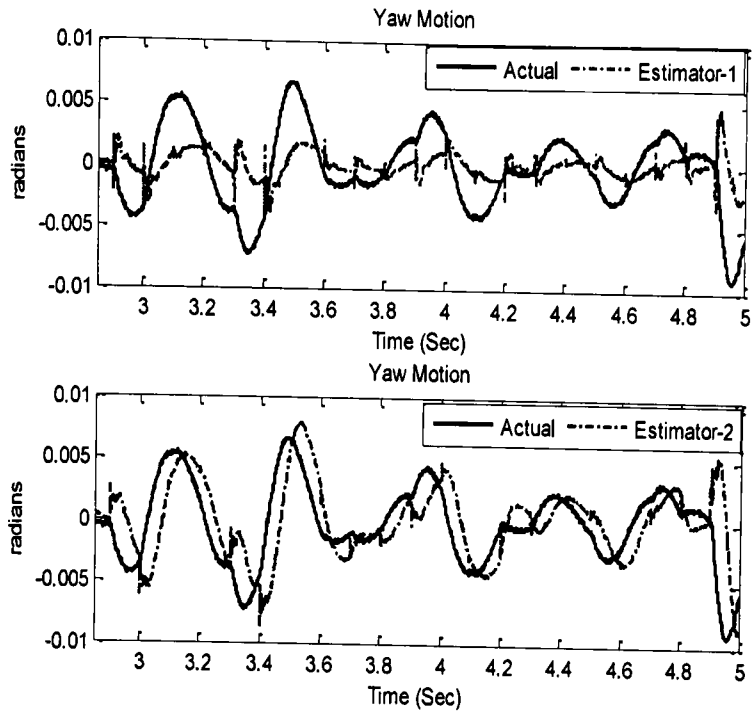

Figure 6: Estimated state and actual state

A Switching Block compares the residuals of both estimators and selects the estimated states which are close to actual states. The result is shown in the figure 7.

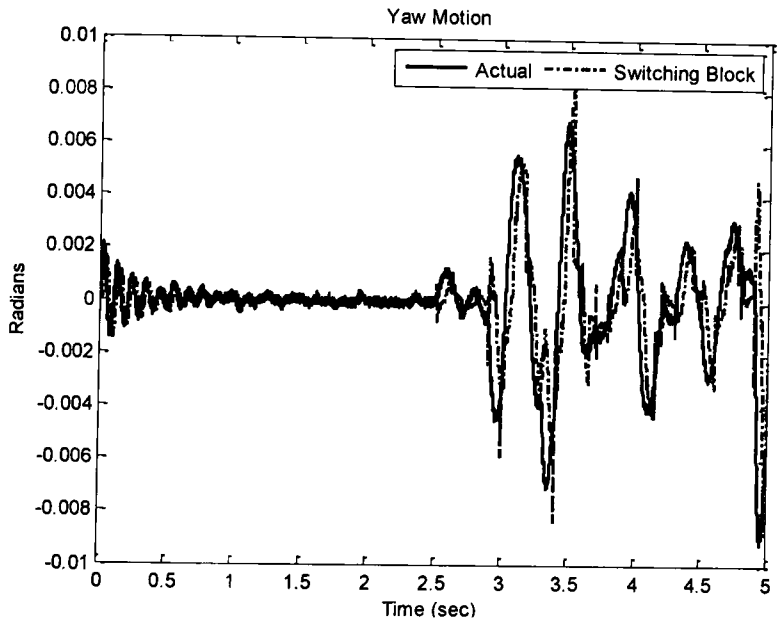

Figure 7: Output of switching block

In this way an accurate estimation of states can be obtained along the entire creep curve by adding more filters designed to operate on different points on the creep curve. Error produced by the switching block is comparatively very small and estimated states can be trusted for further operation.

4. CONCLUSION

The dynamic behaviour of a railway wheelset at different wheel rail contact conditions is an important factor in the performance of a railway vehicle. Reliable knowledge of available contact condition enables the related control system to optimize the use of adhesion available. In this research a multiple model based approach is used to estimate the states in different contact condition. A comprehensive wheelset model is taken under study which includes all main motions of the wheelset. A bank of locally linearized Kalman filters is proposed to estimate the states in all possible contact conditions. The potential usefulness of the research is demonstrated by taking a simple model with two filters and corresponding results are presented. Further research is ongoing to develop a sophisticated control scheme to optimize the use of the available adhesion level at the wheel rail contact in order to improve the traction braking and ride comfort of the railway vehicle.

REFERENCES

1. Mei, T.X., J.H. Yu, and D.A. Wilson, *Mechatronic approach for effective wheel slip control in railway traction.* Proceedings of the Institution of Mechanical Engineers, Part F: Journal of Rail and Rapid Transit: p. 1-10.
2. Yu, J.H., T.X. Mei, and D.A. Wilson, *RE-ADHESION CONTROL BASED ON WHEELSET DYNAMICS IN RAILWAY TRACTION SYSTEM.*
3. Mei, T.X., J.H. Yu, and D.A. Wilson, *A Mechatronic Approach for Anti-slip Control in Railway Traction.*
4. Charles, G. and R. Goodall. *Low Adhesion Estimation.* 2006.
5. Charles, G., R. Goodall, and R. Dixon, *Model-based condition monitoring at the wheel-rail interface.* Vehicle System Dynamics, 2008. **46**(Supplement 1): p. 415-430.
6. Polach, O., *Creep forces in simulations of traction vehicles running on adhesion limit.* Wear, 2005. **258**(7-8): p. 992-1000.
7. Yu, J.H., *Re-adhesion control for AC traction system in railway application*, PhD Thesis, The University of Leeds, 2007.
8. Welch, G. and G. Bishop, *An Introduction to the Kalman Filter.* University of North Carolina at Chapel Hill, Chapel Hill, NC, 1995.

Appendix A: List of symbols

ω_L, ω_R	Left and right wheel angular velocities
v	Forward Speed of Vehicle
M_v, m_w	Mass of vehicle and mass of wheelset
I_R, I_L	Moment of inertia of right wheel, left wheel
I_w	Yaw moment of inertia
ψ	Yaw Movement
y	Lateral Motion
λ_L, λ_R	Left and right wheel Creepages
$\lambda_{xL}, \lambda_{xR}$	Left and right wheel creepage in longitudinal direction
$\lambda_{yL}, \lambda_{yR}$	Left and right wheel creepage in lateral direction
γ	Conicity of wheel
L_g	Half Gauge
r_L, r_R	Left and right wheel radius
r_o	Radius of each wheel when wheelset is centred
f_{11}, f_{22}	Longitudinal and lateral Creep force coefficients
y_t	Lateral Disturbance Caused by Track irregularities
T_s, T_t	Torsional Torque, Traction Torque
T_L, T_R	Tractive torque Left wheel and Right Wheel respectively

Detection of wheel-rail conditions for improved traction control

***T.X. Mei, **I. Hussain**

School of Computing Science and engineering
University of Salford, UK
*t.x.mei@salford.ac.uk **I.Hussain@edu.salford.ac.uk

Keywords: Wheel-rail contact, Wheel slip, estimation.

Abstract

Novel detection techniques of wheel-rail contact condition that exploit the dynamic properties of the conventional solid axle wheelset in response to changes at the wheel-rail interface, are studied in this paper. The main aim is to develop an ability to identify/predict adhesion limit to overcome the problem of wheel slip/slide in poor contact conditions where the adhesion is low. Two possible solutions are introduced. One of the proposed methods detects the wheel slip indirectly from the wheelset dynamic changes caused by the wheelsets operating in the unstable region of the non-linear contact characteristics as a consequence of wheel slip. The second method estimates the contact force saturation and identifies the maximum adhesion using a model based technique that involves the use of multiple Kalman filters.

1 Introduction

Adhesion at the wheel-rail interface is essential to the delivery of tractive effort from traction and braking systems in railway vehicles. Adhesion forces have nonlinear features in relation to the relative motion of the two surfaces at the wheel-rail contact point(s) and are strongly affected by contact conditions. Wheel slip/slide occurs when applied tractive effort exceeds the maximum adhesion available which can potentially increase severe wear of wheel and rail surfaces, increase mechanical stress in the system and affect stability. Therefore re-adhesion schemes are required to reduce the risk of slip.

The most commonly used wheel slip protection schemes are achieved by measuring and controlling the slip ratio (relative speed between a wheel and the train), and in more extremely cases to control the wheel rotational acceleration below a pre-defined threshold [1-4]. Also, hybrid anti-slip methods with the use of slip, wheel speed and acceleration information are proposed [4, 5]. Those controllers are difficult to obtain optimal performance and also require accurate measurement of slip wheel. Disturbance observers are proposed to detect slip conditions [6, 7], where traction torque is treated as a disturbance input and estimated either through state observers using motor speed and torque information. The performances of the anti-slip schemes based on a disturbance observer are to a large extent affected by noises in the system which can be very substantial in the wheel-rail contact environment.

This paper presents two novel schemes to tackle the problem of wheel slip/slide in poor contact conditions which are fundamentally different from the existing methods. Section 2 presents a scheme that exploits the effect of wheel slip on the wheelset dynamic behaviour and focuses on the axle vibrations caused by the negative damping of the non-linear contact characteristics. In section 3, the second scheme uses a set of Kalman filters that are optimised for different operating conditions of the wheel-rail contact and then use a 'best match' strategy to estimate the adhesion conditions.

2 Wheel Slip Detection via Axle Vibration

The contact forces at the wheel-rail interface are widely recognised to present non-linear characteristics as a function of creep/slip as shown in Figure 1. In normal running conditions where the creep is small, the contact forces provide a damping effort to the dynamic modes of a wheelset and are very useful in stabilising those modes which would otherwise be almost critically damped (e.g. with material damping only). There is a problem of kinematic instability due to the creep forces (or wheelset hunting), but it is a separate issue and overcome mainly by the use of primary suspensions.

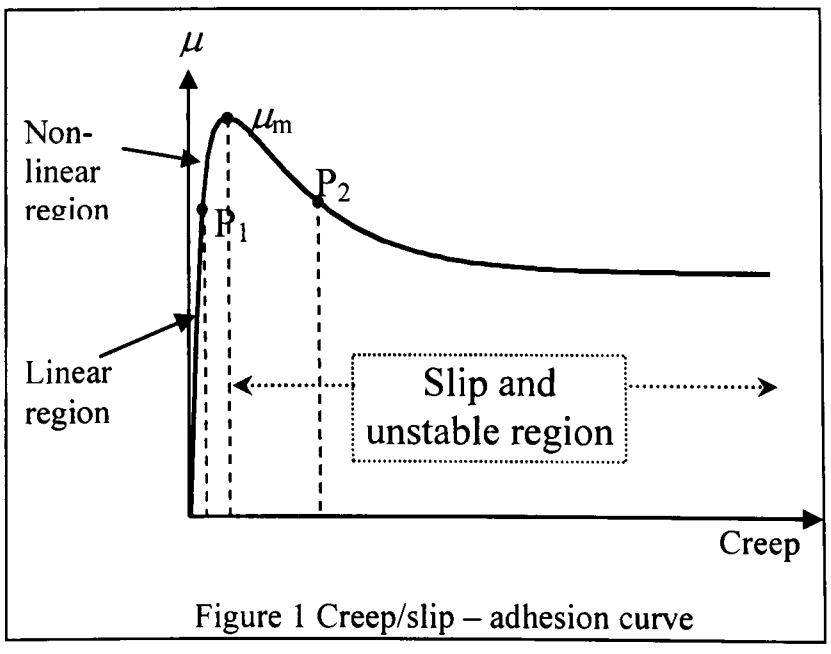

Figure 1 Creep/slip – adhesion curve

As the creep increases, the contact forces can operate in the second (or non-linear) region where the rate of change of the creep forces and associated damping effect is much lower. However, when the creep is beyond the point of maximum adhesion (μ_m) available at the wheel-rail interface and enters the slip or unstable region, the contact forces will then become a destabilising element, which not only cause the well known problem of wheel slip (in traction) or slide (in braking) but also can cause other undesirable mechanical oscillations in the wheelset. Most noticeably, it can cause severe torsional vibrations in the wheelset axle which is considered in railway industry as a highly undesirable problem because they may lead to component failure or rail corrugation [8].

The problem of the torsional vibrations may be overcome in the vehicle design by for example introducing additional damping components. However, the link between the level of damping (or stability) for the torsional mode of a wheelset and the wheel-rail contact conditions provides an excellent indication for wheel slip and therefore is exploited in this study for the development of an anti-slip control scheme. As long as the wheel slip/slide can be effectively controlled, no lasting oscillations and associated damages to the contact surfaces are expected in the wheelset.

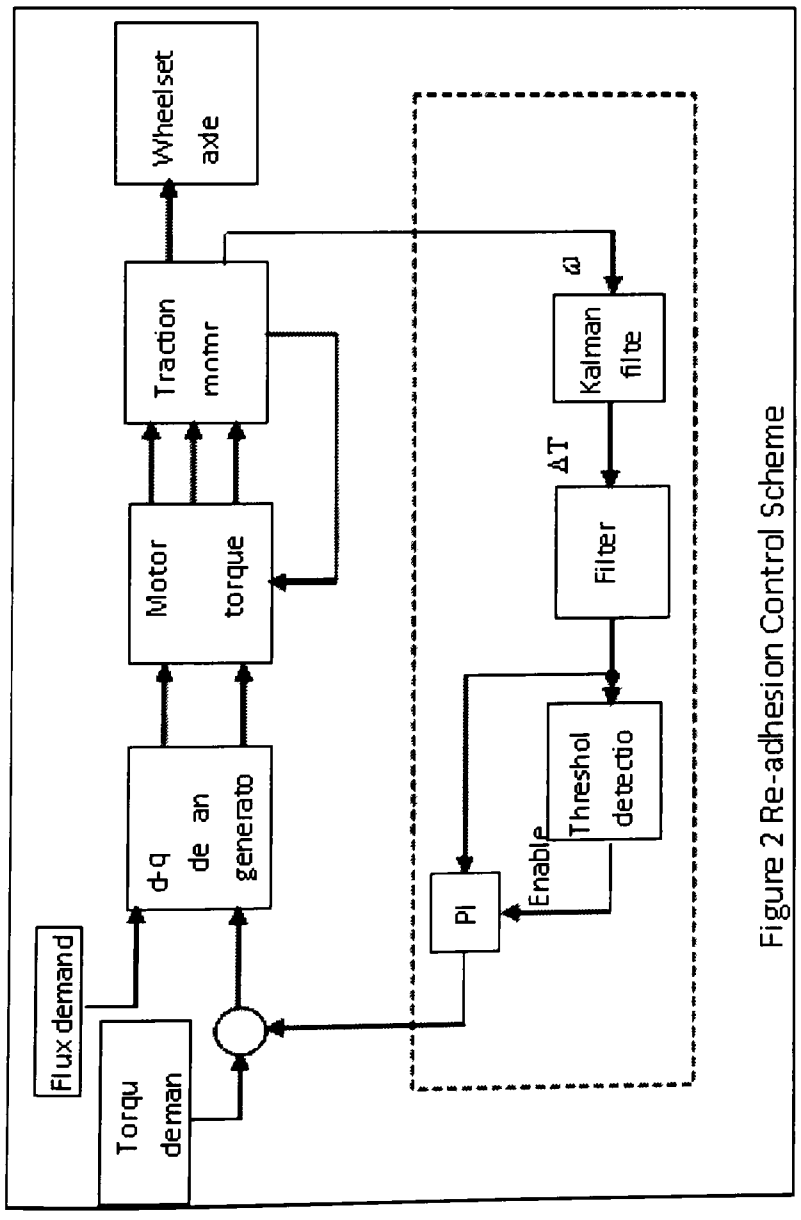

Figure 2 Re-adhesion Control Scheme

The proposed anti-slip (or re-adhesion) control scheme is presented in the dashed block in Figure 2, but a standard AC traction motor and a vector control for the provision of a precise tractive effort are considered in the study as indicated in the diagram. Although the torsional dynamics provide an excellent possibility for wheel slip detection, the direct implementation of the idea will be problematic in practice as it requires a measurement of the torsional torque. Strain gauges (or other torque sensors) would have to be mounted on the (rotating) axle which would present very difficult challenges in terms of the sensor reliability and transmission of the measured signals because of the harsh working environment. Therefore, it is essential that the practicality of sensing is properly tackled. A number of estimation techniques are possible, but a Kalman filter is chosen in this study to provide an estimation of the torsional oscillations from the speed of the traction motor in the system [9]. The speed measurement in railway traction is always available and is normally achieved through the use of inductive sensors to detect the time shifts between the teeth of the traction transmission gears or to count the number of teeth. The estimated output of the Kalman filters is then further processed to extract the magnitude of the torsional vibration signal at the frequency corresponding to the axle torsional mode using conventional filtering methods. A band pass filter is used and tuned to coincide with that of the torsional mode of a particular wheelset which is normally known. The output of the filter is then processed in a rectifier to detect the magnitude before a low pass filter that removes any noises and other disturbances in the system.

The computer simulation results in Figures 3 - 5 show the potential performance of the proposed anti-slip control in two different working conditions [9]. In Figure 3, the vehicle accelerates from an initial speed of 10 km/h on a track with a high adhesion coefficient of 0.4 which is then dropped to 0.05 at t=4s. The change of contact condition causes severe wheel slip where the rotational speed of the wheels becomes substantially greater than the equivalent of the vehicle speed. The wheel slip in turn causes the torsional vibrations in the axle, the magnitude of which at the torsional frequency is detected from estimations using the Kalman filter as shown in Figure 4. The magnitude of the vibration is then detected in a small fraction of a second and used to reduce the demand in tractive effort. Then the torque output from the traction motor is reduced accordingly after the torque reduction controller is enabled and the wheel speeds are 'pulled' back to the vehicle's speed in around 1s to restore the adhesion.

In Figure 5, the vehicle simulated operates at an initial speed of 100km/h on a track where the adhesion is reduced at the time t=4s from a dry condition (μ=0.4) to a low adhesion at μ=0.05. At the higher speed of 100km/h under the sudden change of adhesion, the detection of the wheels slip (in about 0.7s) appears to be slower because of the less rapid increase in the relative wheel speed, i.e. the wheel slip is less severe. The entire time for slip detection and re-adhesion is around 3s.

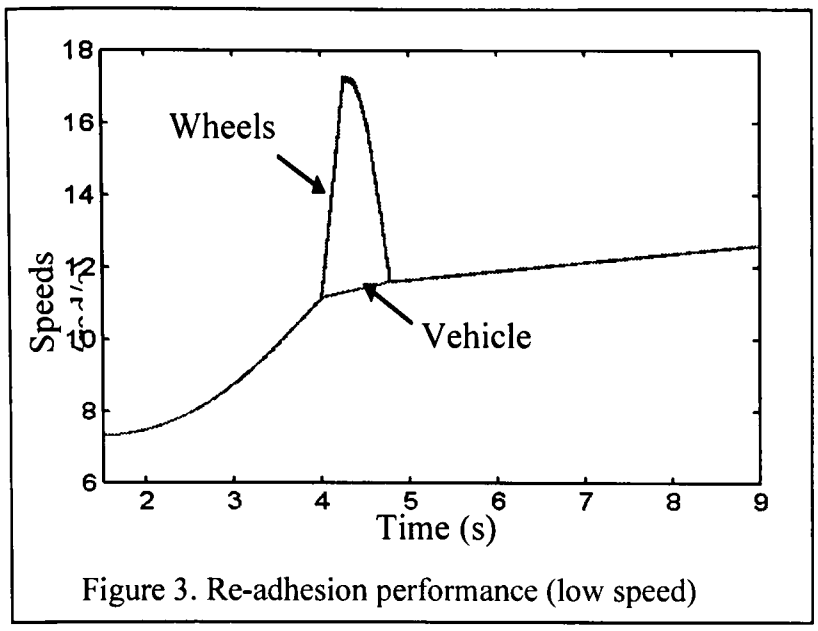

Figure 3. Re-adhesion performance (low speed)

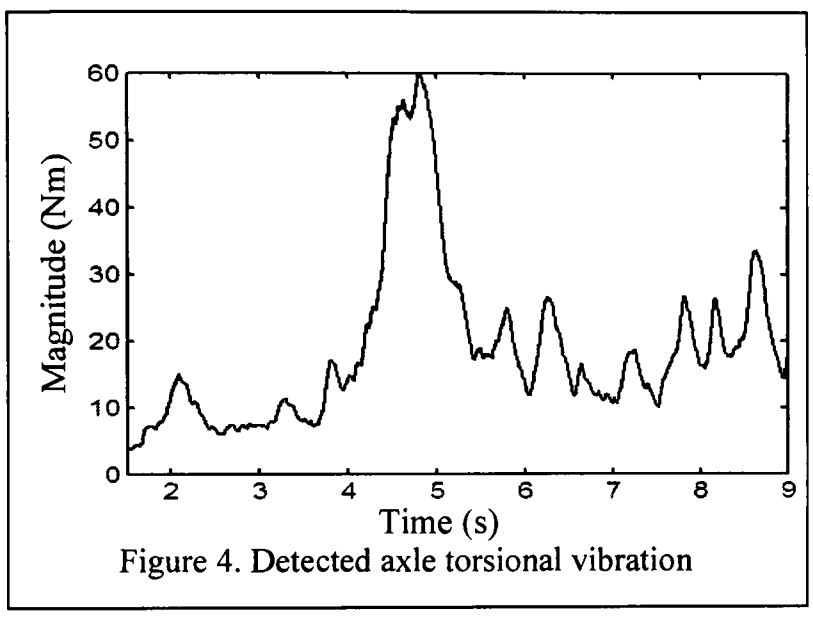

Figure 4. Detected axle torsional vibration

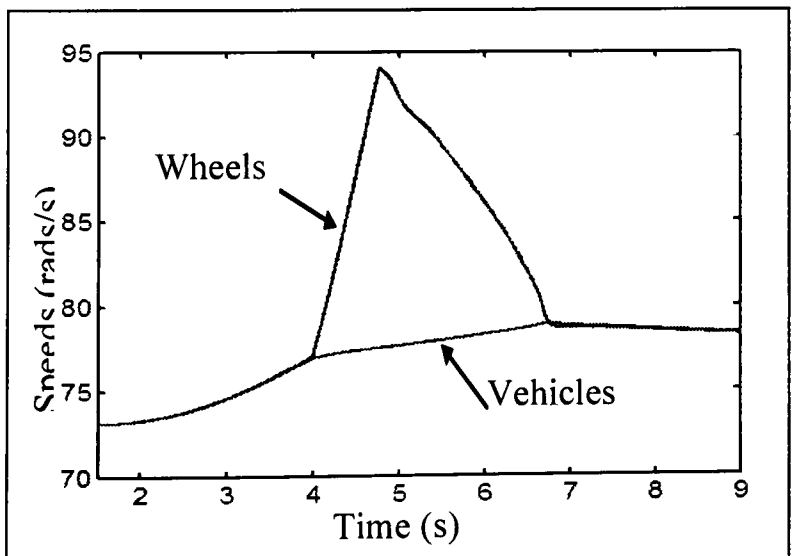

Figure 5. Re-adhesion performance (high speed)

3 Contact Condition Estimation with Multiple Kalman Filters

All present anti-slip protection/control schemes are focussed on the detection of wheel slip/slide and can only take measures to reduce/overcome the problem only after a wheel slip is identified to have occurred. There is no provision of preventative measures that could fundamentally stop wheel spinning (or locking in braking) by e.g. limiting tractive effort below the adhesion level on the track which would require reliable and real time information of the contact conditions to become available. The second part of this study is one of the first attempts to develop a practical method for real time estimation of the contact condition/adhesion on a track a vehicle is travelling. A previous study has tried to estimate the creep coefficient at the wheel-rail contact and use this as an indirect indicator of the adhesion [10].

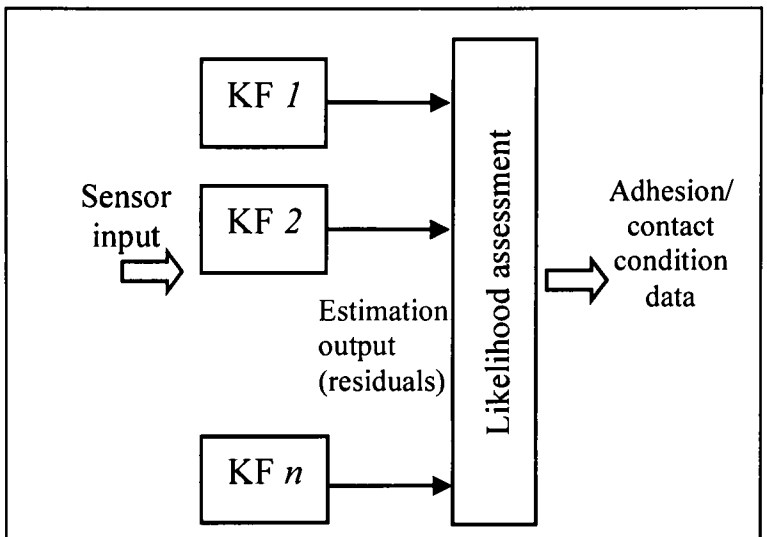

Figure 6. Contact condition monitoring scheme

The contact mechanics are highly non-linear in nature and are subject to large variations due to condition changes at the wheel-rail interface. The use of a single estimator, which is in general designed based on a linear (or linearised) model will be very difficult to cover all different operation conditions and account for the uncertainties. In this study, a set of Kalman filters are designed based on models linearised at different operating points on a creep curve (shown in Figure 1) each of which is tuned to provide the best estimation under its specific condition. The overall scheme is illustrated in Figure 6.

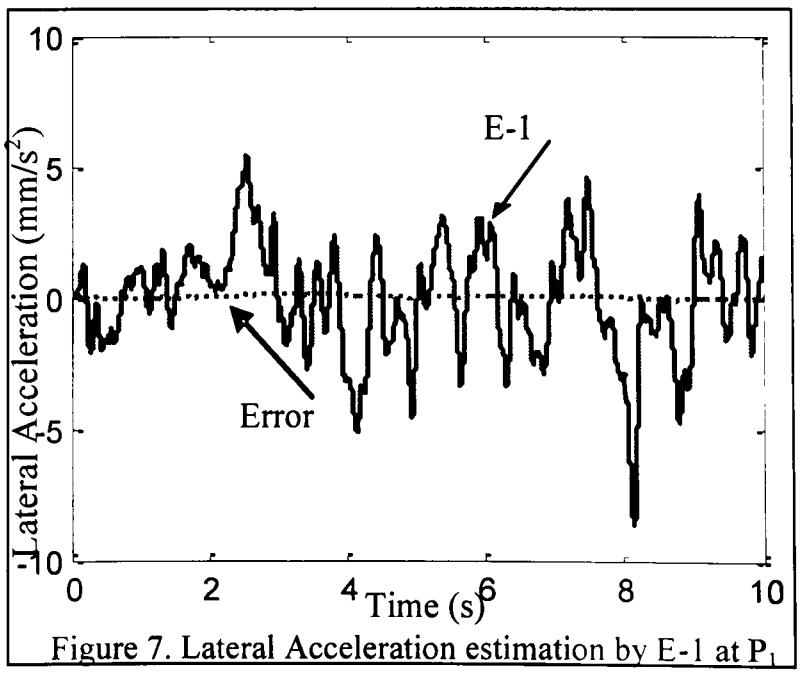

Figure 7. Lateral Acceleration estimation by E-1 at P_1

As each of the estimators is tuned to match one particular condition and will only give the best results at the linearised point, increased estimation errors are expected if the contact condition is not at or near the chosen operating point which will be reflected in the estimation residuals of the estimator. The output residuals from all the estimators can then be assessed using a likelihood approach to determine which of the estimators provide a best match to the present operating condition and hence an indication of the status of the wheel-rail contact.

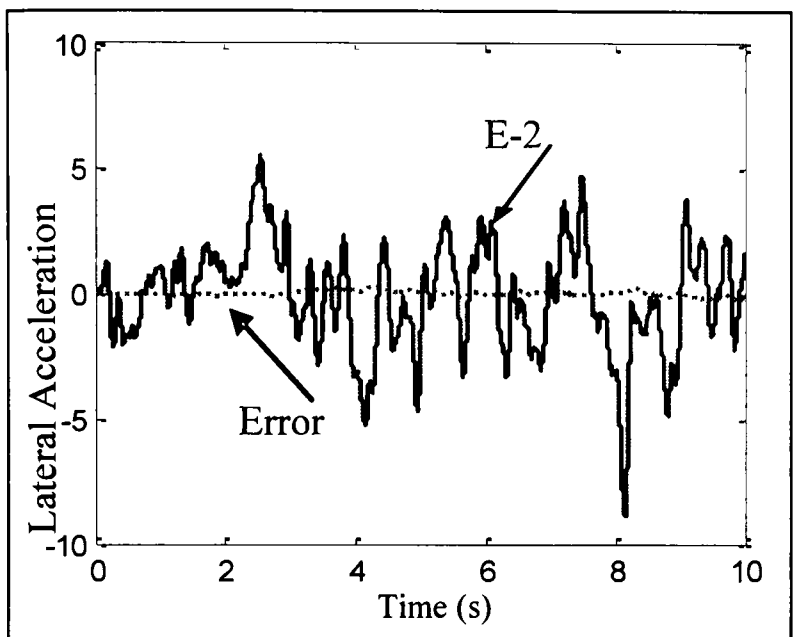

Figure 8. Lateral Acceleration estimation by E-2 at P_1

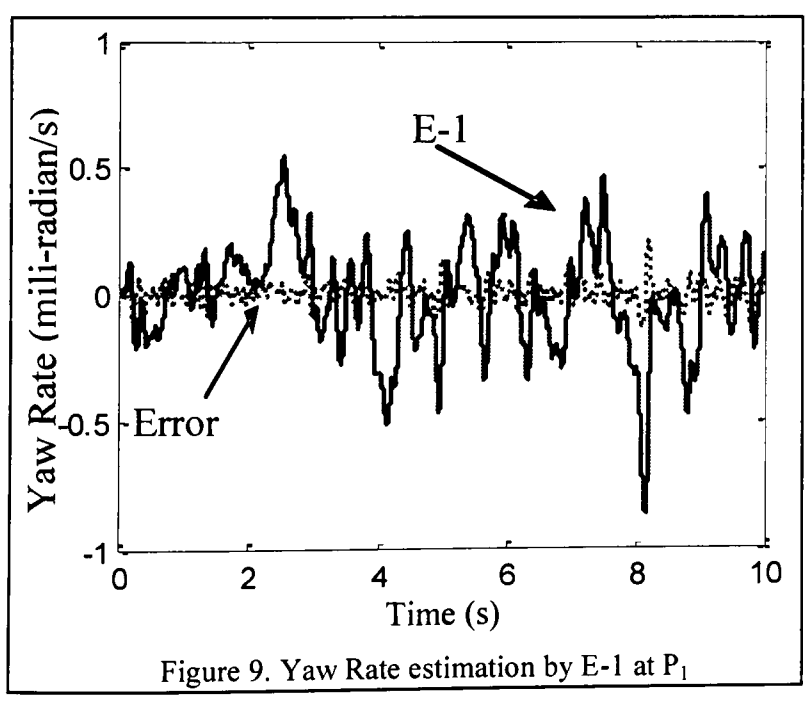

Figure 9. Yaw Rate estimation by E-1 at P_1

Kalman filter is used extensively for state estimation/prediction in many different applications because of its simplicity and robustness. The design/optimisation of Kalman filters is now considered a standard procedure and many design tools are available, e.g. in Matlab toolboxes.

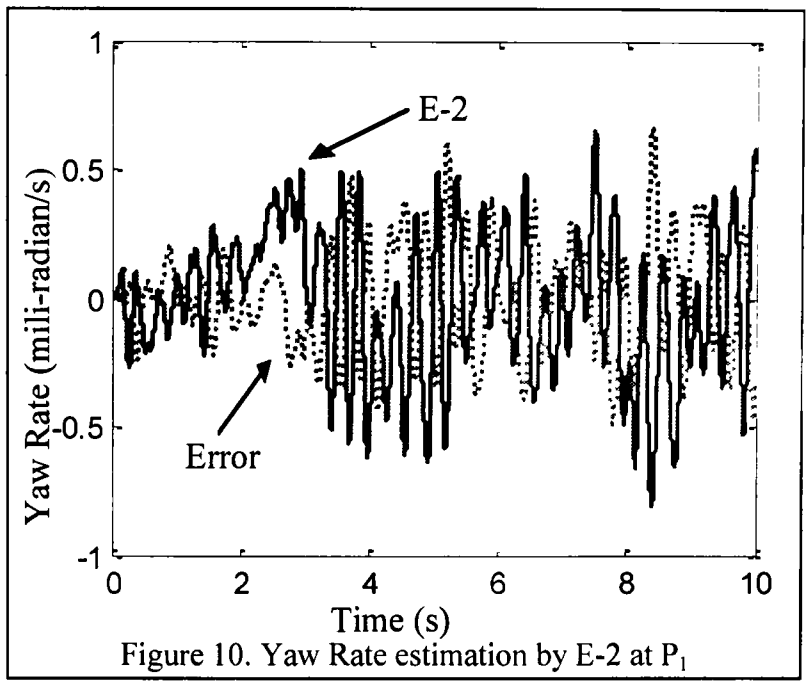

Figure 10. Yaw Rate estimation by E-2 at P_1

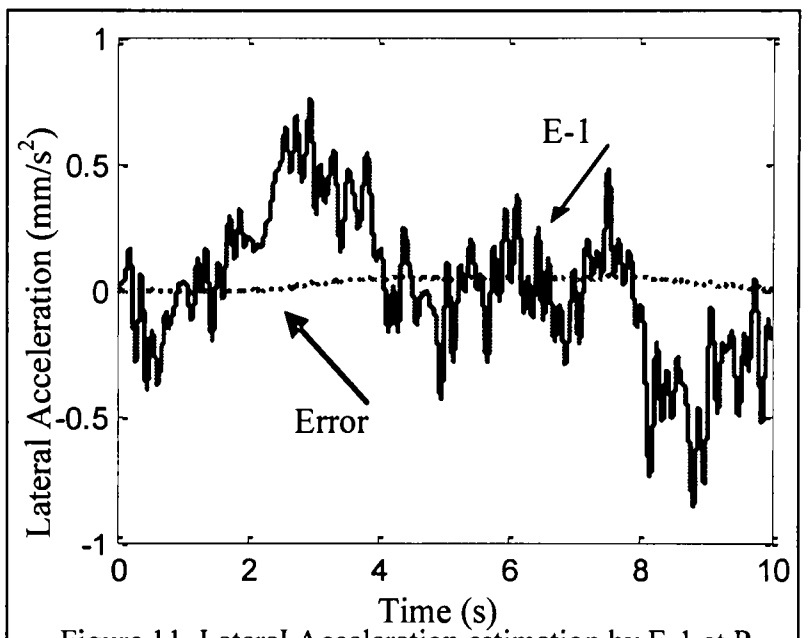

Figure 11. Lateral Acceleration estimation by E-1 at P_2

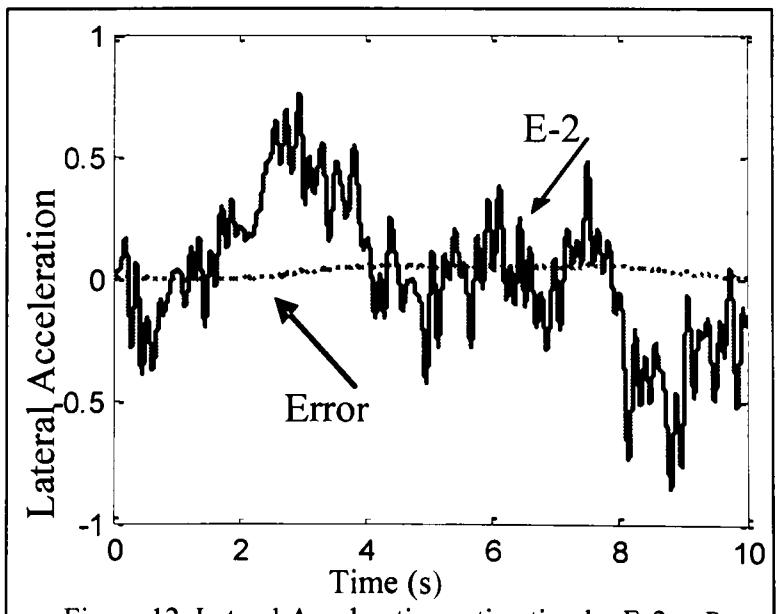

Figure 12. Lateral Acceleration estimation by E-2 at P_2

The potential benefit of this ongoing research is demonstrated by using two Kalman filters. Estimator-1 is

optimised in the linear region of the creep curve (P1) and Estimator-2 is tuned for an operating point in the unstable region just beyond the point of maximum adhesion (P3). Figures 7, 8, 9 and 10 show the result of estimation when the vehicle is set in the computer simulation to operate at the first operating point. It is clear from the figure Estimator-1 is producing smaller residuals compared to Estimator-2, which is especially evident for the yaw rate of the wheelset.

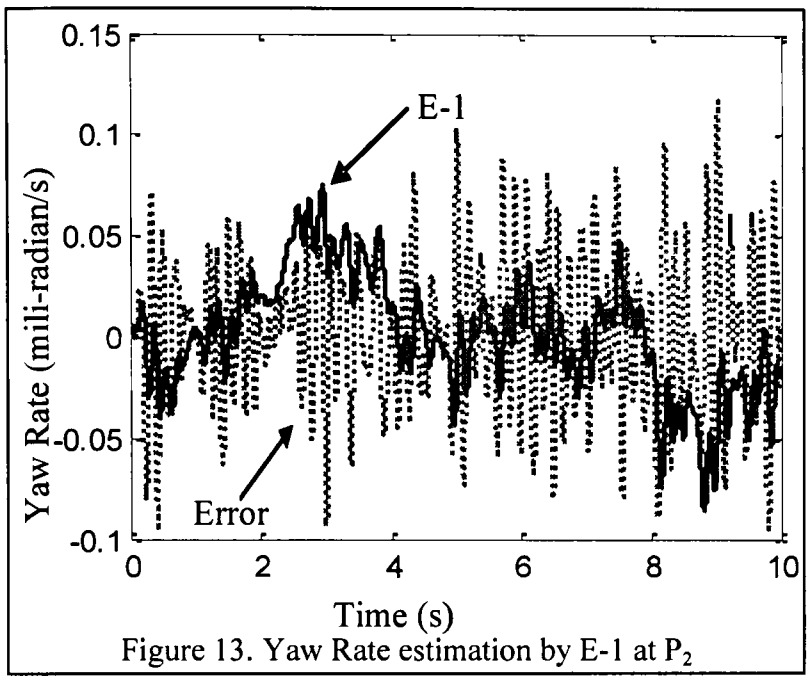

Figure 13. Yaw Rate estimation by E-1 at P_2

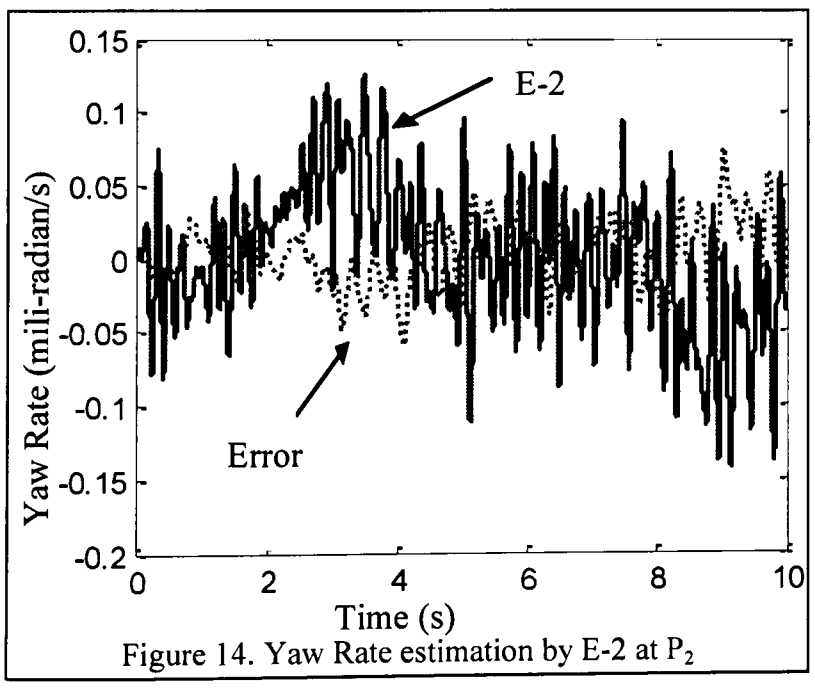

Figure 14. Yaw Rate estimation by E-2 at P_2

4 Concluding Remarks

Conventional anti slip/slide control methods based on the measurement of the wheel slip/slide and wheel rotational acceleration are considered effectively and widely used in industry, but can only act after the undesirable phenomenon has occurred and require the accurate measurement of both wheel (rotational) speed and absolute vehicle speed – the latter can be problematic in the wheel slip/slide conditions.

Two new approaches that aim to overcome the main drawbacks are introduced in this paper. The proposed methods detect wheel-rail contact conditions and the adhesion in particular from the wheelset dynamic behaviour in response to track condition changes and the potential benefits and performance gains are demonstrated using computer simulations.

References

[1] Watanabe T, and Yamanaka A, "Optimisation of readhesion control of Shinkansen Trains with wheel-rail adhesion", IEEE Power Conversion Conference (PCC'97), 1997.

[2] Schwartz H J, and Krebe R "Implementation of an advanced wheel creep control with searching strategy on a light rail vehicle". European Power Electronics Conference (EPE'97), 1997.

[3] Yasuoka I, and Henmi T, "Improvement of re-adhesion for commuter trains with vector control traction inverter" IEEE Power Conversion Conference (PCC'97), 1997.

[4] Park D, and Kim M S et al "Hybrid re-adhesion control method for traction system of high speed railway" IEEE International Conference on Electrical Machines and Systems (ICEMS'01), 2001

[5] Kadowaki,S., Ohishi, K., Miyashita I. and Yasukawa. Re-adhesion control of electric motor coach based on disturbance observer and sensor-less vector control, Proceedings of the Power Conversion Conference, Volume 3, 2002, p1020 – 1025.

[6] Hyoun-Chul Choi, Suk-Kyo Hong. Hybrid control for longitudinal speed and traction of vehicles, IEEE 2002 Annual Conference of the Industrial Electronics society, Volume 2, 2002, p1675 – 1680.

[7] Woo-Seok Kim, Yong-Seok Kim, Jun-Koo Kang and Seung-Ki Sul (1999). Electro-mechanical re-adhesion control simulator for inverter-driven railway electric vehicle, Conference Record of the 1999 IEEE Industry Applications Conference, Volume 2, 1999, p1026 – 1032.

[8] Lu G, and Harwood N A "Prediction of torsional vibration on mass transit vehicle", Computers in Railways'96, Volume 2: Railway Technology and Environment, 1996

[9] Mei, T X, Yu J H and Wilson D A, "Mechatronic approach for effective wheel slip control in railway traction", IMechE Proceedings (Part F) - Rail and Rapid Transit, Vol 223, No 3, 2009, pp 295-304.

[10] Charles, G.A. and Goodall, R.M., "Low Adhesion Estimation", Proceedings of IET International Conference on Railway Condition Monitoring 2006, Birmingham, November 2006, pp 96-101

Identification of Wheel-Rail Contact Condition Using Multi-Kalman Filtering Approach

I Hussain* and T. X. Mei**

School of Computing, Science and Engineering,
Salford University, Salford M5 4WT, UK,
* I.Hussain@pgr.salford.ac.uk** t.x.mei@salford.ac.uk

Abstract: Condition changes at the rail surface due to the fallen tree leaves and/or other contaminations can cause the low adhesion levels which present a serious challenge for the traction/braking control systems to avoid the problem of wheel slip/slide. This paper presents a multiple model based method for the identification of the adhesion limit to overcome the problem of the wheel slip/slide in poor contact conditions. The proposed scheme is an indirect method that exploits the dynamic properties of the conventional solid axle wheelset in response to changes in contact condition at the wheel-rail interface avoiding difficult and expensive measurement requirements. A nonlinear model of lateral and yaw dynamics of a conventional solid axle wheelset is used for the study. The non-linearity and changes in the interaction with the rail are modelled by using a set of non-linear creep/slip curves. The scheme consists of a bank of Kalman filters based on the linearized wheelset models. Each Kalman filter in the filter bank is optimally tuned to operate in a specific contact condition. Normalized root mean square values from the residual of each filter calculated using time moving windows are assessed to identify the operating condition of the wheelset. This paper mainly covers: (1) the modelling of wheelset dynamics and non-linear contact laws and that of condition changes at the wheel-rail interface; (2) the design detail of the Kalman filters; (3) Identification of wheel-rail contact conditions and; (4) simulation results to demonstrate potential effectiveness of the proposed scheme.

Keywords: Wheel rail contact, Estimation, Kalman filters, Fuzzy logic

1. INTRODUCTION

The traction and braking performance of the railway vehicle is governed by the contact forces generated at the wheel rail interface. These contact forces are a non-linear function of the creepages and vary substantially when the conditions of the rail surfaces change due to the contaminations. The overall adhesion can therefore becomes very low which results in wheel slip/slide. The wheel Slip/slide is a highly undesirable phenomenon that causes the mechanical parts to wear down quickly affects the stability and leads to the inconsistent traction performance causing problems in train scheduling.

In order to avoid the wheel slip/slide various different techniques have been used in past. (Watanabe and Yamanaka, 1997, Watanabe et al., 1997) presented a conventional technique of controlling the wheel slip based on the measurement of the relative speed between the wheel and the train which was supplemented with the control of the wheel acceleration. Also hybrid anti-slip methods which are also based on the relative speed measurement are proposed (Choi and Hong, 2002, Park et al., 2001). These controllers require an accurate measurement of the train and wheel rotational speeds that makes it difficult to obtain the optimal performance. Another method based on disturbance observers are proposed to detect the slip conditions (Kim et al., Choi and Hong, 2002). These controllers do not require direct speed measurement rather the adhesion coefficient is estimated by using the information of rotor speed and the torque current but the performances of the anti-slip schemes based on a disturbance observer are to a large extent affected by noises in the system which can be very substantial in the wheel-rail contact environment. (Mei et al., 2009) proposes an indirect technique that exploits the wheelset dynamics to develop wheel slip protection.

The real time information about the maximum adhesion available as a train travels through a track would help to tackle the problem of the wheel slip/slide. The provision of the tractive effort in either traction or braking could then be optimised to make the most out of the wheel-rail contact conditions.

This paper is an extension of an ongoing research that uses the multiple model based estimation approach for the identification of the contact conditions (T X Mei, 2010, I Hussain, 2009, I Hussain, 2010). In a previous study, the residual of estimated states were examined to determine the operating condition. In this paper a fuzzy logic based identification method is developed to determine the contact condition.

2. WHEELSET MODELLING

A solid axle railway wheelset (figure-1) with both the wheels fixed with the axle is used for this study. Both the wheels have profiled tread with the conicity γ. This coned

tread provides a natural feedback (due to the difference in the rolling radius) for the wheelset to adjust itself on the centre position when it is slightly displaced laterally. The motions of the wheelset are governed by the nonlinear creep forces generated at the wheel rail contact patch in the lateral and longitudinal directions. Creep is said to exist when the railway wheels deviate from pure rolling and can be described as the relative motion of wheels to the rails given in equations (1), (2) & (3). Delivery of tractive effort in traction and braking is achieved via longitudinal creep.

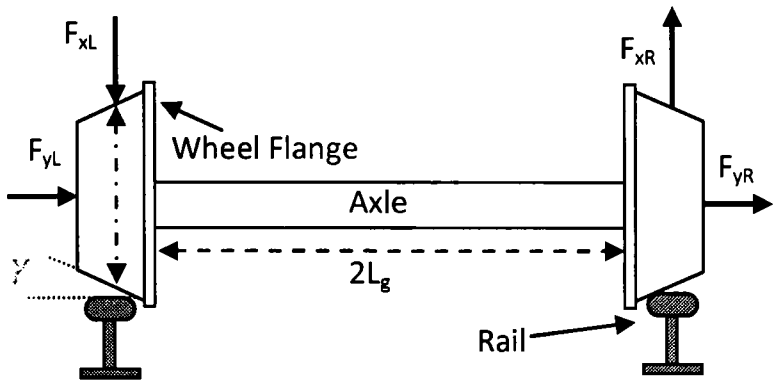

Fig.1. Railway Wheelset

$$\lambda_{xL} = \frac{r_o \omega_L - v}{v} + [\frac{L_g \dot{\psi}}{v} + \frac{\gamma(y - y_t)}{r_o}] \quad (1)$$

$$\lambda_{xR} = \frac{r_o \omega_R - v}{v} - [\frac{L_g \dot{\psi}}{v} + \frac{\gamma(y - y_t)}{r_o}] \quad (2)$$

$$\lambda_{yL} = \lambda_{yR} = \frac{\dot{y}}{v} - \psi \quad (3)$$

In above equations the subscript L, R are used for left and right wheels respectively, x and y are used to indicate the longitudinal and lateral directions, and λ_{xL}, λ_{xR}, λ_{yL} and λ_{yR} are creepages in the longitudinal and lateral directions for left and right wheels. ω_R and ω_L are angular speeds of right and left wheels respectively, Ψ is yaw angle, y is lateral motion, L_g is the half track gauge, v is forward speed of the vehicle, γ is conicity of wheel and r_o is the radius of wheel when it is at centre position and y_t is disturbance applied by track in lateral direction. The total creep at any point on the creep curve is given by following equations.

$$\lambda_L = \sqrt{\lambda_{xL}^2 + \lambda_{yL}^2} \quad (4)$$

$$\lambda_R = \sqrt{\lambda_{xR}^2 + \lambda_{yR}^2} \quad (5)$$

2.1 Simplified model

Only lateral and yaw dynamics are found to be sufficient to identify the track condition (I Hussain, 2010). The simplified equations of longitudinal creep for the left and the right wheel are given below.

$$\lambda_{xL} = \frac{L_g \dot{\psi}}{v} + \frac{\gamma(y - y_t)}{r_o} \quad (6)$$

$$\lambda_{xR} = -\frac{L_g \dot{\psi}}{v} - \frac{\gamma(y - y_t)}{r_o} \quad (7)$$

The yaw angle is the result of the difference in the longitudinal creep forces between the two wheels and the lateral dynamics are determined by the total creep force of the two wheels in the lateral direction. The equations for the lateral and the yaw motions of the railway wheelset are given in (8) and (9).

$$m_w \ddot{y} = -f_{yR} - f_{yL} + F_c \quad (8)$$

$$I_w \ddot{\psi} = f_{xR} L_g - f_{xL} L_g - k_w \psi \quad (9)$$

Where m_w is the wheelset mass, F_c is the centrifugal component of the force and can be ignored if the wheelset is not running on the curved track, I_w is the yaw moment of inertia and k_w is the yaw stiffness of a spring used to stabilise the wheelset. f_{yL}, f_{yR}, f_{xL} and f_{xR} are the creep forces of left and right wheels in lateral and longitudinal directions.

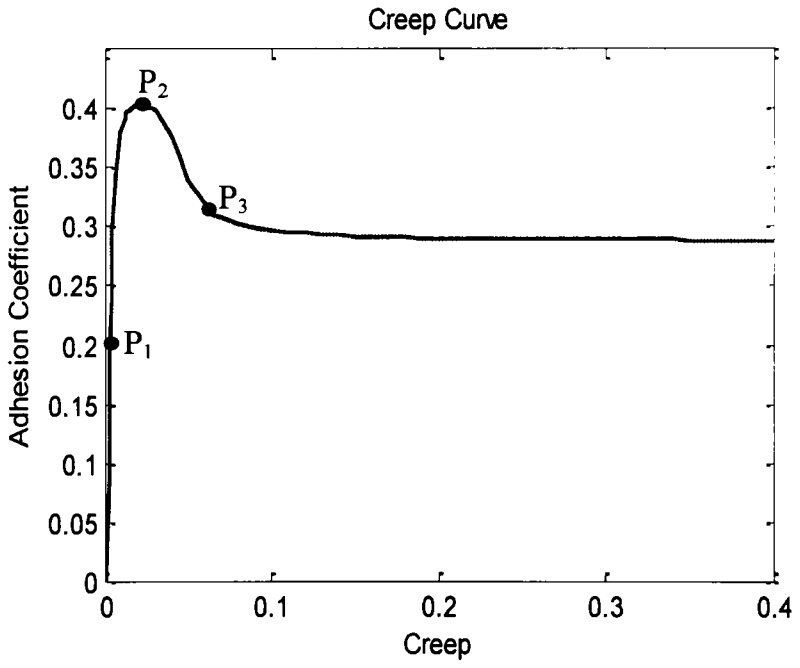

Fig.2. Adhesion Coefficient variation

The creep forces in equation (8) and (9) are widely recognised to present the non-linear characteristics as a function of creep as shown in Figure 2. In normal running conditions where the creep is small, the contact forces provide a damping effort to the dynamic modes of a wheelset and are very useful in stabilising those modes. As the creep increases, due to application of tractive effort, the contact forces can operate in the second (or non-linear) region where the rate of change of the creep forces and associated damping effect is much lower. However, when the creep is beyond the point of maximum adhesion (μ_m) available at the wheel-rail interface and enters the slip or unstable region, the contact forces will then become a destabilising element, which not only cause the well known problem of wheel slip (in traction) or slide (in braking) but also can cause other

undesirable mechanical oscillations in the wheelset (T X Mei, 2010).

3. KALMAN FILTER DESIGN

Kalman filter is a useful tool to estimate the parameters of a linear stochastic process with unknown disturbances, such as the railway wheelset with unknown track disturbance, with some knowledge of the process output and the model. As it works well when the system is linear the nonlinear creep forces are linearized at specific point on the creep curve (λ_o, μ_o) as shown in equation (10) (I Hussain, 2009).The derivative terms represent the slope on the creep curve at the point of linearization which is simplified and represented by g_{11} and g_{12}.

$$f_{xR} = f_{xRo} + \left.\frac{\partial f_{xR}}{\partial \lambda_{xR}}\right|_{(\lambda_{xRo},\lambda_{yRo})} \times \Delta\lambda_{xR} + \left.\frac{\partial f_{xR}}{\partial \lambda_{yR}}\right|_{(\lambda_{xRo},\lambda_{yRo})} \times \Delta\lambda_{yR} \quad (10)$$

Or

$$f_{xR} = f_{xRo} + g_{11}\Delta\lambda_{xR} + g_{12}\Delta\lambda_{yR} \quad (11)$$

All the creep forces are linearized in the similar way and the linearized small signal model of the lateral and yaw dynamics of the railway wheelset is obtained.

$$\begin{bmatrix} \Delta\dot{y} \\ \Delta\dot{\psi} \\ \Delta\ddot{y} \\ \Delta\ddot{\psi} \end{bmatrix} = \begin{bmatrix} 0 & 0 & 1 & 0 \\ 0 & 0 & 0 & 1 \\ 0 & \frac{2g_{22}}{m_w} & -\frac{2g_{22}}{vm_w} & 0 \\ -\frac{2L_g\gamma g_{11}}{r_o I_w} & -\frac{k_w}{I_w} & 0 & -\frac{2L_g^2 g_{11}}{vI_w} \end{bmatrix} \begin{bmatrix} \Delta y \\ \Delta\psi \\ \Delta\dot{y} \\ \Delta\dot{\psi} \end{bmatrix} + \begin{bmatrix} 0 \\ 0 \\ 0 \\ \frac{2L_g\gamma g_{11}}{r_o I_w} \end{bmatrix} \Delta y_t \quad (12)$$

This model is valid only at specific point on the creep curve and best estimation results may be obtained when the wheelset is operated in the vicinity of the point where it is linearized. Equation (12) gives us idea how dynamics of wheelset are affected when operating point of the wheelset (i-e g_{11} and g_{22}) is changed.

3.1 Kalman filter formulation

The wheelset dynamics are excited by the unknown track disturbance. In order to obtain a good estimation results the unknown track disturbance is treated as part of the state vector as shown in the following equation.

$$\frac{d}{dt}\begin{bmatrix} \Delta\psi \\ \Delta\dot{y} \\ \Delta\dot{\psi} \\ \Delta y_t \\ \Delta y - \Delta y_t \end{bmatrix} = \begin{bmatrix} 0 & 0 & 1 & 0 & 0 \\ \frac{2g_{22}}{m_w} & -\frac{2g_{22}}{vm_w} & 0 & 0 & 0 \\ -\frac{k_w}{I_w} & 0 & -\frac{2L_g^2 g_{11}}{vI_w} & 0 & -\frac{2L_g\gamma g_{11}}{r_o I_w} \\ 0 & 0 & 0 & -0.001 & 0 \\ 0 & 1 & 0 & 0 & 0 \end{bmatrix} \begin{bmatrix} \Delta\psi \\ \Delta\dot{y} \\ \Delta\dot{\psi} \\ \Delta y_t \\ \Delta y - \Delta y_t \end{bmatrix} + \begin{bmatrix} 0 \\ 0 \\ 0 \\ 1 \\ -1 \end{bmatrix} \dot{y}_t \quad (13)$$

Two sensors (A gyro sensor for the yaw rate measurement and an accelerometer for the lateral acceleration measurement) as indicated in (14) (v is a vector representing noise level of the sensors with the covariance R) appear to be sufficient for the Kalman filter to provide satisfying estimation results.

$$z(t) = \begin{bmatrix} 0 & 0 & 1 & 0 & 0 \\ \frac{2g_{22}}{m_w} & -\frac{2g_{22}}{vm_w} & 0 & 0 & 0 \end{bmatrix} \begin{bmatrix} \Delta\psi \\ \Delta\dot{y} \\ \Delta\dot{\psi} \\ \Delta y_t \\ \Delta y - \Delta y_t \end{bmatrix} + v \quad (14)$$

Following figure shows the multiple Kalman filter based estimators. Each Kalman filter design is based on the small signal model linearized at specific point on the creep curve. The Kalman filters are optimally tuned by selecting optimal value of covariance matrix *R*.

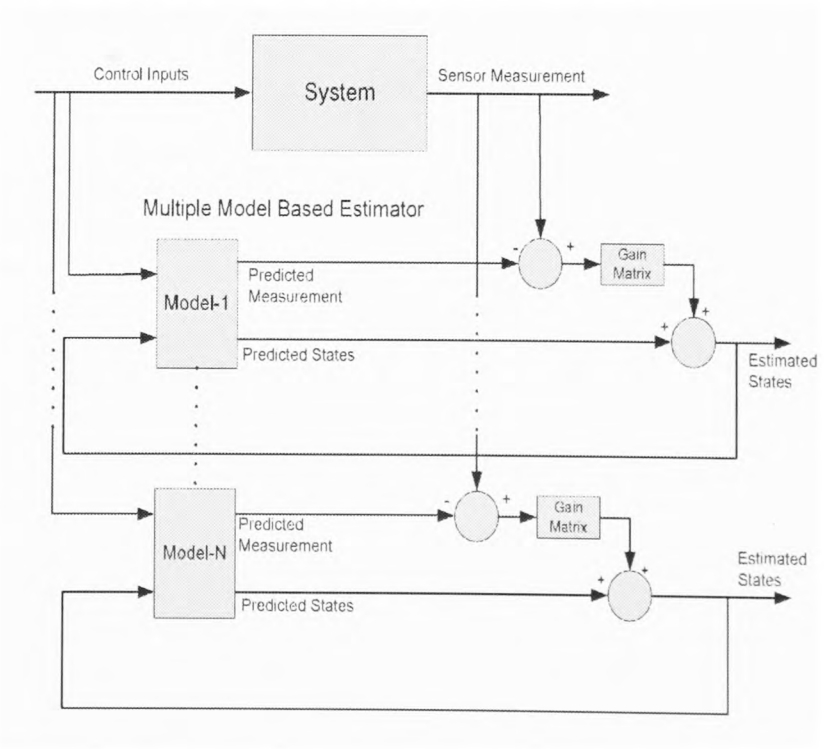

Fig.3. Multiple Model Based Estimation (I Hussain, 2009)

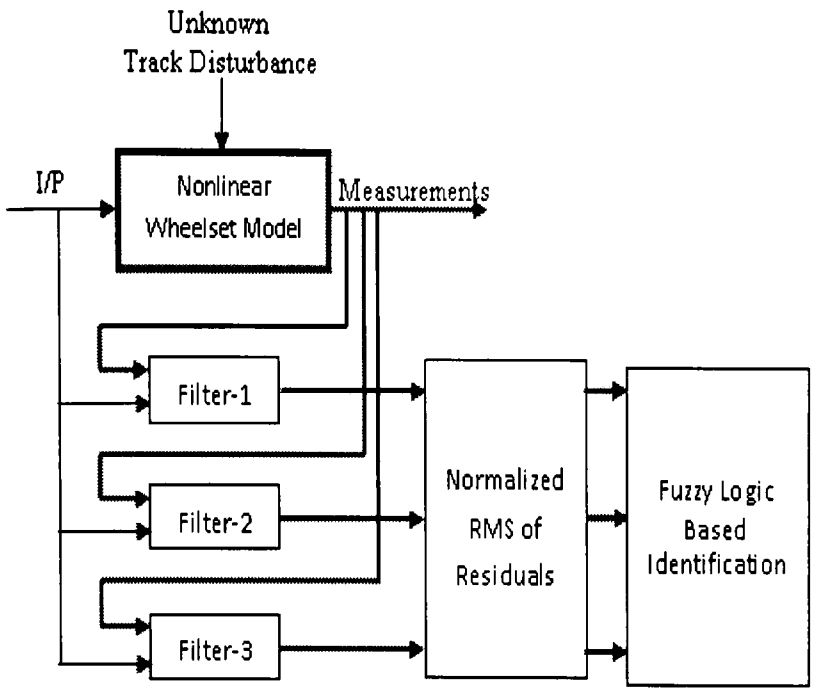

Fig.4. Contact Condition Identification Scheme

The complete proposed scheme is shown in the figure-4. Only three filters are used here to show the potential of the research. The three chosen operating points are shown in figure-2 as P_1 (Linear region of the creep Curve), P_2 (Maximum Point of the creep curve where rate of change of creep force is zero) and P_3 (Unstable Region). Filter-1, filter-2 and filter-3 are designed to operate at these points respectively. Number of Kalman filters can be increased easily to include all possible contact conditions. The normalized values of the residuals of estimated states are then calculated with moving time window of one second. Normalized values of residuals of lateral acceleration are shown in figures (5), (6) and (7) when the wheelset was operated at P_1, P_2 and P_3 respectively. Error-1, Error-2 and Error-3 are the errors produced by Filter-1, Filter-2 and Filter-3 respectively.

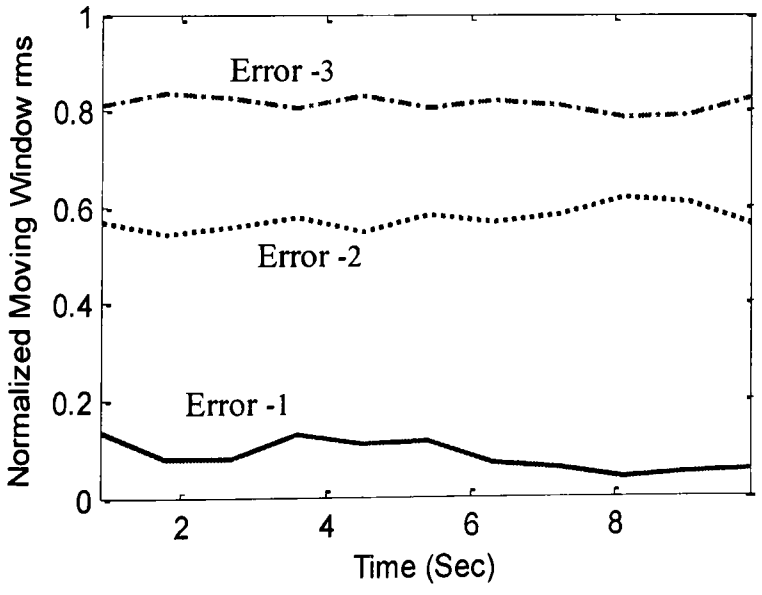

Fig.5. Normalized rms of residuals at P_1

The results show when the wheelset is operated around a point where the any specific filter is optimally tuned to operate the respective filter has minimum error around that point also the amount of error is increased or decreased depending upon how far the wheelset is operating from that point. This provides an excellent opportunity to develop a fuzzy logic based identification system based on these results as shown in the figure below.

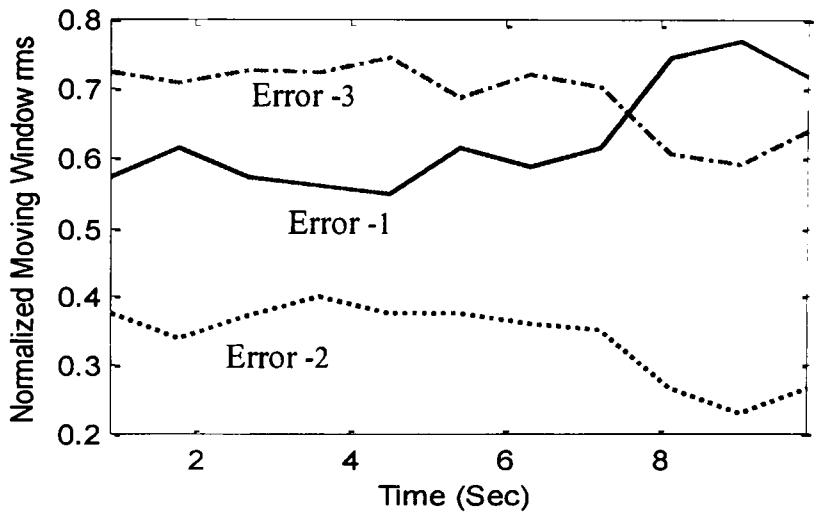

Fig.6. Normalized rms of residuals at P_2

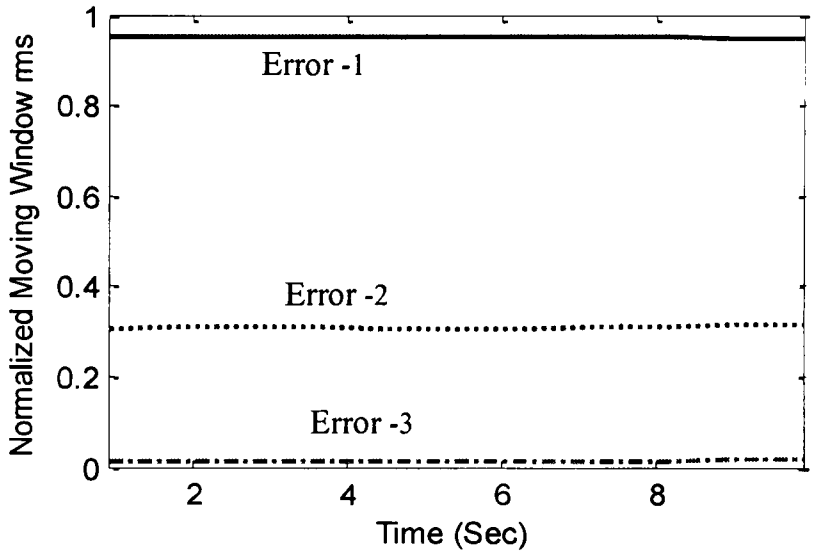

Fig.7. Normalized rms of residuals at P_3

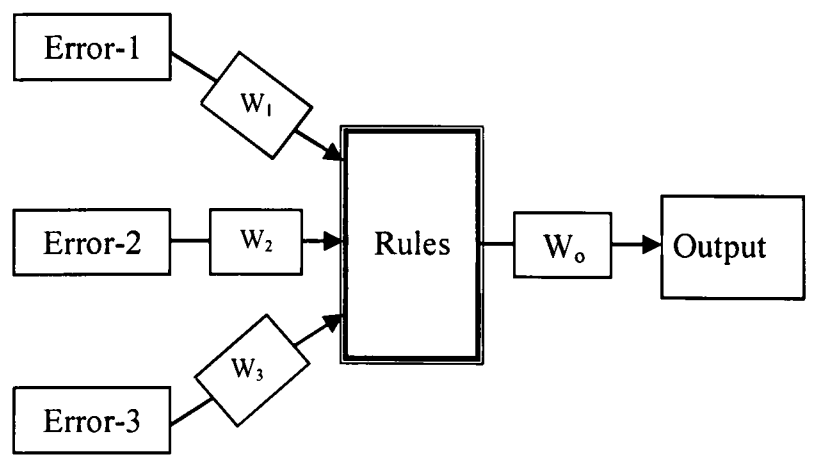

Fig.8. Fuzzy Logic Based Identification System

The normalized values of the residuals are fed to the fuzzy logic system with specific membership function which associates a weighting with each of the input that are processed. The weighting function determines the amount of participation of each input in the producing the output. The rules use the input membership values as weighting factors to determine their influence on the output. Output is produced in terms of the probability of

the operating point near to P_1, P_2 and P_3. Figure (9) is an example out of the system when the wheelset was operated in the vicinity of P_1. The fuzzy output indicates 90% probability of operating point is around P_1. The simulation was carried out at various different operating points and the results showed excellent agreement with the theory.

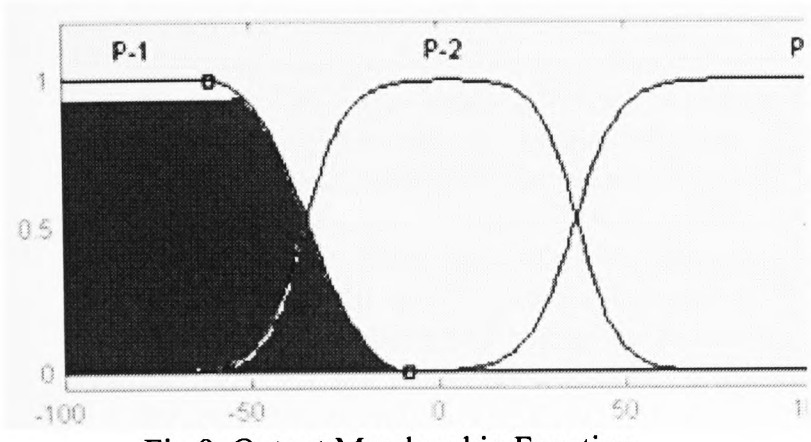

Fig.9. Output Membership Function

4. CONCLUSIONS AND FURTHER WORK

The good delivery of the tractive effort in the traction and braking can be achieved through the real time knowledge of the contact condition. This research proposes a novel technique to identify the contact condition by investigating the changes in the dynamic properties of the wheelset as the train travel through the track. The proposed scheme indirectly identifies the contact condition with minimum measurement requirement. The results presented show the satisfactory performance. However the simulation is carried out using only one creep curve representing good/dry contact condition with small changes in the creep due to application of the tractive torque. Further research is been carried out to validate this model on different creep curves representing low adhesion conditions with large changes in the creep forces.

REFERENCES

CHOI, H. & HONG, S. (2002). Hybrid control for longitudinal speed and traction of vehicles. pp. 1675-1680

I HUSSAIN, Mei. T. X. (2010). Multi Kalman Filtering Approach for Estimation of Wheel-Rail Contact Conditions *Proceedings of the United kingdom Automatic Control Conferecne 2010*. pp.459-464

I HUSSAIN, M. T. X. A. A. H. J. (2009). Modeling and Estimation of Nonlinear Wheel-rail Contact Mechanics. *Proceedings of the twentieth Intenational conference on System Engineering*, pp. 219-223.

KIM, W., KIM, Y., KANG, J. & SUL, S. (1999).Electro-mechanical re-adhesion control simulator for inverter-driven railway electric vehicle. pp.1026-1032

MEI, T.X, YU, J. & WILSON, D. (2009). A mechatronic approach for effective wheel slip control in railway traction. *Proceedings of the Institution of Mechanical Engineers, Part F: Journal of Rail and Rapid Transit,* 223, pp. 295-304.

PARK, D., KIM, M., HWANG, D., LEE, J. & KIM, Y. (2001). Hybrid re-adhesion control method for traction system of high-speedrailway. pp.739-742

T X MEI, I. Hussain. (2010). Detection of wheel-rail contact conditions for improved traction control. *Proceedings of the 4th international conference on Railway Traction systems.*

WATANABE, T. & YAMANAKA, A. (1997). Optimisation of readhesion control of Shinkansen trains with wheel–rail adhesion.

WATANABE, T., YAMANAKA, A., HIROSE, T. & NAKAMURA, S. (1997). Optimization of readhesion control of Shinkansen trains with wheel-rail adhesion prediction. *In*, pp. 47-50.

Multi Kalman Filtering Approach for Estimation of Wheel-Rail Contact Conditions

I Hussain* and T. X. Mei**

School of Computing, Science and Engineering,
Salford University, Salford M5 4WT, UK,
* I.Hussain@pgr.salford.ac.uk** t.x.mei@salford.ac.uk

Abstract: This paper presents a novel detection technique of wheel-rail contact conditions from the dynamic properties of the railway wheelset. The proposed scheme is an indirect method which avoids difficult and expensive measurement requirements. A nonlinear model of lateral and yaw dynamics of a conventional solid axle wheelset is used for study. The scheme consists of a bank of Kalman filters based on linearized wheelset models that represent different characteristics of typical creep/slip curves. Normalized rms values from the residual of each filter calculated using time moving windows are assessed to identify the operating condition of the wheelset at the interface with the rail surface. Simulation results are presented to demonstrate the effectiveness of the proposed scheme.

Keywords: Wheel rail contact, Estimation, Kalman filters

1. INTRODUCTION

The delivery of tractive effort in traction and braking is achieved through the contact forces at the wheel-rail interface. The contact forces are a non-linear function of creepages caused by small relative motions between the two contact surfaces and this relationship can vary substantially when conditions of the surfaces change due to for example existence of fallen tree leaves and/or contaminations by snow/ice etc. The level of overall adhesion (the maximum contact force available) can therefore become very low under the poor contact conditions which present a serious challenge for the traction/braking control systems to avoid the problem of wheel slip/slide. Wheel slip/slide is a highly undesirable phenomenon in railway operations as it increases the wear of wheel and rail, adds to mechanical stress in the system, affects stability and, furthermore, and leads to poor traction performance.

The commonly used wheel slip protection schemes are mostly based on the control of the relative speed between a wheel and the train (also known as slip ratio) which is supplemented with the control of the wheel rotational acceleration (Park et al., 2001, Schwartz and Kresse, 1997, Yasuoka et al., 1997, Watanabe and Yamanaka, 1997). Also, hybrid anti-slip methods with the use of slip, wheel speed and acceleration information are proposed (Park et al., 2001, Kadowaki et al., 2002). Those controllers are difficult to obtain optimal performance and also require accurate measurement of slip wheel. Disturbance observers are proposed to detect slip conditions (Kim et al., Choi and Hong, 2002), where traction torque is treated as a disturbance input and estimated either through state observers using motor speed and torque information. The performances of the anti-slip schemes based on a disturbance observer are to a large extent affected by noises in the system which can be very substantial in the wheel-rail contact environment. The destabilising effect of the slip on the wheelset dynamics has also been exploited to develop wheel slip protection solutions that do not require the measurement of the wheel slip (Mei et al., 2009).

However, there is a lack of effective solutions that can provide real time information about the maximum adhesion available as a train travels through a track which would be able to tackle fundamentally the problem of wheel slip/slip as the provision of tractive effort in either traction or braking could then be optimised to make the most out of the wheel-rail contact conditions.

This paper examines the use of a model based estimation approach for the detection of the contact conditions. A previous study has tried to estimate the creep coefficient at the wheel-rail contact and use this as an indirect indicator of the adhesion(Charles et al., 2008). In this study, however, the use of a multiple Kalman filters is studied, which represents different operating conditions of the wheel-rail contact. A 'best match' strategy is then used to estimate the adhesion available.

2. MODELLING OF CONTACT MECHANICS

Railway wheelset is a complex mechanical system with several degrees of freedom. The motions of the wheelset are governed by the creep forces generated at wheel rail contact patch. The contact forces at the wheel rail interface can be split into normal and tangential forces. The tangential forces at the two wheels of a wheelset can be represented using (1) and (2)

$$F_R = \mu_R N \tag{1}$$

$$F_L = \mu_L N \tag{2}$$

where μ_R and μ_L are adhesion coefficients that vary nonlinearly with the creep and N is the normal force applied to the wheel. The tangential forces can be further divided into longitudinal and lateral components, which are governed by (Polach, 2005):

$$f_{xL} = F_L \frac{\lambda_{xL}}{\lambda_L} \tag{3}$$

$$f_{xR} = F_R \frac{\lambda_{xR}}{\lambda_R} \tag{4}$$

$$f_{yL} = F_L \frac{\lambda_{yL}}{\lambda_L} \tag{5}$$

$$f_{yR} = F_R \frac{\lambda_{yR}}{\lambda_R} \tag{6}$$

In above equations the subscript L, R are used for left and right wheels respectively, x and y are used to indicate the longitudinal and lateral directions, and λ_{xL}, λ_{xR}, λ_{yL} and λ_{yR} are creepages in the longitudinal and lateral directions for left and right wheels given as:

$$\lambda_{xL} = [\frac{L_g \dot{\psi}}{v} + \frac{\gamma(y - y_t)}{r_o}] \tag{7}$$

$$\lambda_{xR} = -[\frac{L_g \dot{\psi}}{v} + \frac{\gamma(y - y_t)}{r_o}] \tag{8}$$

$$\lambda_{yL} = \lambda_{yR} = \frac{\dot{y}}{v} - \psi \tag{9}$$

Where L_g is the half track gauge, v is forward speed of the vehicle, γ is conicity of wheel and r_o is the radius of wheel when it is at centre position and y_t is disturbance applied by track in lateral direction. The total creep at any point on the creep curve is given by following equations.

$$\lambda_L = \sqrt{\lambda_{xL}^2 + \lambda_{yL}^2} \tag{10}$$

$$\lambda_R = \sqrt{\lambda_{xR}^2 + \lambda_{yR}^2} \tag{11}$$

3. DESIGN OF MUTIPLE KALMAN FILTERS

3.1 Simplified models

Only the lateral and yaw dynamics of a wheelset are considered in this study as represented in (12) and (13), as other degrees of freedom are largely decoupled to the plan view motions and are not indirectly relevant to this study.

$$m_w \ddot{y} = -f_{yR} - f_{yL} + F_c \tag{12}$$

$$I_w \ddot{\psi} = f_{xR} L_g - f_{xL} L_g - k_w \psi \tag{13}$$

where m_w is the wheelset mass, I_w is yaw moment of inertia and k_w is yaw stiffness of a spring used to stabilise the wheelset.

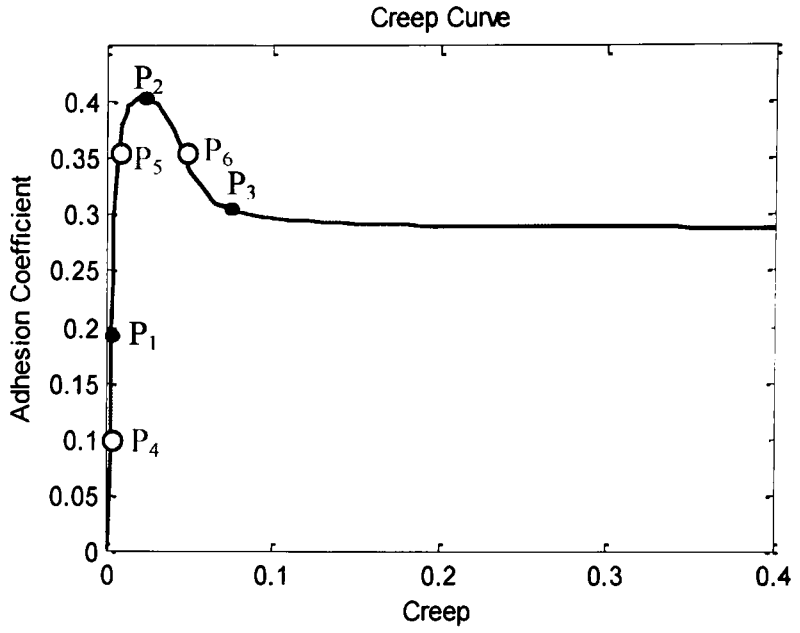

Fig.1. Adhesion Coefficient variation

The variation of adhesion coefficient (μ) with respect to the total creep is illustrated in Fig.1. In most operation conditions, a wheelset tends to operate in the linear region of the creep curve. However, the presence of contaminations on the track may result in a significant reduction in the maximum adhesion and cause the wheels to slip when a high level of tractive effort is applied leading to increased creepages at the wheel-rail interface and pushing the operating point of the wheelset towards the nonlinear and even the unstable sections.

3.2 Linearization

Because the contact forces are highly nonlinear in nature, a single linear model will not be able to represent adequately the complex dynamics of the system. To enable the use of linear Kalman filters, the creep force equations are linearized at a number of selected operating points on the creep curve, each of the model would only be valid when the wheelset is operating in the vicinity of a specific point. The first order approximation of the creep force around a point (λ_o, μ_o) is shown in the following equation(I Hussain, 2009).

$$f_{xR} = f_{xRo} + \frac{\partial f_{xR}}{\partial \lambda_{xR}}\Big|_{(\lambda_{xRo}, \lambda_{yRo})} \times \Delta\lambda_{xR} + \frac{\partial f_{xR}}{\partial \lambda_{yR}}\Big|_{(\lambda_{xRo}, \lambda_{yRo})} \times \Delta\lambda_{yR} \tag{14}$$

The derivative terms represent the slope on the creep curve at the point of linearization which is simplified and represented by g_{11} and g_{12}. The equations for the other contact forces can be similarly linearized which give a small signal state-space model as shown in (15). It is clear that the dynamics behaviour of the wheelset is highly dependent on the different slope of the curve where the main difference between different operating points on the

creep/slip curve will be the different coefficient values, and the forward speed (v) of the vehicle.

$$\begin{bmatrix} \Delta\dot{y} \\ \Delta\dot{\psi} \\ \Delta\ddot{y} \\ \Delta\ddot{\psi} \end{bmatrix} = \begin{bmatrix} 0 & 0 & 1 & 0 \\ 0 & 0 & 0 & 1 \\ 0 & \frac{2g_{22}}{m_w} & -\frac{2g_{22}}{vm_w} & 0 \\ -\frac{2L_g\gamma g_{11}}{r_o I_w} & -\frac{k_w}{I_w} & 0 & -\frac{2L_g^2 g_{11}}{vI_w} \end{bmatrix} \begin{bmatrix} \Delta y \\ \Delta\psi \\ \Delta\dot{y} \\ \Delta\dot{\psi} \end{bmatrix} + \begin{bmatrix} 0 \\ 0 \\ 0 \\ \frac{2L_g\gamma g_{11}}{r_o I_w} \end{bmatrix} \Delta y_t \tag{15}$$

3.3 Kalman filter design

A Kalman filter based on small signal model of (15) can be designed to estimate the states of the system at specific point on the creep curve. But lateral and yaw dynamics of the railway wheelset are excited by unknown track disturbance y_t which makes design of the Kalman filters more complex. This problem can be solved by formulating the unknown parameter into the state equation as part of the state vector rather than as an input such that dynamics of the system remain unchanged. The modified state space model is given in (16), where w represents the track noises with covariance Q. Two sensors (A gyro sensor for yaw rate measurement and an accelerometer for lateral acceleration measurement) as indicated in (17) (v is a vector representing noise level of sensors with covariance R) appear to be sufficient for the Kalman filter to provide satisfying estimation results.

$$\frac{\mathrm{d}}{\mathrm{dt}} \begin{bmatrix} \Delta\psi \\ \Delta\dot{y} \\ \Delta\dot{\psi} \\ \Delta y_t \\ \Delta y - \Delta y_t \end{bmatrix} = \begin{bmatrix} 0 & 0 & 1 & 0 & 0 \\ \frac{2g_{22}}{m_w} & -\frac{2g_{22}}{vm_w} & 0 & 0 & 0 \\ -\frac{k_w}{I_w} & 0 & -\frac{2L_g^2 g_{11}}{vI_w} & 0 & -\frac{2L_g\gamma g_{11}}{r_o I_w} \\ 0 & 0 & 0 & -0.001 & 0 \\ 0 & 1 & 0 & 0 & 0 \end{bmatrix} \begin{bmatrix} \Delta\psi \\ \Delta\dot{y} \\ \Delta\dot{\psi} \\ \Delta y_t \\ \Delta y - \Delta y_t \end{bmatrix} + \begin{bmatrix} 0 \\ 0 \\ 0 \\ 1 \\ -1 \end{bmatrix} \dot{y}_t \tag{16}$$

$$z(t) = \begin{bmatrix} 0 & 0 & 1 & 0 & 0 \\ \frac{2g_{22}}{m_w} & -\frac{2g_{22}}{vm_w} & 0 & 0 & 0 \end{bmatrix} \begin{bmatrix} \Delta\psi \\ \Delta\dot{y} \\ \Delta\dot{\psi} \\ \Delta y_t \\ \Delta y - \Delta y_t \end{bmatrix} + v \tag{17}$$

A Kalman Bucy filter can be formulated as shown in (18).

$$\frac{d}{dt}\hat{x}(t) = A\hat{x}(t) + K[z(t) - C\hat{x}(t)] \tag{18}$$

In (18) $\hat{x}$ represents estimated state vector K is weighting factor calculated by (19).

$$K = PC_T R^{-1} \tag{19}$$

Where P is the estimate error covariance that depends upon the selection of measurement noise covariance R and process noise covariance Q.

4. STATE ESTIMATION

The estimation results show that the properly tuned Kalman filter can provide a reliable estimation of the wheelset states at any specific operating condition. Fig.2 shows the estimated lateral motion with estimation error less than 7% and estimated yaw angle is shown in fig.3 with estimation error less than 3%. Lateral Motion is directly affected by track noise therefore its estimation is greater than that of the yaw angle.

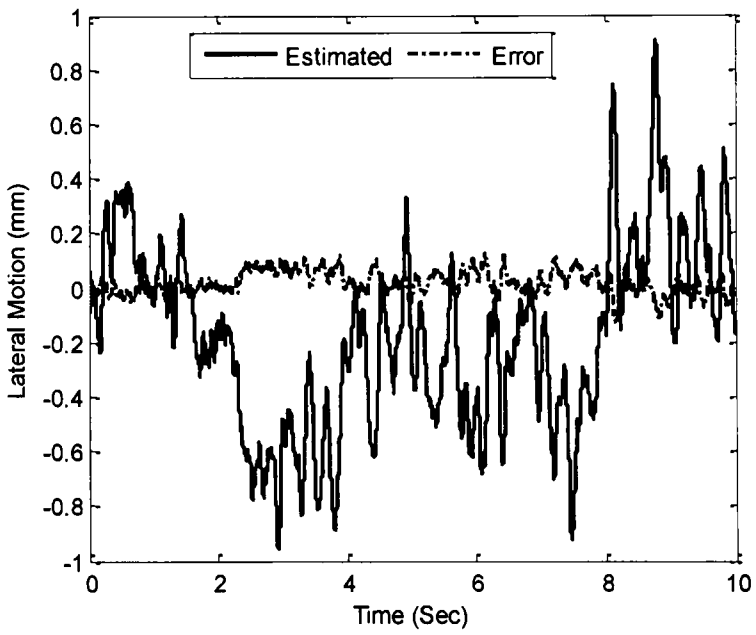

Fig.2. Lateral Motion Estimation

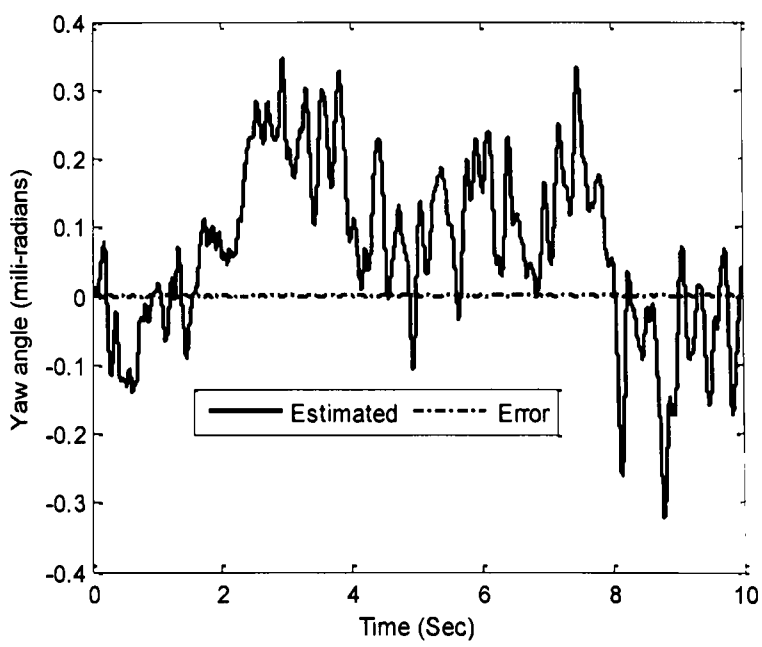

Fig.3. Yaw Angle Estimation

If a wheelset is operating in various different contact conditions, multiple Kalman filters can used to estimate the wheelset states in different contact conditions – this is then explored in this study for the estimation of the contact conditions as discussed in the next section.

5. ESTIMATION OF CONTACT CONDITIONS

Fig.4 shows the principle of the proposed scheme based on well known filter bank technique used in various applications (Kobayashi and Simon, 2003, Kobayashi and Simon, 2005). A bank of Kalman filters that are derived from different operating points of the creep/slip curve and therefore can be used to provide the estimation in different contact conditions as each of the Kalman filter is tuned to match one specific contact condition. All the filters are run in parallel and normalized rms values of the residuals of each filter are calculated using a moving time window and the output of all the Kalman filters are compared to determine the operating point (contact condition) of the wheelset according to the estimation errors. The number of Kalman filters required depends upon the extent of the variation of the wheelset dynamics on the entire creep curve.

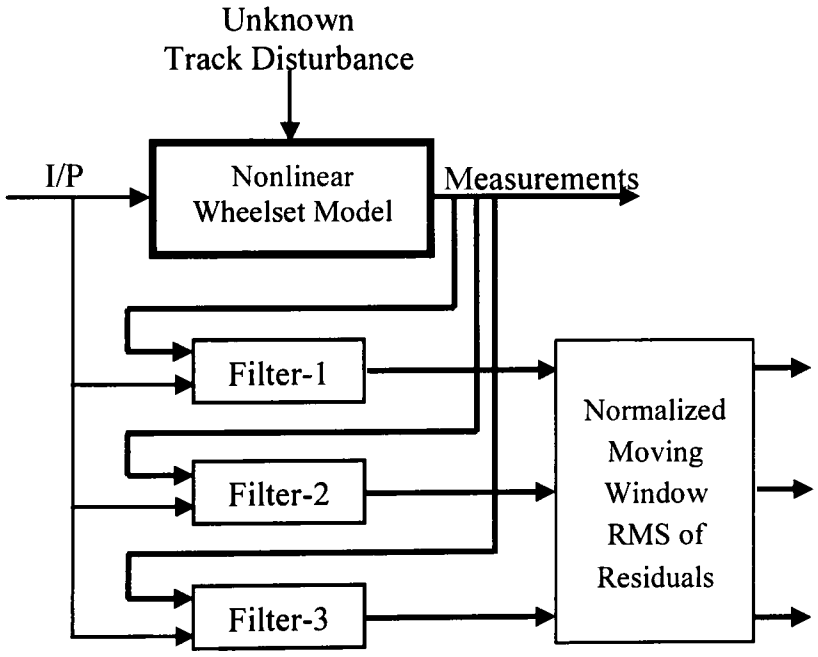

Fig.4. Contact Condition Estimation Scheme

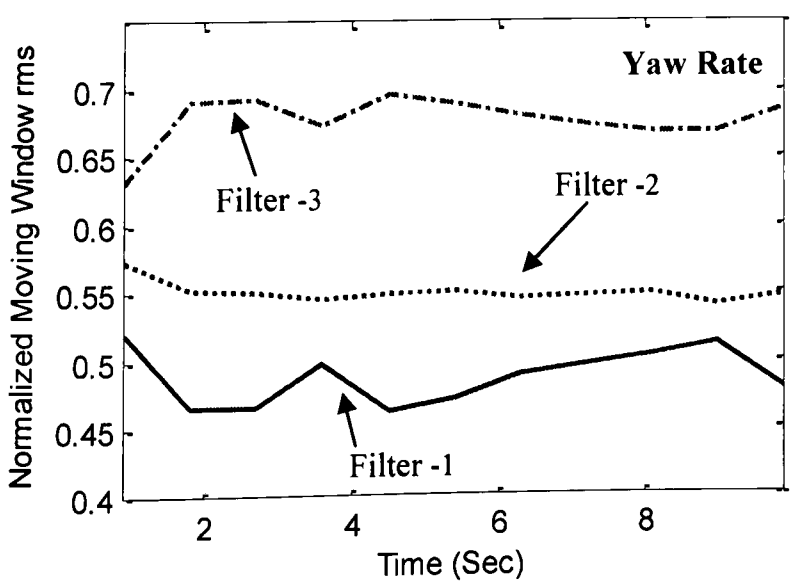

Fig.5. Normalized rms of residuals at P_1

In this research three Kalman filters, Filter -1, Filter -2 and Filter-3, are found to be sufficient to detect different operating points of the wheelset. Estimator-1 is optimally tuned to perform at the P_1 (as in Fig.1) in the linear region of the creep curve where slope of the curve is positive. Estimator-2 is designed to operate at maximum point (P_2) of the creep curve where the slope of the creep curve is zero and Estimator-3 is designed to operate in the unstable region (P_3) where the slope of the creep curve is negative. Normalized rms values of the residuals using a moving time window of one second are presented in figures (5-10), which show an excellent agreement between the Kalman filters and the operating conditions.

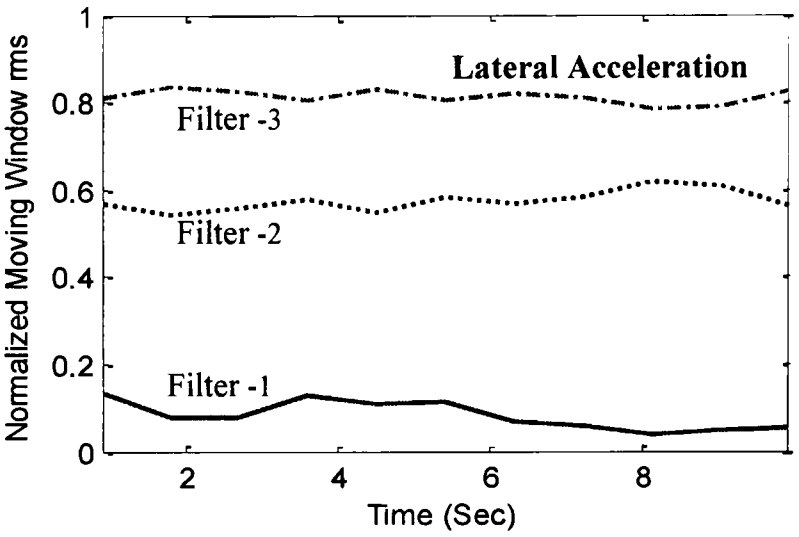

Fig.6. Normalized rms of residuals at P_1

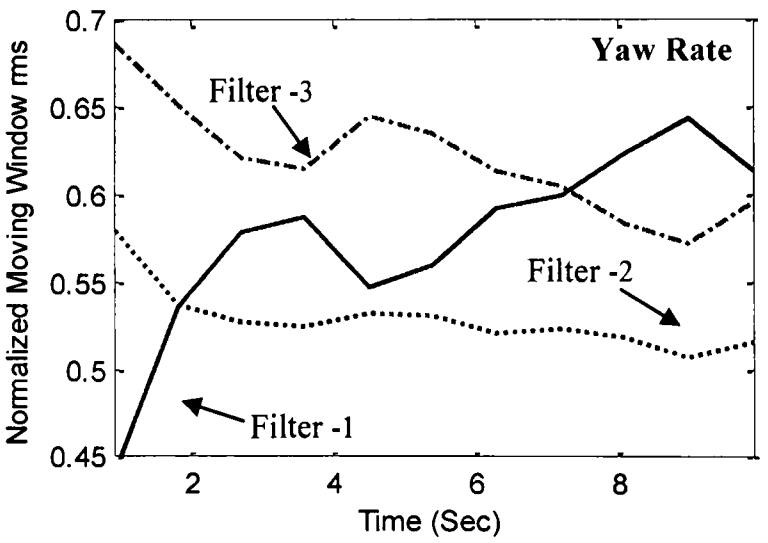

Fig.7. Normalized rms of residuals at P_2

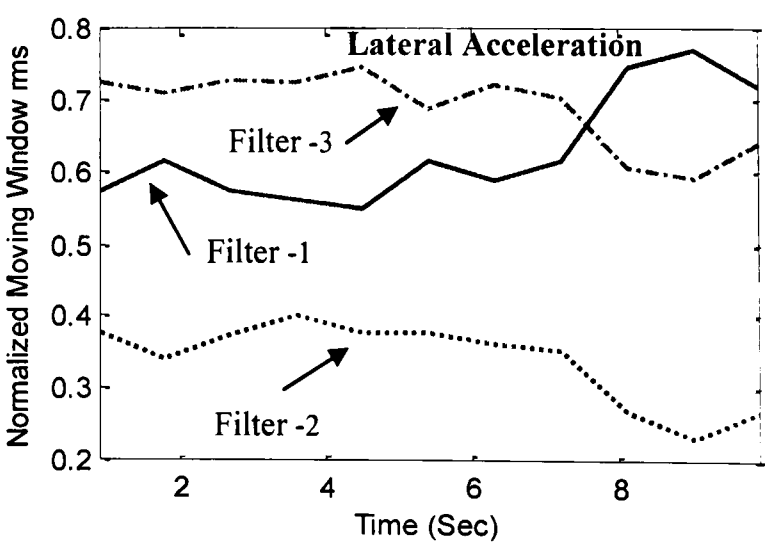

Fig.8. Normalized rms of residuals at P_2

In order to identify the contact conditions at operating points other than those selected for the Kalman filter design, it is possible to use the combination of the results from all three Kalman filters to assess the likelihood of which one(s) is closest to the contact condition. This avoids the need to increase the number of Kalman filters which can be problematic for practical applications. Further simulation results are given in figures (11-16).

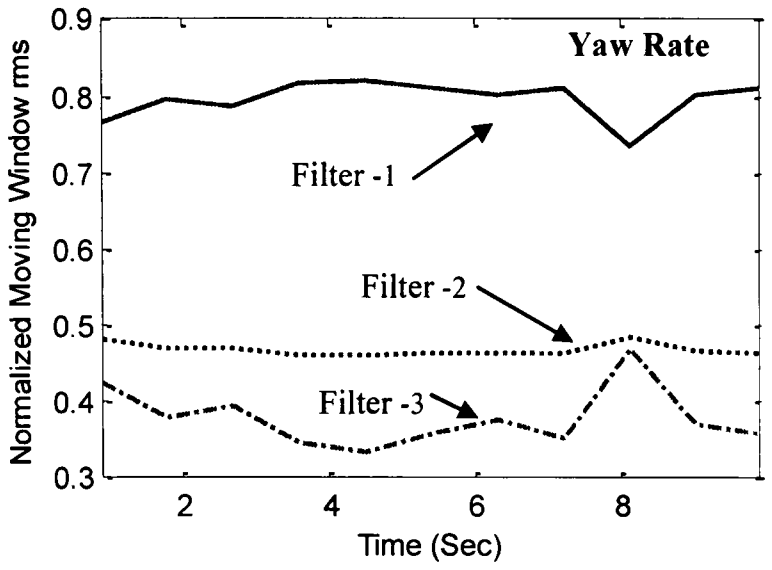

Fig.9. Normalized rms of residuals at P_3

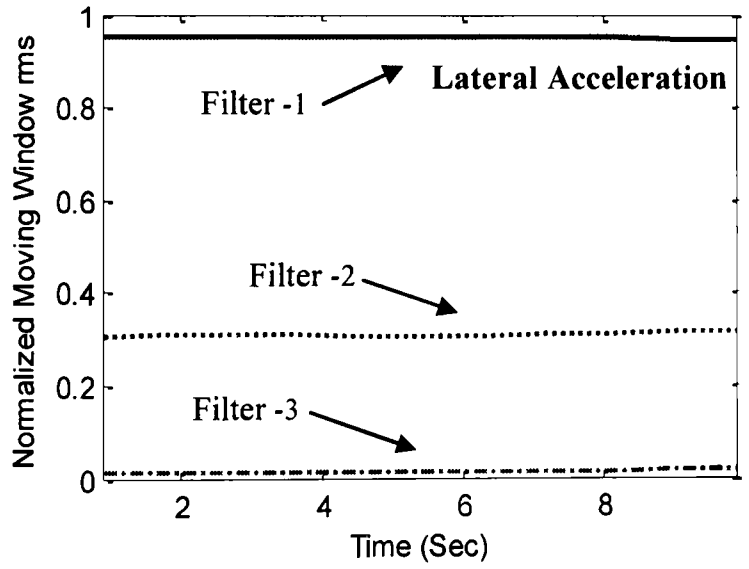

Fig.10. Normalized rms of residuals at P_3

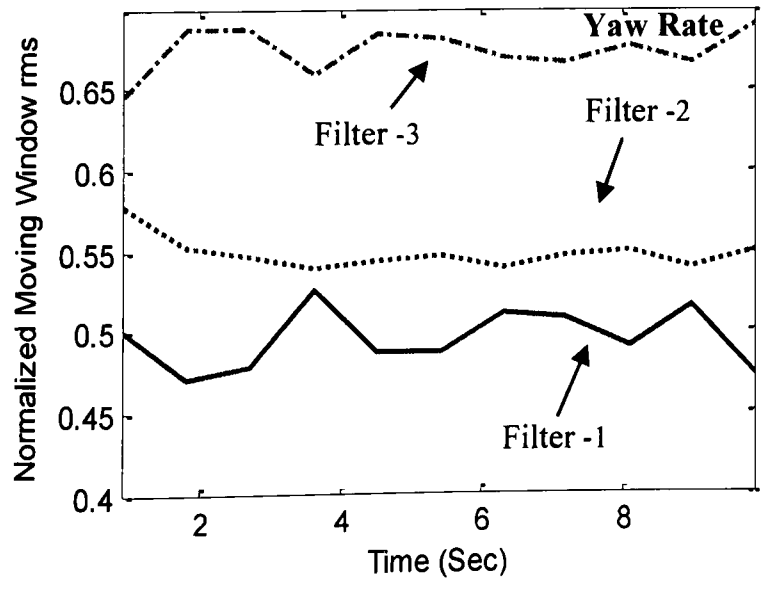

Fig.11. *Normalized rms of residuals at P_4*

When the wheelset is operated in linear part around P_4 filter-1 is producing the best results (fig.11-12). This is because the dynamic properties of the wheelset are nearly equal along the linear part of the creep curve. Around P_5 (where the creep forces start to behave non-linearly) filter-1 and filter-2 have better results than filter-3 and at point P_6 filter-2 and filter-3 are better than filter-1.

Figures (10-15) allow us to divide creep curve into five different segments. First segment is the linear part of the curve where filter-1 is producing least error. Second segment is the part of the curve where filter-1 and filter-2 are overlapping with each other whereas filter-3 has still large error. Third segment is the part of the curve around P_2 at this point filter-2 is tuned to provide best results. Fourth segment is the part of the curve between P_2 and P_3. In this part filter-2 and filter-3 have overlapping outputs whereas filter-1 has largest error. And the fifth segment is the part of the curve around P_3 where filter-3 has least error.

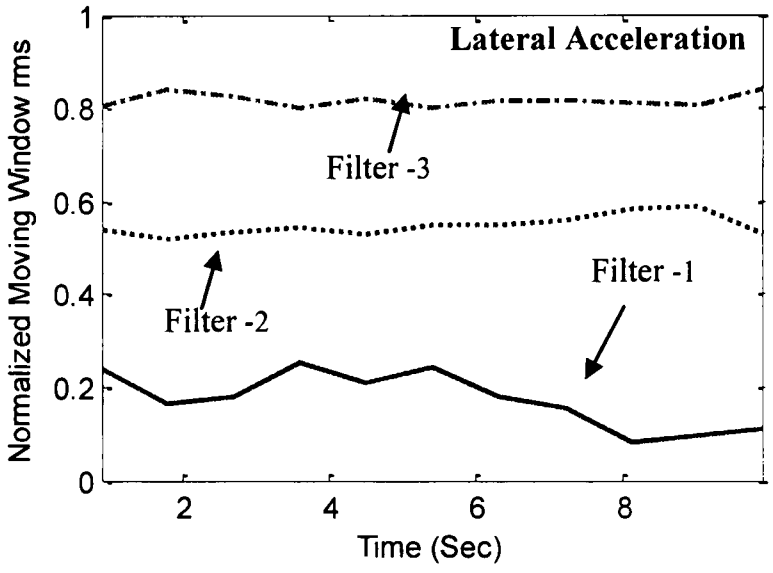

Fig.12. *Normalized rms of residuals at P_4*

Dividing the creep curve into five different segments makes the identification of wheel-rail contact condition simpler. Using these results a suitable identification method can be developed using Fuzzy logic to identify the operating conditions (Wheel-rail contact conditions).

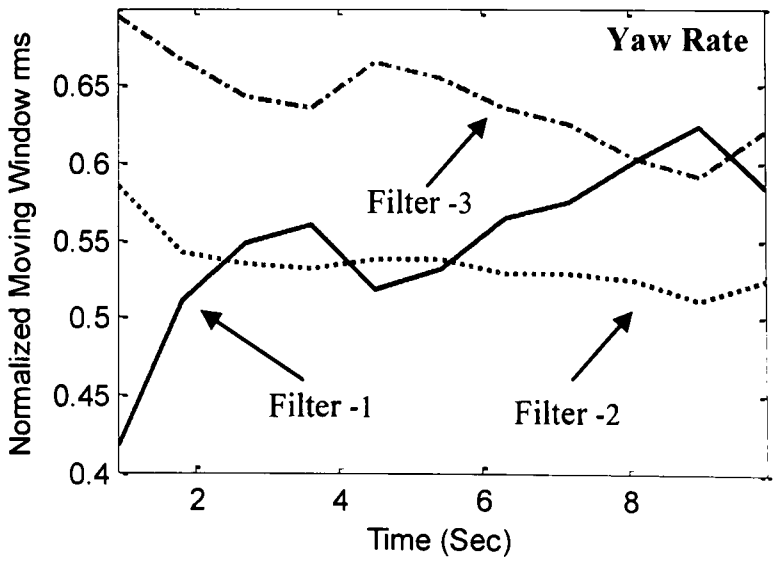

Fig.13. *Normalized of residuals at P_5*

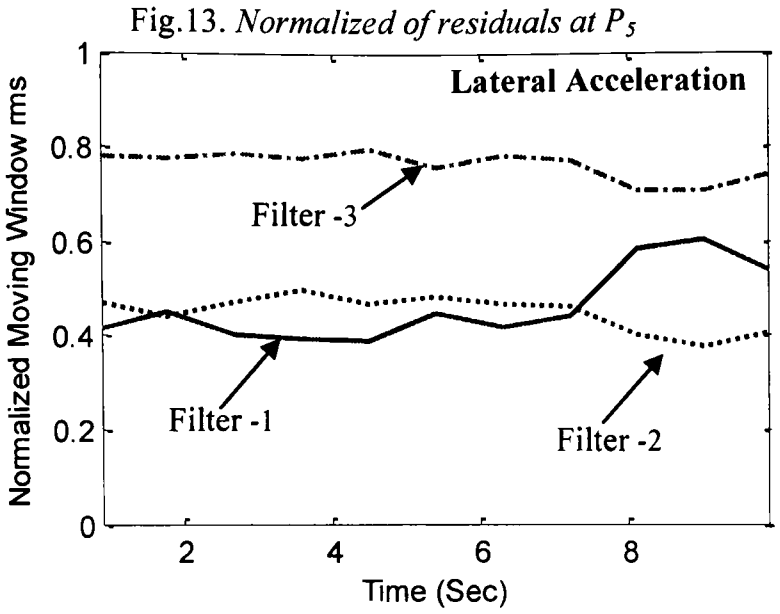

Fig.14. *Normalized of residuals at P_5*

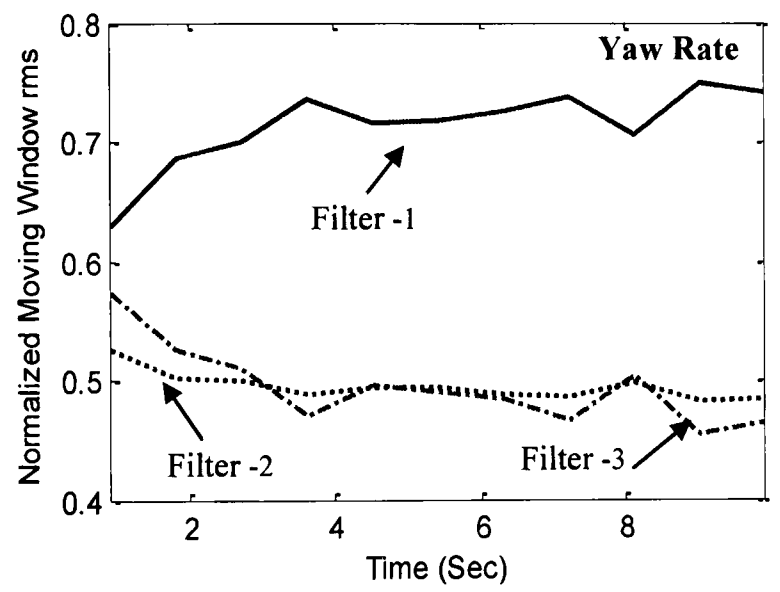

Fig.15. *Normalized rms of residuals at P_6*

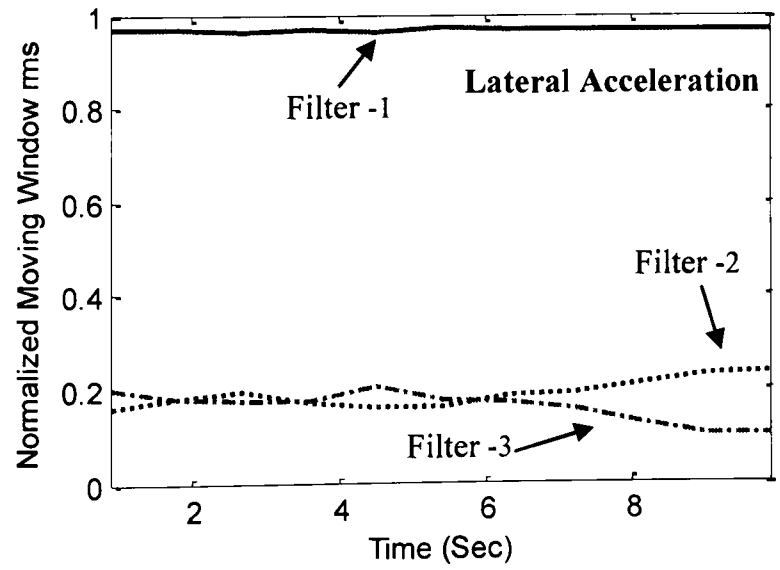

Fig.16. *Normalized rms of residuals at P_6*

6. CONCLUSIONS AND FURTHER WORK

Real time knowledge of the adhesion level between wheel and rail is necessary to improve the efficiency of the traction and braking performance of railway vehicle. The proposed multiple model based estimator provides good clue to identify the operating condition. Further research is ongoing to use this technique to identify adhesion limit in various different contact conditions. Later on an identification method can then be developed to identify the wheelset operating conditions. The accurate information about the contact condition will then allow the control system to optimize the traction and braking performance.

REFERENCES

CHARLES, G., GOODALL, R. & DIXON, R. 2008. Model-based condition monitoring at the wheel-rail interface. *Vehicle System Dynamics,* 46, 415-430.

CHOI, H. & HONG, S. Year. Hybrid control for longitudinal speed and traction of vehicles. *In,* 2002.

I HUSSAIN, M. T. X. A. A. H. J. 2009. Modeling and Estimation of Nonlinear Wheel-rail Contact Mechanics. *Proceedings of the twentieth Intenational conference on System Engineering,* 219-223.

KADOWAKI, S., OHISHI, K., MIYASHITA, I. & YASUKAWA, S. Year. Re-adhesion control of electric motor coach based on disturbanceobserver and sensor-less vector control. *In,* 2002.

KIM, W., KIM, Y., KANG, J. & SUL, S. Electro-mechanical re-adhesion control simulator for inverter-driven railway electric vehicle.

KOBAYASHI, T. & SIMON, D. 2003. Application of a bank of Kalman filters for aircraft engine fault diagnostics. NATIONAL AERONAUTICS AND SPACE ADMINISTRATION CLEVELAND OH GLENN RESEARCH CENTER.

KOBAYASHI, T. & SIMON, D. 2005. Evaluation of an enhanced bank of kalman filters for in-flight aircraft engine sensor fault diagnostics. *Journal of Engineering for Gas Turbines and Power,* 127, 497.

MEI, T., YU, J. & WILSON, D. 2009. A mechatronic approach for effective wheel slip control in railway traction. *Proceedings of the Institution of Mechanical Engineers, Part F: Journal of Rail and Rapid Transit,* 223, 295-304.

PARK, D., KIM, M., HWANG, D., LEE, J. & KIM, Y. Year. Hybrid re-adhesion control method for traction system of high-speedrailway. *In,* 2001.

POLACH, O. 2005. Creep forces in simulations of traction vehicles running on adhesion limit. *Wear,* 258, 992-1000.

SCHWARTZ, H. & KRESSE, R. Year. Implementation of an advanced wheel creep control with searching strategy on a light rail vehicle. *In,* 1997. PROCEEDINGS PUBLISHED BY VARIOUS PUBLISHERS, 3-3.

WATANABE, T. & YAMANAKA, A. Year. Optimisation of readhesion control of Shinkansen trains with wheel–rail adhesion. *In,* 1997.

YASUOKA, I., HENMI, T., NAKAZAWA, Y. & AOYAMA, I. Year. Improvement of re-adhesion for commuter trains with vector controltraction inverter. *In,* 1997.

Identification of the Wheel-Rail Contact Condition for Traction and Braking Control

I Hussain[1] and TX Mei[2]
School of Computing, Science and Engineering
Salford University, UK
Emails: [1] I.Hussain@edu.salford.ac.uk [2]t.x.mei@salford.ac.uk

The traction and braking performance of the railway vehicle is governed by the contact forces generated at the wheel rail interface. These contact forces are a non-linear function of the creepages and vary substantially when the conditions of the rail surfaces change due to the fallen tree leaves and/or other contaminations. The overall adhesion can therefore becomes very low which present a serious challenge for the traction/braking control systems to avoid the problem of wheel slip/slide. The wheel Slip/slide is a highly undesirable phenomenon that causes the mechanical parts to wear down quickly affects the stability and leads to the inconsistent traction performance causing problems in train scheduling.

In order to avoid the wheel slip/slide various different techniques have been used in past. The conventional and Hybrid anti-slip methods are based on measured relative speed between the wheel and the train (Park et al., 2001. Choi and Hong, 2002, Watanabe and Yamanaka, 1997, Watanabe et al., 1997). These controllers require an accurate measurement of the train and wheel rotational speeds that makes it difficult to obtain the optimal performance. The methods based on disturbance observer have also been used (Kim et al.). These controllers do not require direct speed measurement rather the adhesion coefficient is estimated by using the information of rotor speed and the torque current. But the performances of the anti-slip schemes based on a disturbance observer are to a large extent affected by noises in the system which can be very substantial in the wheel-rail contact environment.

This research is an extension of ongoing research (Mei, 2010, Hussain, 2009, Hussain, 2010) which proposes an indirect technique to overcome the problem of the wheel slip/slide in poor contact conditions. The proposed scheme exploits the dynamic properties of the conventional solid axle wheelset in response to changes in contact condition at the wheel-rail interface avoiding difficult and expensive measurement requirements. A nonlinear model of lateral and yaw dynamics of a conventional solid axle wheelset is used for the study. The non-linearity and changes in the interaction with the rail are modelled by using a set of non-linear creep/slip curves. The scheme consists of a bank of Kalman filters based on the linearized wheelset models. Each Kalman filter in the filter bank is optimally tuned to operate in a specific contact condition. The wheelset is operated at specific operating points on the creep curves and normalized root mean square values from the residual of each filter are calculated using time moving windows. Residuals are then assessed using a fuzzy logic based system to identify the operating condition of the wheelset. Two different creep curves are used, representing good and slightly bad contact conditions, to show the potential of this research.

CHOI, H. & HONG, S. Year. Hybrid control for longitudinal speed and traction of vehicles. *In*, 2002.

HUSSAIN, M. T. X. 2010. Multi Kalman Filtering Approach for Estimation of Wheel-Rail Contact Conditions *Proceedings of the United kingdom Automatic Control Conferecne 2010.*

HUSSAIN, M. T. X. A. A. H. J. 2009. Modeling and Estimation of Nonlinear Wheel-rail Contact Mechanics. *Proceedings of the twentieth Intenational conference on System Engineering*, 219-223.

KIM, W., KIM, Y., KANG, J. & SUL, S. Electro-mechanical re-adhesion control simulator for inverter-driven railway electric vehicle.

MEI, H. 2010. Detection of wheel-rail contact conditions for improved traction control. *Proceedings of the 4th international conference on Railway Traction systems 2010*

PARK, K. T., LEE, H. W., PARK, C. H., KIM, D. H. & LEE, M. H. Year. The characteristics of deriving control of crane [deriving read driving]. *In:* Industrial Electronics, 2001. Proceedings. ISIE 2001. IEEE International Symposium on, 2001. 734-739 vol.2.

WATANABE, T. & YAMANAKA, A. Year. Optimisation of readhesion control of Shinkansen trains with wheel–rail adhesion. *In*, 1997.

WATANABE, T., YAMANAKA, A., HIROSE, T. & NAKAMURA, S. Year. Optimization of readhesion control of Shinkansen trains with wheel-rail adhesion prediction. *In*, 1997. 47-50.

Fuzzy Logic Based Identification of Wheel-Rail Contact Condition

I Hussain* and T. X. Mei**

School of Computing, Science and Engineering,
Salford University, Salford M5 4WT, UK,
* *l.Hussain@pgr.salford.ac.uk*** *t.x.mei@salford.ac.uk*

The low adhesion problem between the wheel and the rail has been since the beginning of the railway a crucial parameter in the design and operation of the railway vehicles, particularly in autumn when the leaves on the line and the humid conditions combine to form a low-adhesion contaminant film on the rail surface. A large number of measures have been developed; nevertheless the trouble caused by the low adhesion still occurs. The available knowledge is largely based on subjective observations, for the most part offered by drivers. It is therefore important to provide the real time information about the track condition to the traction and braking control system to maximize the use of available adhesion which will help the control system to maintain the stable operation of the railway vehicle. This paper proposes a novel technique to identify the adhesion condition by using the fact that the dynamic properties of the wheelset are affected by the change in the contact condition. Multiple Kalman filters are used to estimate the wheelset dynamics in different contact conditions. Each Kalman filter in the filter bank is optimally tuned to operate in a specific contact condition. All the Kalman filters are run in parallel and the normalized value of residuals (difference generated by the observations and the system's mathematical model) is calculated with a moving time window. The residuals are then assessed by a fuzzy logic system. The fuzzy logic system identifies the contact condition by investigating the residuals values and the tractive torque.

IDENTIFICATION OF THE WHEEL-RAIL CONTACT CONDITION FOR TRACTION AND BRAKING CONTROL

I Hussain[1] and TX Mei[2]
School of Computing, Science and Engineering
Salford University, UK
Emails: [1] l.Hussain@edu.salford.ac.uk [2]t.x.mei@salford.ac.uk

Abstract

The contact conditions at the wheelset-rail interface have a dominant effect on the performance of the traction and braking control systems. This paper proposes a novel approach for the identification of the adhesion condition by exploiting the fact that the dynamic properties of the wheelset are affected by changes in the contact condition. Multiple Kalman filters are used to estimate the wheelset dynamics in different contact conditions. The residuals of all the filters are assessed by a fuzzy logic system to identify the different contact conditions.

1. INTRODUCTION

The low adhesion problem between the wheel and the rail has been a crucial parameter in the design and operation of the railway vehicles since the beginning of the railway, particularly in the autumn when the tree leaves on the line and the humid conditions combine to form a low-adhesion contaminant film on the rail surface. The rapid increase in railway traffic across the globe demands a better acceleration and braking performance. This means a shorter braking distance and higher acceleration in order to travel at cruising velocity for longer distances possible. Figure-1 shows possible variations of the adhesion coefficient which can be dramatically affected by the presence of a third body layer in the wheel-rail contact.

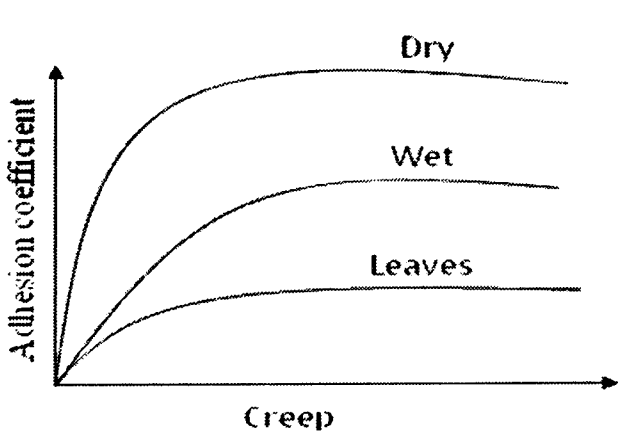

Figure 1. Creep Curves

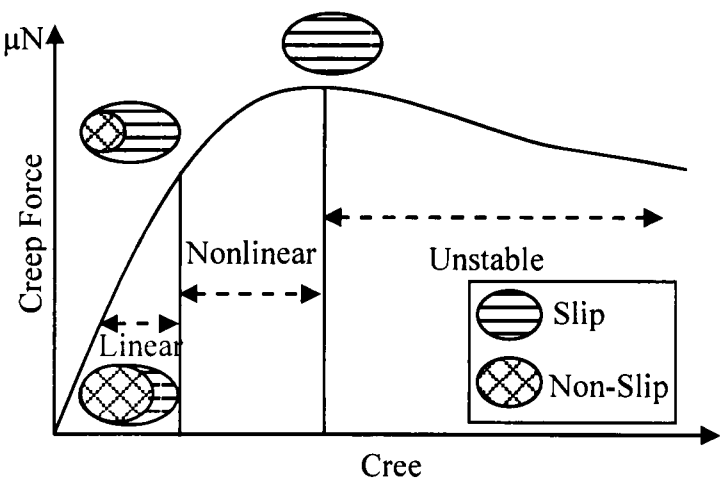

Figure 2. Creep Force vs Creep

An improved knowledge of the contact conditions will help to prevent the occurrence of wheel slip/slide of traction and braking systems on slipper tracks. This paper proposes a novel idea to identify the contact condition at wheel-rail contact. The main approach of the proposed scheme is to interpret the variations in the dynamic responses of the wheelset under different track conditions into useful contact information. In the past, railway engineers tried to improve the adhesion of wheel/rail with many methods, with mixed success. This is because the adhesion coefficient is very sensitive to the environmental conditions, such as speeds, axle-loads, wheel and rail profiles, contamination of contact surfaces, weather, etc [1].

In some re-adhesion control techniques the adhesion level is identified by measuring the difference between the train speed and the wheel rotational speed [2-3]. These re-adhesion control techniques rely on relative speeds measured by sensors measuring angular speed of the wheel and absolute speed of vehicle. There are several practical issues involved in detecting these parameters. The requirement of robust/reliable sensors for the harsh working environments limits the accuracy of measurements. Also the estimated vehicle speeds were used instead of measured to improve the performance under noisy mechanical environment [4]. Attempts have been made to measure the adhesion level available between wheel and rail but the measured data is not considered reliable because presence of several noises generated from various mechanical parts. There are re-adhesion control and wheel-slip protection

schemes that utilize the use of disturbance observers to estimate the adhesion information. The methods based on disturbance observers estimates adhesion saturation by using the information of rotor speed and the torque current and do not require direct speed measurement. However the performances of the anti-slip schemes based on a disturbance observer are to a large extent affected by noises in the system which can be very substantial in the wheel-rail contact environment. There is a lack of effective solutions that can provide real time information about the maximum adhesion available as a train travels through a track. This paper examines the use of multiple model based estimation approach for the detection of the contact conditions. A previous study has tried to estimate the creep coefficient at the wheel-rail contact and use this as an indirect indicator of the adhesion [5]. In this study, however, the use of a multiple Kalman filters is studied, which represents different operating conditions of the wheel-rail contact.

2. MODELING

Railway vehicles employ steel wheels running on tracks with steel rails, which provide the support and guidance functions. The interface between the two is established at contact point(s) between the wheels and rail surface, and both the vehicle configuration and the track greatly influence how vehicles behave [6]. The contact zone between a railway wheel and rail is very small (about $1cm^2$) compared with their overall dimensions and its shape and can be separated into slip and non-slip regions as shown in figure 2. The maximum level of tractive force depends upon the adhesion level at the wheel-rail contact patch. The way in which forces are generated at a rolling contact between wheel and rail is quite complex and relies upon the concept of "creep" a phenomenon which arises from the elastic deformation of material around the contact patch [7] and is defined as the relative speed of the wheels to rail and characterized as the lateral and longitudinal creep in accordance with the direction of motion. This study is carried out using a single solid axle powered wheelset connected to bogie via a yaw spring that stabilizes the kinematic motion of the wheelset.

2.1 Wheelset Dynamics

The railway wheelset has several degrees of freedom. The lateral displacement, yaw movement, longitudinal motion, wheels rotational motions are considered in the paper for the simulation of the wheelset dynamics and assessment of the multiple Kalman filters for the estimation of the contact conditions. The equations of motion of the wheelset are given below [8-11].

$$M_v\ddot{x} = \frac{F_R}{\lambda_R}\left[\frac{r_o\omega_{wR} - v}{v} - \left[\frac{L_g\dot{\psi}}{v} + \frac{\omega_{wR}\gamma(y - y_t)}{v}\right]\right] + \frac{F_L}{\lambda_L}\left[\frac{r_o\omega_{wL} - v}{v} + \left[\frac{L_g\dot{\psi}}{v} + \frac{\omega_{wL}\gamma(y - y_t)}{v}\right]\right] \quad (1)$$

Where M_v is the mass of the vehicle, x is longitudinal motion of the vehicle with $\ddot{x}$ associated acceleration, F_R and F_L are the right and left wheel creep force respectively and are the nonlinear function of adhesion coefficient (μ) and normal force (N) as shown in figure-2, λ_L and λ_R are the left and right wheel creepages, L_g is the track half gauge, ψ is the yaw angle of the wheelset, y is the lateral motion of the wheelset, v is vehicle forward speed, r_o is the contact radius of the wheel, ω_{wR} and ω_{wL} are the right and left wheel angular speeds, γ is the wheelset conicity and y_t is the track disturbance in lateral direction. The yaw degree of freedom is represented by following equation where k_w represents yaw stiffness and I_w is yaw moment of inertia.

$$I_w\ddot{\psi} = \frac{F_R}{\lambda_R}\left[\frac{r_o\omega_{wR} - v}{v} - \left[\frac{L_g\dot{\psi}}{v} + \frac{\omega_{wR}\gamma(y - y_t)}{v}\right]\right]L_g - \frac{F_L}{\lambda_L}\left[\frac{r_o\omega_{wL} - v}{v} + \left[\frac{L_g\dot{\psi}}{v} + \frac{\omega_{wL}\gamma(y - y_t)}{v}\right]\right]L_g - k_w\psi \quad (2)$$

The lateral dynamics are determined by the total creep force of the two wheels in lateral direction. Where F_c is centrifugal force which is taken into consideration when the wheelset runs on a curved track and given in equation

$$m_w\ddot{y} = -\frac{F_L}{\lambda_L}\left[\frac{\dot{y}}{v} - \psi\right] - \frac{F_R}{\lambda_R}\left[\frac{\dot{y}}{v} - \psi\right] + F_c \quad (3)$$

The wheelset is driven by the traction motor mounted on one side (right side in this case) of the wheelset. The other wheel is driven by the torsional torque.

$$I_R\dot{\omega}_R = T_t - T_s - T_R \tag{4}$$

$$I_L\dot{\omega}_L = T_s - T_L \tag{5}$$

Where T_t is the torque applied by the traction motor, T_s is the torsional torque and T_R and T_L are the tractive torques of the right and left wheel respectively. The torsional torque along the shaft is determined by the difference in rotation between two wheels [10]

$$T_s = k_s\int(\omega_R - \omega_L)dt + C_s(\omega_R - \omega_L) \tag{6}$$

Where C_s is material damping of shaft, usually very small, and therefore can be ignored. It is assumed that there is no bounce motion. In that case the roll motion is constrained by track and it does not have significant affect on creepages therefore it is ignored in further study.

2.2 Estimator Design

For the design of the Kalman filters, the wheelset model is simplified and only lateral and yaw dynamics are considered to be sufficient for this type of study [5, 11-13]. The simplified equation of the creepages involving only yaw and lateral dynamics are given below.

$$\lambda_{xL} = \frac{L_g\dot{\psi}}{v} + \frac{\gamma(y - y_t)}{r_o} \tag{7}$$

$$\lambda_{xR} = -\frac{L_g\dot{\psi}}{v} - \frac{\gamma(y - y_t)}{r_o} \tag{8}$$

$$\lambda_y = \lambda_{yR} = \lambda_{yL} = \frac{\dot{y}}{v} - \psi \tag{9}$$

The creep force equations are linearized and the simplified small signal model of wheelset is given below [8-9]. .

$$\frac{d}{dt}\begin{bmatrix}\Delta y_w\\ \Delta\psi\\ \Delta\dot{y}_w\\ \Delta\dot{\psi}\end{bmatrix} = \begin{bmatrix}0 & 0 & 1 & 0\\ 0 & 0 & 0 & 1\\ 0 & \frac{2g_{22}}{m_w} & -\frac{2g_{22}}{vm_w} & 0\\ -\frac{2L_g\gamma g_{11}}{r_oI_w} & -\frac{k_w}{I_w} & 0 & -\frac{2L_g^2g_{11}}{vI_w}\end{bmatrix}\begin{bmatrix}\Delta y\\ \Delta\psi\\ \Delta\dot{y}_w\\ \Delta\dot{\psi}\end{bmatrix} + \begin{bmatrix}0\\ 0\\ 0\\ \frac{2L_g\gamma g_{11}}{r_oI_w}\end{bmatrix}\Delta y_t \tag{10}$$

Lateral and yaw dynamics of the railway wheelset are excited by track irregularities (y_t) which cannot be applied as an input to the Kalman filter, but cannot be ignored due its direct affect on wheelset dynamic behaviour. Therefore to solve this problem y_t is reformulated and treated as a part of the state vector such that dynamics of the system are unchanged.

$$\frac{d}{dt}\begin{bmatrix}\Delta\psi\\ \Delta\dot{y}\\ \Delta\dot{\psi}\\ \Delta y_t\\ \Delta y - \Delta y_t\end{bmatrix} = \begin{bmatrix}0 & 0 & 1 & 0 & 0\\ \frac{2g_{22}}{m_w} & -\frac{2g_{22}}{vm_w} & 0 & 0 & 0\\ -\frac{k_w}{I_w} & 0 & -\frac{2L_g^2g_{11}}{vI_w} & 0 & -\frac{2L_g\gamma g_{11}}{r_oI_w}\\ 0 & 0 & 0 & -0.001 & 0\\ 0 & 1 & 0 & 0 & 0\end{bmatrix}\begin{bmatrix}\Delta\psi\\ \Delta\dot{y}\\ \Delta\dot{\psi}\\ \Delta y_t\\ \Delta y - \Delta y_t\end{bmatrix} + \begin{bmatrix}0\\ 0\\ 0\\ 1\\ -1\end{bmatrix}\dot{y}_t \tag{11}$$

Where $\dot{y}_t$ represents the track noises with variance Q. Two sensors (A gyro sensor for yaw rate measurement and an accelerometer for lateral acceleration measurement) as indicated in equation (4.29) appear to be sufficient for Kalman filter to provide satisfying estimation results.

$$z(t) = \begin{bmatrix} 0 & 0 & 1 & 0 & 0 \\ \frac{2g_{22}}{m_w} & -\frac{2g_{22}}{vm_w} & 0 & 0 & 0 \end{bmatrix} \begin{bmatrix} \Delta\psi \\ \Delta\dot{y} \\ \Delta\dot{\psi} \\ \Delta y_t \\ \Delta y - \Delta y_t \end{bmatrix} + v \tag{12}$$

Where v is a vector representing noise level of sensors with covariance R. It is assumed that there is no correlation between process and measurement noises.

3. Fuzzy Logic

In this paper, fuzzy logic scheme is developed for the analysis of data from the Kalman filters and for the identification of the contact conditions by producing the numeric output associated with specific data or model. It has already been used in various similar industrial applications [14-16]. The identification of contact condition from the combination of residual values is a multi valued logic problem and the fuzzy logic is suitable and simple solution for such applications.

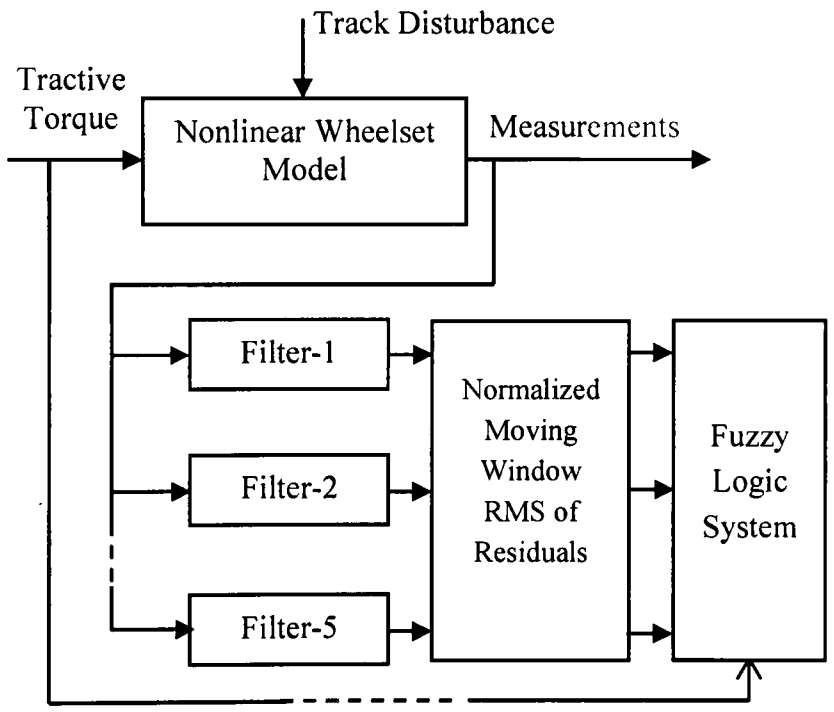

Figure 3. Proposed Scheme

4. Contact Condition Identification

A multiple model based estimation scheme is shown in the figure-3. This scheme identifies the contact condition based on a residual signal, which is the difference generated by the observations and the system's mathematical model. The nonlinear wheelset model is used to simulate the behaviour of the wheelset in presence of an unknown track disturbance in lateral direction. The Kalman filters are optimally tuned to operate on saturation point of different creep curves shown in figures 4 and 5. All the Kalman filters are run in parallel and the normalized rms value of the residuals with moving time window of one second is calculated. The rms values of the residuals are then fed to the fuzzy logic system which examines the rms values along with the tractive torque to identify the contact condition.

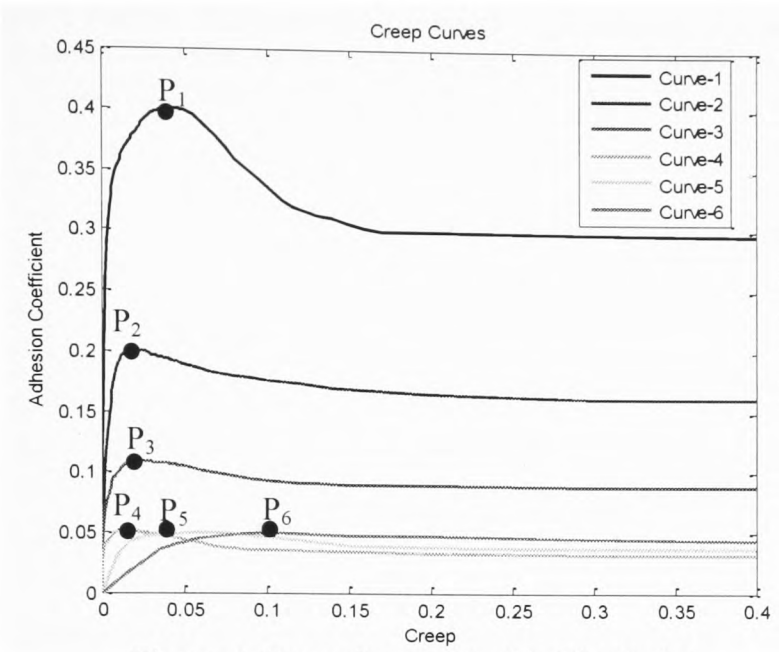

Figure 4. Creep Curves Used in Simulation

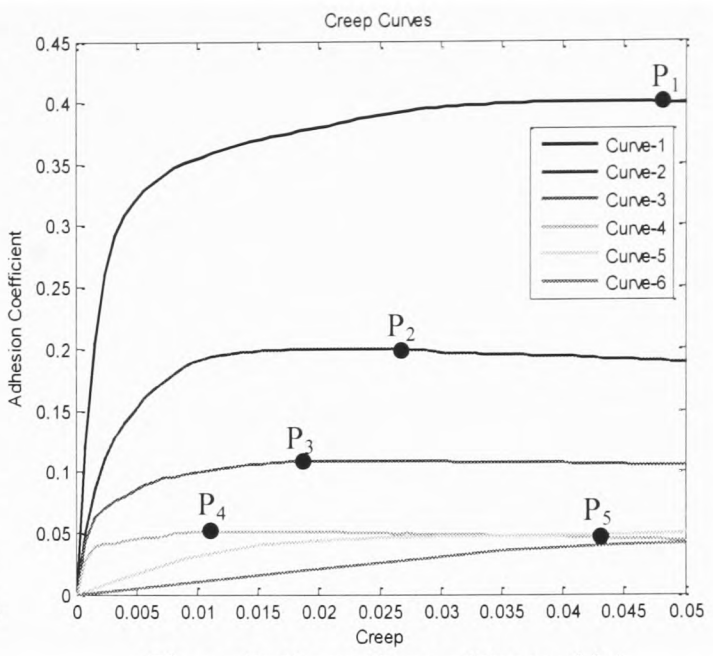

Figure 5. Creep Curves (Zoomed in)

Following figures shows the residual of the filters when the wheelset is operated in different contact conditions. PI controllers are used to control the tractive torque to force the wheelset to operate at specific operating point. Figure-6 shows the residuals of the filters at P_1. The residual of filter-1 is minimum because the filter-1 is optimally tuned to operate at this point. The residuals take approximately 5 seconds to settle down. This delay is caused by two reasons one is the time taken by PI controller to maintain the torque steadily (figure-7) and 1 second time taken consumed in calculating windowed rms value of residuals.

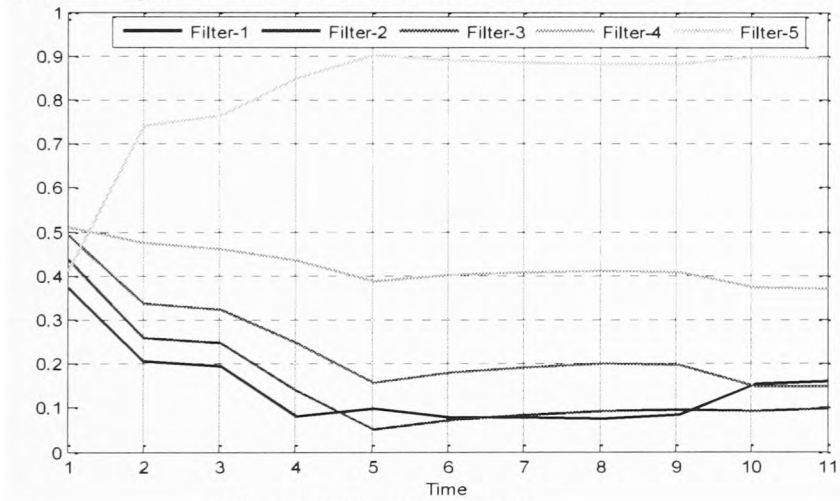

Figure 6. Residuals at P_1

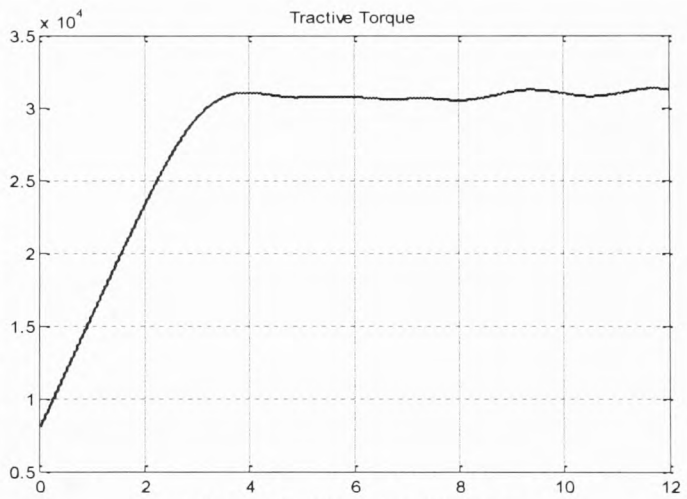

Figure 7. Tractive Torque

Similarly in figure-9 the filter-3 has minimum error during the time window 0f 4 to 10 seconds (this is the time window where PI controller is able to operate the wheelset at P_3). In some cases it is difficult to differentiate the two operating points because the residuals produce similar combination (P1 and P2 in Figure-6 and figure-8). This happens when the two operating point located on different creep curves have the same dynamic response. In such cases tractive torque can be analyzed to distinguish between the two operating points. Figure-10 and figure-11 shows the residual values when the wheelset is operated at P_4 and P_5 respectively. The results show that the Kalman filters show great agreement and consistency with the proposed idea and it is also evident from the results that the residual values give a unique combination at each operating point of the creep curves that makes the contact condition easily identifiable using a fuzzy logic system by building the certain rules.

5. Conclusion

The real time knowledge of available adhesion level is very important for the smooth delivery of traction and braking. This research has proposed a novel technique to identify the contact condition by exploring the dynamic properties of the conventional solid axle wheelset. A multiple model based scheme is proposed to estimate the wheelset dynamics. The fuzzy logic can then be used to identify the contact condition by analyzing the residuals and

tractive torque. Different creep curves (representing typical high, low and moderate adhesion level) are used in simulation. The simulation results presented show the excellent agreement with the proposed idea.

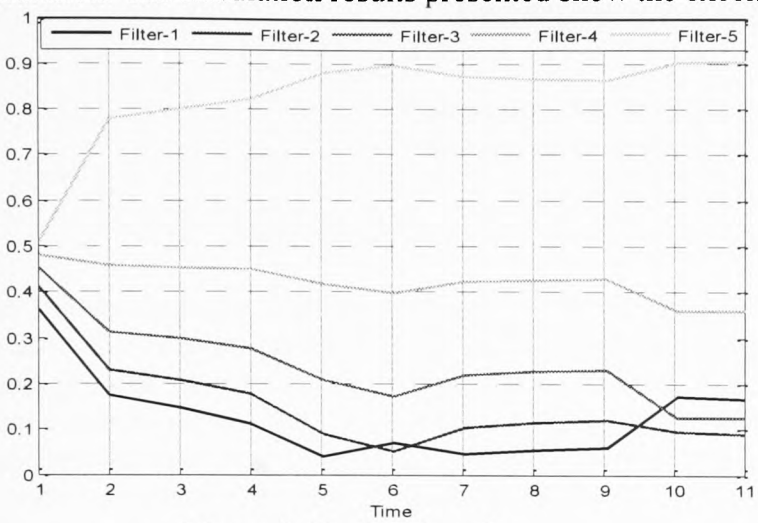

Figure 8. Residuals at P_2

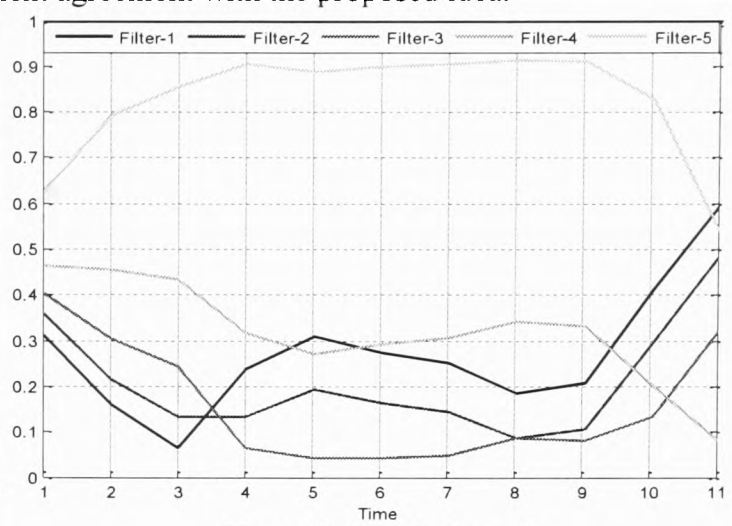

Figure 9. Residuals at P_3

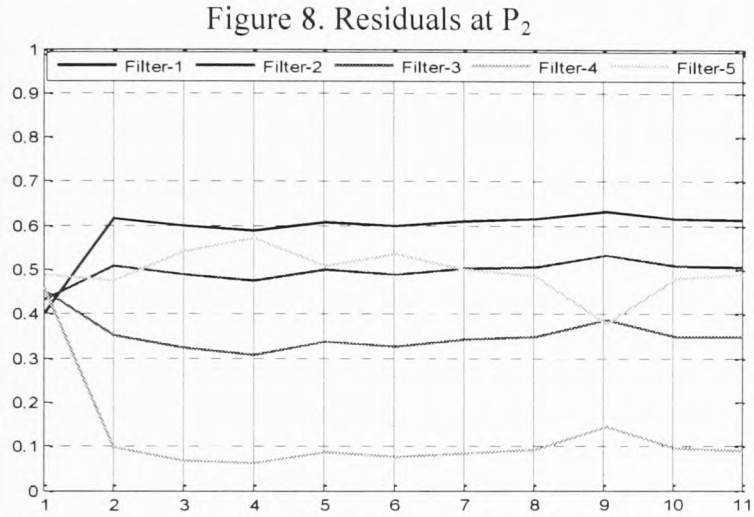

Figure 10. Residuals at P_4

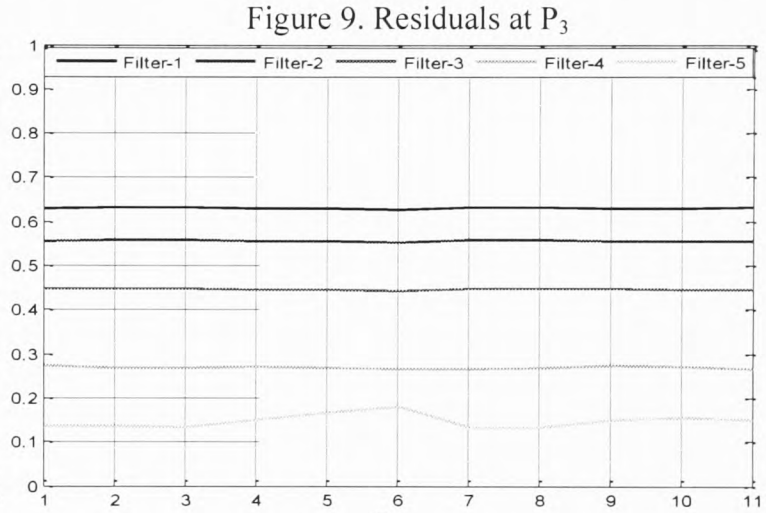

Figure 11. Residuals at P_5

References

[1] Zhang, W., et al., *Wheel/rail adhesion and analysis by using full scale roller rig.* Wear, 2002. **253**(1-2): p. 82-88.

[2] Watanabe, T. and A. Yamanaka. *Optimisation of readhesion control of Shinkansen trains with wheel–rail adhesion.* 1997.

[3] Watanabe, T., et al. *Optimization of readhesion control of Shinkansen trains with wheel-rail adhesion prediction.* 1997.

[4] Yasuoka, I., et al. *Improvement of re-adhesion for commuter trains with vector controltraction inverter.* 1997.

[5] Charles, G. and R. Goodall. *Low adhesion estimation.* 2007: IET.

[6] Iwnicki, S., *Handbook of Railway Vehicle Dynamics.* 2006: CRC Press.

[7] Li, H. and R. Goodall. *Modelling and analysis of a railway wheelset for active control.* 1998.

[8] Hussain, M.T.X.a.A.H.J., *Modeling and Estimation of Nonlinear Wheel-rail Contact Mechanics.* Proceedings of the twentieth Intenational conference on System Engineering, 2009: p. 219-223.

[9] Hussain, M.T.X., *Multi Kalman Filtering Approach for Estimation of Wheel-Rail Contact Conditions* Proceedings of the United kingdom Automatic Control Conferecne 2010, 2010: p. 459-464.

[10] Yu, J.H., T.X. Mei, and D.A. Wilson, *RE-ADHESION CONTROL BASED ON WHEELSET DYNAMICS IN RAILWAY TRACTION SYSTEM.*

[11] Yu, J.H., *Re-adhesion control for AC traction system in railway application*, PhD Thesis, The University of Leeds, 2007.

[12] Mei, T. and R. Goodall. *LQG and GA solutions for active steering of railway vehicles.* 2002: IET.

[13] Charles, G., R. Goodall, and R. Dixon, *Model-based condition monitoring at the wheel-rail interface.* Vehicle System Dynamics, 2008. **46**(Supplement 1): p. 415-430.

[14] Hashmi, K., I. Graham, and B. Mills, *Fuzzy logic based data selection for the drilling process.* Journal of Materials Processing Technology, 2000. **108**(1): p. 55-61.

[15] El Baradie, M., *A fuzzy logic model for machining data selection.* International Journal of Machine Tools and Manufacture, 1997. **37**(9): p. 1353-1372.

[16] Hashmi, K., M. El Baradie, and M. Ryan, *Fuzzy-logic based intelligent selection of machining parameters.* Journal of Materials Processing Technology, 1999. **94**(2-3): p. 94-111.

Multiple Model Based Identification of the Wheel-Rail Contact Condition for Traction and Braking Control

I Hussain[1], TX Mei[2] and Mohammad Mirzapur[3]
School of Computing, Science and Engineering
Salford University, UK
Emails: [1] I.Hussain@edu.salford.ac.uk [2]t.x.mei@salford.ac.uk [3]M.Mirzapour@edu.salford.ac.uk

The traction and the braking performance of the railway vehicle is affected by the changes in contact condition because the contact forces that govern the dynamic behaviour of the wheelset are a non-linear function of the creepages and vary substantially when the conditions of the rail surfaces change due to the fallen tree leaves and/or other contaminations like snow, water and presence of debris particles on the rail surface. The overall adhesion can therefore becomes very low which present a serious challenge for the traction/braking control systems to avoid the problem of wheel slip/slide. The wheel Slip/slide is a highly undesirable phenomenon that causes the mechanical parts to wear down quickly affects the stability and leads to the inconsistent traction performance causing problems in train scheduling. The wear and the traction are the most important aspects from an economic perspective. However, the security point of view in which the friction levels are very low, with the result that a train might not be able to brake within the available distance, is of even higher importance.

The low adhesion problem between the wheel and the rail has been since the beginning of the railway a crucial parameter in the design and operation of the railway vehicles. A large number of measures have been developed; nevertheless the trouble caused by the low adhesion still occurs. The available knowledge is largely based on subjective observations, for the most part offered by drivers. Poor adhesion can be caused by a large number of different factors, and there is often a large variation in local adhesion conditions along a particular section of route. The rapid increase in railway traffic across the globe demands a better acceleration and braking performance. This means a shorter braking distance and higher acceleration in order to travel at cruising velocity for longer distances as possible. It is therefore important to provide the real time information about the track condition to the traction and braking control system to maximize the use of available adhesion which will help the control system to maintain the stable operation of the railway vehicle. This paper proposes a novel technique to identify the adhesion condition by using the fact that the dynamic properties of the wheelset are affected by the changes in the contact condition.

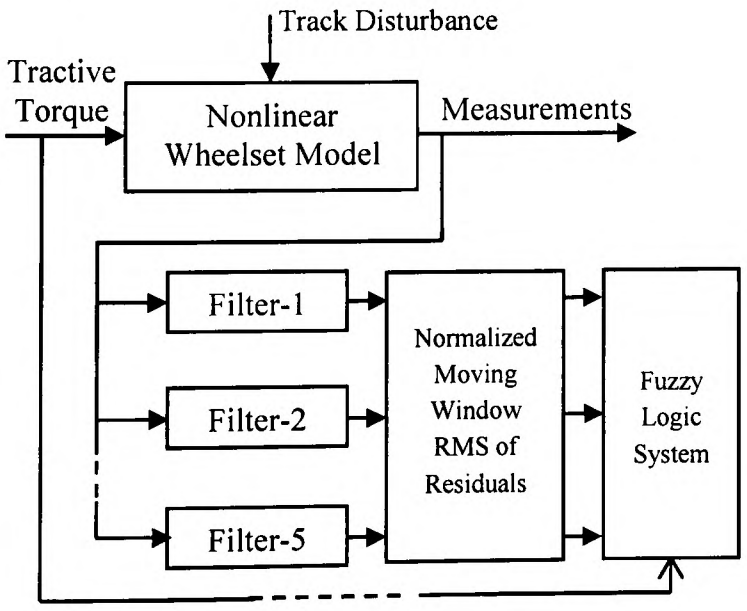

Figure a. Proposed Scheme

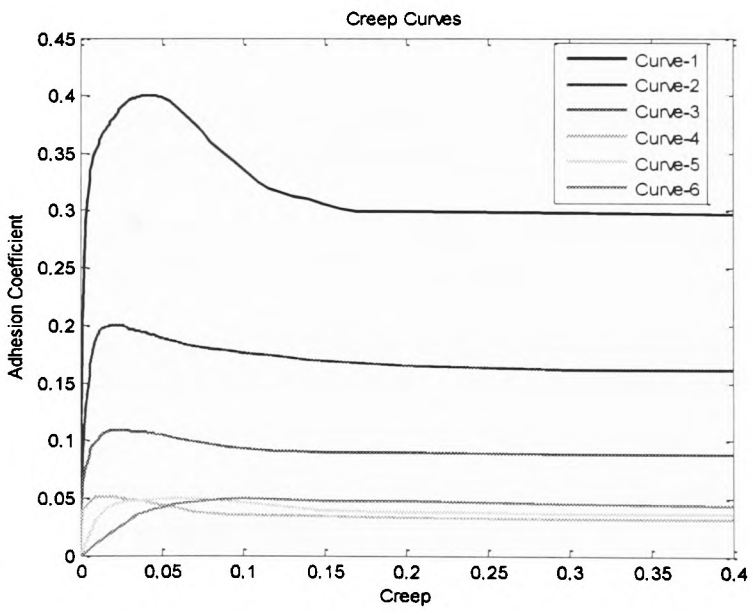

Figure b. Creep Curves Used in Simulation

This research is an extension of ongoing research (Mei, 2010, Hussain, 2009, Hussain, 2010, I Hussain) which proposes an indirect technique to overcome the problem of the wheel slip/slide in poor contact conditions. The proposed scheme exploits the dynamic properties of the conventional solid axle wheelset in response to changes in contact condition at the wheel-rail interface avoiding difficult and expensive measurement requirements. A nonlinear model of Longitudinal, Rotational, Torsional, lateral and yaw dynamics of a conventional solid axle wheelset shown

in figure-c is used for the study. There are various different wheelset arrangements but solid axle wheelset has the ability to steer itself on the curves as a result it is the most commonly used wheelset arrangement around the world. It is called a solid axle wheelset because both the wheels are fixed to a common axle and bound to rotate at the same speed. The proposed scheme (figure-a) consists of a bank of Kalman filters based on the simplified linearized small signal wheelset models. Each Kalman filter in the filter bank is designed to operate in a specific contact condition. The normalized value of residuals (difference generated by the observations and the system's mathematical model) is calculated during the normal running condition using a moving time window of 1 second. Residuals are then assessed using a fuzzy logic based system to identify the operating condition of the wheelset. The proposed idea is validated by simulating the model using various different creep curves (figure-b) representing different contact conditions.

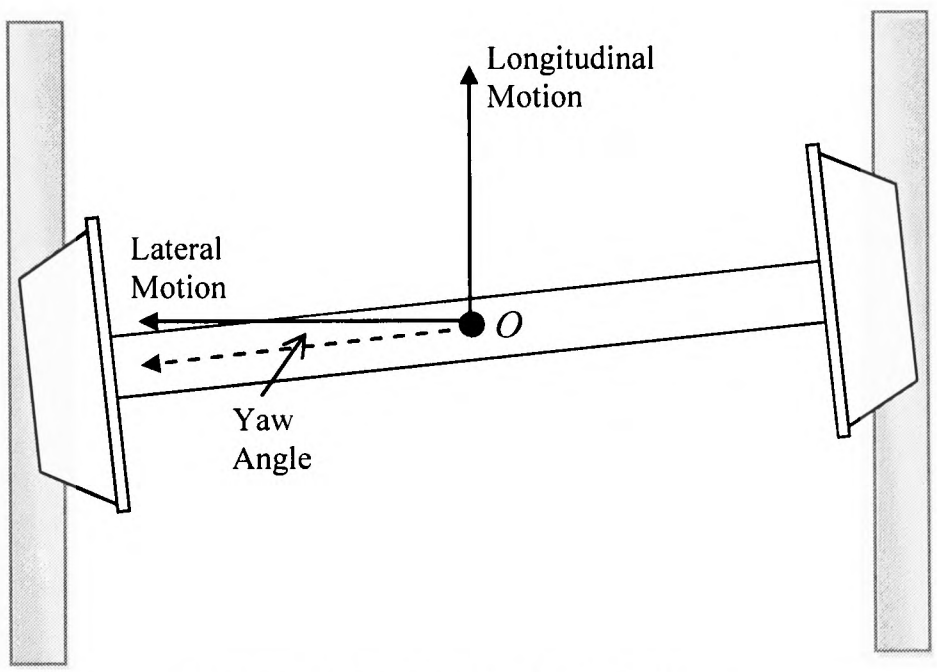

Figure c. Single Solid axle wheelset

References

I. HUSSAIN and Mei. T. X. 2010. Multi Kalman Filtering Approach for Estimation of Wheel-Rail Contact Conditions *Proceedings of the United kingdom Automatic Control Conferecne 2010*, 459-464.

I. HUSSAIN, Mei. T. X. and. A. H. Jones. 2009. Modeling and Estimation of Nonlinear Wheel-rail Contact Mechanics. *Proceedings of the twentieth Intenational conference on System Engineering*, 219-223.

I HUSSAIN, and. T. X. Mei. 2011. Identification of the Wheel Rail Contact Condition for the Traction and Braking Control. *Proceedings of the 22nd International Symposium on Dynamics of Vehicles on Roads and Tracks, Manchester Metropolitan University, 14-19 August 2011.*

MEI. T. X, and I. Hussain. 2010. Detection of wheel-rail contact conditions for improved traction control. *Proceedings of the 4th international conference on Railway Traction systems 2010*

Onboard Estimation of the wheel-rail contact conditions

I Hussain[1] and TX Mei[2]
School of Computing, Science and Engineering
Salford University, UK
Emails: [1] I.Hussain@edu.salford.ac.uk [2] t.x.mei@salford.ac.uk

The low adhesion problem between the wheel and the rail has been since the beginning of the railway a crucial parameter in the design and operation of the railway vehicles. Although in last few decades the railway industry is able to manage the low adhesion to some extent but currently available measures are not sufficient to eliminate the safety incidents and train delays. This research work has led to the development of a novel and vehicle based technique for the real time estimation of the contact conditions by using multiple models to represent variations in the adhesion level and different contact conditions. The proposed solution exploits the fact that the dynamic behaviour of a railway vehicle is strongly affected by the variations in the adhesion level. The purpose of the proposed scheme is to interpret these variations in the dynamic response of the wheelset into useful contact condition information. The proposed system involves the use of a number of carefully selected mathematical models of a rail vehicle to mimic train dynamic behaviours in response to different track conditions. Each of the estimators is tuned to match one particular track. The level of matches/mismatches is reflected in the estimation errors of the models concerned, when compared with the real vehicle (through the measurement output of vehicle mounted inertial sensors). The output residuals from all the models are then be assessed using a fuzzy logic based decision making system to determine which of the models provide a best match to the present operating condition and hence to give real time information about the track conditions.

Real Time Estimation of the Wheel-Rail Contact Condtions using Multi-Kalman Filtering and Fuzzy Logic

I Hussain
School of Computing, Science and Engineering, University of Salford
I.Hussain@edu.salford.ac.uk

T. X. Mei
School of Computing, Science and Engineering, University of Salford
T.X.Mei@edu.salford.ac.uk

Mohammad Mirzapour
School of Computing, Science and Engineering, University of Salford
M.Mirzapour@edu.salford.ac.uk

Abstract— **This paper presents a novel technique for the real time estimation of the contact conditions by using a combination of multi-Kalman filtering and fuzzy logic approach. The proposed solution exploits the variations in the dynamic behaviour of a railway wheelset with the changes in wheel-rail contact condition. The proposed system involves the use of multiple model based estimation of the wheelset dynamics in response to different track conditions. Each of the estimators is tuned to match one particular track condition to give the best results at the specific design point. Residuals of each filter are calculated and the level of matches/mismatches is reflected in the residual values of the models concerned. The residuals from all the models are then be assessed by a fuzzy inference system to determine the present operating condition and hence to give real time information about the track conditions.**

Keywords- Wheel rail contact; State Estimation; Kalman filters; Fuzzy Logic

I. INTRODUCTION

Adhesion is a very important factor in the operation of the railway vehicles. The delivery of traction and braking is achieved through the available adhesion at the wheel-rail interface. Insufficient level of adhesion can lead to severe safety and operational problems resulting in huge financial losses to railway industry around the world. Although in last few decades the railway industry is able to manage low adhesion to some extent but currently available measures are not sufficient to eliminate the safety incidents and train delays. This is because the adhesion is affected by a large number of parameters such as weather, season changes and contaminations and therefore cannot be predicted with certainty. Changes in the adhesion conditions can be rapid and also short-lived, and values can differ from position to position along a route depending upon the type and degree of contamination which presents a great scientific challenge to effectively design a suitable technique to tackle this problem.

Available wheel slip/slide protection (WSP) technologies for traction and braking systems are incorporated in the rail vehicles to maximize the use of available adhesion [1]. WSPs control the slip ratio (relative speed between a wheel and the train) below a pre-defined threshold to avoid slip/slide during traction and braking [1-2]. Those controllers are difficult to obtain optimal performance and also require accurate measurement of wheel slip. In general, WSPs are effectively reactive systems, i.e. only 'activated' to stop wheel slip/slide when detected by the sensors. There is still a need for a system which is proactive and can prevent slip/slide from its occurrence, such that real time information about the track condition can be provided to the traction and braking control systems to maximize the use of available adhesion. On the other hand, the wheel-rail contact mechanics is extremely complex and vary with time which presents a great scientific challenge to effectively design a suitable technique to tackle this problem.

A number of ideas have been proposed to detect the running condition of the wheel-rail interface that use low cost inertial sensing mounted on the vehicle and advanced processing, e.g. an inverse modelling approach for the estimation of creep forces [3]; and a model based estimation [4-5].

We have already presented the idea of use of multiple models and fuzzy logic for the real time estimation of the wheel-rail contact conditions [6-9]. Multiple Kalman filters based on linearized wheelset model are used to estimate the wheelset dynamics in different contact conditions. The contact condition information is reflected in the residual values of the Kalman filters which interpreted by fuzzy logic based decision making system. In previous research the idea was limited to only selected creep curves here it is further extended for all possible contact conditions. This paper also covers the complete design of fuzzy inference system and presents a formula to convert the fuzzy logic output into percentage adhesion.

II. MODELLING OF CONTACT MECHANICS

Wheelsets are the component of railway vehicles that interacts directly with the track and consequently the dynamics of the wheelset are directly influenced by

changing contact conditions - therefore this study focussed on a single solid axle wheelset and the outcome of the study may be readily extended to the full vehicles. [5, 10-20]. The dynamic behaviour of the railway wheelset is governed by the creep forces generated at the wheel rail contact patches. These creep forces are the result of creepages which are the relative speed of the wheels to rail and can be characterized as lateral (λ_y) and longitudinal creep (λ_x) in accordance with the direction of motion as given in equations 1-3 [6-9].

$$\lambda_{xL} = \frac{r_o\omega_L - v}{v} + [\frac{L_g\dot{\psi}}{v} + \frac{\gamma(y - y_t)}{r_o}] \quad (1)$$

$$\lambda_{xR} = \frac{r_o\omega_R - v}{v} - [\frac{L_g\dot{\psi}}{v} + \frac{\gamma(y - y_t)}{r_o}] \quad (2)$$

$$\lambda_y = \lambda_{yR} = \lambda_{yL} = \frac{\dot{y}}{v} - \psi \quad (3)$$

where the subscripts L and R represent left and right wheels, r_o is the nominal radius of the wheels, v is the vehicle forward speed, γ is the conicity of the wheels, Ψ is the yaw angle, L_g is the track half gauge, ω_L and ω_R are the angular velocities of the left and right wheels respectively, y is the lateral motion, and y_t represents the track irregularity in lateral direction. The total creepage λ_j is the combination of the lateral and longitudinal creepages.

$$\lambda_j = \sqrt{\lambda_{ij}^2 + \lambda_{ij}^2} \quad i = x, y \text{ and } j = L, R \quad (4)$$

The total creep force F_j is a nonlinear function of the total creepage and can be represented using equation 5.

$$F_j = \mu_j N_j \quad j = L, R \quad (5)$$

The distribution of the contact forces in the longitudinal and lateral directions is thoroughly studied by Polach [21] and can be represented using (6).

$$F_{ij} = F_j \cdot \frac{\lambda_{ij}}{\lambda_j}, \quad i = x, y \text{ and } j = L, R \quad (6)$$

The equations of motion of the wheelset are given in equations (7-12).

$$M_v\ddot{x} = \frac{\mu_R N_R}{\sqrt{\lambda_{xR}^2 + \lambda_{yL}^2}}\left[\frac{r_o\omega_R - v}{v} - [\frac{L_g\dot{\psi}}{v} + \frac{\gamma(y - y_t)}{r_o}]\right] + \frac{\mu_L N_L}{\sqrt{\lambda_{xL}^2 + \lambda_{yL}^2}}\left[\frac{r_o\omega_L - v}{v} + [\frac{L_g\dot{\psi}}{v} + \frac{\gamma(y - y_t)}{r_o}]\right] \quad (7)$$

$$I_w\ddot{\psi} = \frac{\mu_R N_R}{\sqrt{\lambda_{xR}^2 + \lambda_{yL}^2}}\left[\frac{r_o\omega_R - v}{v} - [\frac{L_g\dot{\psi}}{v} + \frac{\gamma(y - y_t)}{r_o}]\right]L_g - \frac{\mu_L N_L}{\sqrt{\lambda_{xL}^2 + \lambda_{yL}^2}}\left[\frac{r_o\omega_L - v}{v} + [\frac{L_g\dot{\psi}}{v} + \frac{\gamma(y - y_t)}{r_o}]\right]L_g - k_w\psi \quad (8)$$

$$m_w\ddot{y} = -\frac{\mu_L N_L}{\sqrt{\lambda_{xL}^2 + \lambda_{yL}^2}}\left[\frac{\dot{y}}{v} - \psi\right] - \frac{\mu_R N_R}{\sqrt{\lambda_{xR}^2 + \lambda_{yL}^2}}\left[\frac{\dot{y}}{v} - \psi\right] + F_c + F_g \quad (9)$$

$$I_R\dot{\omega}_R = T_t - K_s\theta_s - r_o\frac{\mu_R N_R}{\sqrt{\lambda_{xR}^2 + \lambda_{yL}^2}}[\frac{r_o\omega_R - v}{v} - (\frac{L_g\dot{\psi}}{v} + \frac{\gamma(y - y_t)}{r_o}) \quad (10)$$

$$I_L\dot{\omega}_L = K_s\theta_s - r_o\frac{\mu_L N_L}{\sqrt{\lambda_{xL}^2 + \lambda_{yL}^2}}[\frac{r_o\omega_L - v}{v} + (\frac{L_g\dot{\psi}}{v} + \frac{\gamma(y - y_t)}{r_o})] \quad (11)$$

$$T_s = k_s\int(\omega_R - \omega_L)dt + C_s(\omega_R - \omega_L) \quad (12)$$

where M_v is the mass of the vehicle $\ddot{x}$ is the vehicle forward acceleration, I_w is the yaw moment of inertia, k_w is a yaw stiffness necessary to stabilise the wheelset, m_w is the mass of the wheelset, $\ddot{y}$ is the lateral acceleration, F_c is a centrifugal force which is taken into consideration when the wheelset runs on a curved track, F_g is the gravitational stiffness force related to the lateral displacement and roll angle of the wheelset. The tractive torque T_t is applied to one side of the wheelset (right side in this case) and the other wheel is driven by the torsional torque T_s. $\theta_s = \int(\omega_R - \omega_L)dt$. k_s is the torsional stiffness of the shaft connecting the two wheels and C_s is material damping of the shaft, which is usually very small.

III. Design of Multiple Kalman Filters

The main objective of this study is to detect the changes in the wheel-rail contact condition with practical sensors. The design of the estimator is simplified by considering the wheelset modes that are directly related to contact conditions. Previous studies have shown that the lateral and yaw dynamics are sufficient for the study of plan-view dynamics of a wheelset [5, 7, 9, 16, 22-24]. The simplified model has several advantages in estimator design without having a significant effect on the results [7, 9, 24]. The major advantage is the simple design of the estimator with minimum number of states which will allow the estimator to converge quickly. The yaw and lateral dynamics are excited by lateral track irregularities hence no torque input is required to estimators in simplified model also irregularities in track are not no measureable therefore cannot be applied as input to Kalman filter either. The contact forces given in (5) and (6) are nonlinear in nature and are linearized at specific points on the creep curves in order to enable the design of the Kalman filters. The small signal model of linearized creep forces is given in following equation [7-8].

$$\begin{bmatrix}\Delta\dot{y}\\ \Delta\dot{\psi}\\ \Delta\ddot{y}\\ \Delta\ddot{\psi}\end{bmatrix} = \begin{bmatrix}0 & 0 & 1 & 0\\ 0 & 0 & 0 & 1\\ 0 & \frac{2g_{22}}{m_w} & -\frac{2g_{22}}{vm_w} & 0\\ -\frac{2L_g\gamma g_{11}}{r_o I_w} & -\frac{k_w}{I_w} & 0 & -\frac{2L_g^2 g_{11}}{vI_w}\end{bmatrix}\begin{bmatrix}\Delta y\\ \Delta\psi\\ \Delta\dot{y}\\ \Delta\dot{\psi}\end{bmatrix} + \begin{bmatrix}0\\ 0\\ 0\\ \frac{2L_g\gamma g_{11}}{r_o I_w}\end{bmatrix}\Delta y_t \quad (13)$$

The track disturbances (y_t) are very difficult to measure in practice and therefore highly undesirable to be used as an input to the Kalman filters, therefore (13) is reformulated to overcome the problem, as

$$\frac{d}{dt}\begin{bmatrix}\Delta\psi\\ \Delta\dot{y}\\ \Delta\dot{\psi}\\ \Delta y_t\\ \Delta y-\Delta y_t\end{bmatrix}=\begin{bmatrix}0 & 0 & 1 & 0 & 0\\ \frac{2g_{22}}{m_w} & -\frac{2g_{22}}{vm_w} & 0 & 0 & 0\\ -\frac{k_w}{I_w} & 0 & -\frac{2L_g^2 g_{11}}{vI_w} & 0 & -\frac{2L_g\gamma g_{11}}{r_o I_w}\\ 0 & 0 & 0 & N & 0\\ 0 & 1 & 0 & 0 & 0\end{bmatrix}\begin{bmatrix}\Delta\psi\\ \Delta\dot{y}\\ \Delta\dot{\psi}\\ \Delta y_t\\ \Delta y-\Delta y_t\end{bmatrix}+\begin{bmatrix}0\\ 0\\ 0\\ 1\\ -1\end{bmatrix}\dot{y}_t \quad (14)$$

A gyro sensor to measure yaw rate and accelerometer to measure lateral acceleration are found to be sufficient to produce satisfactory results. The output equation is given in (15).

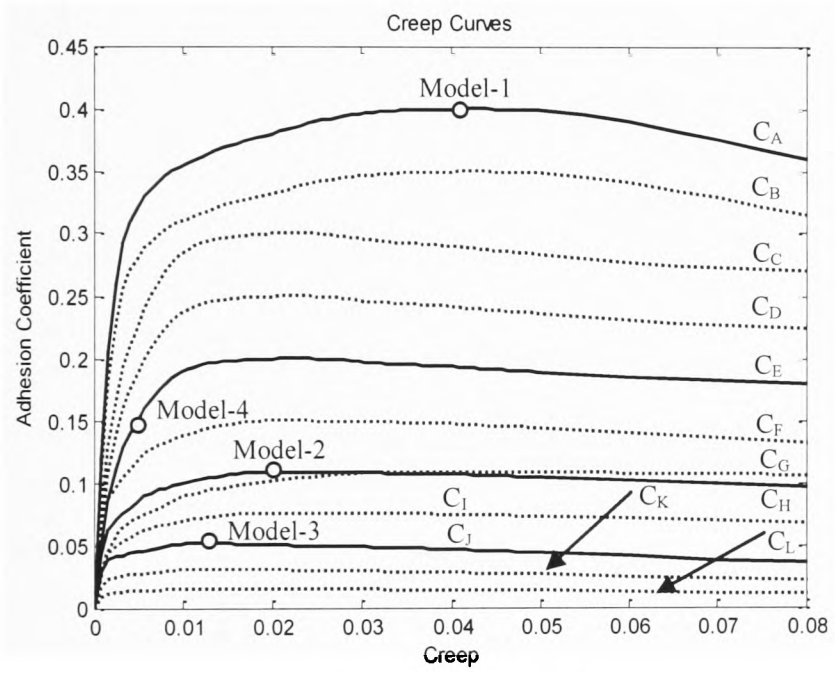

Figure 1. Creep Curves.

$$z(t)=\begin{bmatrix}0 & 0 & 1 & 0 & 0\\ \frac{2g_{22}}{m_w} & -\frac{2g_{22}}{vm_w} & 0 & 0 & 0\end{bmatrix}\begin{bmatrix}\Delta\psi\\ \Delta\dot{y}\\ \Delta\dot{\psi}\\ \Delta y_t\\ \Delta y-\Delta y_t\end{bmatrix}+v \quad (15)$$

IV. Estimation of Contact Conditions

Several creep curves representing high to very lows adhesion conditions are used for design and the testing of the detection system. The creep curves used for Kalman filter design are shown by solid lines and the creep curves shown by dotted lines are used for the testing of detection system. The proposed scheme is shown in Fig.2. This scheme identifies the contact condition based on a residual signal, which is the difference generated by the observations and the system's mathematical model. The design of each Kalman filter is based on g_{11} and g_{22} values. At saturation point of creep curve g_{11}, which depends upon the slope of the creep curve $d\mu/d\lambda$, is zero and g_{22}, which depends upon traction ratio μ/λ, is different for different adhesion levels. Therefore the residual signal of Kalman filter designed and tuned to operate in specific contact condition would be at lowest whenever the vehicle is operated in similar contact condition. After trials and errors four Kalman filters are found to be sufficient to detect the changes in the contact conditions. Model-1 is tuned to operate at the saturation region of the creep curve C_A, model-2 is designed to operate on the saturation region of the creep curve C_C, model-3 is designed to operate on the saturation region of creep curve C_D and model-4 is designed to operate in the linear region of creep curve C_B. The purpose of the model-4 is to identify whether the wheelset is operating at saturation region of the creep curve or not.

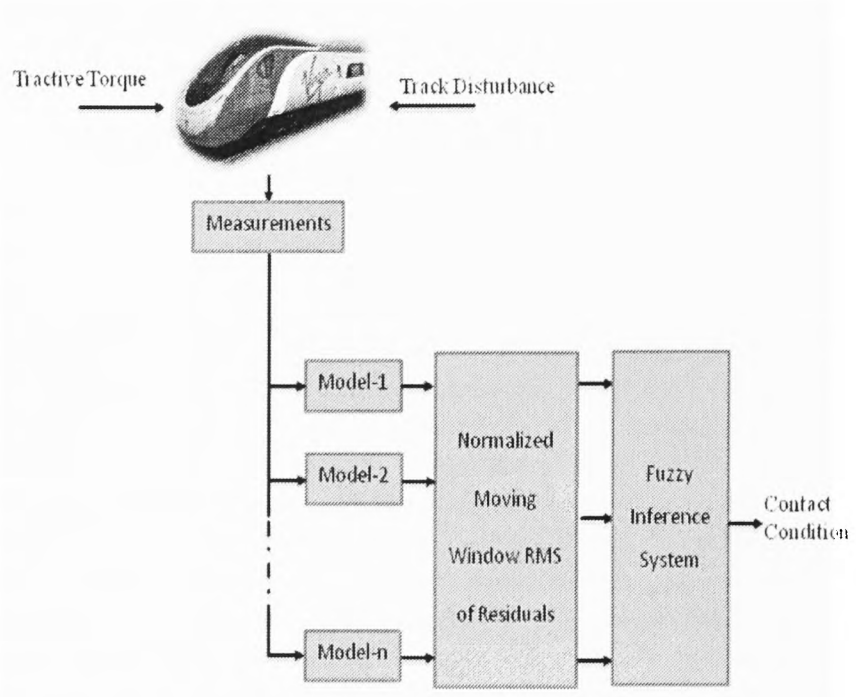

Figure 2. Contact Condition Estimation Scheme

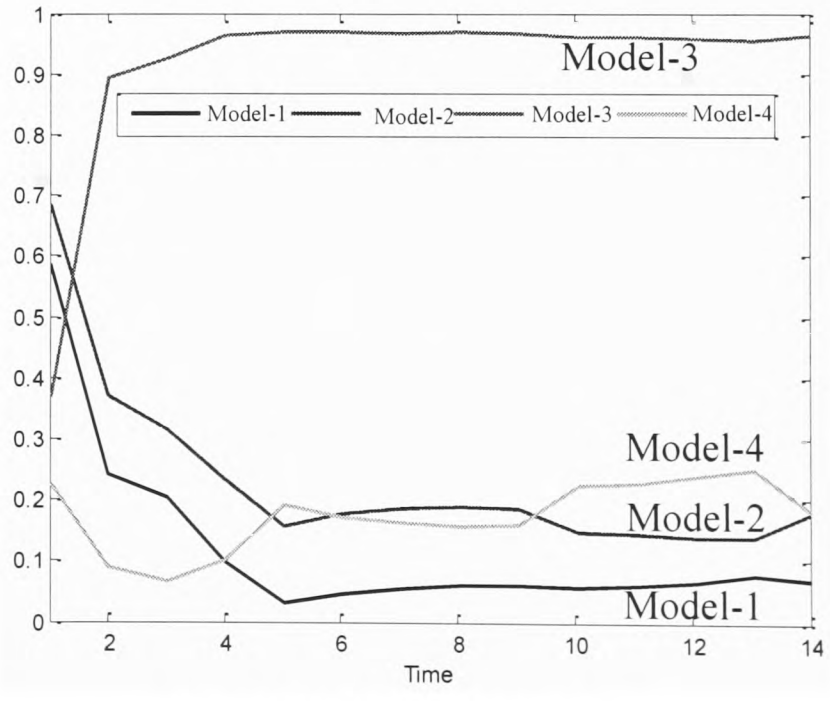

Figure 3. Residuals of filters at P_1

Fig.3 shows the residuals of filters when the wheelset is operated at the saturation region of the creep curve-1. The residual of model-1 is lowest as expected indicting that the wheelset is operating at P_a. When the wheelset is operated at P_c the residual of model-2 is at the lowest and

the residual of model-1 is increased as shown in Fig.4. If the wheelset is not operated on the saturation points of the creep curves the residual of model-4 designed at P_e is lowest. For instance when the wheelset is operated in the linear region of the creep curve-1 the residual of model-4 is at the lowest as shown in Fig.5. In general when the vehicle operates in a contact condition similar to model-1 the residual of model-1 are smaller as compare to rest of the models and in this way the information about the contact condition is reflected in the residual values.

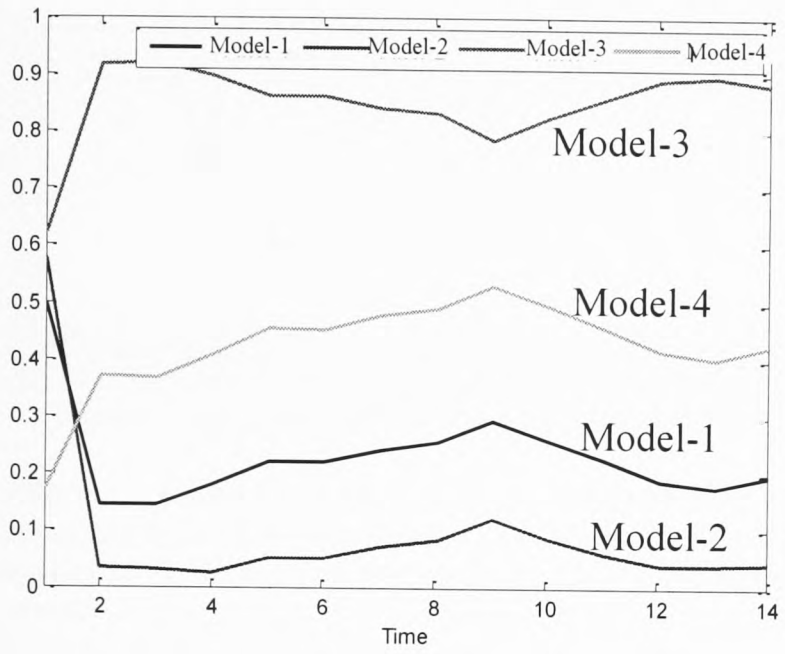

Figure 4. Residuals of filters at P_3

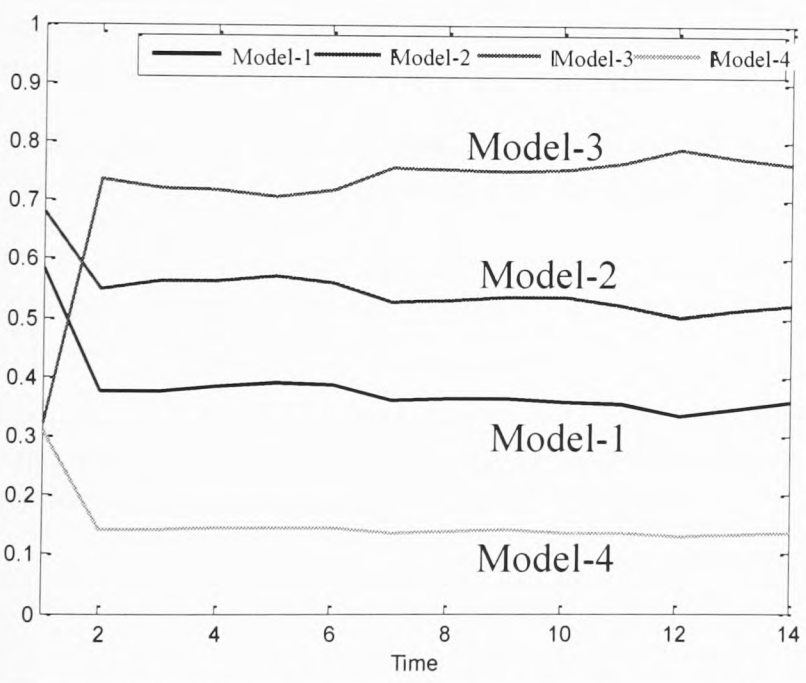

Figure 5. Residuals the when the wheelset is operated in linear region of C_A

As only four models are used in the proposed detection scheme, it is necessary to evaluate how the models would respond to other contact conditions that are not directly included in the design. This is carried out by simulating the filters in different contact conditions shown in figure-1 and the residual data is interpolated (Fig.6) to develop a fuzzy logic based detection system to detect all possible contact conditions.

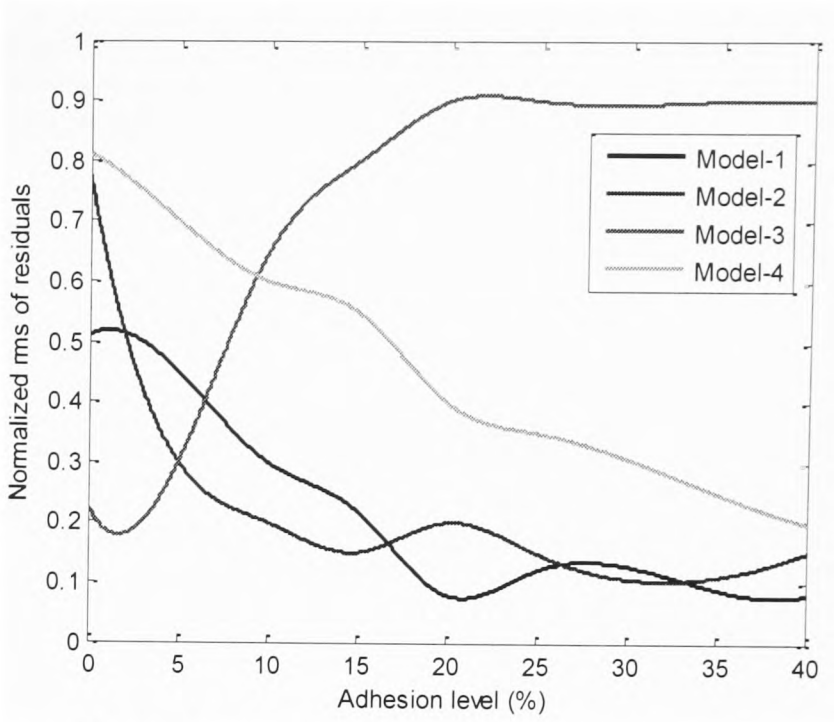

Figure 6. Residuals of filters after interpolation

V. Design Of Fuzzy Inference System

The basic idea of the fuzzy inference system is that if wheelset operating point is at saturation region of the creep curve then the residual information together with the tractive torque can easily be used to determine the adhesion level. The fuzzy inference system (FIS) that analyzes the residuals and the tractive torque is shown in Fig.7. As any other fuzzy logic system it has three main divisions. First part is input division which scales and weights the inputs and determines the magnitude of participation in producing output. The inputs are then processed according to set rules and the final output is determined by the averaging the output of individual rules.

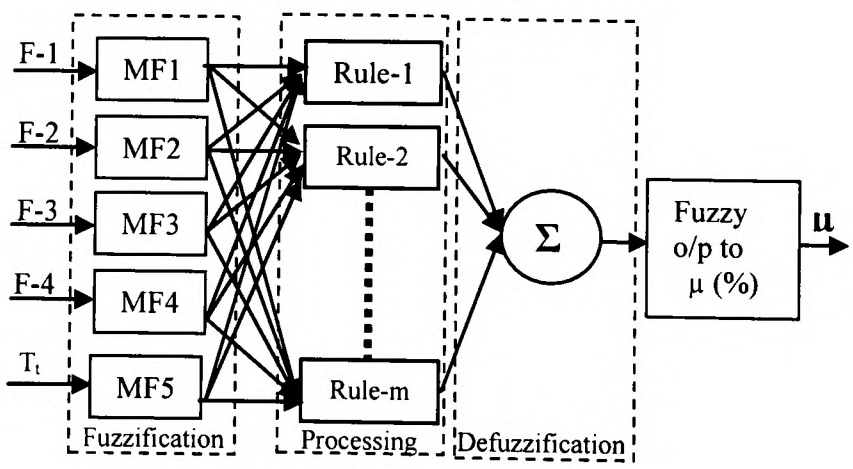

Figure 7. Fuzzy Inference System

The residual of each model in Fig.6 is divided as 'Low', 'Moderate' and 'High' to develop input membership function. Input membership function for residual of model and modle-2 are shown in Fig.8 and Fig.9 respectively.

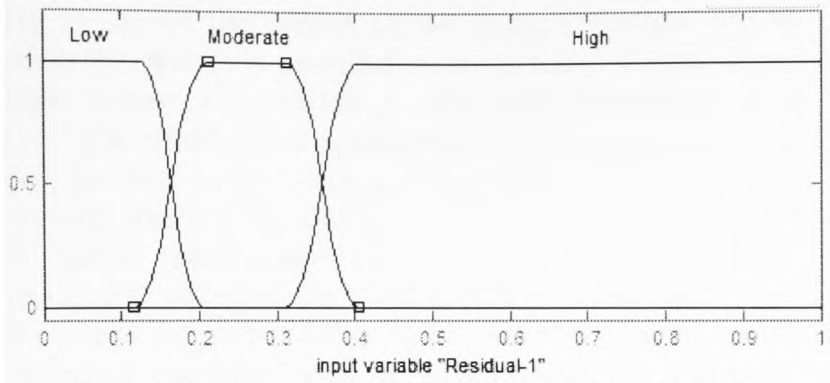

Figure 8. Input membership function of Residual-1

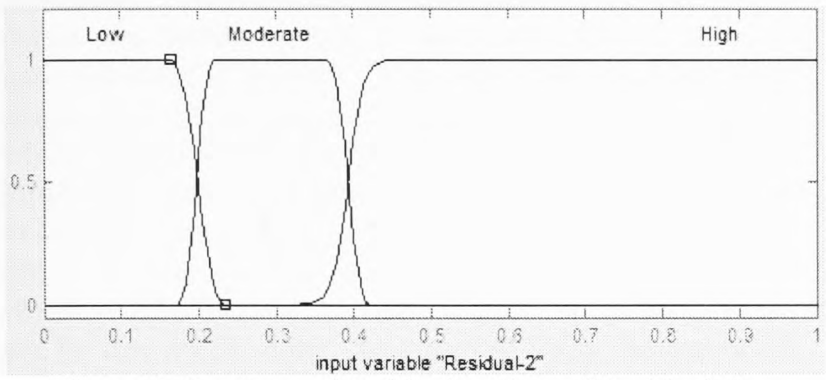

Figure 9. Input membership function of Residual-2

After the residual values are scaled and weighted they are processed according to set rules. The fuzzy logic rules are developed by looking at the residual values in different contact conditions e.g. in 40% adhesion level the value of residual of model-1 is 'Low', the value of residual of Model-2 is 'Low', the value of residual of model-3 is 'High' and the value of residual of model-4 is 'Moderate'. Similarly rules for other possible contact conditions are developed and some of the rules are given below.

If *Residual-1* is '*Low*' and *Residual-2* is '*Low*' and *Residual-3* is '*High*' and *Residual-4* is '*Moderate*' and T_t is 'T_8' then '$\mu \geq 40\%$'.
If *Residual-1* is '*Low*' and *Residual-2* is '*Low*' and *Residual-3* is '*Moderate*' and *Residual-4* is '*Low*' and T_t is 'T_3' then '$20\% \geq \mu \geq 10\%$'.

Output is determined by averaging the outcome of all the rules and final numeric output ranging from 0 to 100 is produced. The output fuzzy set is shown in Fig-10.

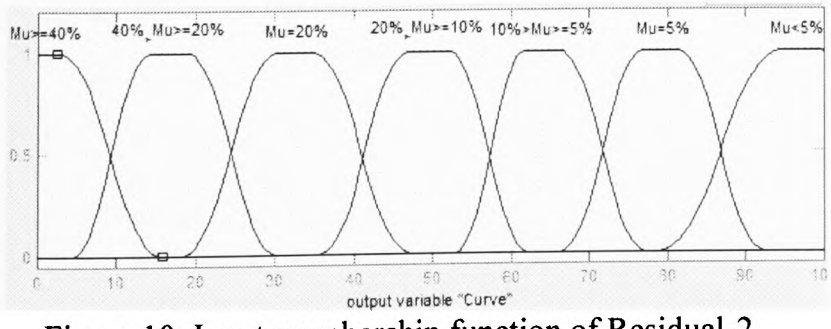

Figure 10. Input membership function of Residual-2

Final stage is to convert the fuzzy logic output into percentage adhesion. Which is done by fitting a sixth order polynomial on fuzzy output data set and following equation is obtained.

$$\mu = -2.213\times10^{-6} n_1^4 + 0.00042 n_1^3 - 0.0205 n_1^2 - 0.38 n_1 + 42 \quad (16)$$

where n_1 is fuzzy logic output and μ is percentage adhesion level. The simulations are run different contact conditions and the results are given below.

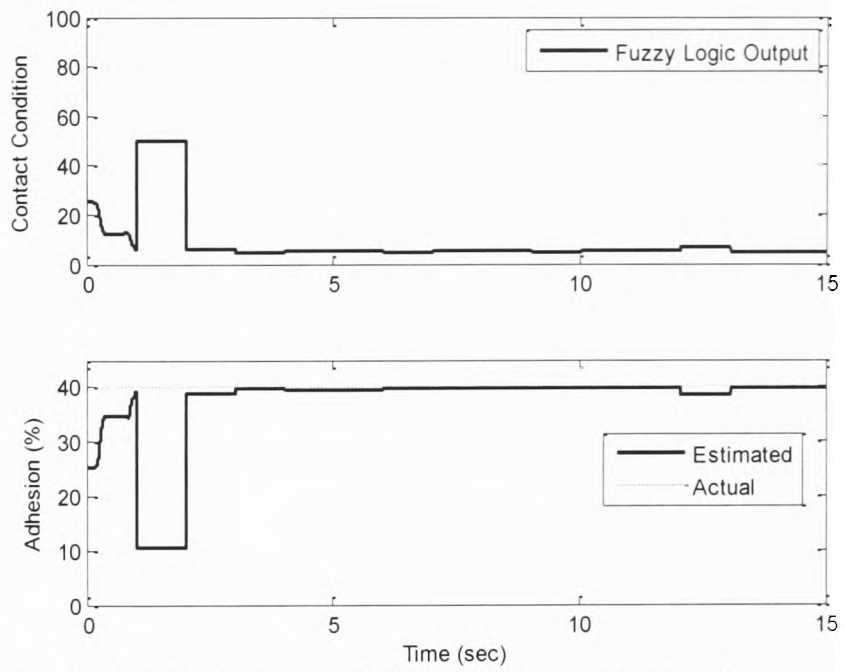

Figure 11. Simulation carried out using creep Curve C_A

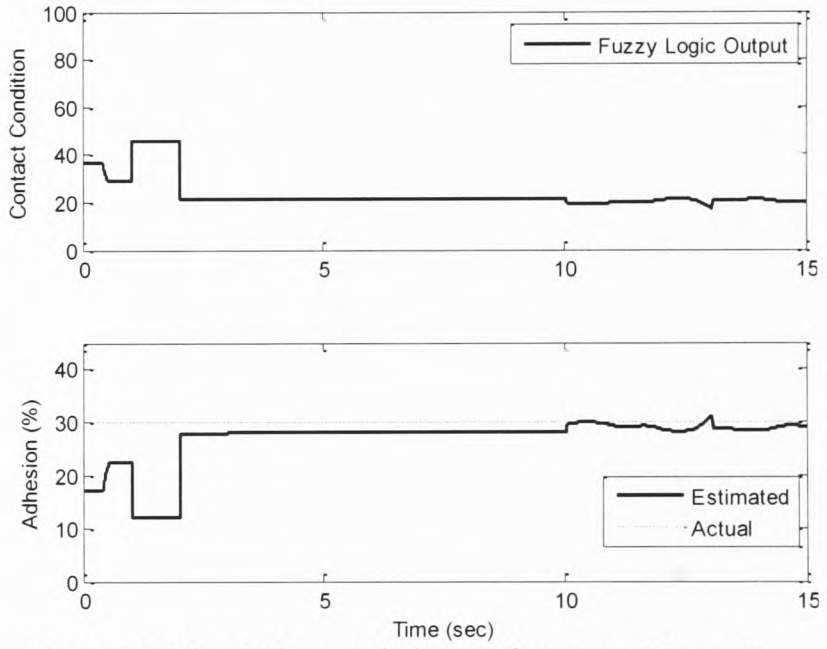

Figure 12. Simulation carried out using creep Curve C_C

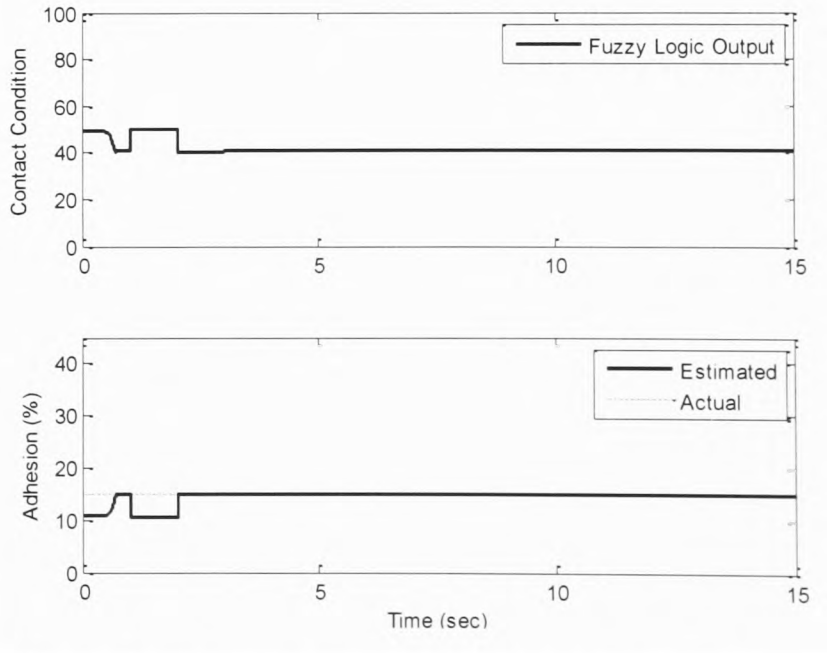

Figure 13. Simulation carried out using creep Curve C_F

Fig.11 shows the output of the fuzzy inference system when the system is operated on creep curve C_A. the fuzzy logic output is converted to adhesion information using (16). The system takes approximately two seconds to react and produce correct output. The delay in this case is 2 seconds which is the result of the time consumed by the PI to control the tractive torque steadily and 1 second is required to calculate the windowed rms of residuals. After 2 seconds the output fuzzy logic system is steady and the estimated adhesion level is almost equal to the actual adhesion level. Fig.12 shows the result obtained by simulating the Simulink model using creep curve C_C. Again the steady output is produced after a delay of approximately 2 seconds. It is worth noticing here that almost half of the delay is caused by the PI controller which during simulation gradually increases the tractive torque from zero until it reaches to saturation point and try to hold the operating point for sufficient amount of time in order to analyze the residuals. In practice while the wheelset already be in motion the amount of delay would not be that much. After the expected delay the estimated adhesion level is approximately equal to the actual adhesion level. The difference in the actual output and the estimated output is caused by several reasons that include inaccuracy in fuzzy interpretation and the error due to curve fitting formula. Similarly Fig.13 shows the result of the simulation when the wheelset is operated on creep curve C_F.

VI. Conclusion and Further Work

The problem of low adhesion and its adverse impact on train control systems and rail network operations present a significant technological challenge to the railway industry. Measures taken by railway industries around the world, such as sanding, water jetting, WSPs e.t.c, have solved this problems to some extent. But these measures are not sufficient to eliminate the problems completely. The adhesion detection method presented in this paper lays a scientific foundation for a new way forward. The simulation results presented in this paper affirm the potential of the idea presented. But further work, e.g. track testing and experimental validation, will be needed before it can be put into practice.

References

1. Watanabe, T. and A. Yamanaka. *Optimisation of readhesion control of Shinkansen trains with wheel–rail adhesion*. 1997.
2. Watanabe, T., et al. *Optimization of readhesion control of Shinkansen trains with wheel-rail adhesion prediction*. 1997.
3. Xia, F., C. Cole, and P. Wolfs, *An inverse railway wagon model and its applications.* Vehicle System Dynamics, 2007. **45**(6): p. 583-605.
4. C. Ward, P.W., E. Stewart, H. Li, R. Goodall, C. Roberts, T.X. Mei, G. Charles and R. Dixon, *Condition monitoring opportunities using vehicle based sensors* IMechE proceedings, Part F: Rail and Rapid Transit, Vol 225, No.2/2011, pp.202-218.
5. Charles, G., R. Goodall, and R. Dixon, *Model-based condition monitoring at the wheel-rail interface.* Vehicle System Dynamics, 2008. **46**(Supplement 1): p. 415-430.
6. Hussain, I. and M.T. X, *Identification of the Wheel Rail Contact Condition for the Traction and Braking Control* Proceedings of the 22nd International Symposium on Dynamics of Vehicles on Roads and Tracks, Manchester Metropolitan University, 14-19 August 2011.
7. Hussain, M.T.X., *Multi Kalman Filtering Approach for Estimation of Wheel-Rail Contact Conditions* Proceedings of the United kingdom Automatic Control Conferecne 2010, 2010: p. 459-464.
8. Hussain, M.T.X.a.A.H.J., *Modeling and Estimation of Nonlinear Wheel-rail Contact Mechanics.* Proceedings of the twentieth Intenational conference on System Engineering, 2009: p. 219-223.
9. Mei, T.X. and I. Hussain. *Detection of wheel-rail conditions for improved traction control.* in *Railway Traction Systems (RTS 2010), IET Conference on*. 2010.
10. Park, K.T., et al. *The characteristics of deriving control of crane [deriving read driving].* in *Industrial Electronics, 2001. Proceedings. ISIE 2001. IEEE International Symposium on*. 2001.
11. Mei, T.X., J.H. Yu, and D.A. Wilson, *A Mechatronic Approach for Anti-slip Control in Railway Traction.*
12. Mei, T., J. Yu, and D. Wilson, *A mechatronic approach for effective wheel slip control in railway traction.* Proceedings of the Institution of Mechanical Engineers, Part F: Journal of Rail and Rapid Transit, 2009. **223**(3): p. 295-304.
13. Li, H. and R. Goodall. *Modelling and analysis of a railway wheelset for active control*. 1998.
14. Mei, T.X. and R.M. Goodall, *Practical Strategies for Controlling Railway Wheelsets Independently Rotating Wheels.* Journal of Dynamic Systems, Measurement, and Control, 2003. **125**(3): p. 354-360.
15. Yu, J.H., T.X. Mei, and D.A. Wilson, *RE-ADHESION CONTROL BASED ON WHEELSET DYNAMICS IN RAILWAY TRACTION SYSTEM.*
16. Yu, J.H., *Re-adhesion control for AC traction system in railway application*, PhD Thesis, The University of Leeds, 2007.
17. Iwnicki, S., *Simulation of wheel-rail contact forces.* Fatigue & Fracture of Engineering Materials & Structures, 2003. **26**(10): p. 887-900.
18. Goodall, R. and H. Li, *Solid Axle and Independently-Rotating Railway Wheelsets-A Control Engineering Assessment of Stability.* Vehicle System Dynamics, 2000. **33**(1): p. 57-67.
19. Goodall, R., *Tilting trains and beyond. The future for active railwaysuspensions. 2. Improving stability and guidance.* Computing &

Control Engineering Journal, 1999. **10**(5): p. 221-230.

20. Beagley, T., I. McEwen, and C. Pritchard, *Wheel/rail adhesion--Boundary lubrication by oily fluids.* Wear, 1975. **31**(1): p. 77-88.
21. Polach, O., *Creep forces in simulations of traction vehicles running on adhesion limit.* Wear, 2005. **258**(7-8): p. 992-1000.
22. Charles, G. and R. Goodall. *Low adhesion estimation.* 2007: IET.
23. Mei, T. and R. Goodall. *LQG and GA solutions for active steering of railway vehicles.* 2002: IET.
24. I Hussain, a.T.X.M., *Identification of the Wheel Rail Contact Condition for the Traction and Braking Control.* Proceedings of the 22nd International Symposium on Dynamics of Vehicles on Roads and Tracks, Manchester Metropolitan University, 14-19 August 2011.

Estimation of wheel-rail contact conditions and adhesion using multiple model approach

I Hussain[a], TX Mei[a], and R T Ritchings[a]

[a] School of Computing Science & Engineering University of Salford

This paper presents the development of a multiple model estimation approach for the identification of the adhesion limit to overcome the problem of the wheel slip/slide at the rail wheel-rail contact. The contact characteristics at the rail wheel-rail interface are both highly nonlinear and subject to changes due to exposure to external contaminations. The detection of adhesion and its changes is therefore scientifically challenging, but would provide a critical information in the control of trains to avoid undesirable wear of the wheels/track but also the safety compromise of rail operations. The study exploits the variations in the dynamic behaviour of the railway wheelset caused by the contact condition changes and applies a bank of Kalman filters designed at selected operation points for the adhesion estimation. A fuzzy logic system is then developed to identify the contact conditions by examining the residuals from the Kalman filters.

Keywords: contact condition estimation; Kalman filters; railway wheelset; fuzzy logic.

1. INTRODUCTION

The wheel rail interaction is the most important element in the dynamics of railway vehicles and the contact forces that govern the dynamic performance of the railway vehicles vary substantially when the conditions of the rail surfaces change. The change in the contact condition can cause subsequent changes on the traction and braking responses of a rail vehicle, especially when the rail and/or wheel contact surfaces are contaminated by e.g. fallen tree leaves, oil or rain/snow, leading the well known problem of low adhesion. The low adhesion problem presents a serious challenge to the traction/braking control systems to avoid the problem of wheel slip/slide which can potentially cause the severe wear of wheel and rail surfaces, increase mechanical stress in the system, affect stability and lead to the inconsistent traction performance causing problems in train scheduling.

The most commonly used wheel slip protection schemes are based on controlling measured slip ratio (relative speed between a wheel and the train) to control the wheel rotational acceleration below a pre-defined threshold [1-4]. In some techniques adhesion coefficient is estimated by use of disturbance observer [5-8]. An indirect method has also been introduced that detects the slip by investigating the torsional vibrations in the wheelset axle [9-11]. The controllers based on these techniques are reactive in nature and only if wheel slip/slide is detected.

However there is a real need for an effective solution to provide the real time information about the maximum adhesion level which could then be used to determine appropriate provision of the tractive effort in either traction or braking in an optimized manner to make the most out of the wheel-rail contact conditions without the risk of causing the undesirable wheel slip/slide. The main technical difficulty for developing such a solution is due to the fact the contact mechanics at the wheel-rail interface are extremely complex. The relationship between the creepage (relative velocity between the wheel and rail surfaces) and the contact forces, i.e. the creep

curve, is known to be highly non-linear, but also can change quickly due to contaminations.

Model based estimation approach has been proposed previously to estimate the initial slope of the creep curves (in the linear region) or the contact forces [12-13], but it is not yet clear how the outcome could be correlated to generate adhesion information.

This paper studies a multiple Kalman filter approach to provide real time information about contact condition variations by exploiting the fact that the dynamic behaviour of a railway wheelset can change substantially in response to different track conditions. The multiple model based estimation and identification methods have been used for other applications previously [14-15] and are well suited to tackle the problems of this kind due to the non-linear nature of wheelset dynamics. A bank of Kalman filters will be developed to represent different operating points/conditions, the residuals of which are then processed using fuzzy logic reasoning to identify the contact conditions. The idea was first presented by the authors using only single creep curve representing good/dry contact condition [16-18]. This paper however takes into account various different creep curves representing different contact conditions. The development is based on a single railway wheelset, but can be readily extended for full vehicles.

2. Wheelset modelling

A conventional solid axle wheelset with coned wheels is used in the study and the longitudinal, lateral, rotational and yaw dynamics of the wheelset are included in the model. The bounce and roll motions are not considered in that case as they are constrained by the track. The track irregularities in the lateral direction are considered because of its direct effect on yaw and lateral dynamics. The railway wheelset dynamic behaviours are dominated by the creep forces generated at the wheel rail contact patches. These creep forces are the result of creepages which are the relative speed of the wheels to rail and can be characterized as lateral (λ_y) and longitudinal creep (λ_x) in accordance with the direction of motion as given in equations 1-3.

$$\lambda_{xL} = \frac{r_o\omega_L - v}{v} + [\frac{L_g\dot{\psi}}{v} + \frac{\gamma(y - y_t)}{r_o}] \tag{1}$$

$$\lambda_{xR} = \frac{r_o\omega_R - v}{v} - [\frac{L_g\dot{\psi}}{v} + \frac{\gamma(y - y_t)}{r_o}] \tag{2}$$

$$\lambda_y = \lambda_{yR} = \lambda_{yL} = \frac{\dot{y}}{v} - \psi \tag{3}$$

where the subscripts L and R represent left and right wheels, r_o is radius of the wheels, v is vehicle forward speed, γ is the conicity of the wheels, Ψ is yaw angle, L_g is track half gauge, ω_L and ω_R are the angular velocities of the left and right wheels respectively, y is lateral motion, $\dot{y}$ is speed associated with lateral motion and y_t is track disturbance in lateral direction. The total creepage λ_j is the combination of the lateral and longitudinal creepages.

$$\lambda_j = \sqrt{\lambda_{ij}^2 + \lambda_{ij}^2} \quad i = x, y \text{ and } j = L, R \tag{4}$$

The total creep force F_j is a nonlinear function of the total creepage and can be represented using equation 5. For small creep values (microslip) F_j varies linearly with the creep. As the slip velocity is increased it varies nonlinearly and reaches to maximum value (saturation) and decreased beyond that point if the slip velocity is increased further as shown in Fig 1. However, this non-linear relationship can be severely affected by different contact environments such as the contaminations and the weather and the creep force is subject to large and uncertain variations. A selection of creep curves representing different contact conditions are illustrated in Fig 1.

$$F_j = \mu_j N_j \qquad j = L, R \tag{5}$$

The distribution of the contact forces in the longitudinal and lateral directions is thoroughly studied by Polach [19] and can be represented using equation 6.

$$F_{ij} = F_j . \frac{\lambda_{ij}}{\lambda_j}, \qquad i = x, y \text{ and } j = L, R \tag{6}$$

The equations of motion of the wheelset are given below 7-12.

$$M_v \ddot{x} = \frac{\mu_R N_R}{\sqrt{\lambda_{xR}^2 + \lambda_{yL}^2}} \left[\frac{r_o \omega_R - v}{v} - [\frac{L_g \dot{\psi}}{v} + \frac{\gamma(y - y_t)}{r_o}] \right] + \frac{\mu_L N_L}{\sqrt{\lambda_{xL}^2 + \lambda_{yL}^2}} \left[\frac{r_o \omega_L - v}{v} + [\frac{L_g \dot{\psi}}{v} + \frac{\gamma(y - y_t)}{r_o}] \right] \tag{7}$$

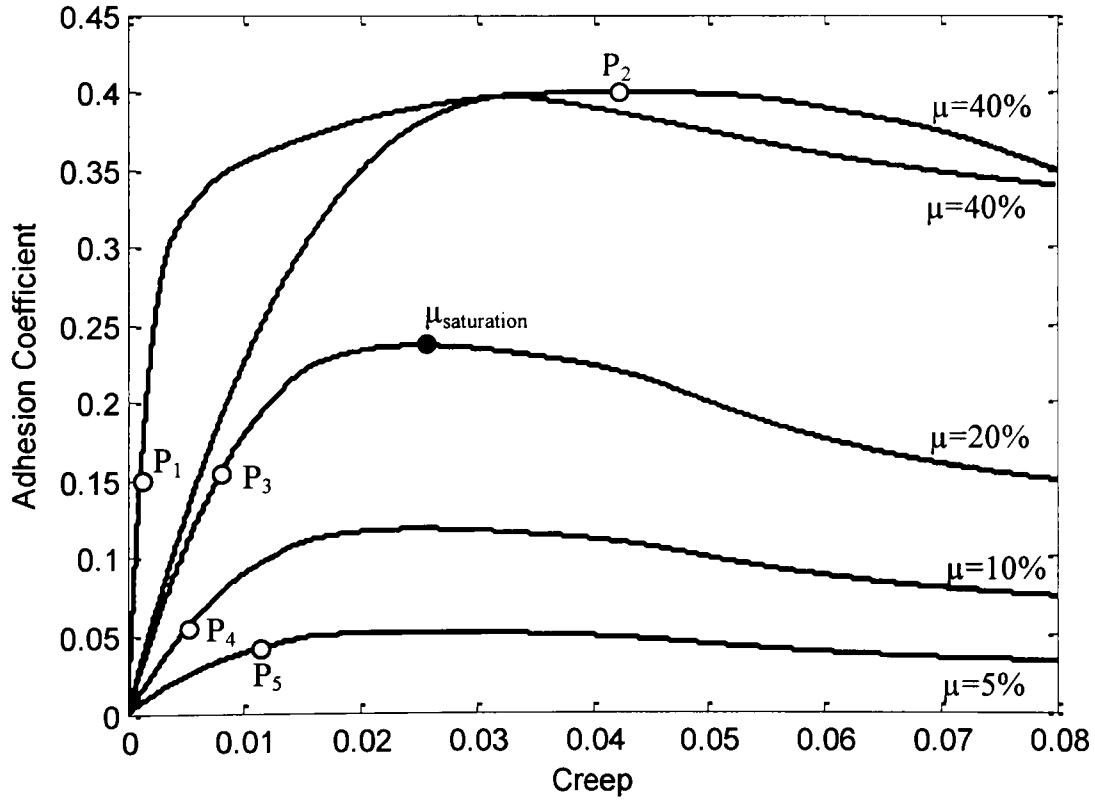

Fig. 1. Creep Curves

$$I_w \ddot{\psi} = \frac{\mu_R N_R}{\sqrt{\lambda_{xR}^2 + \lambda_{yL}^2}} \left[\frac{r_o \omega_R - v}{v} - [\frac{L_g \dot{\psi}}{v} + \frac{\gamma(y - y_t)}{r_o}] \right] L_g - \frac{\mu_L N_L}{\sqrt{\lambda_{xL}^2 + \lambda_{yL}^2}} \left[\frac{r_o \omega_L - v}{v} + [\frac{L_g \dot{\psi}}{v} + \frac{\gamma(y - y_t)}{r_o}] \right] L_g \tag{8}$$
$$- k_w \psi$$

$$m_w \ddot{y} = -\frac{\mu_L N_L}{\sqrt{\lambda_{xL}^2 + \lambda_{yL}^2}} \left[\frac{\dot{y}}{v} - \psi \right] - \frac{\mu_R N_R}{\sqrt{\lambda_{xR}^2 + \lambda_{yL}^2}} \left[\frac{\dot{y}}{v} - \psi \right] + F_c + F_g \tag{9}$$

$$I_R\dot{\omega}_R = T_t - K_s\theta_s - r_o\frac{\mu_R N_R}{\sqrt{\lambda_{xR}^2+\lambda_{yL}^2}}[\frac{r_o\omega_R - v}{v} - (\frac{L_g\dot{\psi}}{v} + \frac{\gamma(y-y_t)}{r_o})] \quad (10)$$

$$I_L\dot{\omega}_L = K_s\theta_s - r_o\frac{\mu_L N_L}{\sqrt{\lambda_{xL}^2+\lambda_{yL}^2}}[\frac{r_o\omega_L - v}{v} + (\frac{L_g\dot{\psi}}{v} + \frac{\gamma(y-y_t)}{r_o})] \quad (11)$$

$$T_s = k_s\int(\omega_R - \omega_L)dt + C_s(\omega_R - \omega_L) \quad (12)$$

Where M_v is the mass of the vehicle $\ddot{x}$ is vehicle acceleration, I_w is yaw moment of inertia, k_w is a yaw stiffness necessary to stabilise the wheelset, m_w is mass of the wheelset, $\ddot{y}$ is lateral acceleration, F_c is centrifugal force which is taken into consideration when the wheelset runs on a curved track, F_g is gravitational stiffness force related to the lateral displacement and roll angle of the wheelset. The tractive torque T_t is applied to one side of the wheelset (right side in this case) the other wheel is driven by the torsional torque T_s. $\theta_s=\int(\omega_R-\omega_L)dt$ and T_R and T_L are the tractive torques of the right and left wheels respectively. k_s is torsional stiffness of the shaft connecting two wheels and C_s is material damping of the shaft, which is usually very small.

3. Estimation scheme

The model based techniques such as Kalman filters have been used successfully for the estimation of states as well as parameters.[13, 20-21]. However, the use of a single estimator (through linerisation and/or extension) has been found insufficient to tackle the complex problem, because of the high level of non-linearity and uncertainty (i.e. time varying) associated with the wheel-rail contact mechanics. A multiple model based estimation scheme is therefore proposed and the system scheme is shown in Fig 2. Each of the Kaman filters in the filter bank is designed and optimally tuned to operate in a specific contact condition. All the Kalman filters are run in parallel and the normalized rms value of the residuals with moving time windows is calculated. The rms values of the residuals are then fed to the fuzzy logic system which examines the rms values along with the tractive torque to identify the different contact conditions. The nonlinear wheelset model introduced in section II is used to simulate the wheelset dynamic behaviour and to assess the effectiveness of the proposed scheme.

2.1 Kalman filter design

The plain view dynamics (lateral and yaw degrees of freedom) are used to design the Kalman filter to simplify the design. The plan view model represents the dominant wheelset dynamic properties and is nearly always used for studies of this kind [12-13, 18, 22]. Due to the presence of nonlinearities in the wheel-rail contact mechanics, the creep forces are linearized. The first order small signal approximation of the longitudinal creep force of the right wheel is given below.

$$\Delta F_{xR} = g_{11}\lambda_{xR} + g_{12}\lambda_{yR} \quad (13)$$

where g_{11} and g_{12} represent the slope of the curve at the point of linearization. The lateral creep forces and those for the left wheel are linearized similarly and the small signal model of the yaw and lateral dynamics is then obtained as given in equation 14. The model is reformulated to include the track input y_t as one of the states as it is not

easily measurable in practice and cannot be treated as a simple plant disturbance because it has a significant effect on the lateral and yaw dynamics [22]. In the reformulated equation lateral displacement of the wheelset is replaced by the estimator state representing the lateral displacement relative to the track, ie. Δy_w-Δy_t. A small constant N is added to the reformulated equation to keep the system matrix full ranked which will allow the Kalman filters to converge [22].

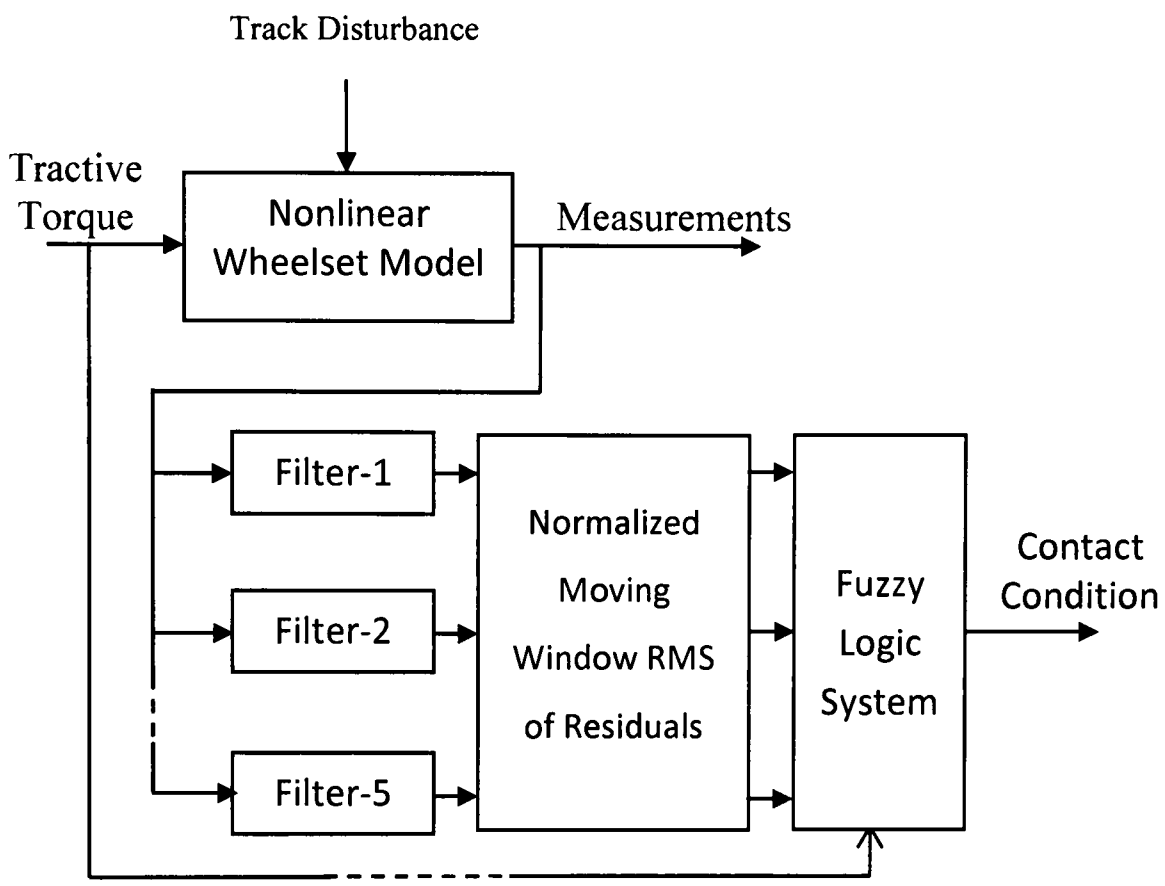

Fig. 2. Estimation Scheme

$$\frac{\mathrm{d}}{\mathrm{dt}}\begin{bmatrix}\Delta\psi\\ \Delta\dot{y}\\ \Delta\dot{\psi}\\ \Delta y_t\\ \Delta y-\Delta y_t\end{bmatrix}=\begin{bmatrix}0 & 0 & 1 & 0 & 0\\ \frac{2g_{22}}{m_w} & -\frac{2g_{22}}{vm_w} & 0 & 0 & 0\\ -\frac{k_w}{I_w} & 0 & -\frac{2L_g^2 g_{11}}{vI_w} & 0 & -\frac{2L_g\gamma g_{11}}{r_o I_w}\\ 0 & 0 & 0 & N & 0\\ 0 & 1 & 0 & 0 & 0\end{bmatrix}\begin{bmatrix}\Delta\psi\\ \Delta\dot{y}\\ \Delta\dot{\psi}\\ \Delta y_t\\ \Delta y-\Delta y_t\end{bmatrix}+\begin{bmatrix}0\\ 0\\ 0\\ 1\\ -1\end{bmatrix}\Delta\dot{y}_t \quad (14)$$

Two sensors (A gyro sensor to measure the yaw rate and an accelerometer to measure the lateral acceleration) are found to be sufficient to detect the contact condition.

$$z(t)=\begin{bmatrix}0 & 0 & 1 & 0 & 0\\ \frac{2g_{22}}{m_w} & -\frac{2g_{22}}{vm_w} & 0 & 0 & 0\end{bmatrix}\begin{bmatrix}\Delta\psi\\ \Delta\dot{y}\\ \Delta\dot{\psi}\\ \Delta y_t\\ \Delta y-\Delta y_t\end{bmatrix}+v \quad (15)$$

Where v is a vector representing noise level of the sensors with the covariance R and Q is said to be the process noise covariance. By properly tuning the covariance matrix for the track noises, process noise covariance and selecting suitable value for N the performance of the Kalman filter can be optimized at different operating points to form a bank of Kalman filters. Five different creep curves, representing high to very

low adhesion conditions, are used. After a thorough study of behaviour of Kalman filters in different contact conditions and keeping in view the practical aspects, only five Kalman filters are used to identify the contact condition. The filters-1 to filter-5 are optimally tuned at P_1 (linear region of the creep curve where μ=40%), P_2 (saturation point of the creep curve where μ=40%), P_3 (nonlinear region away from saturation region of the creep curve where μ=20%), P_4 (linear region of the creep curve where μ=10%) and P_5 (nonlinear region near to saturation region of the creep curve where μ=5%) respectively. The wheelset dynamics on selected operating points are entirely different from each other avoiding any redundant Kalman filters. Kalman filter tuned at P_1 is robust enough to work at the linear region of the other creep curves as well with a slight increase in error. The results of state estimation carried out in the linear region of the creep curve representing 40% overall adhesion are shown in Figs 3 and 4, where filter parameters Q ($6\times10^{-9}I_5$) and R ($diag[9\times10^{-8}, 6\times10^{-11}]$) are found to give the best estimation.

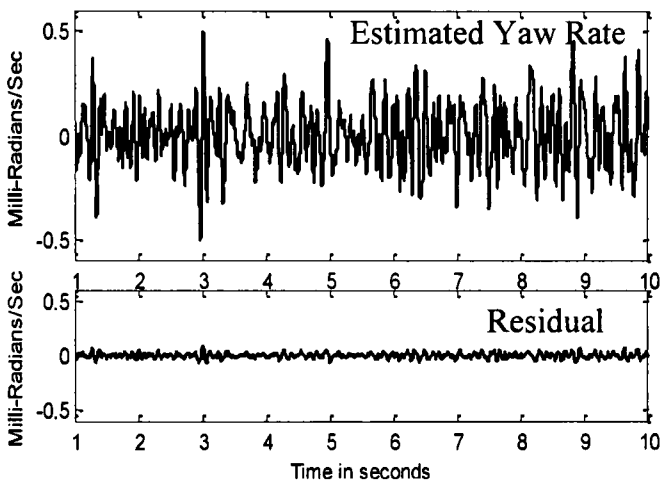

Fig-3. Yaw Rate ($\Delta\dot{\psi}$) Estimation

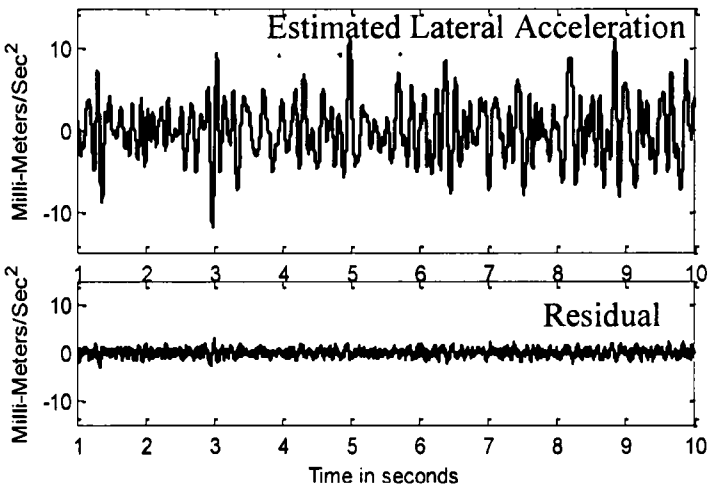

Fig-4. Lateral Acceleration ($\Delta\ddot{y}$) Estimation

2.2 *Fuzzy logic design*

Normalized rms values of the residuals from the bank of filters are calculated using a moving time window and processed further with fuzzy logic reasoning in the proposed monitoring system to identify the contact conditions. There are various industrial applications in which fuzzy logic is used as data selector [23-24]. The detailed view of the fuzzy logic system is shown in Fig 5. The rms residual from each of the filters has an associated membership function (e.g. MF1 for residual of filter-1 and so on). Figure-6 shows the membership function of input R_1 (R_1 is the normalized root mean square value of the residual of the filter-1 calculated using equation-16). The horizontal axis represents the normalized value of residual. The value of residual then determines the magnitude of participation of the input and the category it belongs to (e.g. 'Large' if the residual value is 0.6 and the degree of membership is 1).

$$R_1 = \frac{\frac{1}{\Delta t}\int_{t-\Delta t}^{t}(R_1(t)^2 dt}{\sqrt{\frac{1}{\Delta t}\int_{t-\Delta t}^{t}(R_1(t)^2 dt + \frac{1}{\Delta t}\int_{t-\Delta t}^{t}(R_2(t)^2 dt + \ldots + \frac{1}{\Delta t}\int_{t-\Delta t}^{t}(R_5(t)^2 dt}} \qquad (16)$$

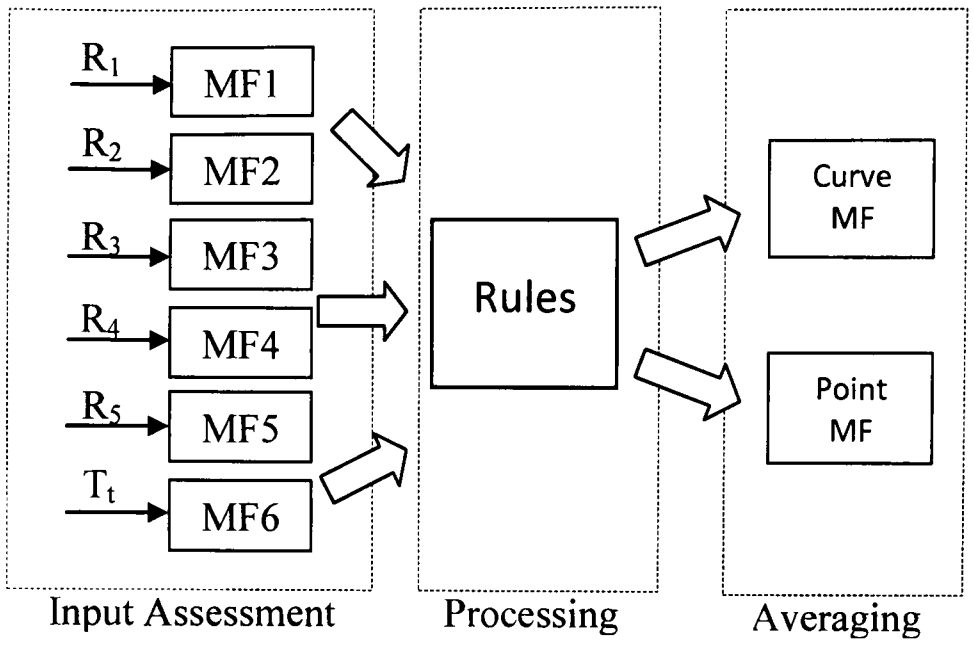

Fig. 5. Fuzzy Logic System

The numbers of categories in each MF depend upon the variation of residual value of filters in different operating conditions. For instance, the value of the residual of filter-1 remain approximately same for creep curves representing overall adhesion less than 20% therefore only three categories are found to be sufficient to distinguish the operating point information. However in the case of filter-2 the residual values are substantially different for the different curves and hence 4 categories are required to distinguish the operating conditions.

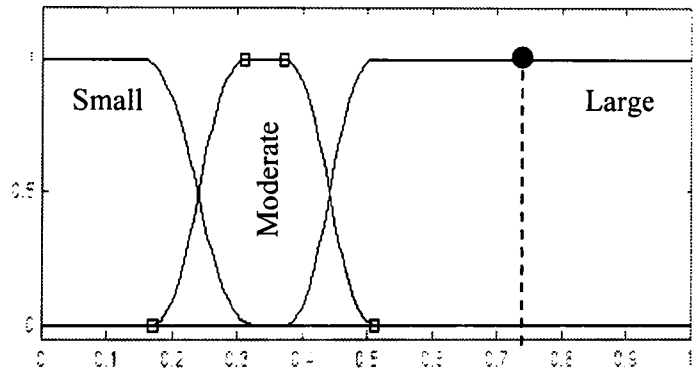

Fig. 6. Membership function of Residual of Filter-1

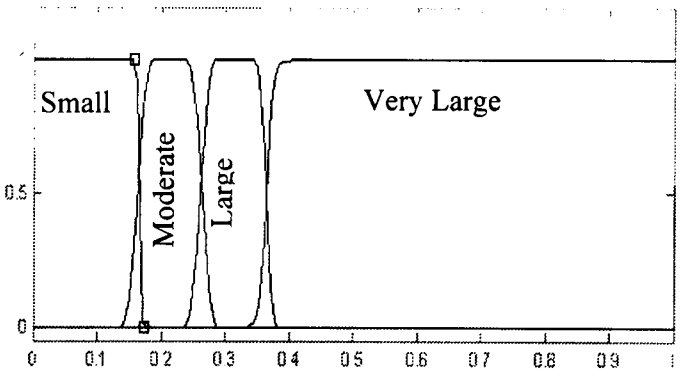

Fig. 7. Membership function of Residual of Filter-2

The boundaries and the shape of the categories are formed by carefully analyzing the residual values at each operating point. The general idea of setting the boundaries of categories is to divide the entire horizontal space into three categories, near, far and very far. This will allow extracting the maximum information by using least possible number of filters. For instance in figure 6 the residual value falling in 'Small' indicates that the wheelset is operating in good contact condition ($\mu \approx 40\%$) and the residual value falling in 'large' indicates the wheelset is operating in a relatively load adhesion condition ($10\% > \mu \geq 5\%$) ruling out rest of the curves and making it easy for fuzzy logic system to make decisions. The shape of the membership functions are chosen on the basis of behaviour of residual values which varies gradually and can have same values at multiple operating points. A triangular or step functions would not be suitable in those circumstances. The membership functions for the rest of the inputs are formed in similar way.

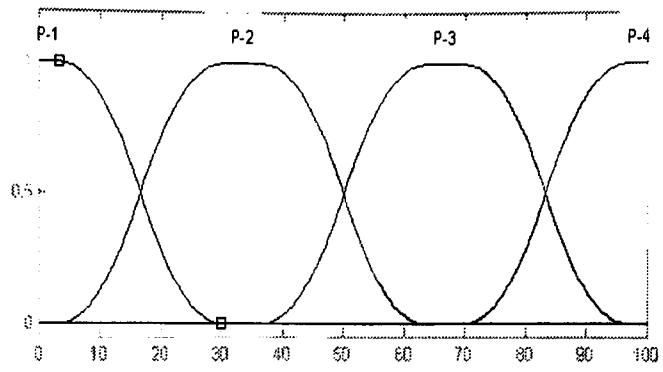

Fig. 8. Output Membership function-1 identifying operating point

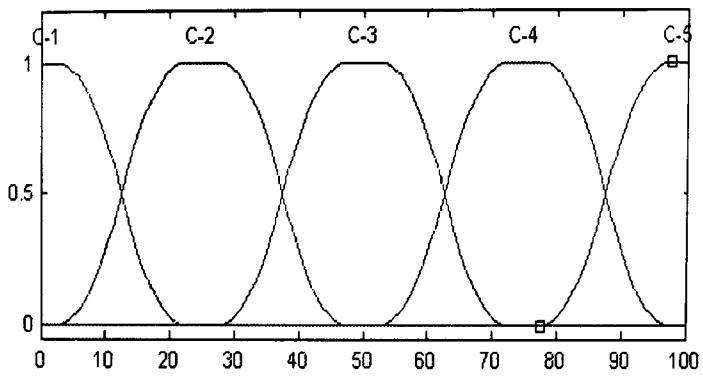

Fig. 9. Output Membership function-2 identifying Creep curve

Once all the inputs are scaled and combined they are processed according to the rules. The resulting outputs from all the individual rules are averaged and weighted by output membership functions. There are two output membership functions. One for determining the creep curves (figure-9) and other for operating points (figure-8). The fuzzy logic system is designed to identify the contact condition based on following figure. This figure shows a typical variation of adhesion with the creep. The outputs of fuzzy logic are numeric on a scale of 0 to 100. Each numeric value represents specific adhesion level and the operating point. For example the values of output membership function-1=33 and output membership function-2=50 suggest that the wheelset is operating in nonlinear region and the overall adhesion is 20%. On each curve there are four designated point one in linear region (i-e. P_a), two in nonlinear region (i.e. P_b and P_c) such that P_b is labelled as nonlinear region away from saturation and P_c is labelled as nonlinear region near to saturation and fourth point is the saturation point of the creep curve (i.e. P_d). The relation between the fuzzy logic outputs and the operating condition is given by the following equations.

$$\mu = -4.714\times10^{-6} n_1^4 + 0.0011 n_1^3 - 0.08 n_1^2 + 1.8 n_1 + 33 \qquad (17)$$

Where μ in this equation is adhesion level in percentage and n_1 is the numeric fuzzy logic output for adhesion level. If the operating point in the linear region is represented by 1 and the operating point in the non linear and saturation regions are represented by 2,3 and4 respectively then the relation between fuzzy logic out and the operating point is given below.

$$P = 1.714\times10^{-6} n_2^3 - 0.00027 n_2^2 + 0.044 n_2 + 0.79 \qquad (18)$$

Where P is the operating point on a specific curve and n_2 is the fuzzy logic output for operating point.

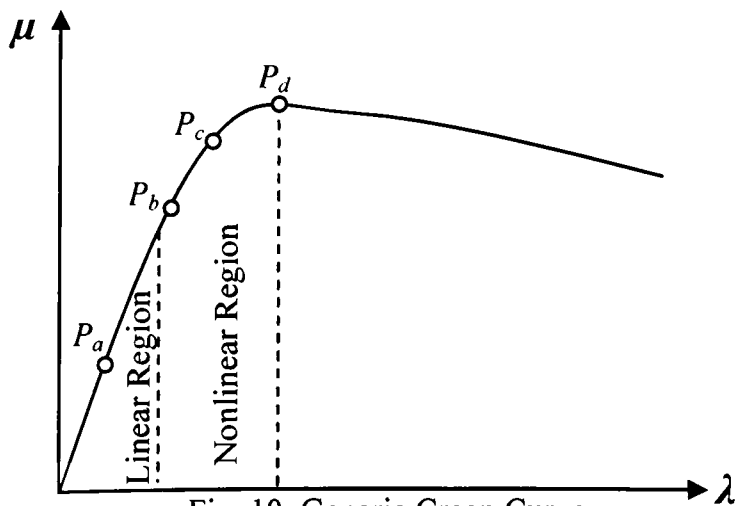

Fig. 10. Generic Creep Curve

4. Contact condition estimation

In railway research, it is a normal practice to use computer simulation in the study of new concepts and/or vehicle designs due to the difficulty and high cost of real track testing. Therefore a Simulink model of the proposed estimation scheme as presented in section-II is used for performance assessment. Figure-11 shows the residual of lateral acceleration of all the filters when the wheelset is operated in the linear region of the creep curve representing 40% adhesion. The residual of filter-1 is the smallest because the filter-1 is optimally tuned to operate in the linear region. Similarly in figure-12 the residual of filter-3 has minimum value and residual of filter-1 is increased as the wheelset operating point moves away from linear region and finally reaches to its maximum value as shown in figure-13 where wheelset is operated in the nonlinear region of the creep curve representing 5% adhesion. Conclusively it is clear that the residual of each filter tends to produce the lowest residual when the wheelset is operated at the point where it is optimally tuned to operate and increase gradually when the operating point is moved away from that point.

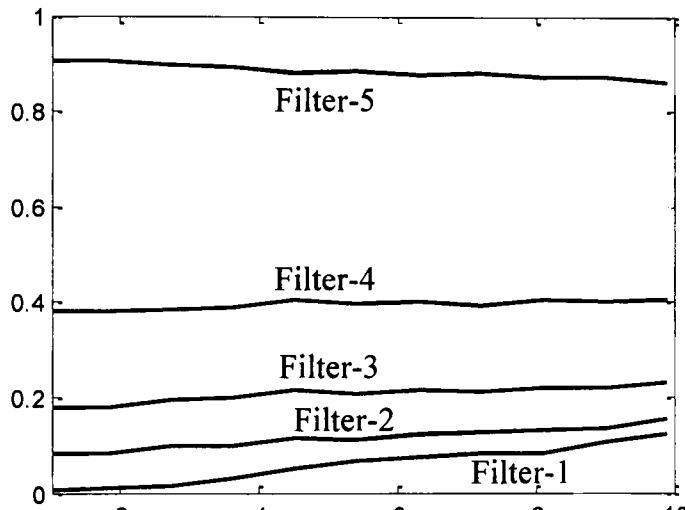

Fig. 11. Residuals when the wheelset is operated in the linear region (μ=40%)

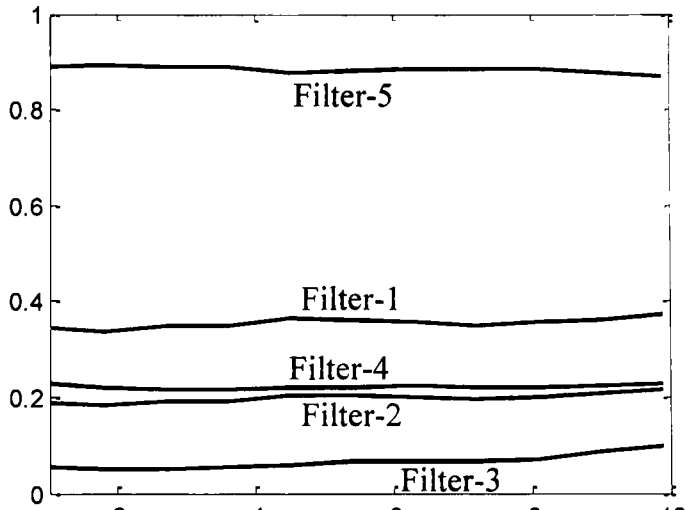

Fig. 12. Residuals when the wheelset is operated in the nonlinear region (μ=40%)

In some cases it is difficult to differentiate the two operating points because the residuals produce similar combination. This happens when the two operating points located on different creep curves have the similar dynamic responses. In such cases the tractive torque can be analyzed to distinguish between the two operating points. The Kalman filters show great agreement with the theory and the results show the good consistency of the Kalman filters. From the results it is evident that the residual values give a unique combination at each operating point of the creep curves that makes the contact condition easily identifiable using a fuzzy logic system by building the certain rules (as given below). A table containing the values of the residuals of lateral acceleration is developed by simulating the model at various different operating points. The rules are developed by looking at the values of residuals in the table. The output is produced in the form of a numeric value representing the operating point and the adhesion value. Some fuzzy logic outputs are shown in following figures. The vertical axis of the figures show the numeric values produced by fuzzy logic outputs representing specific adhesion level and operating point.

If R_1 is '*Small*' and R_2 is '*Small*' and R_3 is '*Moderate*' and R_4 is '*Large*' and R_5 is '*Large*' and T_t is T_5 then contact condition is 'μ=*40%*' and Operating Point is *'Linear Region'*.

If R_1 is '*Large*' and R_2 is '*Moderate*' and R_3 is '*Moderate*' and R_4 is '*Small*' and R_5 is '*Moderate*' and T_t is T_7 then contact condition is 'μ=*40%*' and the operating point is *'Saturation Region'*.
If R_1 is '*Moderate*' and R_2 is '*Moderate*' and R_3 is '*Small*' and R_4 is '*Moderate*' and R_5 is '*Large*' and T_t is T_4 then contact condition is 'μ=*20%*' and Point is *'nonlinear region away from saturation'*.

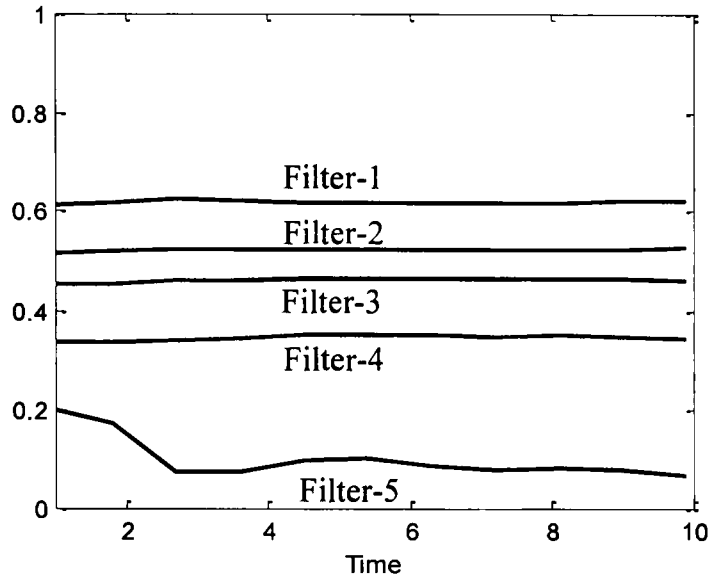

Fig. 13. Residuals at P_{53}

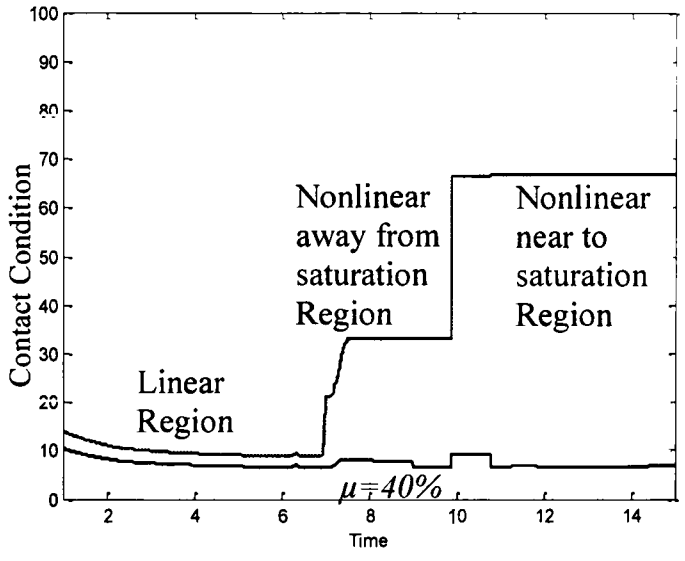

Fig. 14. Fuzzy Logic Output shows the operating point is changed during the simulation (μ=*40%*)

Fig14 shows the fuzzy logic output when the operating point of the wheelset is changed during the simulation. At first wheelset is operating in the linear region then after 5 seconds tractive torque is increased causing the operating pint to move in the nonlinear region. There is small delay which is caused by the time consumed by the *PI* controller to adjust the tractive torque to force the operating point and plus the time consumed in calculating the windowed rms of the residuals. When the tractive torque is increased further the operating point moves towards the saturation.

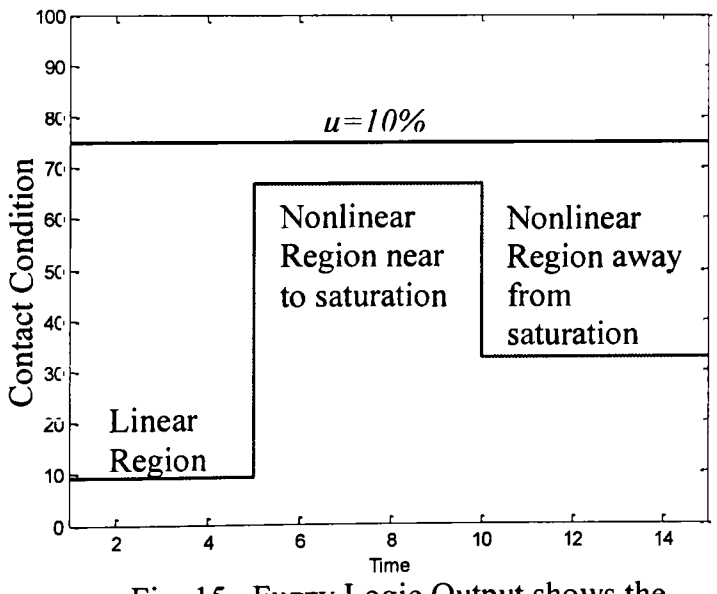

Fig. 15. Fuzzy Logic Output shows the operating point is changed during simulation (μ=*10%*)

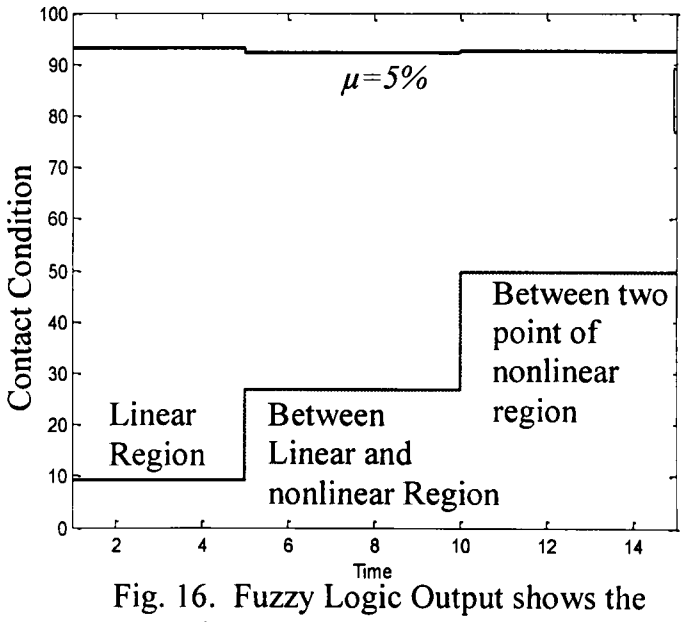

Fig. 16. Fuzzy Logic Output shows the operating point is changed from during simulation (μ=*5%*)

In Fig-15 the wheelset is operated on creep curve representing 10% adhesion level. The operating point of the wheelset is varied after 6 seconds from linear region to nonlinear region near to saturation point and then after 9 seconds to nonlinear region away from saturation point. In Fig-16 the wheelset is operated on creep curve representing 5% adhesion level. Here the wheelset is operating on the operating points which are not used in filter design (such as between linear and nonlinear). The tractive

torque is varied manually to drive the wheelset at desired operating points. The fuzzy logic outputs show the wheelset operating point is changed from linear region to the operating point located between linear and nonlinear regions. Referring to Fig-8 the numeric value 27 in Fig-16 suggests that the point is located nearer to nonlinear region After 9 seconds the operating is changed again but this time the numeric value 50 suggests that the point is located exactly in the middle of two operating points in nonlinear region.

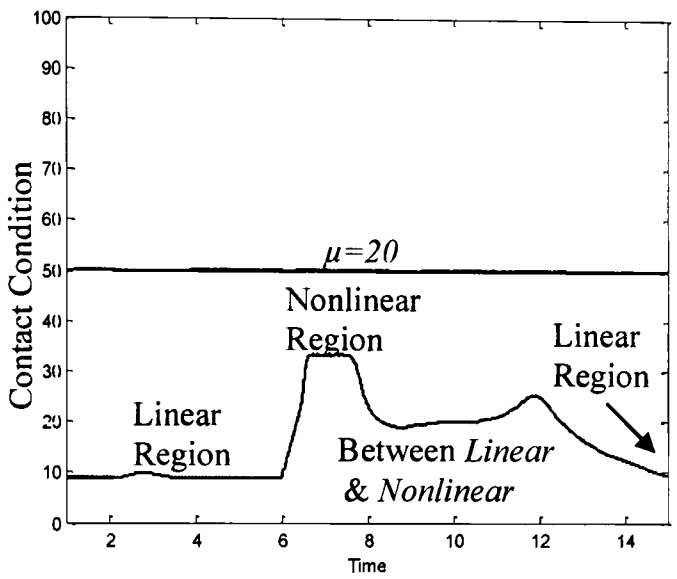

Fig. 17. Fuzzy Logic Output shows the operating point is randomly changed

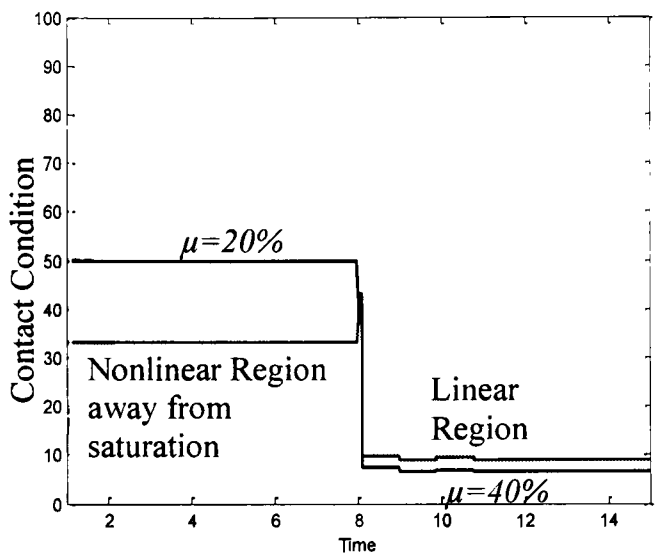

Fig. 18. Fuzzy Logic Output shows the large variation in the operating point

In Fig-17 the operating point is randomly changed by randomly varying the tractive torque. The wheelset is operated on creep curve representing 20% adhesion level. When the tractive torque is increased, the operating is moved up on the creep curve from linear region to nonlinear region away from saturation. After a couple of second, the tractive torque is slightly reduced therefore the operating point is moved down the curve and the wheelset is operated on the point between linear and nonlinear region. Finally the tractive torque is further reduced causing the wheelset to operate back in linear region. In figure-18 the wheelset is subjected to a large variation in contact condition and not only the operating point is changed during the simulation but the creep curve is also switched. First the wheelset is operated on the creep curve representing 20% adhesion level. After 6 seconds the condition is changed to creep curve representing 40% adhesion level keeping the tractive torque same. The fuzzy logic output indicates the condition is changed to 40% adhesion level and the wheelset is now operating in the linear region. Simulation is also carried out by using the creep curves other than five creep curves used in Kalman filter design (Fig-1). The result of the simulation is shown in Fig-19. The creep curve used represents 15% adhesion level. At the start of the simulation wheelset is operating at adhesion level of 10%. During the simulation the condition is switched to new curve as indicated by the fuzzy logic output.

5. Conclusion

The real time information about the wheel-rail contact condition is necessary to ensure the consistent traction and braking performance of the railway vehicles. This paper has presented a novel technique to identify the wheel-rail contact conditions which are difficult to measure in practice. Different creep curves representing different contact conditions are used in simulations and the results are found to

produce robust and accurate estimations. The fuzzy reasoning developed in the study has helped to identify different wheel-rail conditions, not only at the operating points where the Kalman filters are designed/tuned but also for different operating points and/or contact characteristics' to account for a variety of conditions in practical applications.

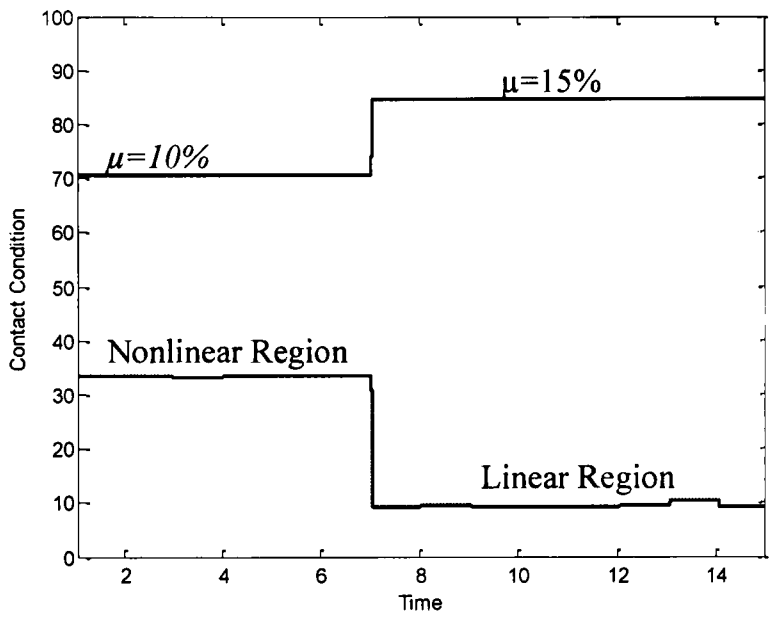

Fig. 19. Fuzzy Logic Output shows the operating point is changed from during the simulation

References

1. Schwartz, H. and R. Kresse. *Implementation of an advanced wheel creep control with searching strategy on a light rail vehicle*. 1997: PROCEEDINGS PUBLISHED BY VARIOUS PUBLISHERS.
2. Yasuoka, I., et al. *Improvement of re-adhesion for commuter trains with vector controltraction inverter*. 1997.
3. Watanabe, T. and A. Yamanaka. *Optimisation of readhesion control of Shinkansen trains with wheel–rail adhesion*. 1997.
4. Watanabe, T., et al. *Optimization of readhesion control of Shinkansen trains with wheel-rail adhesion prediction*. 1997.
5. Ohishi, K., et al. *Anti-slip control of electric motor coach based on disturbance observer*. 1998.
6. Shimizu, Y., et al. *Anti-slip re-adhesion control based on disturbance observer considering bogie vibration*. 2007.
7. Hata, T., et al. *Anti-slip re-adhesion control based on speed sensor-less vector control and disturbance observer for electric multiple units, series 205-5000 of East Japan Railway Company*. 2003.
8. Ohishi, K., et al. *Anti-slip Readhesion Control of Electric Commuter Train Based on Disturbance Observer Considering Bogie Dynamics*. 2006.
9. Mei, T., J. Yu, and D. Wilson, *A mechatronic approach for effective wheel slip control in railway traction.* Proceedings of the Institution of Mechanical Engineers, Part F: Journal of Rail and Rapid Transit, 2009. **223**(3): p. 295-304.
10. Mei, T.X., J.H. Yu, and D.A. Wilson, *Mechatronic approach for effective wheel slip control in railway traction.* Proceedings of the Institution of Mechanical Engineers, Part F: Journal of Rail and Rapid Transit: p. 1-10.
11. Mei, T.X., J.H. Yu, and D.A. Wilson, *Wheelset dynamics and wheel slip detection.* STECH2006, Chengdu, China, 2006.

12. Charles, G. and R. Goodall. *Low adhesion estimation*. 2007: IET.
13. Charles, G., R. Goodall, and R. Dixon, *Model-based condition monitoring at the wheel-rail interface.* Vehicle System Dynamics, 2008. **46**(Supplement 1): p. 415-430.
14. Smith, K., C. Rahn, and C. Wang, *Model-based electrochemical estimation and constraint management for pulse operation of lithium ion batteries.* Control Systems Technology, IEEE Transactions on, 2010. **18**(3): p. 654-663.
15. Ru, J. and R. Li, *Variable-structure multiple-model approach to fault detection, identification, and estimation.* Control Systems Technology, IEEE Transactions on, 2008. **16**(5): p. 1029-1038.
16. Mei, H., *Detection of wheel-rail contact conditions for improved traction control.* Proceedings of the 4th international conference on Railway Traction systems 2010 2010.
17. Hussain, M.T.X.a.A.H.J., *Modeling and Estimation of Nonlinear Wheel-rail Contact Mechanics.* Proceedings of the twentieth Intenational conference on System Engineering, 2009: p. 219-223.
18. Hussain, M.T.X., *Multi Kalman Filtering Approach for Estimation of Wheel-Rail Contact Conditions* Proceedings of the United kingdom Automatic Control Conferecne 2010, 2010: p. 459-464.
19. Polach, O., *Creep forces in simulations of traction vehicles running on adhesion limit.* Wear, 2005. **258**(7-8): p. 992-1000.
20. Ortega, R., et al., *Estimation of Rotor Position and Speed of Permanent Magnet Synchronous Motors With Guaranteed Stability.* Control Systems Technology, IEEE Transactions on, 2011. **19**(3): p. 601-614.
21. Hsu, Y.H.J., S.M. Laws, and J.C. Gerdes, *Estimation of Tire Slip Angle and Friction Limits Using Steering Torque.* Control Systems Technology, IEEE Transactions on, 2010. **18**(4): p. 896-907.
22. Mei, T. and R. Goodall. *LQG and GA solutions for active steering of railway vehicles*. 2002: IET.
23. Hashmi, K., et al., *Adjustment approach for fuzzy logic model based selection of non-overlapping machining data in the turning operation.* Journal of Materials Processing Technology, 2003. **142**(1): p. 152-162.
24. Hashmi, K., I. Graham, and B. Mills, *Fuzzy logic based data selection for the drilling process.* Journal of Materials Processing Technology, 2000. **108**(1): p. 55-61.